UNIVERSIDADE FEDERAL DE MINAS GERAIS
Instituto de Ciênicas Biológicas
Programa de Pós-Graduação em Zoologia

Daniel de Melo Casali

EXPLORING MORPHOLOGICAL DATA PARTITIONING AND REASSESSING THE PHYLOGENY, DIVERGENCE TIMES AND MORPHOLOGICAL EVOLUTION IN PILOSA (MAMMALIA: XENARTHRA)

Belo Horizonte
2021

Daniel de Melo Casali

EXPLORING MORPHOLOGICAL DATA PARTITIONING AND REASSESSING THE PHYLOGENY, DIVERGENCE TIMES AND MORPHOLOGICAL EVOLUTION IN PILOSA (MAMMALIA: XENARTHRA)

Tese apresentada ao Programa de Pós-Graduação em Zoologia da Universidade Federal de Minas Gerais, como requisito parcial à obtenção do título de Doutor em Zoologia.

Orientador: Fernando Araújo Perini

Belo Horizonte

2021

043 Casali, Daniel de Melo.
Exploring morphological data partitioning and reassessing the phylogeny, divergence times and morphological evolution in Pilosa (Mammalia: Xenarthra) [manuscrito] / Daniel de Melo Casali. – 2021.

202 f. : il. ; 29,5 cm.

Orientador: Prof. Dr. Fernando Araújo Perini.
Tese (doutorado) – Universidade Federal de Minas Gerais, Instituto de Ciências Biológicas. Programa de Pós-Graduação em Zoologia.

1. Zoologia. 2. Eutérios. 3. Filogenia. 4. Morfologia (Animais). 5. Cingulados. I. Perini,Fernando Araújo. II. Universidade Federal de Minas Gerais. Instituto de Ciências Biológicas. III. Título.

CDU: 591

Ficha catalográfica elaborada pela bibliotecária Rosilene Moreira Coelho de Sá – CRB 6 - 2726

UNIVERSIDADE FEDERAL DE MINAS GERAIS
INSTITUTO DE CIÊNCIAS BIOLÓGICAS
PÓS-GRADUAÇÃO EM ZOOLOGIA

FOLHA DE APROVAÇÃO DE TESE

Exploring morphological data partitioning and reassessing the phylogeny, divergence times and morphological evolution in Pilosa (Mammalia: Xenarthra)

DANIEL DE MELO CASALI

Esta tese foi apresentada em sessão pública e submetida a avaliação em 24 de agosto de 2021, sendo aprovada pela Banca Examinadora composta pelos seguintes membros:

Prof. Dr. Almir Rogério Pepato (Membro / UFMG)

Prof. Dr. Fernando Araújo Perini (Orientador / UFMG)

Prof. Dr. François Roger Francis Pujos (Membro / Instituto Argentino de Nivologia, Glaciologia y Ciencias Ambientales)

Profa. Dra. Mariela Cordeiro de Castro (Membro / Universidade Federal de Catalão)

Prof. Dr. Mario Alberto Cozzuol (Membro / UFMG)

Belo Horizonte, 24 de agosto de 2021

Documento assinado eletronicamente por **Fernando Araujo Perini, Professor do Magistério Superior**, em 25/08/2021, às 09:11, conforme horário oficial de Brasília, com fundamento no art. 5º do Decreto nº 10.543, de 13 de novembro de 2020.

Documento assinado eletronicamente por **Mario Alberto Cozzuol, Membro**, em 25/08/2021, às 13:18, conforme horário oficial de Brasília, com fundamento no art. 5º do Decreto nº 10.543, de 13 de novembro de 2020.

Documento assinado eletronicamente por **Almir Rogerio Pepato, Professor do Magistério Superior**, em 26/08/2021, às 10:12, conforme horário oficial de Brasília, com fundamento no art. 5º do Decreto nº 10.543, de 13 de novembro de 2020.

Documento assinado eletronicamente por **François Roger Francis Pujos, Usuário Externo**, em 26/08/2021, às 10:35, conforme horário oficial de Brasília, com fundamento no art. 5º do Decreto nº 10.543, de 13 de novembro de 2020.

Documento assinado eletronicamente por **Mariela Cordeiro de Castro, Usuário Externo**, em 26/08/2021, às 22:10, conforme horário oficial de Brasília, com fundamento no art. 5º do Decreto nº 10.543, de 13 de novembro de 2020.

A autenticidade deste documento pode ser conferida no site https://sei.ufmg.br/sei/controlador_externo.php?acao=documento_conferir&id_orgao_acesso_externo=0, informando o código verificador **0922861** e o código CRC **0D0F9EFF**.

ACKNOWLEDGMENTS

I thank Fernando Perini for the guidance during those more than four years, for being supportive and providing invaluable orientations in the construction of this thesis, always giving me freedom to commit my own mistakes, and learn from them in the process. I'm indebted to him for much of what I learned in my academic journey so far.

I'm also truly indebted to my collaborators: Felipe Freitas, José Eustáquio dos Santos, Flávia Miranda, Fabrício Santos, Alberto Boscaini and Timothy Gaudin. Their varied expertise hugely contributed to the studies composing this thesis, and their support and friendship were essential to my personal and professional development.

For the financial support, I thank the Coordenação de Aperfeiçoamento de Pessoal de Nível Superior (CAPES), the Field Museum of Natural History and the Paleontological Society.

I am very grateful to the curators and staff of the collections of Field Museum of Natural History, Yale Peabody Museum, American Museum of Natural History, Museo de Historia Natural Bernardino Rivadavia, Museo de La Plata, Museu PUC Minas Gerais and the taxonomic collection of UFMG, which grant me access to the studied specimens.

To the evaluation committee members, for kindly accepting the invitation: Almir Pepato, Mario Cozzuol, Adalberto Santos, Mariela Castro, François Pujos and Rafaela Missagia.

To all colleagues and to professors of the university, who taught me so much. My special thanks to Guilherme Garbino, Cayo Dias and Rafaela Missagia for many constructive conversations which helped me to improve the studies composing this thesis, to Rodrigo Parisi Dutra and Thiago Quintão for always "being ridiculous", to Carla Melo, Carla Nobre, Maria Clara Nascimento, Leonardo Cotts and Luciano Vilaboin, for all the funny moments and for their constant help. I also thank Germán Gasparini for helping me in many occasions.

To my dear friends outside the university: Mairon Oliveira, Victor Costa, Elvis Pimenta, Rafael Figueiredo, Raul Torres, André Villas-Boas, Fernanda Alvarenga, Michael Renzetti, Edgardo Mourão, Stefan Salej, Vitor Casarin, Diogo Fleury and Tulaci Bhakti. Thanks for your friendship. More so in this last year and a half – while locked up at home due to Covid-19 pandemic – having the chance to laugh together or a to have nice conversation with you, even if at distance, was very important to me.

To my family, specially to my parents, Ana and Ramon, for continuously encouraging me to keep studying and pursuing my goals. To my sister Gabriela, my aunt Nilda, my uncles Luiz and Tolomeu, and their families, and to my wife's family as well, thanks for all support.

Most of all, to my wife, Gabi, for being by my side in all good and bad times, for helping me in many direct and indirect ways. I cannot stress how much I’m indebted to her, and the completion of this thesis would not be possible if it was not for her constant support and comprehension. Also, to my dog, Fox, for his unconditional companionship and for making me happy even in the tougher times.

“Nature creates unity even in the parts of a whole” (Eugène Delacroix)

RESUMO

A evolução morfológica é heterogênea e os métodos analíticos devem levar isso em consideração para produzir inferências confiáveis, tanto filogenéticas quanto em estudos de evolução morfológica baseados em caracteres discretos. O particionamento de dados é bem compreendido para dados moleculares, mas só recentemente começou a ser aplicado à morfologia, e seus impactos nas inferências filogenéticas e evolutivas para este tipo de dados permanecem pouco estudados. Esta tese avalia o desempenho do particionamento de dados morfológicos com diferentes abordagens e objetivos, incluindo simulações e explorações empíricas sistemáticas. Esta tese também teve como objetivo reavaliar a filogenia, tempos de divergência e evolução morfológica de Vermilingua e Folivora, e essas investigações empíricas servem também como estudos de caso para avaliar o desempenho de particionamento de dados morfológicos e do uso da morfologia em análises de datação. Evidências das simulações e dados empíricos sugerem que o particionamento anatômico não é uma maneira eficiente de segregar caracteres de acordo com suas taxas evolutivas, mas que isso pode ser alcançado usando partições baseadas em homoplasias em análises filogenéticas. No entanto, as partições orientadas pela anatomia podem ser valiosas ao estudar a disparidade morfológica e as taxas evolutivas, permitindo investigar esses padrões para distintas regiões de interesse, que poderiam ser obscurecidos avaliando os dados de forma não particionada. As investigações filogenéticas de Vermilingua e Folivora retornaram resultados gerais semelhantes aos obtidos anteriormente, mas forneceram algumas novas evidências relacionadas à posição de táxons contenciosos, estimativas de tempos de divergência e novas sinapomorfias para clados previamente reconhecidos. Alguns insights metodológicos também foram obtidos. Para o estudo de Vermilingua, a importância de uma maior amostragem de táxons e caracteres e a presença de sinais filogenéticos ocultos em conjuntos de dados separados somente se tornaram evidentes quando estes foram combinados. Para o estudo filogenético de Folivora, a consistência com os resultados publicados anteriormente foi afetada pelo modelo de partição aplicado, com partições definidas por critérios de homoplasia sendo preferidas e levando a topologias semelhantes às obtidas por inferências de máxima parcimônia. Ambos os estudos reafirmaram a importância da seleção de modelos nas análises filogenéticas bayesianas utilizando dados morfológicos. Ao investigar os padrões de evolução morfológica em Folivora, o particionamento em dados cranianos e pós-cranianos foi fundamental para esclarecer o padrão distinto apresentado por esses subconjuntos de caracteres, com a morfologia craniana refletindo principalmente a inércia filogenética, enquanto para o pós-crânio, as adaptações ecológicas

parecem ter também desempenhado um importante papel, levando a convergências relacionadas à morfologia funcional.

PALAVRAS-CHAVE: Pilosa. Vermilingua. Folivora. Morfologia. Particionamento. Filogenética bayesiana. Disparidade. Taxas evolutivas.

ABSTRACT

Morphological evolution is heterogeneous and analytical methods should take this into consideration in order to produce reliable inferences, both for phylogenetic analyses and for studies of morphological evolution based on discrete characters. Data partitioning is well understood for molecular datasets, but only recently has begun to be applied to morphology, and its impacts on phylogenetic and evolutionary inferences for this kind of data remain underinvestigated. This thesis evaluates the performance of morphological data partitioning with different approaches and goals, including simulations and systematic empirical explorations. This thesis also aimed to reassess the phylogeny, divergence times and morphological evolution of Vermilingua and Folivora, and these empirical investigations also work as case studies for evaluating the performance of morphological data partitioning and the use of morphology in dating analyses. Evidence from simulations and empirical data suggests that anatomical partitioning is not an efficient way to segregate characters according to their evolutionary rates, what can be achieved using homoplasy-based partitions in phylogenetic analyses. Nevertheless, anatomically-oriented partitions can be valuable when studying morphological disparity and evolutionary rates, allowing to investigate these patterns for different regions of interest, which could be obscured if unpartitioned datasets are considered. Phylogenetic investigations of Vermilingua and Folivora returned overall similar results with those previously obtained, but provided some novel evidences related to the position of contentious taxa, divergence time estimates and new synapomorphies for previously recognized clades. Some methodological insights were also obtained. For the study of Vermilingua, the importance of sampling additional taxa and characters and the presence of hidden phylogenetic signals in separate datasets only became evident when they were combined. For the phylogenetic study of Folivora, the consistency with previously published results was affected by the partitioning model applied, with homoplasy-based partitioning being preferred and leading to similar topologies to those obtained by maximum parsimony inferences. Both studies reafirmed the importance of model selection in Bayesian phylogenetics of morphological data. While investigating the patterns of morphological evolution in Folivora, partitioning of cranial and postcranial data was fundamental to shed light in the distinct evolutionary patterns in these subsets of characters, with cranial morphology mostly reflecting phylogenetic inertia, whereas for postcranium, ecological adaptations seem to have also played an important role, leading to convergences related to the functional morphology.

KEYWORDS: Pilosa. Vermilingua. Folivora. Morphology. Partitioning. Bayesian phylogenetics. Disparity. Evolutionary rates.

SUMMARY

INTRODUCTION

Morphological data constitutes a fundamental source of evidence for understanding the evolutionary patterns observed in living and fossil organisms (Wiens 2004; Lee and Palci 2015). In the last few years, there was a renewed interest in morphology, with the emergence of new analytical approaches, including the application of Bayesian phylogenetic methods for morphological datasets (Wright 2019). Studying morphological variation is appealing not only because of the astonishing variability found among organisms, but also because of the heterogeneity observed in how distinct characters and anatomical regions evolve (Clarke and Middleton 2008). This variability, nevertheless, also poses important methodological challenges, requiring that analytical methods take this evolutionary heterogeneity into consideration in order to achieve reliable inferences, and only a few studies have explored this for discrete morphology (e.g., Rosa et al. 2019; Stubbs et al. 2019). Understanding how to best partition morphological data can be invaluable for phylogenetic inferences, divergence time estimations and for studies of morphological evolution. This thesis aims to evaluate the performance of morphological data partitioning with different approaches and goals, including simulations and systematic empirical explorations of morphological data.

This thesis has also a second, and equally important goal, which is to improve our knowledge on the phylogeny, divergence times and morphological evolution of Vermilingua (anteaters) and Folivora (sloths), which together comprises the clade Pilosa (Gaudin and McDonald 2008; Gibb et al. 2016). Pilosa is an autochthonous South American group of placental mammals, with a rich fossil record but few living species (Patterson and Pascual 1968; McDonald and De Iuliis 2008; McDonald et al. 2008). The phylogeny of anteaters and sloths have been widely studied in the last few decades, almost exclusively with parsimony-based methods for morphology (e.g., Gaudin and Branham 1998; Gaudin 2004; Pujos et al. 2007; Amson et al. 2016; Boscaini et al. 2019; but see Varela et al. 2019), with statistical phylogenetic methods mostly applied for molecular data (e.g., Gibb et al. 2016; Delsuc et al. 2019; Presslee et al. 2019). Additionally, the patterns of morphological evolution in these groups were frequently assessed through limited morphometric data of dental and postcranial elements (Bargo et al. 2012; Toledo 2016; Kalthoff and Green 2018; Serio et al. 2020), or with discrete character for an unpartitioned dataset of the complete skeleton (Varela et al. 2019). Therefore, reassessing pilosan phylogeny, divergence times and patterns of morphological discrete

character evolution with methodologies that explicitly consider the heterogeneous evolutionary patterns present in morphology is necessary.

The thesis is composed of four chapters, which were written and formatted as manuscripts to be submitted to scientific journals. Chapter 1 is a methodological exploration of anatomical partitioning and its impact in the precision and accuracy of consensus tree topologies obtained in Bayesian phylogenetic analyses, evaluated with simulated and empirical morphological datasets. This manuscript was submitted and it is under review in Systematic Biology. In chapter 2, a combined analysis of morphological and molecular data was performed, investigating the phylogeny and divergence times of Vermilingua, with anatomical partitioning being applied to morphological characters. This study was published in Systematics and Biodiversity in 2020. In chapter 3, the phylogeny and divergence times of Folivora were reassessed, and a systematic exploration of alternative models of morphological data partition was conducted. Finally, in chapter 4, folivoran morphological disparity and rates of evolution for cranial and postcranial partitions were evaluated separately, investigating how these patterns relate to phylogenetic and ecological groups of sloths. Chapters 3 and 4 are intended to be submitted to high impact scientific journals, such as Zoological Journal of the Linnean Society and Evolution.

REFERENCES

Amson E., de Muizon C., Gaudin T.J. 2016. A reappraisal of the phylogeny of the Megatheria (Mammalia: Tardigrada), with an emphasis on the relationships of the Thalassocninae, the marine sloths. Zool. J. Linn. Soc. 179:217–236.

Bargo M.S., Toledo N., Vizcaíno S.F. 2012. Paleobiology of Santacrucian sloths and anteaters. In: Vizcaíno S.F., Kay R.F., Bargo M.S., editors. Early Miocene Paleobiology in Patagonia. Cambridge University. p. 216–242.

Boscaini A., Pujos F., Gaudin T.J. 2019. A reappraisal of the phylogeny of Mylodontidae (Mammalia, Xenarthra) and the divergence of mylodontine and lestodontine sloths. Zool. Scr. 48:691–710.

Clarke J.A., Middleton K.M. 2008. Mosaicism, modules, and the evolution of birds: results from a Bayesian approach to the study of morphological evolution using discrete character data. Syst. Biol. 57:185–201.

Delsuc F., Kuch M., Gibb G.C., Karpinski E., Hackenberger D., Szpak P., Martínez J.G., Mead J.I., McDonald H.G., MacPhee R.D.E., Billet G., Hautier L., Poinar H.N. 2019. Ancient mitogenomes reveal the evolutionary history and biogeography of sloths. Curr. Biol. 29:2031-2042.e6.

Gaudin T.J. 2004. Phylogenetic relationships among sloths (Mammalia, Xenarthra, Tardigrada): the craniodental evidence. Zool. J. Linn. Soc. 140:255–305.

Gaudin T.J., Branham D.G. 1998. The phylogeny of the Myrmecophagidae (Mammalia, Xenarthra, Vermilingua) and the relationship of *Eurotamandua* to the Vermilingua. J. Mamm. Evol. 5:237–265.

Gaudin T.J., McDonald H.G. 2008. Morphology-based investigations of the phylogenetic relationships among extant and fossil xenarthrans. In: Vizcaíno S.F., Loughry W.J., editors. The biology of the Xenarthra. Gainesville: University of Florida Press. p. 24–36.

Gibb G.C., Condamine F.L., Kuch M., Enk J., Moraes-Barros N., Superina M., Poinar H.N., Delsuc F. 2016. Shotgun mitogenomics provides a reference phylogenetic framework and timescale for living xenarthrans. Mol. Biol. Evol. 33:621–642.

Kalthoff D.C., Green J.L. 2018. Feeding ecology in Oligocene mylodontoid sloths (Mammalia, Xenarthra) as revealed by orthodentine microwear analysis. J. Mamm. Evol. 25:551–564.

Lee M.S.Y., Palci A. 2015. Morphological phylogenetics in the genomic age. Curr. Biol. 25:R922–R929.

McDonald G.H., Vizcaíno S.F., Bargo S.M. 2008. Skeletal anatomy and the fossil history of the Vermilingua. In: Vizcaíno S.F., Loughry W.J., editors. The Biology of the Xenarthra. Gainesville: University Press of Florida. p. 64–78.

McDonald H.G., De Iuliis G. 2008. Fossil history of sloths. In: Vizcaino S.F., Loughry W.J., editors. The Biology of the Xenarthra. Gainesville: University Press of Florida. p. 39–55.

Patterson B., Pascual R. 1968. The fossil mammal fauna of South America. Q. Rev. Biol. 43:409–451.

Presslee S., Slater G.J., Pujos F., Forasiepi A.M., Fischer R., Molloy K., Mackie M., Olsen J. V, Kramarz A., Taglioretti M., Scaglia F., Lezcano M., Lanata J.L., Southon J., Feranec R., Bloch J., Hajduk A., Martin F.M., Salas Gismondi R., Reguero M., de Muizon C., Greenwood A., Chait B.T., Penkman K., Collins M., MacPhee R.D.E. 2019. Palaeoproteomics resolves sloth relationships. Nat. Ecol. Evol. 3:1121–1130.

Pujos F., De Iuliis G., Argot C., Werdelin L. 2007. A peculiar climbing Megalonychidae from the Pleistocene of Peru and its implication for sloth history. Zool. J. Linn. Soc. 149:179–235.

Rosa B.B., Melo G.A.R., Barbeitos M.S. 2019. Homoplasy-based partitioning outperforms alternatives in Bayesian analysis of discrete morphological data. Syst. Biol. 68:657–671.

Serio C., Raia P., Meloro C. 2020. Locomotory adaptations in 3D humerus geometry of Xenarthra: testing for convergence. Front. Ecol. Evol. 8:1–12.

Stubbs T.L., Benton M.J., Elsler A., Prieto-Márquez A. 2019. Morphological innovation and the evolution of hadrosaurid dinosaurs. Paleobiology. 45:347–362.

Toledo N. 2016. Paleobiological integration of Santacrucian sloths (Early Miocene of Patagonia). Ameghiniana. 53:100.

Varela L., Tambusso P.S., McDonald H.G., Fariña R.A. 2019. Phylogeny, macroevolutionary trends and historical biogeography of sloths: insights from a Bayesian morphological clock analysis. Syst. Biol. 68:204–218.

Wiens J.J. 2004. The role of morphological data in phylogeny reconstruction. Syst. Biol. 53:653–661.

Wright A.M. 2019. A systematist's guide to estimating bayesian phylogenies from morphological data. Insect Syst. Divers. 3:1–14.

CHAPTER 1. Anatomical partitioning has little influence in topologies from Bayesian phylogenetic analyses of morphological data

ABSTRACT

Morphological data is a fundamental source of evidence to reconstruct the Tree of Life, and Bayesian phylogenetic methods are increasingly being used for this task, along with, or instead of, traditional parsimony approaches. Bayesian phylogenetic analyses require the use of proper evolutionary models and they have been intensively studied in the past few years, with significant improvements to our knowledge regarding their performance. Notwithstanding, it was only recently that partitioned models for morphology received attention in studies of empirical data, but a systematic evaluation of its performances using simulations was never performed. Here we evaluate the influence of partitioned models defined by anatomical criterion in the precision and accuracy of consensus tree topologies, evaluating the possible negative effects of under and overpartitioning. For that, we analysed datasets simulated using parameters and properties of two empirical datasets, using Bayesian phylogenetic analyses in MrBayes. Additionally, we reanalysed 32 empirical datasets for diverse groups of vertebrates, applying unpartitioned and partitioned models. We found that in general, partitioning by anatomy has little to no influences in the performance of Bayesian phylogenetic methods in respect to the metrics studied here, with analyses under alternative partitioning schemes presenting very similar tree precision and accuracy. We discuss the possible reasons for the disagreement between the results obtained here and previous studies for empirical morphological data, and with empirical and simulation studies of molecular data, discussing the adequacy of anatomical partitioning relative to alternative methods to partition morphological datasets and how morphological and molecular partitioning are related.

KEYWORDS: Partition. Morphology. Mk model. Evolutionary rates. Heterogeneity. Topology.

1.1 INTRODUCTION

Morphological data is a fundamental source of evidence to reconstruct the Tree of Life. Almost always, it is the only kind of data available for phylogenetic inferences of fossil taxa and, along with molecular data, it is also a complementary source of information to reconstruct the phylogeny and timescale of living and extinct organisms (Wiens 2004; Lee and Palci 2015). Traditionally, morphological datasets have been analysed exclusively with the maximum parsimony criterion, but more recently, model-based phylogenetic analyses, in particular Bayesian methods, have become widely available and are increasingly being used instead of, or along with, parsimony approaches (Wright 2019; Wright and Lloyd 2020). In parallel with the growing use of probabilistic approaches, we have an increasing number of studies exploring the performance of those alternative phylogenetic methods, using both simulated and empirical morphological data (Wright and Hillis 2014; O'Reilly et al. 2016; Puttick et al. 2017; O'Reilly et al. 2018; Goloboff et al. 2018; Goloboff and Arias 2019; Puttick et al. 2019; Smith 2019b).

Bayesian phylogenetic analyses of discrete morphological data make use of the Mk model (Lewis 2001), which is essentially the Jukes-Cantor model of nucleotide substitution (Jukes and Cantor 1969) generalized for any number of states. Since its original proposal, extensions of that model have been presented in order to account for the heterogeneity in evolutionary patterns present in morphological datasets, like allowing for unequal character state frequencies, or the use of alternative distributions to model among-character rate variation, with their performances being evaluated for empirical and simulated data (Harrison and Larsson 2015; Wright et al. 2016).

Another important way to account for data heterogeneity in phylogenetic analyses is through the use of partitioned models, in which subsets of the data have its parameters estimated independently from those of other such subsets (Brown and Lemmon 2007; Lanfear et al. 2012). Those partitioned models have been widely used for molecular datasets and their performance are well explored and understood (Nylander et al. 2004; Brandley et al. 2005; Marshall et al. 2006; Brown and Lemmon 2007; Kainer and Lanfear 2015; Duchêne et al. 2020). More recently, data partitioning began to be applied in studies using empirical morphological data, some of which provided a broad evaluation of alternative partitioning models for these datasets, including partitioning by anatomy, homoplasy, evolutionary rates and number of character states (Clarke and Middleton 2008; Close et al. 2015; Tarasov and Génier 2015; Gavryushkina et al. 2017; King et al. 2017; Rosa et al. 2019; Varela et al. 2019; Brazeau et al. 2020; Lucena and Almeida 2021; Porto et al. 2021).

Although studying the performance of models using empirical datasets ensure a greater degree of realism, the use of simulated data allow the assessment of the accuracy of a given method or model and the systematic exploration of a broad range of factors that can potentially affect the results of the analyses (Hillis 1995), something not feasible to do using empirical datasets. To the best of our knowledge, no study to date evaluated the performance of partitioned models for morphological data making use of simulations.

Here we focus on the evaluation of the performance of data partitioning according to the anatomical criterion as it has been used recently in the literature (Clarke and Middleton 2008; Tarasov and Génier 2015; Rosa et al. 2019; Varela et al. 2019; Porto et al. 2021). The anatomical partitioning criterion considers that subsets of characters associated with distinct anatomical modules evolve at different rates (Clarke and Middleton 2008; Tarasov and Génier 2015), and these modules can be defined according to hypotheses of structural, functional or developmental integration of characters (Clarke and Middleton 2008). Frequently, those partitions are defined for general and localized body regions like cranial x postcranial skeleton (Varela et al. 2019) or internal x external anatomy (Porto et al. 2021), but fine-grained hypotheses of partitioning have also been evaluated (Clarke and Middleton 2008; Tarasov and Génier 2015; Varela et al. 2019; Porto et al. 2021). Distinctly from other partitioning criteria, and especially from those applied to molecular data, anatomical partitioning requires specific knowledge from researchers studying the morphology of a given taxonomic group.

We applied anatomical partitioned models for simulated morphological datasets in a Bayesian framework, and evaluated their impact on the precision and accuracy of the estimated consensus topologies, evaluating the effects of using the correct partitioning scheme used to simulate the data, and also different partitioning schemes to explore under and overpartitioning. Complementarily, we also reanalyzed 32 vertebrate empirical datasets originally proposed to be composed of two anatomical partitions – cranial and postcranial – considering unpartitioned and partitioned models in Bayesian analyses, and comparing their performance.

We show that, in general, partitioning data by anatomy has only a minor effect in the precision and accuracy of inferred topologies, and we discuss the adequacy of anatomical partitioning relative to alternative methods to partition morphological data, also comparing to what we know the about the performance of partitioned models for molecular datasets.

1.2 MATERIAL AND METHODS

1.2.1 Simulated data

1.2.1.1 Simulations

All simulations conducted in the present study were informed by properties and parameters obtained from two empirical datasets, which were previously analyzed using anatomical partitioning with Bayesian phylogenetic inferences. In both studies, models including anatomical partitioning proved to better fit the data than unpartitioned models, according to Bayes factors. The first dataset was obtained from Clarke and Middleton (2008), the first study that evaluated the use of anatomical partitioning in Bayesian phylogenetics. This study investigated the phylogeny of birds (Dinosauria: Avialae), and included 25 taxa, almost all of them extinct. It explored alternative anatomical partitioning schemes with two, three and four partitions, and will henceforth be referred as dataset A. The second dataset was obtained from Porto et al. (2021), a recent study that also investigated anatomical partitioning studying the phylogeny of corbiculate bees (Hymenoptera: Apidae) and several outgroups, including 50 extant taxa. Anatomical partitioning schemes with two and seven partitions were proposed for this dataset in the original study, that will henceforth be referred as dataset B.

Both datasets were reanalyzed considering the anatomical partitions and partitioning schemes originally proposed by the authors (Table 1) and phylogenetic inferences were performed in MrBayes 3.2.7a (Huelsenbeck and Ronquist 2001; Ronquist and Huelsenbeck 2003) with two approaches – i) Unlinking partition topologies and branch lengths, to obtain partition-specific trees to be used to simulate the data – henceforth referred to as partition trees, ii) Linking partition topologies and branch lengths to produce a single phylogenetic tree for each partitioning scheme, which will be used as a reference for evaluating topological accuracy and precision of trees inferred from simulated data – henceforth referred to as reference trees. For these reference trees, among-partition rate variation was accounted for using partition-specific rate multipliers. To account for among-character rate variation, discrete gamma distributions with four rate categories were applied, with unlinked estimates of shape (α) for each partition. Those analyses resulted in three reference trees and nine partition trees for dataset A, and two reference and nine partition trees for dataset B. Also, anunpartitioned analysis was performed for each dataset, with the resulting tree being used both for simulations and as a reference tree of unpartitioned models, and in these cases, a single gamma distribution was used for modeling among-character rate variation for the entire dataset. We replicated the settings of character ordering (or lack thereof) and coding (*coding* = *variable*) as used in the

original analyses. We set runs (two for dataset A with 5M generations and four for dataset B, with 10M generations, as in the original studies), with four chains each, sampling every 1000th generation, and discarding 25% of the samples before summarizing parameters. Unlinked analyses of dataset A required a larger number of generations (20-30M) to converge. Tree summaries were set to return a maximum compatibility consensus tree (*contype* = *allcompat*). The samples of continuous parameters and topologies were checked with the function *analyze.rwty* in the package *rwty* (Warren et al. 2017) in R environment (R Core Team 2021). We visually inspected all trace plots, and considered that analyses have converged when individual runs achieved a minimum effective sample size (ESS) >100 with all runs sampling in the same region of parameter space, average standard deviation of split frequencies (ASDFD) < 0.01 and correlation of splits between runs = 1.0. All input, output and convergence files from those analyses are available as Supplementary Data S1.

Partition-specific topologies and branch lengths from partition trees estimated in the reanalysis of the two empirical datasets were used to generate the partitions in our study, ensuring that simulated patterns of phylogenetic signal and among-partition rate variation are consistent with those present in the empirical datasets. Other properties obtained from partitions of datasets A and B were applied in the simulations, further ensuring consistency among those empirical datasets and the ones simulated here (Fig. 1, Table 1). Those properties were: partition size, frequency of characters by the number of states, degree of rate asymmetry between states of binary characters, distribution of homoplasy and missing data, and number of non-informative characters. For dataset A, simulations were conducted considering four partitioning schemes (s1 – data unpartitioned, s2 – two partitions, s3 – three partitions and s4 – four partitions) and for dataset B, three partitioning schemes were applied (s1 – data unpartitioned, s2 – two partitions and s7 – seven partitions), following the partitioning schemes proposed in the empirical studies (Table 1).

Table 1. Properties of all partitions that compose empirical datasets A and B, used in simulations, and their respective association with a partitioning scheme. CI – Ensemble consistency index. Characters – total number of characters per partition. Non-info – number of non-informative characters per partition. st. – states.

Dataset	Scheme	Partition	CI	Characters	Non-info	Binary	Three st.	Four st.	Five st.	Six st.
A	s1	ALL	0.64	205	16	0.75	0.22	0.02	0.01	-
A	s4	CRANIAL	0.66	52	7	0.81	0.19	-	-	-
A	s4	AXIAL	0.7	19	0	0.58	-	0.37	-	0.05
A	s2, s3, s4	PECTORAL	0.6	83	3	0.81	0.14	0.02	0.02	-
A	s3, s4	PELVIC	0.66	51	6	0.65	0.31	0.04	-	-
A	s3	CRANIAL_AXIAL	0.67	71	7	0.75	0.14	0.10	-	0.01
A	s2	CRANIAL_AXIAL_PELVIC	0.67	122	13	0.70	0.21	0.07	-	0.01
B	s1	ALL	0.38	282	1	0.69	0.26	0.06	-	-
B	s2	EXT	0.34	181	0	0.71	0.25	0.04	-	-
B	s2	INT	0.45	101	1	0.64	0.27	0.09	-	-
B	s7	HD	0.3	42	0	0.74	0.24	0.02	-	-
B	s7	MP	0.41	52	0	0.79	0.17	0.04	-	-
B	s7	MS	0.31	57	0	0.68	0.26	0.05	-	-
B	s7	WG	0.43	16	0	0.56	0.44	-	-	-
B	s7	LG	0.38	49	0	0.49	0.37	0.14	-	-
B	s7	MT	0.57	11	0	0.82	0.18	-	-	-
B	s7	GN	0.49	55	1	0.75	0.20	0.05	-	-

EXT – external, INT – internal, HD – head, MP – mouthparts, MS – mesosoma, WG – wings, LG – legs, MT – metasoma, GN – genitalia.

Characters for each partition were simulated in R (R Core Team 2021) using the package *dispRity* (Guillerme 2018). We used the function *sim.morpho* to simulate variable characters, with the number of character per states in each partition following proportions obtained from empirical datasets (Table 1). Binary characters were simulated using HKY model (Hasegawa et al. 1985), whereas multistate characters were simulated with the Mk model (equal rates). For HKY, values of *pi* were sampled from a uniform distribution and divided by their sum to obtain their proportional frequencies. The parameter governing among-states rate asymmetry (*kappa*) was sampled from a uniform distribution composed of values obtained from empirical datasets (Fig. 1c-d). This distribution was obtained fitting the all rates different (ARD) model to all binary characters from the empirical datasets and calculating the ratio between the faster and the slower rates estimated for each character. Those rate distributions were obtained for each partition using their respective partition tree, and applied accordingly to simulate the data. For example, if a two-partition dataset was being simulated, we used values of *kappa* obtained fitting ARD to the data of the two empirical partitions in the partition trees estimated from them. Model fitting was performed using marginal reconstructions with the package and function *corHMM* (Beaulieu et al. 2021) in R.

After simulating each character, we checked if it was generated as a parsimony-informative character, and if not, the character was discarded and re-simulated until this condition was satisfied. This procedure was repeated until we achieved the desired partition size, as informed by the empirical data (Table 1).

Partition-specific branch lengths from partition trees ensured that all simulated partitions of a given dataset present among-partition rate variation comparable to those observed in empirical data. Additionally, to account for among-character rate variation in our simulations, character-specific rates were drawn from an exponential distribution with its rate parameter sampled from a second, uniform distribution. The minimum and maximum values of the uniform distributions were empirically adjusted, aiming to simulate partitions that match the distribution of homoplasy observed in their respective generative empirical partition. The final values (min = 1, max = 10 for dataset A, min = 1, max = 2 to dataset B) produced distributions of character consistency indices (ci, Kluge and Farris 1969) and partition ensemble consistency index (CI, Farris 1989, Table 1) comparable to those observed in the empirical datasets (Fig. 1a-b, Table 1, Supplementary Files S1-S2). Consistency indices were calculated with the function *check.morpho* in the package *dispRity*.

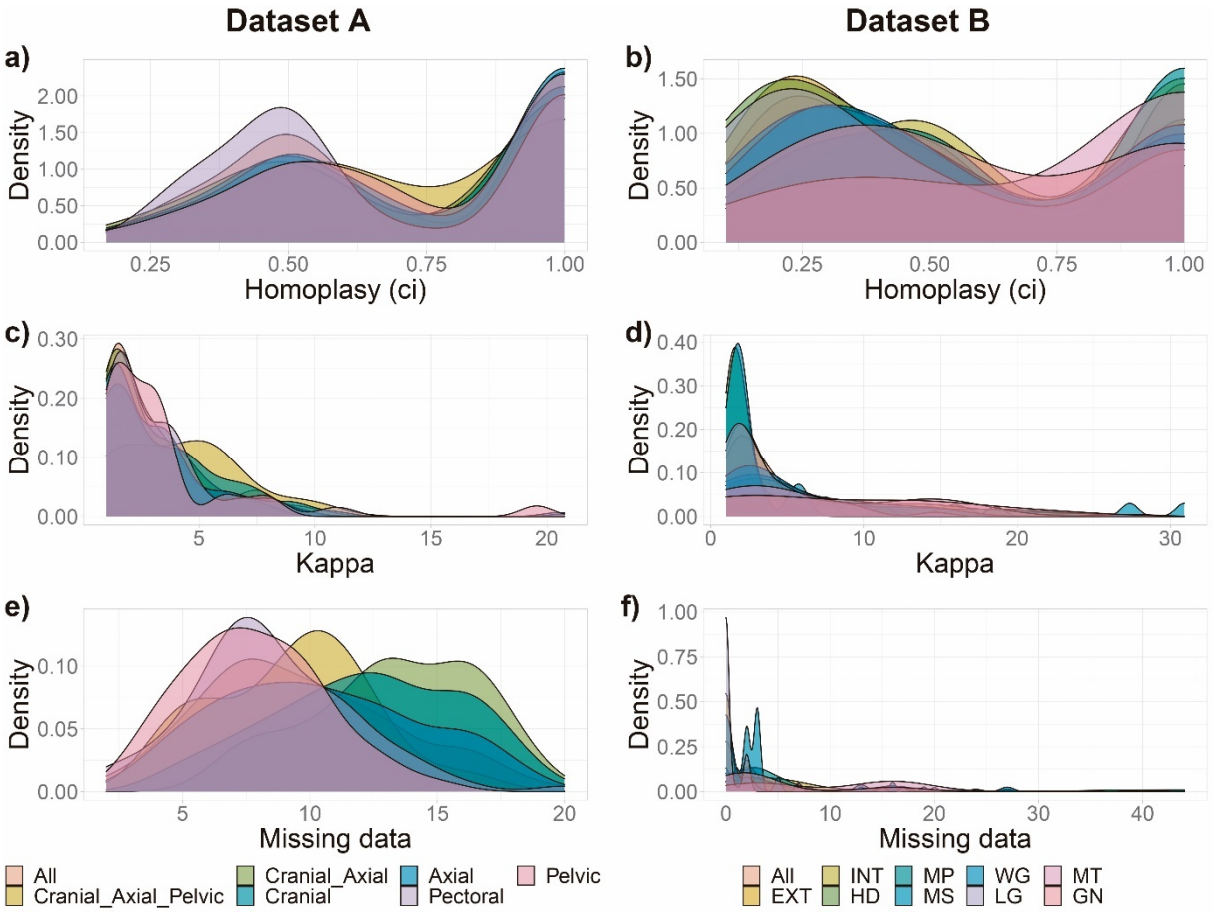

Figure 1. Density plots summarizing properties of all partitions of empirical datasets A and B, used in simulations. a-b) Distributions of homoplasy, measure by character consistency index (ci); c-d) Distributions of values of *kappa*, measured as the ratio of among-state rates for binary characters; e-f) Distributions of missing data, measured by the number of missing cells per character.

Missing data is frequently present in morphological datasets, especially in those including or totally composed of fossil taxa, with their distribution being rarely at random (Prevosti and Chemisquy 2009). We attributed missing data to the simulated partitions recoding cells to "?", sampling the number of cells per character to be recoded from a uniform distribution obtained from the values observed in the empirical partitions (Fig. 1e-f), mimicking non-random empirical distributions of missing data. Whenever a character was turned non-informative due to this process, the missing data attribution was redone, ensuring that all modified characters were kept as parsimony-informative. After that, we converted some characters to non-informative in the proportion they were observed in this condition in

empirical partition (Table 1). We generated 500 replications of each partition/datasets to account for the stochastic variation present in the simulation of the characters. The custom R scripts used to extract the information from the empirical dataset and to conduct the simulations are available in Supplementary Material.

1.2.1.2 Phylogenetic analyses

We analyzed each dataset using all strategies of data partitioning (x) also used to simulate them (s), resulting in 16 combinations for dataset A and nine for dataset B (Fig. 2). In this way, we were able to explore underpartitioned, correctly partitioned (i.e. matching the number of partitions that data was simulated and analyzed with) and overpartitioned models. Analyses were performed with Bayesian inferences in MrBayes. We set all analyses with two runs of 10M generations, with four chains each, sampling every 500th generation. In partitioned analyses, branch lengths were linked and per-partition rate multipliers were defined to account for among-partition rate variation, as this setting has been shown to outperform unlinking branch lengths (Rosa et al. 2019; Duchêne et al. 2020; Porto et al. 2021) and avoid overly parametrized models that can make analyses unnecessarily long or even fail to converge (e.g., Tarasov and Génier 2015). To account for among-character rate variation, a discrete gamma distribution with four rate categories was applied, and a single gamma distribution was defined for the entire dataset in the case of unpartitioned models. We used ascertainment bias correction for branch lengths (*coding* = *variable*), to be consistent with the conditions used to simulate the data. The initial 25% of the samples were discarded as a burn-in phase before summarizing continuous parameters and trees, with the latter being summarized into a maximum compatibility consensus tree. The analyses were interrupted when ASDFD reached values below 0.01, a widely used diagnostic of topological convergence among runs. We set the *diagnfreq* to 5M generations to ensure a minimum sample size before interrupting each analysis. We also obtained consensus trees collapsed by posterior probabilities (PPs) thresholds of 0.5 and 0.95 using the functions *read_annotated* of package *phylotate* (Beer and Beer 2019) and *collapseUnsupportedEdges* of the package *ips* (Heibl 2008). Convergence was checked using ASDFD < 0.01, and ESS >100 for each run, using functions *mcmc* and *effectiveSize* in R package *coda* (Plummer et al. 2006). All input, consensus tree, log and convergence output files from those analyses are available as Supplementary Data S2.

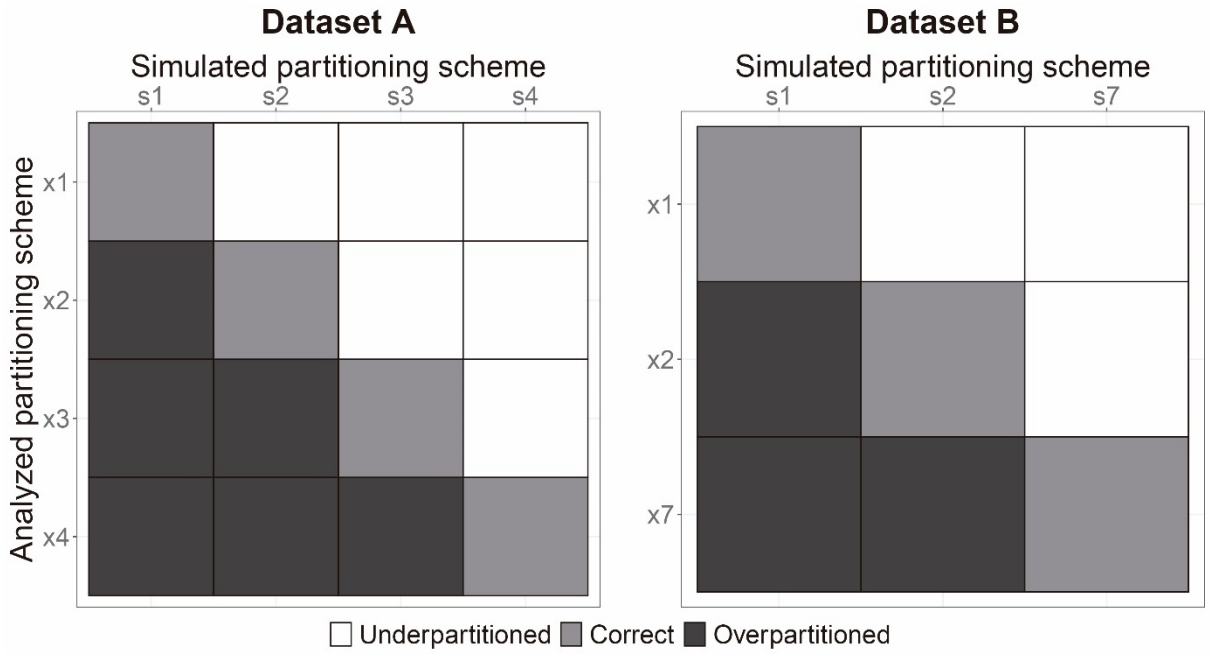

Figure 2. All combinations for simulated (s) and analyzed (x) partitioning schemes for datasets A and B, indicating those which are under, correct and overpartitioned.

1.2.1.3 Topological precision and accuracy

Robinson-Foulds distances (Robinson and Foulds 1981) are usually considered as a proxy of the accuracy of phylogenetic trees obtained from simulated data, comparing them to "true" trees used to generate it (Puttick et al. 2019; Smith 2019b). In spite of that, the Robinson-Foulds distance is a problematic metric if we wish to make independent assessment of accuracy and precision of phylogenetic trees, since it conflates similarity due to correct resolution and that from lack of resolution (Keating et al. 2020). Trees can be made two units more similar by replacing an incorrect bipartition with a correct one, or by collapsing two incorrect bipartitions (Smith 2019b). Thus, we used two separate metrics, one for accuracy and one precision. Those metrics were evaluated for bipartitions (= nodes) and for quartets, which is less sensitive to rogue taxa (Keating et al. 2020). For accuracy, we verified the proportion of correct nodes/quartets (correctly resolved /total number of resolved node/quartets) and for precision, the proportion of resolved nodes/quartets (actual number of resolved/maximum possible number of resolved nodes/quartets). The last metric applies only to trees after collapsing nodes below a given PP threshold, since *allcompat* trees are completely resolved. Node and quartet status were calculated using the fuctions *SplitStatus* and *QuartetStatus*, respectively, in the package *Quartet* (Smith 2019a).

Metrics were summarized in boxplots using *ggplot* function of ggplot2 package (Wickham 2016) and the function *describeBy* of package psych (Revelle 2020) was used to produce summary statistics tables. We excluded all analyses that fail to converge in at least one of the inspected metrics (34% for dataset A and 15% for dataset B, convergence data available in Supplementary Data S2) before summarizing the results. Convergence issues were present in all groups (i.e. unique combinations of s and x), but were not equally distributed among them, resulting in groups with different sample sizes. To ensure that this was not affecting our results, we also made group size equal by randomly sampling 150 trees from the set of analyses that converged (roughly the size of the smaller group from the converged set – 158 trees, for analysis s3_x1 of dataset A).

The degree of similarity between pairs of distributions of metrics for alternative partitioning schemes was evaluated using Bhattacharyya coefficients (Bhattacharyya 1946) with the function *bhatt.coeff* in the package *dispRity*. Calculations were conducted comparing all analysed partitioning schemes (e.g., x1 to x2, x1 to x3, x1_x3) for each simulated partitioning scheme (e.g., s1, s2, s3). The Bhattacharyya coefficient ranges from 0 (no overlap between distributions) to 1 (full overlap), and we follow Guillerme and Cooper (2016), considering Bhattacharyya coefficients < 0.05 indicative of clearly different distributions, and > 0.95 indicative of clearly similar distributions. We expected that, if anatomical partitioning is an efficient way to account for data heterogeneity, it would produce clearly different (or at least not clearly similar) distributions to those from under and overpartitioned models, including unpartitioned ones. If distributions of metrics of accuracy and precision are clearly similar for alternative partitioning schemes, this indicates that none of them is particularly better or worse in recovering the reference tree topology or to resolve nodes/quartets. Figure 3 depicts a summary of the methodology used to simulate and analyse the data.

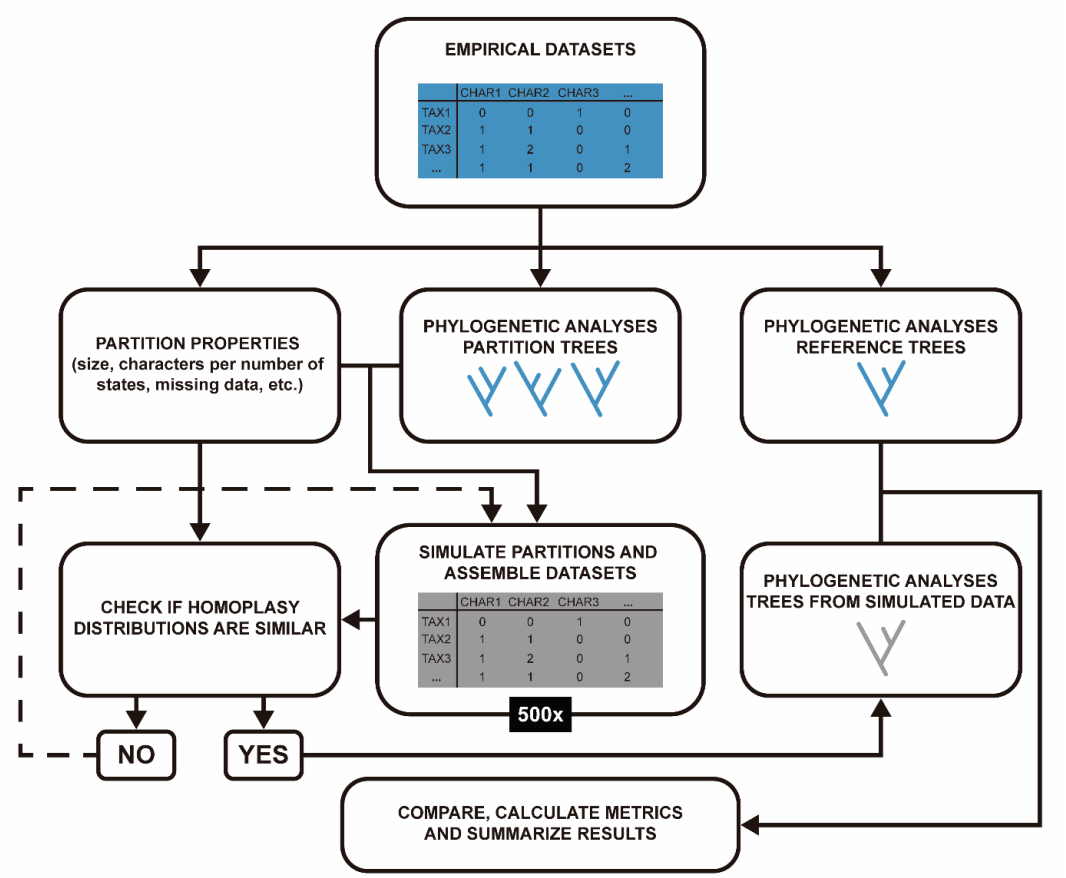

Figure 3. Graphical summary of the methodological steps of the simulation and analyses performed for simulated data. Blue indicates empirical and grey simulated datasets and trees.

1.2.2 Empirical data

1.2.2.1 Datasets

For a systematic evaluation of the performance of anatomical partitioning for empirical morphological data, we investigated datasets previously analyzed by Mounce et al. (2016) using separate analyses with maximum parsimony, and reanalyzed them using partitioned models with Bayesian inference. Mounce et al. (2016) defined two anatomical partitions for all datasets, one for cranial and another for postcranial characters. When analyzed separately, for some instances, those two partitions produced significantly different topologies according to the incongruence relationship difference (IRD) test (Mounce et al. 2016). We selected all 32 datasets that satisfied that condition for one or both versions of IRD test used in the original study, to be reanalyzed here using the same partitions proposed in Mounce et al. (2016). Supplementary File S3 contains a list of those datasets and details of some of their partitions and other properties.

1.2.2.2 Phylogenetic analyses

The datasets were reanalyzed using Bayesian inferences, with two approaches – not partitioning the data and partitioning it by previously proposed anatomical partitions – cranial and postcranial – and applying the character ordering (or lack thereof) as in the original analyses. Coding was set to variable to all datasets. As we did for simulated data, branch lengths were linked and rate multipliers used to account for among-partition rate variation, with gamma distributions used to model among-character rate variation. Analyses were performed in two runs, with four chains each, for 10M generations, sampling every 2000th, although some datasets demanded more generations to converge (20-25M). A burn-in of 25% was applied, and trees were summarized into a maximum compatibility consensus tree. Collapsing of nodes using PP threshold of 0.5 and 0.95 were also investigated. Convergence was checked with *rwty*, as described for analyses of empirical datasets A and B. All input, output and convergence files from those analyses are available in Supplementary Data S3.

1.2.2.3 Topological precision and similarity

The metrics used to evaluate precision in the analyses of simulated data were also applied to empirical datasets, comparing the resolution of consensus of alternative partitioning schemes (unpartitioned x partitioned). Also, the proportion of nodes/quartets resolved in the same way was computed. If the proportion of nodes/quartets resolved for each partitioning scheme is equal or very similar among themselves and to that of nodes/quartets resolved in common, it is evidence that alternative partitioning schemes does not make much difference in the precision of resulting topologies, whereas, if the opposite is true, some partitioning scheme is leading to a different degree of resolution of consensus trees. As for simulated data, boxplots and summary statistics were used to show the results and Bhattacharyya coefficients were calculated to assess similarity between distributions. For Bhattacharyya coefficients, the proportion of resolved nodes/quartets of unpartitioned models was compared to those resolved with partitioned models, and each of them was also compared to the proportion of nodes/quartets commonly resolved for both models.

All R scripts used for calculating the metrics for accuracy and precision, plotting the results, calculating summary statistics and Bhattacharyya coefficients for simulated and empirical datasets are available in Supplementary Material.

1.3 RESULTS

1.3.1 Simulated data

1.3.1.1 General results

Results observed for complete (all analyses that converged, unequal sample sizes) and reduced samples (150 samples for all groups) were in general agreement, so we will focus here on the results of the complete sample. Results of the reduced sample are available as Supplementary Figures S1-S2 and Supplementary Files S4-S7. Also, results of the analyses for datasets A and B were very similar. We will report the general results considering that they apply to trees obtained from simulations using both datasets, unless stated otherwise.

As expected, and irrespective of partitioning scheme, accuracy was greater for more collapsed (PP 0.95) trees if compared to trees with intermediate (PP 0.5) or no collapsing of nodes by support values, whereas the opposite was observed for precision (Figs. 4-5). Data simulated with partitioning schemes with a greater number of partitions tended to result in less precise and accurate consensus trees. Two exceptions to this general trend could be observed – i) For dataset A, tree accuracy for data simulated with two partitions (s2) was lower than the observed for data simulated with three (s3) or four (s4) partitions. This was observed for nodes (Fig. 4c), whereas for quartets (Fig. 4d), accuracy of s2 was lower only when compared to s3. ii) The node precision for dataset B simulations was greater for s7 than for s2 (Fig. 5a), but the same cannot be said for quartets (Fig. 5b). Overall, quartet metrics returned higher absolute precision and accuracy values than their counterparts for nodes, but indicating relative performances consistent with those showed by node metrics.

1.3.1.2 Topological precision and accuracy

Overall, there was no consistent improvement (or worsening) in topological precision or accuracy when data was analyzed with the same partitioning scheme used to simulated it, with all analyses usually showing very similar or identical proportions of resolved and correctly resolved nodes and quartets (Figs. 4-5, Supplementary Files S8-S9). Nevertheless, for some particular comparisons, tree precision and accuracy showed slightly higher median values for datasets analyzed with the correct partitioning, noticeably for quartet metrics of s4 of dataset A simulations, and quartets of s7 of dataset B simulations. But even in those cases, for some node collapsing schemes, this pattern was absent or very subtle.

Bhattacharyya coefficients indicate that in almost all cases, alternative anatomical partitioning schemes showed clearly similar distributions (> 0.95) for metrics of precision and accuracy, irrespective of the model used to analyse it (Supplementary Files S10-S11). In rare exceptions (2 of 396), the coefficients were less than 0.95, but greater than 0.94, which is very close to the threshold of greater similarity adopted here, and very far from indicate clearly different distributions (< 0.05). Those exceptions were only slightly more common for the reduced sample than for the complete (19 of 396), in which all values were greater than 0.93 (Supplementary Files S6-S7). Those comparisons showing Bhattacharyya coefficients below to 0.95 are not consistently associated with the cases of higher medians reported above.

1.3.2 Empirical data

Analyses of empirical datasets showed results aligned to those observed for simulations. For most datasets, the proportion of resolved nodes and quartets are the same – 20 for trees collapsed using PP threshold of 0.5 and 24 for 0.95. For 0.5 collapsing, the number of datasets in which nodes/quartets were resolved differently between partitioning schemes were 12, with six cases of better performance for each partitioning scheme. For trees collapsed using the 0.95 threshold, 8 datasets resolved more nodes/quartets in one or the other partitioning scheme. For nodes, partitioned analyses outperformed the unpartitioned in five datasets, and the opposite was true in the other three, whereas for quartets, partitioning schemes scored better than the alternative in four cases each (Table 2).

When we evaluate the distributions for the proportion of nodes and quartets resolved for unpartitioned and partitioned analyses, partitioned lead to slightly higher medians. Despite that, their distributions are very similar among themselves and to the distribution of the proportions of nodes resolved in common for both analysed schemes (Fig. 6, Supplementary File S12). Also, Bhattacharyya coefficients indicate that all compared distributions are clearly similar (> 0.95, Supplementary File S13).

Table 2. Precision metrics calculated for trees from empirical datasets analyzed with alternative partitioning schemes (Unpart. – unpartitioned and Part. – Partitioned by anatomical criterion – cranial and postcranial partitions). Precision was measure as the proportion of nodes and of quartets resolved. Comm. – the proportion of nodes and quartets resolved in common for both partitioning schemes. All – Maximum compatibility consensus trees (allcompat), Col. 50 – Consensus trees with nodes collapsed using 0.5 posterior probability threshold, Col. 95 – Consensus trees with nodes collapsed using 0.95 posterior probability threshold.

	Nodes						**Quartets**						
Dataset	**All Comm.**	**Col. 50 Unpart.**	**Col. 50 Part.**	**Col. 50 Comm.**	**Col. 95 Unpart.**	**Col. 95 Part.**	**Col. 95 Comm.**	**All Comm.**	**Col. 50 Unpart.**	**Col. 50 Part.**	**Col. 50 Comm.**	**Col. 95 Unpart.**	**Col. 95 Part.**	**Col. 95 Comm.**
Allain2012	0.70	0.70	0.55	0.55	0.25	0.30	0.25	0.84	0.88	0.73	0.73	0.62	0.63	0.62
AllainAquesbi2008	1.00	1.00	1.00	1.00	0.73	0.73	0.73	1.00	1.00	1.00	1.00	0.89	0.89	0.89
Asher2005	0.96	0.77	0.73	0.73	0.27	0.27	0.27	0.99	0.86	0.86	0.86	0.31	0.31	0.31
Asher2007	0.98	0.81	0.81	0.81	0.42	0.42	0.42	0.95	0.64	0.64	0.64	0.46	0.46	0.46
Brochu2010	0.95	0.71	0.71	0.71	0.24	0.24	0.24	1.00	0.93	0.93	0.93	0.47	0.47	0.47
Burns2011	1.00	0.86	0.86	0.86	0.36	0.36	0.36	1.00	0.94	0.94	0.94	0.04	0.04	0.04
Butler2008	1.00	0.92	0.92	0.92	0.65	0.65	0.65	1.00	0.96	0.96	0.96	0.79	0.79	0.79
CarranoSampson2008	1.00	0.78	0.78	0.78	0.67	0.56	0.56	1.00	0.90	0.90	0.90	0.79	0.74	0.74
EzcurraCuny2007	1.00	1.00	0.88	0.88	0.38	0.50	0.38	1.00	1.00	0.98	0.98	0.72	0.78	0.72
GatesSampson2007	1.00	0.50	0.50	0.50	0.20	0.20	0.20	1.00	0.63	0.63	0.63	0.26	0.26	0.26
Gaubert2005	0.97	0.83	0.89	0.83	0.58	0.58	0.58	1.00	0.98	0.99	0.98	0.93	0.93	0.93
Godefroit2008	1.00	0.83	0.92	0.83	0.33	0.33	0.33	1.00	0.97	0.98	0.97	0.52	0.52	0.52
HiltonForey2009	1.00	0.73	0.73	0.73	0.20	0.20	0.20	1.00	0.78	0.78	0.78	0.36	0.36	0.36

Dataset	Nodes							Quartets						
	All Comm.	Col. 50 Unpart.	Col. 50 Part.	Col. 50 Comm.	Col. 95 Unpart.	Col. 95 Part.	Col. 95 Comm.	All Comm.	Col. 50 Unpart.	Col. 50 Part.	Col. 50 Comm.	Col. 95 Unpart.	Col. 95 Part.	Col. 95 Comm.
Hurley2007	0.95	0.76	0.81	0.71	0.19	0.24	0.19	0.98	0.94	0.93	0.91	0.45	0.47	0.45
Ji2013	1.00	0.75	0.80	0.75	0.45	0.45	0.45	1.00	0.83	0.86	0.83	0.78	0.78	0.78
Lu2013	1.00	1.00	1.00	1.00	0.50	0.57	0.50	1.00	1.00	1.00	1.00	0.66	0.72	0.66
MartinelliRougier2007	1.00	1.00	0.92	0.92	0.62	0.62	0.62	1.00	1.00	0.96	0.96	0.79	0.79	0.79
Mauricio2012	0.94	0.66	0.66	0.63	0.43	0.43	0.43	0.99	0.92	0.93	0.92	0.87	0.87	0.87
MullerReisz2006	0.94	0.47	0.47	0.47	0.35	0.29	0.29	0.98	0.62	0.62	0.62	0.30	0.25	0.25
Nesbitt2009	1.00	0.97	0.97	0.97	0.72	0.78	0.72	1.00	1.00	1.00	1.00	0.98	0.98	0.98
Nesbitt2011	0.98	0.96	0.96	0.96	0.79	0.79	0.79	1.00	1.00	1.00	1.00	0.95	0.95	0.95
Nesbittetal2011	0.82	0.82	0.88	0.82	0.41	0.41	0.41	0.96	0.95	0.98	0.95	0.58	0.58	0.58
Parilla-Bel2013	1.00	1.00	1.00	1.00	0.46	0.46	0.46	1.00	1.00	1.00	1.00	0.83	0.83	0.83
Phillips2009	0.94	0.94	0.94	0.92	0.50	0.50	0.50	0.99	0.99	0.99	0.99	0.74	0.74	0.74
Pine2012	0.94	0.48	0.48	0.48	0.79	0.79	0.79	0.94	0.66	0.66	0.66	0.03	0.01	0.01
Sanchez-Villagra2006	1.00	1.00	0.86	0.86	0.64	0.64	0.64	1.00	1.00	0.97	0.97	0.85	0.85	0.85
Sigurdsen2012	1.00	0.82	0.88	0.82	0.35	0.29	0.29	1.00	0.93	0.98	0.93	0.70	0.55	0.55
SkutchasGubin2012	0.94	0.22	0.22	0.22	0.00	0.00	0.00	0.99	0.47	0.47	0.47	0.00	0.00	0.00
SuesAverianov2009	0.95	0.86	0.82	0.77	0.32	0.32	0.32	0.99	0.98	0.96	0.96	0.72	0.72	0.72
SuesRiesz2008	1.00	0.89	0.89	0.89	0.33	0.33	0.33	1.00	0.95	0.95	0.95	0.66	0.66	0.66
VallinLaurin2004	0.98	0.84	0.84	0.84	0.41	0.41	0.41	0.99	0.96	0.96	0.96	0.76	0.76	0.76

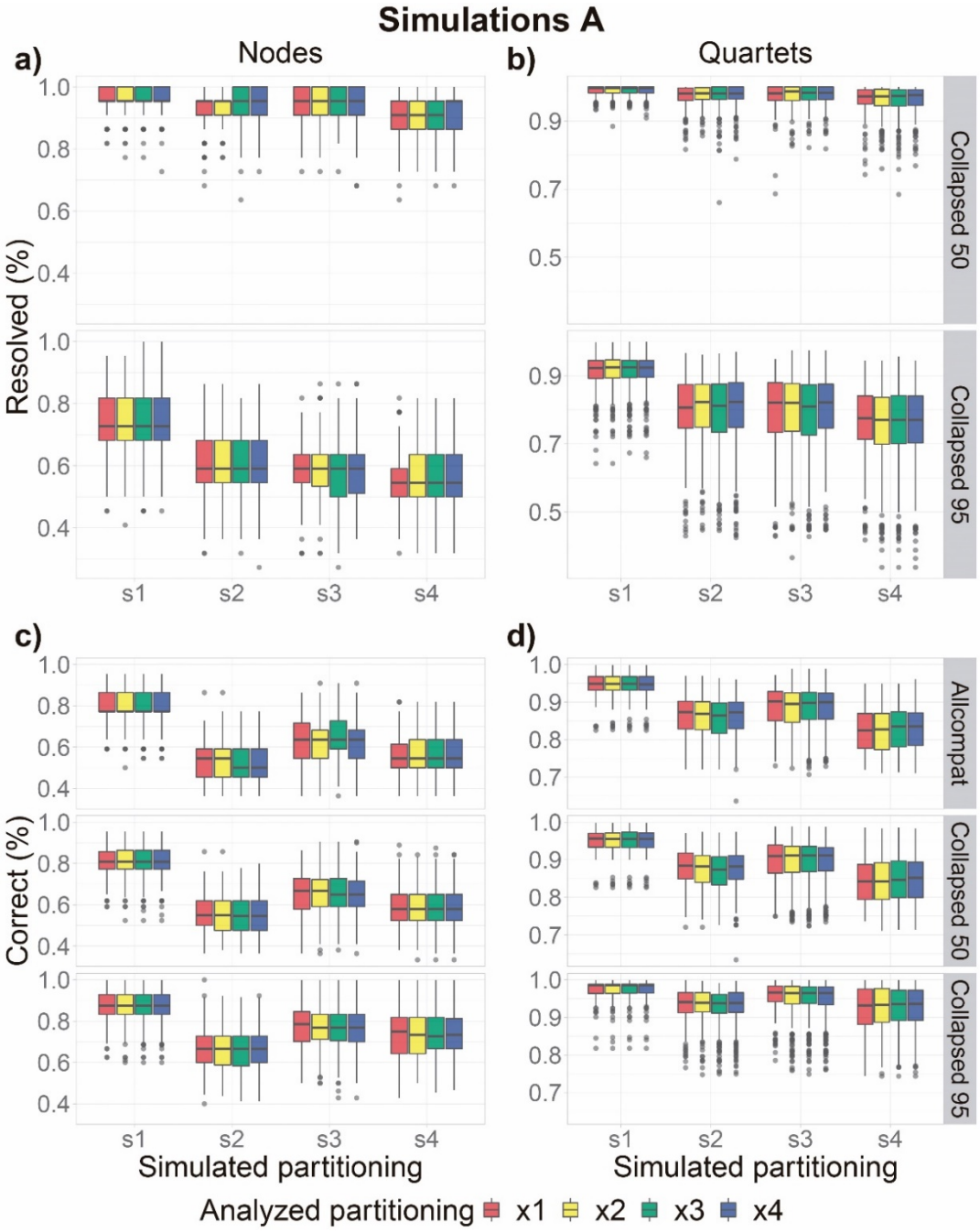

Figure 4. Topological precision and accuracy for the complete sample (all analyses that converged), evaluated comparing trees from simulated data (dataset A) to its respective reference trees. Boxplots summarize the metrics for all combinations of simulated (s) and analyzed (x) partitioning schemes. a) Proportion of resolved nodes. b) Proportion of resolved quartets. c) Proportion of correct nodes. d) Proportion of correct quartets. Allcompat consensus trees are fully resolved and were only evaluated for accuracy.

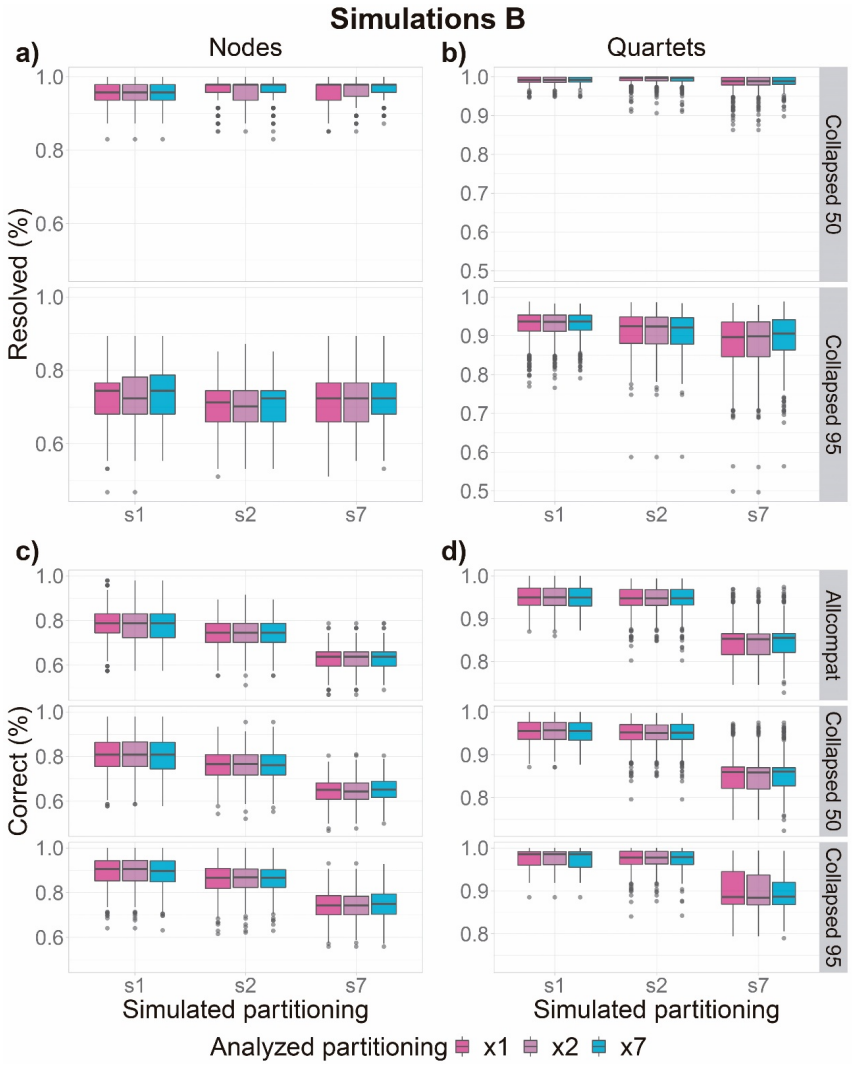

Figure 5. Topological precision and accuracy for the complete sample (all analyses that converged), evaluated comparing trees from simulated data (dataset B) to its respective reference trees. Boxplots summarize the metrics for all combinations of simulated (s) and analyzed (x) partitioning schemes. a) Proportion of resolved nodes. b) Proportion of resolved quartets. c) Proportion of correct nodes. d) Proportion of correct quartets. Allcompat consensus trees are fully resolved and were only evaluated for accuracy.

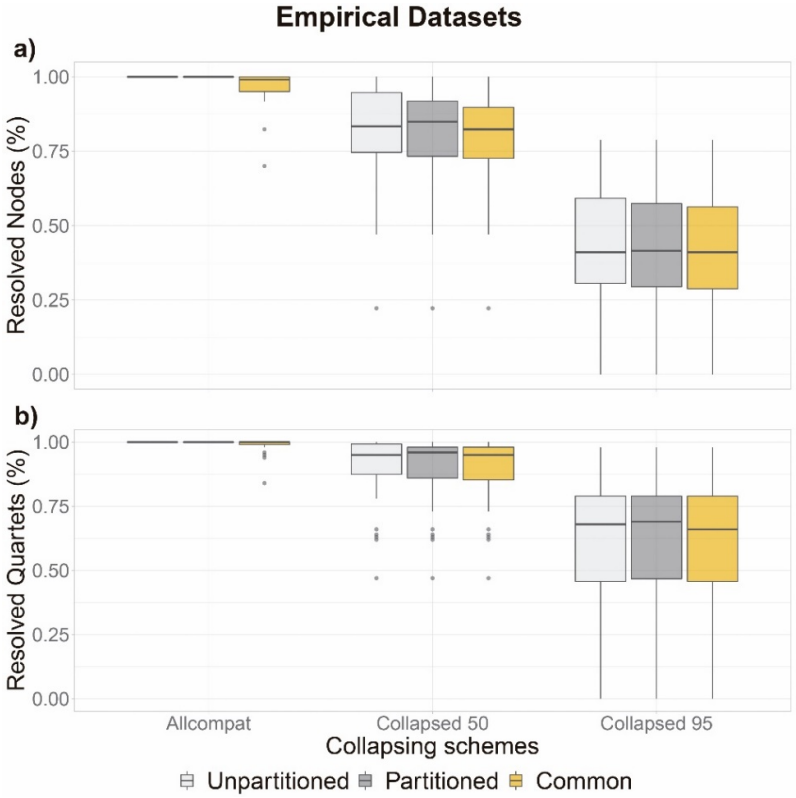

Figure 6. Topological precision and similarity for empirical datasets. Boxplots summarize the proportion of resolved nodes and quartets for alternative partitioning schemes and for those common for both schemes. a) Proportion of resolved nodes. b) Proportion of resolved quartets. Allcompat consensus trees are fully resolved and showed only for completeness.

1.4 DISCUSSION

1.4.1 The performance of anatomical partitioning

We presented here the first simulation study evaluating the performance of anatomical partitioning, as well as the first study of this kind for morphological partitioning in general. We also presented the first systematic evaluation of anatomical partitioning applied to several morphological datasets in Bayesian phylogenetics. Previous studies that evaluated more deeply the use of partitioned models for morphological datasets were limited to explore only one or a few empirical datasets and focused mainly (though not exclusively) in model selection using Bayes factor (Clarke and Middleton 2008; Tarasov and Génier 2015; Rosa et al. 2019; Porto et al. 2021). Model selection is undeniably an important step of statistical phylogenetic reconstructions and Bayes factor reliability as a criterion to select appropriate partitioning schemes for morphological and molecular datasets in a Bayesian framework is well established (Brown and Lemmon 2007; Clarke and Middleton 2008). Nonetheless, a systematic assessment

of the impact of partitioning in estimates of parameters of major interest in phylogenetic analyses – as topological precision and accuracy – was lacking for morphological data, despite being much better understood for molecular data (Brown and Lemmon 2007; Kainer and Lanfear 2015).

Some empirical studies have shown that anatomical partitions can be preferred to unpartitioned analysis using Bayes factor criterion (Clarke and Middleton 2008; Tarasov and Génier 2015; Rosa et al. 2019; Varela et al. 2019; Lucena and Almeida 2021; Porto et al. 2021) and this could be seen to be in disagreement with our findings here. Since we did not explore the performance of Bayes factor, which would require thousands of Stepping-Stone sampling analyses to obtain accurate estimates of marginal likelihoods (Fan et al. 2011; Xie et al. 2011), we are actually dealing with different aspects of the performance of partitioned models and there is not necessarily a disagreement between our results and those of previous empirical studies. Also, we should highlight that it is quite possible for a model to better fit the data with no impact in the topology, or to produce only a slightly different topology if compared to those obtained with an unpartitioned model.

Based on the results from simulated and empirical datasets, we found that topological precision and accuracy were not much affected by anatomical partitioning. Although some individual datasets showed slightly different topologies when analysed under alternative partition schemes, there were no clear differences when multiple replications were considered. Overall, our results are in agreement with previous findings (Tarasov and Génier 2015; Rosa et al. 2019), that reported minor variations in tree topology using anatomical partitioning of empirical datasets, despite considerable differences in estimates of marginal likelihoods among models.

Tree resolution and accuracy were slightly improved by anatomical partitioning only when data was simulated and analysed under schemes with a greater number of partitions, although even this observation was not consistent among all collapsing schemes and datasets used for simulate the data. Rosa et al. (2019) observed some improvement in resolution of the majority-rule consensus, but mainly when datasets were partitioned by the homoplasy criterion, instead of anatomy.

Studies of empirical datasets which separately analysed anatomical partitions, recovered topologies that were significantly different between those partitions, at least for part of the datasets analysed (Mounce et al. 2016; Sansom et al. 2016; Sansom and Wills 2017; Brinkworth et al. 2019; Li et al. 2020). We reanalysed 32 of those datasets, and showed that when we use combined (i.e. total-evidence, Kluge 1989) analysis, those topological differences are

accommodated in the same or very similar consensus topologies irrespective if we use or not anatomical partitions. Is relevant to know that different partitions, if analysed separately, would produce different topologies, but it does not necessary imply that this would affect topologies of partitioned models in combined analyses. In combined analyses, characters from different partitions interact and can reveal a hidden phylogenetic signal (Gatesy et al. 1999; Mounce et al. 2016), influencing the resulting topology.

1.4.2 Comparison with alternative morphological partition schemes

In light of the results obtained here, and those presented by Rosa et al. (2019), we can speculate that the partitioning of morphological datasets using anatomical subsets may not be the best approach to deal with heterogeneities in those datasets. Partitioning by homoplasy was shown to perform consistently better than anatomical partitioning, and methods that partition datasets using other proxies of evolutionary rates (e.g., as implemented in PartitionFinder2, Lanfear et al. 2016) also outperformed partitioning by anatomy for some datasets, although less consistently than when homoplasy is applied to segregate the characters in partitions (Rosa et al. 2019). It seems straightforward to understand why this is the case, since the main goal of partitioning is to model together characters that share similar evolutionary patterns and rates, with their parameters estimated partially or completely separated from those of other subsets of a given dataset. Anatomical partitions may not produce such well segregated subsets of characters since they are usually composed of characters of variable nature, like variations in shape, size, proportions, organization, presence or absence of disparate kinds structures (e.g., processes, foramina), whereas the degrees of homoplasy are good proxies for the evolutionary rates of the characters (Rosa et al. 2019).

Differently from the anatomical criterion, methods using a homoplasy or other rate-based metric are topology-dependent, and their sensibility to a specific topology and the optimality criterion used to obtain such tree remains poorly explored (but see Felsinger 2019). For example, studies exploring homoplasy partitions calculated the homoplasy indices with implied-weights parsimony with the parameter governing the strength of weighting (k) set to the default value. It would be informative to evaluate the impact of changing this parameter, since it can lead to different topologies, and hence, different allocation of characters in partitions. Also, it would be important to explore alternative homoplasy indices that can be calculated for equal-weights parsimony topologies, and even for those topologies obtained from maximum likelihood methods, as originally proposed for molecular data (Kjer and Honeycutt

2007). More studies evaluating the performance of those methods are necessary, including simulations and systematic evaluations for empirical datasets.

1.4.3 Comparison with molecular data partitioning

The use of partitioned models in molecular phylogenetics is a well-established practice (Brandley et al. 2005; Blair and Murphy 2011; Kainer and Lanfear 2015), and different criteria have been applied to define those data subsets, like genes across the genome, introns x exons, codon positions and stem x loop regions (Brandley et al. 2005; Kainer and Lanfear 2015).

Conceptually, partitioning constitutes the very same procedure for morphological and molecular data, and in both cases, the objective of this approach is to separately infer parameters for data subsets which were hypothesized to evolve – to some extent – independently from the other subsets of a given dataset (Clarke and Middleton 2008; Lanfear et al. 2012). In practice, on the other hand, quite distinct substitution models are often selected and applied to alternative molecular partitions (Lemmon and Moriarty 2004), whereas for morphology, all partitions usually have characters modelled by the Mk model. Although an alternative model which allows frequency asymmetry among states is available (Wright et al. 2016), it has been rarely used (e.g., Simões et al. 2020; May et al. 2021). This model requires a highly parametrized structure to achieve something similar to a F81 model of nucleotide substitution (Felsenstein 1981). This happens because states in morphological data (e.g., 0, 1, 2) have no comparable meaning across characters as nucleotides have for molecular data, and must have its parameters separately inferred (Wright et al. 2016). Those highly parametrized models pose difficulties to convergence and mixing of Markov chains, what may discourage their use (Simões et al. 2020). In that way, in practice, morphological data partitions differ in fewer and, probably, less consequential parameters, potentially explaining part of the disagreements between our results and those obtained evaluating molecular data partitioning.

Differently from what we observed here for morphology, for molecular datasets, alternative partitioning usually lead to moderate to substantial impacts in tree topology (Nylander et al. 2004; Kainer and Lanfear 2015), although in other study, also for molecular data, topological differences were more modest, and mostly associated to weakly supported nodes (Brandley et al. 2005). An improvement of resolution, which is directly related to the increasing on node supports in Bayesian inference, was reported for partitioned analyses of molecular datasets (e.g., Brandley et al. 2005), whereas some other studies reported a general decrease in node supports, but with greater differences observed only for clades presenting

lower support values (e.g., Powell et al. 2013). Systematic assessments of node supports for simulated molecular data using partitioned models and Bayesian inference indicates that mismodelling can increase the variance of estimated PPs, but without a trend for higher or lower values (Brown and Lemmon 2007). A similar pattern was also reported for Bootstrap values in maximum likelihood analyses using empirical datasets (Kainer and Lanfear 2015). Something similar may be happening here, what would explain why precision is not usually affected relative to alternative partitioning schemes.

We observed that both under and overpartitioning can have negligible impacts in tree precision and accuracy. This is quite different from the results observed for empirical molecular data, for which it was observed that the impacts of ignoring partitioning at all are problematic, and more severe than using incorrectly underpartitioned schemes (Kainer and Lanfear 2015). Studies using simulations showed a more continuous loss of precision on estimates of node support from correct to gradually under or overpartitioned schemes for molecular data (Brown and Lemmon 2007), while still indicating a clear pattern of loss of precision when wrong partitioning schemes were applied.

Despite those incongruences observed between the performance of data partitioning for morphological and molecular datasets, it may be hasty to assume that this can be fully explained as a difference about the nature of data used in analyses. Other morphological partitioning criterion, particularly by homoplasy (Rosa et al. 2019), may be more appropriated and achieve more comparable performances if compared to molecular partitioning, but this remains to be investigated. The relation of anatomical to homoplasy/rate-based methods of morphological partitioning may prove to be comparable, to some extent, to the relation of partitioning molecular data by genes versus by codon positions, with the latter being frequently preferable than the former (e.g., Li et al. 2008; Tao et al. 2013).

1.4.4 Limitations of simulations and future directions

Simulated data will always be limited in complexity if compared to empirical datasets. Nevertheless, simulation studies provide complementary insights to those obtained from the exploration of empirical data, and it is noteworthy that the general pattern which emerged from simulations was also recovered for empirical datasets, reinforcing our conclusions.

The list of possible variables to be explored as potential interacting factors in a simulation is extensive and practical limitations should be considered, in order to focus in what seem to be the more relevant parameters for the matter at hand (Barido-Sottani et al. 2020). Here we

adopted a method for data simulation that is directly informed by those parameters and properties of empirical datasets that seemed more relevant to simulate partitioned datasets. Nonetheless, the simulation of morphological data is a complex endeavour, and many important aspects were not considered directly here, as the hierarchical relationship of characters (Tarasov 2019, 2020) or correlations and the presence of serial homology (Billet and Bardin 2019), to cite a few examples. The adoption of only two empirical datasets as references to simulate the data is another limitation of our simulation, although results were, in general, consistent between the simulations originated from them. This is relevant, since they differ in many fundamental properties, like the number of taxa, numbers of partitions per partition scheme, partition sizes and missing data distribution. Future simulation studies may benefit from exploring properties from more datasets and variation in those parameters, among others.

1.5 CONCLUSIONS

Our results indicated that partitioning by anatomy has only minor effects in consensus topologies while conducting Bayesian phylogenetic analyses of morphological data. We should also bear in mind that a few empirical datasets have benefitted from anatomical partitioning, and other parameters like partition-specific evolutionary rates were not explored here, so it would not be reasonable to discourage the use of those models. That being considered, it is likely that other ways of partitioning the data may perform better than the anatomical criterion, as the use of homoplasy and rates to define partitions. Researchers should consider the costs – in time and resources – and the potential benefits of exploring alternative partition schemes in their empirical studies, and hopefully, this study can provide some guidance in this evaluation.

ACKNOWLEDGMENTS

This work was supported by Coordenação de Aperfeiçoamento de Pessoal de Nível Superior (CAPES-Finance Code 0001). Also, this work was partly supported by the grant #2018/09666-5, São Paulo Research Foundation (FAPESP) and by the Brazilian National Council for Scientific and Technological Development (CNPq grant 422019/2018-6). We would like to thank Cayo Dias for suggestions in an early version of the manuscript and Eduardo A. B. Almeida for making computational resources available for preliminary analyses of this study. We are also indebted to the reviewers, Brunno Rosa, Joseph Keating, Thomas Guillerme and two additional anonymous reviewers; and editors, Edward Susko, James Albert and Bryan

Carstens, for suggestions which contributed significantly to improve the manuscript. This research was developed with HPC resources made available by “Superintendência de Tecnologia da Informação” from “Universidade de São Paulo”.

REFERENCES

Barido-Sottani J., Saupe E.E., Smiley T.M., Soul L.C., Wright A.M., Warnock R.C.M. 2020. Seven rules for simulations in paleobiology. Paleobiology. 46:435–444.

Beaulieu J.M., O’Meara B.C., Oliver J., Boyko J. 2021. corHMM: Hidden Markov Models of Character Evolution. .

Beer D., Beer A. 2019. phylotate: Phylogenies with annotations. https://cran.r-project.org/package=phylotate.

Bhattacharyya A. 1946. On a measure of divergence between two multinomial populations. Sankhyā Indian J. Stat. 7:401–406.

Billet G., Bardin J. 2019. Serial homology and correlated characters in morphological phylogenetics: modeling the evolution of dental crests in placentals. Syst. Biol. 68:267–280.

Blair C., Murphy R.W. 2011. Recent trends in molecular phylogenetic analysis: Where to next? J. Hered. 102:130–138.

Brandley M.C., Schmitz A., Reeder T.W. 2005. Partitioned Bayesian analyses, partition choice, and the phylogenetic relationships of scincid lizards. Syst. Biol. 54:373–390.

Brazeau M.D., Giles S., Dearden R.P., Jerve A., Ariunchimeg Y.A., Zorig E., Sansom R., Guillerme T., Castiello M. 2020. Endochondral bone in an Early Devonian ‘placoderm’ from Mongolia. Nat. Ecol. Evol. 4:1477–1484.

Brinkworth A.R., Sansom R., Wills M.A. 2019. Phylogenetic incongruence and homoplasy in the appendages and bodies of arthropods: why broad character sampling is best. Zool. J. Linn. Soc. 187:100–116.

Brown J.M., Lemmon A.R. 2007. The importance of data partitioning and the utility of Bayes factors in Bayesian phylogenetics. Syst. Biol. 56:643–655.

Clarke J.A., Middleton K.M. 2008. Mosaicism, modules, and the evolution of birds: results from a Bayesian approach to the study of morphological evolution using discrete character data. Syst. Biol. 57:185–201.

Close R.A., Friedman M., Lloyd G.T., Benson R.B.J. 2015. Evidence for a mid-Jurassic adaptive radiation in mammals. Curr. Biol. 25:2137–2142.

Duchêne D.A., Tong K.J., Foster C.S.P., Duchêne S., Lanfear R., Ho S.Y.W. 2020. Linking branch lengths across sets of loci provides the highest statistical support for phylogenetic inference. Mol. Biol. Evol. 37:1202–1210.

Fan Y., Wu R., Chen M.-H., Kuo L., Lewis P.O. 2011. Choosing among partition models in Bayesian phylogenetics. Mol. Biol. Evol. 28:523–532.

Farris J.S. 1989. The retention index and the rescaled consistency index. Cladistics. 5:417–419.

Felsenstein J. 1981. Evolutionary trees from DNA sequences: A maximum likelihood approach. J. Mol. Evol. 17:368–376.

Felsinger S.M. 2019. Untangling the tree of life: Which partitioning strategies improve phylogenetic inference? Masters Thesis. Durham: Durham University.

Gatesy J., O'Grady P., Baker R.H. 1999. Corroboration among data sets in simultaneous analysis: hidden support for phylogenetic relationships among higher level artiodactyl taxa. Cladistics. 15:271–313.

Gavryushkina A., Heath T.A., Ksepka D.T., Stadler T., Welch D., Drummond A.J. 2017. Bayesian total-evidence dating reveals the recent crown radiation of penguins. Syst. Biol. 66:57–73.

Goloboff P.A., Arias J.S. 2019. Likelihood approximations of implied weights parsimony can be selected over the Mk model by the Akaike information criterion. Cladistics. 35:695–716.

Goloboff P.A., Torres Galvis A., Arias J.S. 2018. Parsimony and model-based phylogenetic methods for morphological data: comments on O'Reilly et al. Palaeontology. 61:625–630.

Guillerme T. 2018. dispRity: A modular R package for measuring disparity. Methods Ecol. Evol. 9:1755–1763.

Guillerme T., Cooper N. 2016. Effects of missing data on topological inference using a Total Evidence approach. Mol. Phylogenet. Evol. 94:146–158.

Harrison L.B., Larsson H.C.E. 2015. Among-character rate variation distributions in phylogenetic analysis of discrete morphological characters. Syst. Biol. 64:307–324.

Hasegawa M., Kishino H., Yano T. 1985. Dating of the human-ape splitting by a molecular clock of mitochondrial DNA. J. Mol. Evol. 22:160–174.

Heibl C. 2008. PHYLOCH: R language tree plotting tools and interfaces to diverse phylogenetic software packages. http://www.christophheibl.de/Rpackages.html.

Hillis D.M. 1995. Approaches for assessing phylogenetic accuracy. Syst. Biol. 44:3–16.

Huelsenbeck J.P., Ronquist F. 2001. MRBAYES: Bayesian inference of phylogenetic trees. Bioinformatics. 17:754–755.

Jukes T., Cantor C.R. 1969. Evolution of Protein Molecules. In: Munro H.., editor. Mammalian Protein Metabolism. New York: Academic Press. p. 21–132.

Kainer D., Lanfear R. 2015. The effects of partitioning on phylogenetic inference. Mol. Biol. Evol. 32:1611–1627.

Keating J.N., Sansom R.S., Sutton M.D., Knight C.G., Garwood R.J. 2020. Morphological phylogenetics evaluated using novel evolutionary simulations. Syst. Biol. 69:897–912.

King B., Qiao T., Lee M.S.Y., Zhu M., Long J.A. 2017. Bayesian morphological clock methods resurrect placoderm monophyly and reveal rapid early evolution in jawed vertebrates. Syst. Biol. 66:499–516.

Kjer K.M., Honeycutt R.L. 2007. Site specific rates of mitochondrial genomes and the phylogeny of Eutheria. BMC Evol. Biol. 7:1–9.

Kluge A.G. 1989. A concern for evidence and a phylogenetic hypothesis of relationships among Epicrates (Boidae, Serpentes). Syst. Zool. 38:7.

Kluge A.G., Farris J.S. 1969. Quantitative Phyletics and the Evolution of Anurans. Syst. Biol. 18:1–32.

Lanfear R., Calcott B., Ho S.Y.W., Guindon S. 2012. PartitionFinder: Combined selection of partitioning schemes and substitution models for phylogenetic analyses. Mol. Biol. Evol. 29:1695–1701.

Lanfear R., Frandsen P.B., Wright A.M., Senfeld T., Calcott B. 2016. PartitionFinder 2: new methods for selecting partitioned models of evolution for molecular and morphological phylogenetic analyses. Mol. Biol. Evol. 34:msw260.

Lee M.S.Y., Palci A. 2015. Morphological phylogenetics in the genomic age. Curr. Biol. 25:R922–R929.

Lemmon A.R., Moriarty E.C. 2004. The importance of proper model assumption in Bayesian phylogenetics. Syst. Biol. 53:265–277.

Lewis P.O. 2001. A likelihood approach to estimating phylogeny from discrete morphological character data. Syst. Biol. 50:913–925.

Li C., Lu G., Ortí G. 2008. Optimal data partitioning and a test case for ray-finned fishes (Actinopterygii) based on ten nuclear loci. Syst. Biol. 57:519–539.

Li Y., Ruta M., Wills M.A. 2020. Craniodental and postcranial characters of non-avian Dinosauria often imply different trees. Syst. Biol. 69:638–659.

Lucena D.A.A., Almeida E.A.B. 2021. Morphology and Bayesian tip-dating recover deep Cretaceous-age divergences among major chrysidid lineages (Hymenoptera: Chrysididae). Zool. J. Linn. Soc. 0:1–44.

Marshall D.C., Simon C., Buckley T.R. 2006. Accurate branch length estimation in partitioned Bayesian analyses requires accommodation of among-partition rate variation and attention to branch length priors. Syst. Biol. 55:993–1003.

May M.R., Contreras D.L., Sundue M.A., Nagalingum N.S., Looy C. V., Rothfels C.J. 2021. Inferring the total-evidence timescale of marattialean fern evolution in the face of model sensitivity. Syst. Biol. 0:1–22.

Mounce R.C.P., Sansom R., Wills M.A. 2016. Sampling diverse characters improves phylogenies: Craniodental and postcranial characters of vertebrates often imply different trees. Evolution (N. Y). 70:666–686.

Nylander J.A.A., Ronquist F., Huelsenbeck J.P., Nieves-Aldrey J.L. 2004. Bayesian phylogenetic analysis of combined data. Syst. Biol. 53:47–67.

O'Reilly J.E., Puttick M.N., Parry L., Tanner A.R., Tarver J.E., Fleming J., Pisani D., Donoghue P.C.J. 2016. Bayesian methods outperform parsimony but at the expense of precision in the estimation of phylogeny from discrete morphological data. Biol. Lett. 12:20160081.

O'Reilly J.E., Puttick M.N., Pisani D., Donoghue P.C.J. 2018. Probabilistic methods surpass parsimony when assessing clade support in phylogenetic analyses of discrete morphological data. Palaeontology. 61:105–118.

Plummer M., Best N., Cowles K., Vines K. 2006. CODA: convergence diagnosis and output analysis for MCMC. R News. 6:7–11.

Porto D.S., Almeida E.A.B., Pennell M.W. 2021. Investigating morphological complexes using informational dissonance and Bayes factors: A case study in corbiculate bees. Syst. Biol. 70:295–306.

Powell A.F.L.A., Barker F.K., Lanyon S.M. 2013. Empirical evaluation of partitioning schemes for phylogenetic analyses of mitogenomic data: An avian case study. Mol. Phylogenet. Evol. 66:69–79.

Prevosti F.J., Chemisquy M.A. 2009. The impact of missing data on real morphological phylogenies: influence of the number and distribution of missing entries. Cladistics. 26:326–339.

Puttick M.N., O'Reilly J.E., Pisani D., Donoghue P.C.J. 2019. Probabilistic methods outperform parsimony in the phylogenetic analysis of data simulated without a probabilistic model. Palaeontology. 62:1–17.

Puttick M.N., O'Reilly J.E., Tanner A.R., Fleming J.F., Clark J., Holloway L., Lozano-Fernandez J., Parry L.A., Tarver J.E., Pisani D., Donoghue P.C.J. 2017. Uncertain-tree: discriminating among competing approaches to the phylogenetic analysis of phenotype data. Proc. R. Soc. B Biol. Sci. 284:20162290.

R Core Team. 2021. R: A language and environment for statistical computing. https://www.r-project.org/.

Revelle W. 2020. psych: Procedures for psychological, psychometric, and personality research. https://cran.r-project.org/package=psych.

Robinson D.F., Foulds L.R. 1981. Comparison of phylogenetic trees. Math. Biosci. 53:131–147.

Ronquist F., Huelsenbeck J.P. 2003. MrBayes 3: Bayesian phylogenetic inference under mixed models. Bioinformatics. 19:1572–1574.

Rosa B.B., Melo G.A.R., Barbeitos M.S. 2019. Homoplasy-based partitioning outperforms alternatives in Bayesian analysis of discrete morphological data. Syst. Biol. 68:657–671.

Sansom R.S., Wills M.A. 2017. Differences between hard and soft phylogenetic data. Proc. R. Soc. B Biol. Sci. 284:20172150.

Sansom R.S., Wills M.A., Williams T. 2016. Dental data perform relatively poorly in reconstructing mammal phylogenies: Morphological partitions evaluated with molecular benchmarks. Syst. Biol. 66:813–822.

Simões T.R., Caldwell M.W., Pierce S.E. 2020. Sphenodontian phylogeny and the impact of model choice in Bayesian morphological clock estimates of divergence times and evolutionary rates. BMC Biol. 18:1–30.

Smith M. 2019a. Quartet: comparison of phylogenetic trees using quartet and split measures. doi:10.5281/zenodo.2536318.

Smith M.R. 2019b. Bayesian and parsimony approaches reconstruct informative trees from simulated morphological datasets. Biol. Lett. 15:20180632.

Tao W., Mayden R.L., He S. 2013. Remarkable phylogenetic resolution of the most complex clade of Cyprinidae (Teleostei: Cypriniformes): A proof of concept of homology assessment and partitioning sequence data integrated with mixed model Bayesian analyses. Mol. Phylogenet. Evol. 66:603–616.

Tarasov S. 2019. Integration of anatomy ontologies and Evo-Devo using structured Markov models suggests a new framework for modeling discrete phenotypic traits. Syst. Biol. 68:698–716.

Tarasov S. 2020. The invariant nature of a morphological character and character state: insights from gene regulatory networks. Syst. Biol. 69:392–400.

Tarasov S., Génier F. 2015. Innovative Bayesian and parsimony phylogeny of dung beetles (Coleoptera, Scarabaeidae, Scarabaeinae) enhanced by ontology-based partitioning of morphological characters. PLoS One. 10:e0116671.

Varela L., Tambusso P.S., McDonald H.G., Fariña R.A. 2019. Phylogeny, macroevolutionary trends and historical biogeography of sloths: insights from a Bayesian morphological clock analysis. Syst. Biol. 68:204–218.

Warren D.L., Geneva A.J., Lanfear R. 2017. RWTY (R We There Yet): An R package for examining convergence of Bayesian phylogenetic analyses. Mol. Biol. Evol. 34:1016–1020.

Wickham H. 2016. ggplot2: Elegant graphics for data analysis. https://ggplot2.tidyverse.org.

Wiens J.J. 2004. The role of morphological data in phylogeny reconstruction. Syst. Biol. 53:653–661.

Wright A.M. 2019. A systematist's guide to estimating bayesian phylogenies from morphological data. Insect Syst. Divers. 3:1–14.

Wright A.M., Hillis D.M. 2014. Bayesian analysis using a simple likelihood model outperforms parsimony for estimation of phylogeny from discrete morphological data. PLoS One. 9:e109210.

Wright A.M., Lloyd G.T. 2020. Bayesian analyses in phylogenetic palaeontology: interpreting the posterior sample. Palaeontology. 63:997–1006.

Wright A.M., Lloyd G.T., Hillis D.M. 2016. Modeling character change heterogeneity in phylogenetic analyses of morphology through the use of priors. Syst. Biol. 65:602–611.

Xie W., Lewis P.O., Fan Y., Kuo L., Chen M.-H. 2011. Improving marginal likelihood estimation for Bayesian phylogenetic model selection. Syst. Biol. 60:150–160.

SUPPLEMENTARY MATERIAL

Supplementary Figures

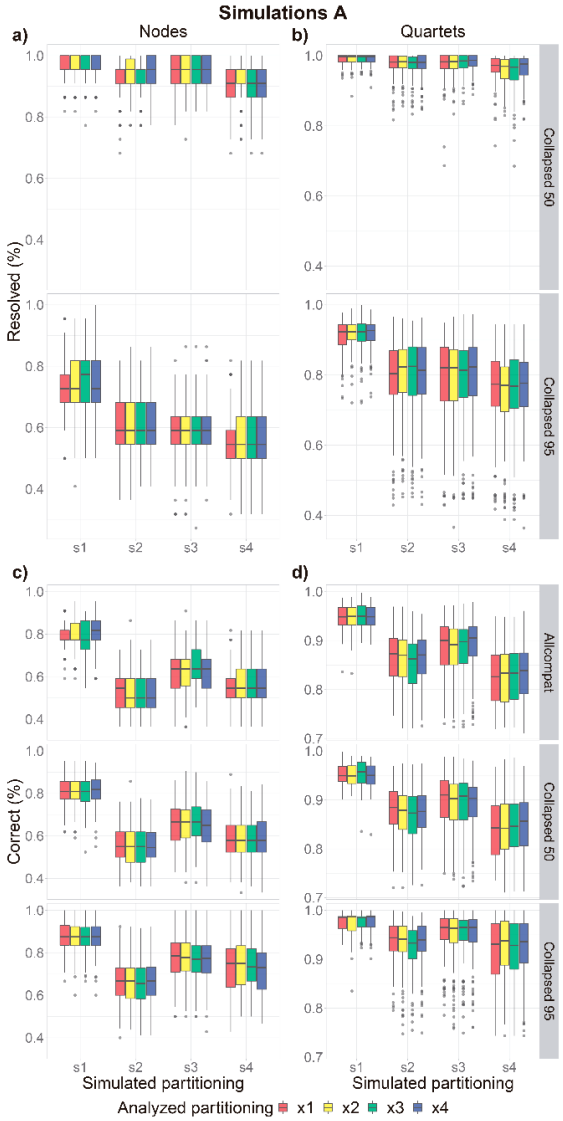

Supplementary Figure S1. Topological precision and accuracy for the reduced sample (150 trees), evaluated comparing trees from simulated data (dataset A) to its respective reference trees. Boxplots summarize the metrics for all combinations of simulated (s) and analyzed (x) partitioning schemes. a) Proportion of resolved nodes. b) Proportion of resolved quartets. c) Proportion of correct nodes. d) Proportion of correct quartets. Allcompat consensus trees are fully resolved and were only evaluated for accuracy.

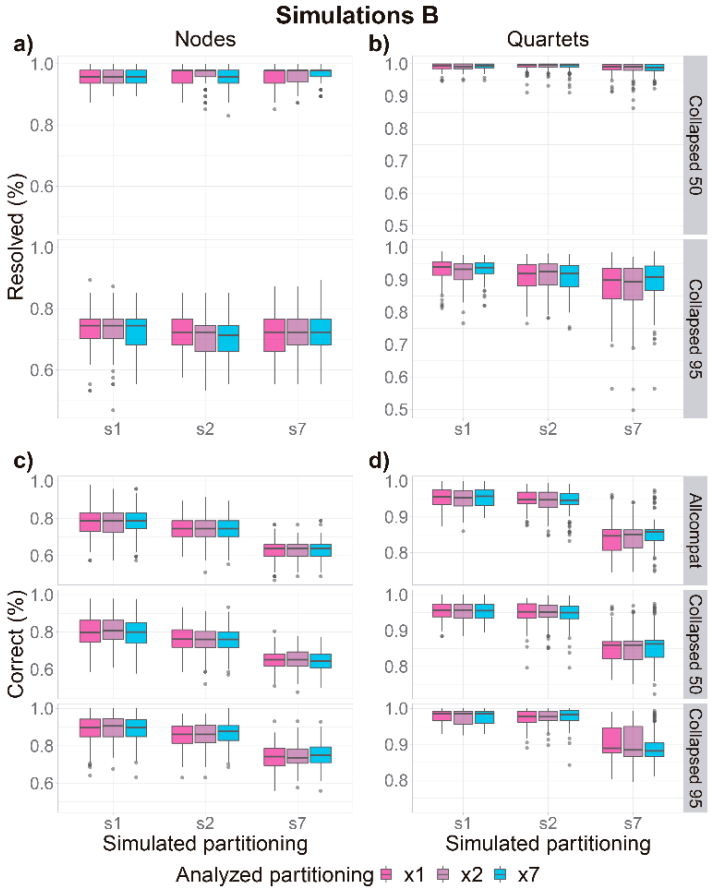

Supplementary Figure S2. Topological precision and accuracy for the reduced sample (150 trees), evaluated comparing trees from simulated data (dataset B) to its respective reference trees. Boxplots summarize the metrics for all combinations of simulated (s) and analyzed (x) partitioning schemes. a) Proportion of resolved nodes. b) Proportion of resolved quartets. c) Proportion of correct nodes. d) Proportion of correct quartets. Allcompat consensus trees are fully resolved and were only evaluated for accuracy.

Supplementary Files

Supplementary File S1. Density plots with per-partition character consistency indices (ci) and tables with per-partition ensemble consistency indices (CI) for the 500 datasets simulated using trees and properties from empirical dataset A. Consistency indices were calculated for partition (unlinked) and reference (linked) topologies.

Supplementary File S2. Density plots with per-partition character consistency indices (ci) and tables with per-partition ensemble consistency indices (CI) for the 500 datasets simulated using trees and properties from empirical dataset B. Consistency indices were calculated

for partition (unlinked) and reference (linked) topologies.

Supplementary File S3. Empirical datasets from Mounce et al. (2016) reanalyzed here (modified for Mounce et al. 2016, Supplementary Table 1).

Supplementary File S4. Summary statistics for metrics of precision and accuracy, calculated for trees from simulations using empirical dataset A, with groups of equal sample sizes (150 consensus trees).

Supplementary File S5. Summary statistics for metrics of precision and accuracy, calculated for trees from simulations using empirical dataset B, with groups of equal sample sizes (150 consensus trees).

Supplementary File S6. Bhattacharyya coefficients for metrics of precision and accuracy of alternative partitioning schemes. Data simulated using empirical dataset A, with groups of equal sample sizes (150 consensus trees).

Supplementary File S7. Bhattacharyya coefficients for metrics of precision and accuracy of alternative partitioning schemes. Data simulated using empirical dataset B, with groups of equal sample sizes (150 consensus trees).

Supplementary File S8. Summary statistics for metrics of precision and accuracy, calculated for trees from simulations using empirical dataset A, with groups of unequal sample sizes (trees from all analyses that converged).

Supplementary File S9. Summary statistics for metrics of precision and accuracy, calculated for trees from simulations using empirical dataset B, with groups of unequal sample sizes (trees from all analyses that converged).

Supplementary File S10. Bhattacharyya coefficients for metrics of precision and accuracy of alternative partitioning schemes. Data simulated using empirical dataset A, with groups of unequal sample sizes (trees from all analyses that converged).

Supplementary File S11. Bhattacharyya coefficients for metrics of precision and accuracy of alternative partitioning schemes. Data simulated using empirical dataset B, with groups of unequal sample sizes (trees from all analyses that converged).

Supplementary File S12. Summary statistics for metrics of precision and similarity, calculated for trees from 32 empirical datasets.

Supplementary File S13. Bhattacharyya coefficients for metrics of precision and similarity for two alternative partitioning schemes applied to 32 empirical datasets.

Supplementary Data

Supplementary Data S1. Input and output files from analyses of empirical datasets A and B.

1) Dataset A - empirical analyses
    a. Aves_1 to Aves_4U_4 - Folders with nexus input files and all standard MrBayes (Ronquist et al., 2012; Ronquist & Huelsenbeck, 2003) output files from Bayesian phylogenetic analyses of empirical Dataset A (Aves), with results for 13 trees from alternative partitioned models. Numbers at the beginning of folder names indicate the number of partitions and at the end, the partition identity. U for unliked topologies and branch lengths and L linked topologies and branch lengths. e.g. Aves_4U_3 – Four partitions, unlinked topologies and branch lengths, trees from partition 3;
    b. Convergence_check - plots summarizing convergence assessment using R package rwty (R Core Team, 2021; Warren et al., 2017) for all 13 trees and continuous parameters estimated for the partitioning scheme which produced this tree.
2) Dataset A - empirical analyses
    a. Bees_1 to Bees_7U_7 - Folders with nexus input files and all standard MrBayes output files from Bayesian phylogenetic analyses of empirical Dataset A (Aves), with results for 13 trees from alternative partitioned models. Numbers at the beginning of folder names indicate the number of partitions and at the end, the partition identity. U for unliked topologies and branch lengths and L linked topologies and branch lengths. e.g. Bees_7U_2 – Seven partitions, unlinked topologies and branch lengths, trees from partition 2;
    b. Convergence_check - plots summarizing convergence assessment using R package rwty (R Core Team, 2021; Warren et al., 2017) for all 13 trees and continuous parameters estimated for the partitioning scheme which produced this tree.

Supplementary Data S2. Input and output files from analyses of simulated data.

1) Dataset A - simulation analyses: input and output files from 8000 Bayesian analyses performed for datasets simulated using empirical dataset A.
    a. A_consensus_trees - All maximum compatibility consensus trees;
    b. A_convergence -
        i. All log files from those analyses;
        ii. Windows cmd script used to assess convergence using average standard deviation of split frequencies (ASDSF);
        iii. R script used to assess effective sample sizes (ESS);

iv. Outputs produced by the two above-mentioned scripts:
    1. fail_splits – text file reporting all analyses the failed to converge according to ASDSF;
    2. ESS_list – R .rds file with a list of ESS values, computed for all parameters and all runs of all analyses;
    3. Status_list - R .rds file with the convergence status assessed for all runs of all analyses;
    4. fail_all – text file reporting all analyses the failed to converge both for ASDSF and for ESS;
    5. summary_final – summary of analyses that fail to converge per group (i.e. unique combinations of simulated – s, and analyzed partitioning scheme - x).

c. A_inputs – Nexus input files for all Bayesian analyses of this dataset.

2) Dataset B - simulation analyses: input and output files from 4500 Bayesian analyses performed for datasets simulated using empirical dataset B.

a. B_consensus_trees - All maximum compatibility consensus trees.

b. B_convergence -

i. All log files from those analyses;

ii. Windows cmd script used to assess convergence using average standard deviation of split frequencies (ASDSF);

iii. R script used to assess effective sample sizes (ESS);

iv. Outputs produced by the two above-mentioned scripts:
    1. fail_splits – text file reporting all analyses the failed to converge according to ASDSF;
    2. ESS_list – R .rds file with a list of ESS values, computed for all parameters and all runs of all analyses;
    3. Status_list - R .rds file with the convergence status assessed for all runs of all analyses;
    4. fail_all – text file reporting all analyses the failed to converge both for ASDSF and for ESS;
    5. summary_final – summary of analyses that fail to converge per group (i.e. unique combinations of simulated – s, and analyzed partitioning scheme - x).

c. B_inputs – Nexus input files for all Bayesian analyses of this dataset.

Supplementary Data S3. Input and output files from analyses of 32 vertebrate empirical datasets from Mounce et al. (2016).

1) consensus_trees – maximum compatibility consensus trees;
2) inputs – input nexus files;
3) logs – logs from analyses;
4) p&t - .p and .t output files;
5) rwty – convergence assessment with rwyt R package.

Main Scripts

1) Simulation
    a. A_info_script – Script used to extract information from empirical dataset A;
    b. A_simulation_script – script used to simulate data using dataset A trees and properties;
    c. A_simulation_script – scrip used to summarize the results after Bayesian phylogenetic analyses of data simulated with dataset A trees and properties
    d. B_info_script – Script used to extract information from empirical dataset B;
    e. B_simulation_script – script used to simulate data using dataset B trees and properties;
    f. B_simulation_script – scrip used to summarize the results after Bayesian phylogenetic analyses of data simulated with dataset B trees and properties.
2) Empirical
    a. E_matrices_script – script used to create nexus input files for 32 vertebrate empirical datasets.
    b. E_results_script – script used to summarize results for 32 vertebrate empirical datasets.

Files available in:

https://drive.google.com/drive/folders/1G7CqfV68QU0nbd8NH3WsYRNcxfEP78Tx?usp=sharing

CHAPTER 2. Total-evidence phylogeny and divergence times of Vermilingua (Mammalia: Pilosa)

ABSTRACT

Vermilingua is a peculiar group of xenarthran placental mammals with well-established phylogenetic relationships based on morphological and molecular data, but until now, no combined analysis of those data types. Here we perform the first total-evidence phylogenetic analysis of Vermilingua and estimate divergence times for living and fossil anteaters with a tip-dating approach, using the Fossilized Birth-Death model in a Bayesian framework. Using combined analyses, we recovered as monophyletic the two families, Cyclopedidae and Myrmecophagidae, as in previous studies, although our revised morphological data alone do not support the monophyly of Cyclopedidae. We show how the combination of molecular and morphological data indirectly affects the position and support for fossil taxa even though molecular datasets do not contain direct information for them. The estimated divergence times of *Palaeomyrmidon* and *Protamandua* are much older than the ages of those fossils, reinforcing the scarcity of the vermilinguan fossil record. In addition, we obtained evidence that the extinct *Neotamandua* is an ancestor of the extant *Myrmecophaga*, not a sister taxon as in previous studies, that did not incorporate the possibility of anagenetic evolution between fossil and living taxa.

KEYWORDS: Anagenesis. Anteaters. Cyclopedidae. *Palaeomyrmidon*. *Protamandua. Neotamandua.*

2.1 INTRODUCTION

New World anteaters are peculiar xenarthran placental mammals that display a characteristic set of morphological adaptations in the skull, mandible, masticatory myology, digestive organs and forelimbs, related to an extreme adaptation to myrmecophagy (Owen 1856; Taylor 1978; Reiss 1997; Naples 1999; McDonald et al. 2008; Casali et al. 2017). They are included in the suborder Vermilingua and, together with sloths (suborder Folivora), compose the order Pilosa (McKenna and Bell 1997; Gardner 2008). Traditionally, Vermilingua includes four living species, the giant anteater (*Myrmecophaga tridactyla* Linnaeus 1758), the southern (*Tamandua tetradactyla* (Saussure 1860)) and northern (*Tamandua mexicana*

(Linnaeus 1758)) tamanduas in the family Myrmecophagidae, and the silky anteater (*Cyclopes didactylus* (Linnaeus 1758)) in the family Cyclopedidae (Wetzel 1982; Gardner 2008). Recently, Miranda et al. (2018) recognized six additional species of silky anteaters, elevating three subspecies to species status (*Cyclopes dorsalis* (Gray 1965); *Cyclopes catellus* Thomas 1928*; Cyclopes ida* Thomas 1900), and describing three entirely new species (*Cyclopes xinguensis* Miranda et al. 2018; *Cyclopes thomasi* Miranda et al. 2018; *Cyclopes rufus* Miranda et al. 2018), raising the number of species in the suborder to ten.

The fossil record of Vermilingua is scarce, particularly compared to its sister clade Folivora, which includes a rich array of extinct species (Gaudin and Branham 1998; McDonald et al. 2008; Gaudin and Croft 2015). The earliest record of Vermilingua is an undescribed specimen from the Early Miocene (Colhuehuapian) (Carlini et al. 1992), whereas the earliest putative sloth, *Pseudoglyptodon* Engelmann 1987, is from Late Eocene (McKenna et al. 2006), suggesting a long undocumented early evolutionary history of anteaters.

At least two uncontroversial fossil genera (and their respective species) of Vermilingua are recognized, *Protamandua rothi* Ameghino 1904 from the Early Miocene (Santacrucian), and *Palaeomyrmidon incomptus* Rovereto 1914 from the Late Miocene (Huayquerian) (Hirschfeld 1976; Gaudin and Branham 1998; McDonald et al. 2008). A third fossil genus, *Neotamandua* Rovereto 1914, is recognized by most authors (Hirschfeld 1976; Engelmann 1985; Gaudin and Branham 1998; McDonald et al. 2008), but its validity was questioned by Patterson et al. (1992), who suggested that it could be congeneric with *Myrmecophaga* Linnaeus 1758. Five species have been proposed for *Neotamandua*, *Neotamandua conspicua* Rovereto 1914, *Neotamandua australis* Scillato-Yané and Carlini 1998*, Neotamandua borealis* Hirschfeld 1976, *Neotamandua greslebini* Kraglievich 1940 and *Neotamandua magna* Ameghino 1919 (McDonald et al., 2008).

Previous studies explored the phylogenetic relationships among Vermilingua using morphological (Hirschfeld 1976; Engelmann 1985; Patterson et al. 1992; Gaudin and Branham 1998) or molecular data in a broader context (Delsuc et al. 2001, 2002; Möller-Krull et al. 2007; Gibb et al. 2016), and estimated divergence times with molecular data for living anteaters, also in broader contexts (Delsuc et al. 2004, 2012, 2018, 2019; Gibb et al. 2016; Coimbra et al. 2017; Miranda et al. 2018). None of the previous studies combined both kinds of data in a total-evidence analysis of the phylogeny and divergence times of Vermilingua, despite its potential advantages (Wortley and Scotland 2006; Ronquist et al. 2012). Consequently, divergence times for fossil Vermilingua remain unknown. Morphological characters for anteaters also were never analysed with Bayesian phylogenetic methods, which seem to produce more accurate

phylogenetic inferences for morphology than parsimony analysis (Wright and Hillis 2014; O'Reilly et al. 2016, 2018; Puttick et al. 2017, 2019, but see also Goloboff et al. 2018b, 2018a; Goloboff and Arias 2019)

Recent advances allowing the incorporation of fossil taxa as terminals, including their morphology and ages in the diversification process (Heath et al. 2014), gives us the opportunity to fill this gap in our knowledge about the evolutionary history of anteaters. They also allow us to explore, probabilistically, scenarios of anagenetic evolution among fossil and extant taxa (Gavryushkina et al. 2014), a possibility that was until recently precluded by limitations of the phylogenetic models available and restricted to a parsimony-based approach (Fisher 2008). Here, we investigate the phylogenetic relationships of Vermilingua with morphological, molecular and combined data. We produce a time-calibrated tree using tip-dating that includes all recognized genera of Vermilingua, and test the support of fossil species as ancestors of living lineages.

2.2 MATERIAL AND METHODS

2.2.1 Morphological phylogenetic analysis

We obtained morphological characters from skull, mandible and postcranial skeleton from Gaudin and Branham (1998). We re-evaluated all characters and observed new specimens, leading to the addition of new information and modifications to the definition of some characters and states, division and merging of other characters, and exclusion of a few others, resulting in 98 revised characters. Additionally, we included seven characters from Casali and Perini (2017) that capture variations in the hyoid apparatus, and 27 lingual characters from Casali (2016), resulting in a final dataset with 132 morphological characters (see Supplementary Files S1 and S2 for a detailed account of the characters, Supplementary File S3 for the list of observed specimens; and Supplementary File S4 for the morphological character matrix). Our ingroup is composed of *M. tridactyla, Neotamandua, T. mexicana, T. tetradactyla, Pr. rothi, Pa. incomptus, Cy. didactylus, Cy. xinguensis* and *Cy. rufus*, the last two of which have not been included in previous analyses of Vermilingua because of their recent recognition by Miranda et al. (2018). It is unclear how many valid species of *Neotamandua* exist because of its fragmentary nature and the incompatibility of the skeletal parts available for each species, which hampers a definitive taxonomic revision (McDonald et al. 2008). Following Gaudin and Branham (1998), we provisionally consider the genus monophyletic. Our coding for *Neotamandua* is based on specimens of two different species (*N. conspicua* and *N. borealis)*.

We studied *Neotamandua conspicua* directly, whereas we took data for *N. borealis* from literature sources (Hirschfeld 1976; Gaudin and Branham 1998). As outgroups, we included the sloths *Choloepus didactylus* and *Bradypus tridactylus*, and the armadillos *Dasypus novemcinctus* and *Euphractus sexcinctus*.

To model the morphological characters of Vermilingua in a Bayesian framework, we used the MK model (Lewis 2001). We tested three partitioning schemes: unpartitioned data, two partitions (cranium/hyoid/tongue x postcranium), and three partitions: (cranium x hyoid/tongue x postcranium). We also evaluated the option of ordering some multistate characters versus keeping all multistate characters unordered. Ordered characters included those ordered in Gaudin and Branham (1998), and we proposed an additional ordering of characters using the criteria of position, orientation and structural morphoclines (Gaudin and Branham 1998; Gaudin 2004) (see ordered characters in Supplementary File S1). We combined the partitioning and ordering schemes in all possible ways, leading to six alternative models. For all six, we considered the coding bias as variable and accounted for rate heterogeneity with a four-category gamma distribution. We evaluated the relative support for each model by estimating the marginal likelihood, using stepping-stone sampling (Fan et al. 2011; Xie et al. 2011) in MrBayes 3.2.7 (Huelsenbeck and Ronquist 2001; Ronquist and Huelsenbeck 2003). We performed the stepping-stone analysis in two runs of 50 steps for five million generations, sampling every 100 generations, with a step burn-in of 50%. Additionally, 500,000 generations (five steps) were performed and discarded as initial burn-in. We assessed convergence via an overlay plot for the initial burn-in phase, a joined plot of the 50 steps, and the precision of estimated values between runs. The marginal likelihood values were compared by Bayes factor (2*(lnBF)), using the decision rules of Kass and Raftery (1995) to evaluate relative model support.

We submitted the data and the best-fitting model to an MCMC analysis with two independent runs of two million generations and four chains each, sampling every 200 generations, unlinking gamma shapes and setting relative rates among partitions to variable. We discarded a burn-in phase consisting of 25% initial samples before summarizing parameters and trees. Convergence was evaluated with Average Standard Deviation of Split Frequencies (ASDSF, <0.01) in MrBayes, and inspecting trace plots and Effective Sample Size (ESS, >200) in Tracer 1.7 (Rambaut et al. 2018). Support was assessed with Posterior Probabilities (PP, Huelsenbeck et al. 2001) displayed in a majority-rule consensus tree (*allcompat*), visualized in FigTree v. 1.4.4 (http://tree.bio.ed.ac.uk/software/figtree/).

2.2.2 Molecular phylogenetic analysis

New nucleotide sequences for eight nuclear genes (ADORA3, ADRB2, ATP7A, BCHE, BDNF, BRCA1, CNR1 and RAG2) were generated for two recently-described species of the genus *Cyclopes*, *Cy. xinguensis* and *Cy. rufus*. DNA was extracted from muscle preserved in absolute alcohol using the phenol–chloroform method (Sambrook and Russel 2001), and the extracted DNA was re-suspended in 100 μL of TE buffer. DNA was quantified using Nanodrop (Thermo Fisher Scientific), and a working aliquot of ~20 ng/μL of genomic DNA was separated for use in the PCRs (polymerase chain reaction). We amplified all nuclear gene regions according to primers described in Meredith et al. (2011). The amplifications were done in a 20 μL PCR mix, including 0.3 units of Platinum Taq DNA Polymerase (Thermo Fisher Scientific), 2 mM $MgCl_2$, in 1x PCR buffer, 0.5 μM of each primer, 2.5 mM of dNTPs and about 20 ng of genomic DNA. PCR products were visualized in a 2% agarose gel. All PCRs that generated a single product were purified using polyethylene glycol 20% (PEG) precipitation following Santos Júnior et al. (2015). After purification, PCR products were sequenced using the ABI 3130x1 following the manufacturer's guidelines (Applied Biosystems). Two forward and two reverse reads per sample were grouped into a consensus sequence, and checked using Applied Biosystems' SeqScape ® v.2.6 software.

We obtained published sequences from Genbank for 16 nuclear (ADORA3, ADRA2B (A2AB), ADRB2, APOB, ATP7A, BCHE, BDNF, BRCA1, BRCA2, CNR1, ENAM, PLCB4, RAG1, RAG2, TTN, vWF) and two mitochondrial genes (COI and CYTB). We selected these genes to minimize the number of missing sequences for the extant ingroup and outgroup taxa included in our dataset. Access numbers and gene coverage are available in Supplementary File S5.

We aligned the sequences of each gene with MUSCLE (Edgar 2004) in AliView 1.18.1 (Larsson 2014) with minor manual editing, and concatenated them in FASconCAT-G (Kück and Longo 2014). The final alignment contains 23,204 nucleotide sites and is available as Supplementary File S6.

Best-fitting models of nucleotide substitution and best partition schemes were jointly estimated in PartitionFinder 2.1.1 (Lanfear et al. 2016), using the Bayesian Information Criterion (BIC), greedy algorithm, and considering branch lengths as linked. All but one of the sampled genes were coding sequences, and were submitted to PartitionFinder with separated codon positions to be evaluated as potential partitions. The pseudogene ENAM was submitted

as a single block. The best scheme, with partitions and their respective models, is available in Supplementary File S7.

We submitted the molecular dataset to a Bayesian phylogenetic analysis in MrBayes, unlinking all estimated parameters among partitions aside from branch lengths. Two runs with four chains were run for 50 million generations, sampling every 5000 generations. Burn-in, convergence and support follow the procedure described for the morphological analysis. This analysis and the total evidence analyses were conducted on CIPRES (Miller et al. 2010).

2.2.3 Total-evidence phylogenetic analysis and tip-dating divergence times' estimation

We combined the morphological and molecular datasets and performed non-clock and clock analyses in MrBayes, repeating all settings applied in previous analyses for morphology and nucleotide sequences, running two MCMC runs with four chains for 50 million generations, and sampling every 5000 generations. For non-clock analysis, we compared, via Bayes factor, an unconstrained analysis, which recovers Cyclopedidae as monophyletic, with an analysis in which Cyclopedidae is constrained to be non-monophyletic. Stepping-stone sampling was set for two parallel runs, with 100 million generations, sampling every 1000 generations, with an initial burn-in of 10 million generations, and all other settings the same as in the marginal likelihood estimations for morphological models.

For clock analyses, we compared a strict clock, an uncorrelated relaxed clock (IGR), and an autocorrelated relaxed clock (TK02), estimating the marginal likelihood for Bayes factor comparisons. We ran 300 million generations, sampling every 1000 generations, and 30 million generations of initial burn-in. All other configurations were the same as for previous stepping-stone analyses. We used the stratigraphic ranges of the fossil taxa as age priors for tip-dating, with a uniform distribution. Stratigraphic provenance was obtained from McDonald et al. (2008), with ages in millions of years ago (Ma) updated by information from Fossilworks (Paleobiology Database). The ages for the fossil species were Huayquerian (6.8-9.0 Ma) for *Pa. incomptus* and Santacrucian (16.3-17.5 Ma) for *Pr. rothi*; the Huayquerian-Colloncuran (6.8-15.5 Ma) range for *Neotamandua* covers the entire fossil record of the genus. The root was calibrated using a uniform distribution (58.5-71.6 Ma), with the minimum age representing the estimated age of the earliest xenarthran fossil, *Riostegotherium yanei* Oliveira and Bergqvist, 1998, used by Meredith et al. (2011) and Gibb et al. (2016), and the maximum representing the 95% HPD superior limit estimated by Gibb et al. (2016). To account for the diversification process, we used the Fossilized Birth-Death model (FBD, Heath et al. 2014). This model allows

us to estimate rates of speciation, extinction, and fossil sampling (preservation and recovery), and adds the possibility of testing whether fossil taxa are tips or ancestors (i.e., part of a lineage leading to an extant taxon, Gavryushkina et al. 2014). We utilized default priors for speciation, extinction, fossilization and sampling, and sampling probability was set to = 0.3 to approximately represent the proportion of living taxa sampled given the current diversity of Vermilingua and the outgroups (Gardner 2008; Abba et al. 2015; Feijó and Cordeiro-Estrela 2016; Feijó et al. 2018, 2019; Miranda et al. 2018). The clock rate prior was modelled by a gamma distribution with alpha=1 and beta=1. We constrained the topology for clock analyses to recover Cingulata and Pilosa in order to assure proper rooting (following the well-supported results of our combined non-clock analysis and previous studies), but the remaining relationships among taxa were jointly estimated with divergence times and all other model parameters.

We verified the proportion of trees in which each fossil taxon was recovered as a possible ancestor relative to the total number of trees (after burn-in, 15,000 trees), considering three levels of stringency: zero branch length, branch length < 0.001 and branch length < 0.01. The tabulation was performed using a Python script developed by Cayo Dias and is available upon request. We also inspected the 95% HPDs for clock branch lengths for fossil taxa to verify if they included zero or very short branch lengths, as defined above.

2.3 RESULTS

Based on the Bayes factor Criterion, the best-fitting model for the morphological data was the one in which all characters are unordered and partitioned in three blocks (cranium, hyoid/tongue, postcranium). Using the rules suggested by Kass and Raftery (1995), the support for this partitioning scheme is weak relative to the other two unordered schemes (BF: 3_part_unord/unpart_unord = 1.8, 3_part_unord/2_part_unord = 1.92), whereas its support relative to all ordered models is positive (BF: 2.08-5.86). Vermilingua was recovered as monophyletic (Fig. 1a), and strongly supported (PP = 1.0). The genus *Cyclopes* was recovered as the sister taxon of all other Vermilingua, followed by *Palaeomyrmidon;* the family Cyclopedidae was not recovered as a clade. The positions of these two taxa are poorly supported, however (PP = 0.54, and 0.57, respectively). The same can be said about the resolution among *Cyclopes* species. This effectively put *Palaeomyrmidon* and the three *Cyclopes* species in a polytomy with the clade that includes the remaining anteaters. This clade, (total group Myrmecophagidae) shows high support (PP = 0.95), and the same is true for the

clade excluding *Protamandua* (crown group Myrmecophagidae, PP = 1.0). The genus *Tamandua* received moderate support (PP = 0.86), whereas its sister clade, composed by *M. tridactyla* and *Neotamandua*, is strongly supported (PP = 0.98).

The molecular analysis recovered the same relationships between living taxa as observed in the morphological analysis, but for this dataset the relationships among *Cyclopes* and the remaining Vermilingua, and between the species of the genus *Cyclopes*, are fully resolved. *Cyclopes rufus* is recovered as the sister taxon of a clade composed of *Cy. xinguensis* and *Cy. didactylus.* All clades in the tree are strongly supported (PP = 1.0) in the molecular analysis (Fig. 1b).

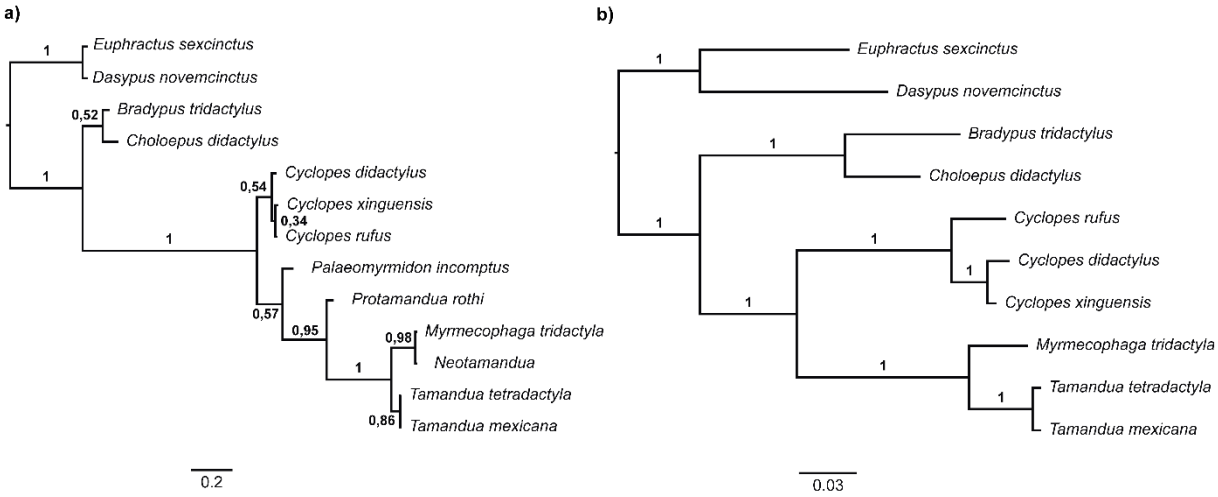

Figure 1. Bayesian majority-rule consensus depicting the phylogenetic relationships among Vermilingua: a) morphological b) and molecular datasets. Values at the branches indicate support from Posterior Probabilities.

Interestingly, combining the two datasets resulted in moderate support for a monophyletic Cyclopedidae (*Palaeomyrmidon* + *Cyclopes*) and *Cyclopes* (PP = 0.79 for both), whereas the clade composed of *Cy. didactylus* and *Cy. xinguensis* was strongly supported (PP = 0.95). Bayes factor analysis suggests positive support for the unconstrained analysis in which Cyclopedidae is monophyletic relative to the analysis constraining Cyclopedidae as non-monophyletic (BF = 4.74). In the combined analysis, the support for total group Myrmecophagidae decreased relative to the morphology-only analysis (PP = 0.76), but the crown group remained strongly supported (PP = 0.99). The genus *Tamandua* and the clade comprising *Myrmecophaga* + *Neotamandua* were both well supported (PP = 1.0) in the combined analysis (Fig. 2).

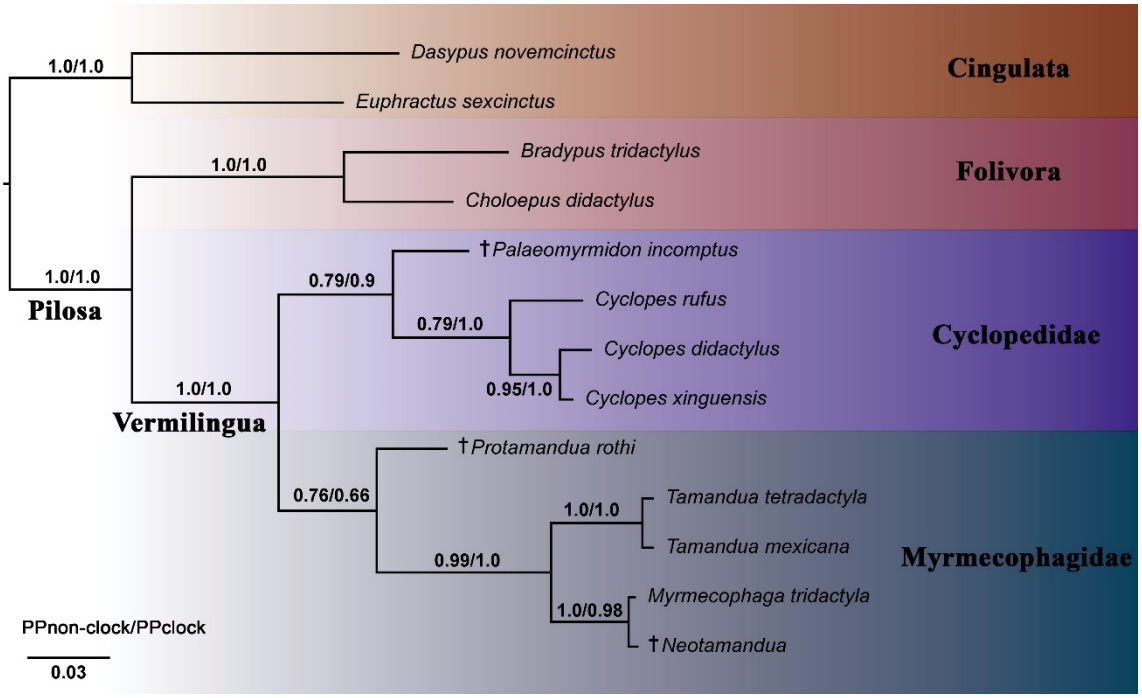

Figure 2. Bayesian majority-rule consensus for non-clock combined analysis for Vermilingua. Values at the branches indicate support from Posterior Probabilities for non-clock and clock analyses, respectively.

The Bayes factor analyses indicated that both relaxed clocks produced a better fit to the data than a strict clock (BF: IGR/STRICT = 81.76, TK02/STRICT = 88.74), with very strong support. The autocorrelated relaxed clock (TK02) was favoured in comparison with the uncorrelated relaxed clock (IGR) (BF: IGR/TK02 = 6.98), with strong support. The resulting topology was identical to the one obtained in the non-clock combined analysis (Fig. 3) and generally had high values of support, with all clades but three having posterior probabilities of 1.0. Cyclopedidae was moderately supported (PP = 0.90), whereas total group Myrmecophagidae had lowest support of all analyses (PP = 0.66). *Myrmecophaga* + *Neotamandua* received high support (PP = 0.98) (Fig. 2). The initial divergence of Vermilingua was estimated at approximately 43.7 Ma, whereas Cyclopedidae was predicted to have diverged around 23.9 Ma and Myrmecophagidae (total group) at 30.9 Ma. Table 1 summarizes all node estimates.

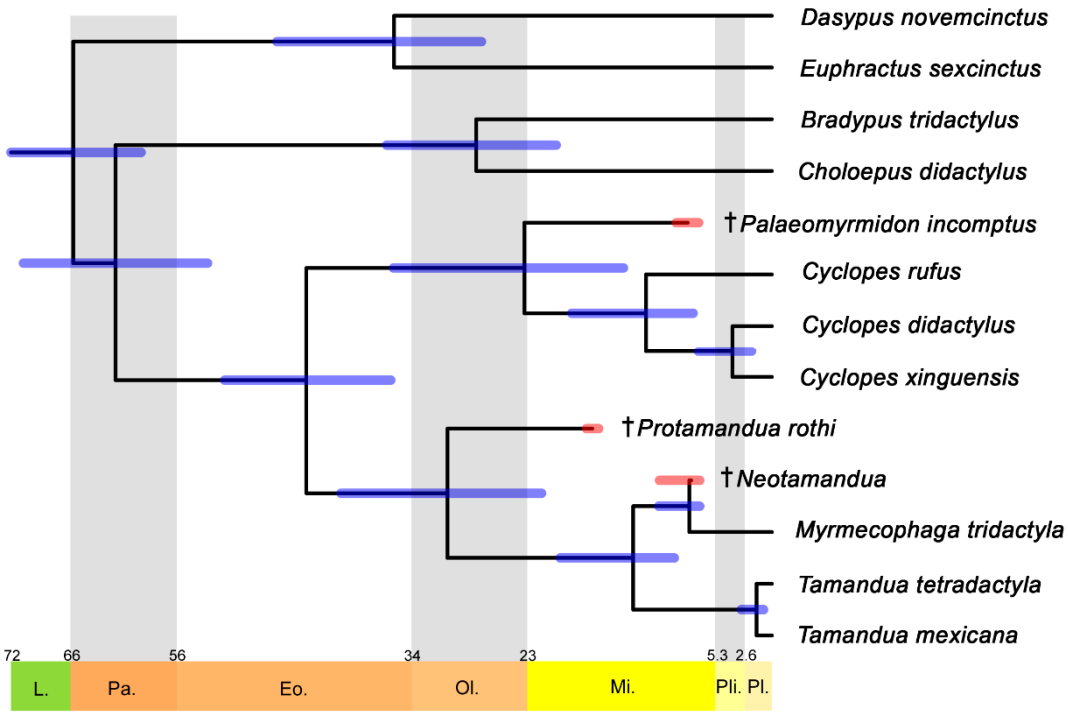

Figure 3. Bayesian chronogram of a majority-rule consensus obtained from combined autocorrelated clock analysis with FBD model. Node bars depicting the uncertainty (95% HPDs) of age estimates (blue in digital version), and tip bars showing the uncertainty for fossil tip ages (red in the digital version). Geological scale ages in millions of years ago. We used the package MCMCtreeR (Puttick 2019) in R (R Core Team 2019) to plot the uncertainty bars and geological scale. L. – Late Cretaceous, Pa. – Palaeocene, Eo. – Eocene, Ol. – Oligocene, Mi. – Miocene, Pli. – Pliocene and Pl. – Pleistocene.

Table 1. Divergence times of Vermilingua.

Taxon	Mean age	95% HPDs
Xenarthra	65.5	59.3-71.6
Cingulata	36.3	27.3-46.6
Pilosa	61.6	53.1-70.4
Folivora	28.1	20.3-36.2
Vermilingua	43.7	35.9-51.5
Cyclopedidae	23.9	14.0-35.6
Cyclopes	12.4	7.4-18.8
Cy. didactylus/Cy. xinguensis	4.0	1.9-6.9
Myrmecophagidae (total)	30.9	21.7-40.5
Myrmecophagidae (crown)	13.6	9.2-19.9
Myrmecophaga/Neotamandua	8.1	6.8-10.6
Tamandua	1.6	0.8-2.9

Summary of mean ages and 95% Highest Posterior Densities (HPDs) estimated with an autocorrelated clock and FBD diversification model for combined dataset for Vermilingua and outgroups. Ages in millions of years ago.

In our clock analysis with the Fossilized Birth-Death model, we observed very short to zero branch lengths leading to *Neotamandua*, indicating that this taxon could be an ancestor of *M. tridactyla* instead of its sister taxon (F. Ronquist & C. Zhang, personal communication, May 15, 2019). Counting the frequency of zero or very short branch lengths for each fossil across the trees obtained in MCMC sampling lead us to recover a very high proportion of trees in which *Neotamandua* was strongly supported as an ancestor, whereas this was not the case for the other two fossil vermilinguans included in the analysis. Mean and median values for branch lengths reinforced this pattern. Also, the rare short branches for *Palaeomyrmidon* fell outside the 95% HPD of clock branch length. The *Protamandua* branch length 95% HPD included some branches <0.01, but none shorter than 0.001, whereas the confidence interval for *Neotamandua* includes very short (<0.001) and zero branch lengths (Table 2).

Table 2. Branch lengths of fossil Vermilingua in clock analysis.

TAXON	BL = 0	BL < 0.001	BL < 0.01	MEAN	MEDIAN	95% HPDs
Palaeomyrmidon	0.01	0.01	0.01	0.049	0.044	0.012-0.096
Protamandua	0.01	0.01	0.02	0.041	0.038	0.007-0.084
Neotamandua	0.55	0.84	0.99	0.001	0.000	0.000-0.003

Frequencies (percentage) of zero and short branch lengths (BL), mean, median, and 95% HPDs for the branches of three fossil Vermilingua, according to the autocorrelated clock analysis using FBD model, counted across a set of 15,000 trees sampled from two MCMC runs.

2.4 DISCUSSION

The phylogenetic relationships recovered using the combined dataset are congruent with previous analyses using exclusively morphological (Engelmann 1985; Patterson et al. 1992; Gaudin and Branham 1998) or molecular data (Delsuc et al. 2001, 2002; Möller-Krull et al. 2007; Gibb et al. 2016), reflecting a general consistency between the two data types for Vermilingua. Nevertheless, the fact that *Cyclopes* and *Palaemyrmidon* did not form a monophyletic group in the analysis of the revised morphological dataset indicates some instability in the position of these taxa when considering solely morphological characters, something already observed by Gaudin and Branham (1998). Although Gaudin and Branham (1998) recovered a monophyletic Cyclopedidae with their preferred scheme of weighting and ordering, they reported that alternative manipulations of those variables returned a tree in which Cyclopedidae is paraphyletic, with *Palaeomyrmidon* diverging earlier and *Cyclopes* forming the sister group of Myrmecophagidae (Gaudin and Branham 1998). Gaudin (1993) also recovered a paraphyletic Cyclopedidae, but with *Cyclopes* diverging first (cited in Gaudin & Branham, 1998). We used Bayes factor to evaluate models including different character ordering and partitioning schemes, and our best-fitting model treated multistate characters as unordered. The topology remained the same when the characters were ordered, however.

The inclusion of molecular data had an important impact in this region of the tree, leading to a moderately supported Cyclopedidae. Bayes factor analysis offers further support for this topology over alternatives in which Cyclopedidae is constrained to be non-monophyletic. Molecular data being conclusive over the resolution among *Cyclopes* species, as opposed to the lower supported relationships recovered by morphology alone, probably also lead to this emergent support for Cyclopedidae. Instances of this kind of hidden support are not uncommon and typically manifest only when independent datasets are combined, underscoring the potential value of combining data from different sources even if they seem to agree when analysed separately (Barrett et al. 1991; Gatesy et al. 1999; de Queiroz and Gatesy 2007). In contrast, the strong support for *Protamandua* as the sister of the remaining Myrmecophagidae in the morphology-only analysis decreased with the addition of molecular data, suggesting that the support for this taxon is also affected by the resolution in Cyclopedidae. In both morphological and total-evidence analyses, *Neotamandua* is consistently recovered as closely related to *Myrmecophaga.*

The inclusion of fossil taxa as part of the diversification process, along with the temporal information they provide, is a significant advantage of tip-dating methods because it minimizes

the need to define arbitrary prior distributions for node times, as required by node-dating methods (Ronquist et al. 2012; Zhang et al. 2016). Some studies have pointed out that divergence time estimates from tip-dating can be much older than estimates based on node-dates or a combination of tip-dates and node calibrations, particularly near the root of the tree (Wood et al. 2013; Beck and Lee 2014; Arcila et al. 2015; O'Reilly et al. 2015; Ronquist et al. 2016). Those older estimates are probably artefacts resulting from large morphological datasets, in which many unlikely events like convergences would take more time to occur (Ronquist et al. 2016), but this is not the case for the moderate size morphological matrix used in this study. Applying a single node calibration at the root of the tree along with tip-dates returned highly congruent estimates with those observed in previous node-dating analyses for living taxa (Delsuc et al. 2004, 2012, 2018, 2019; Gibb et al. 2016; Coimbra et al. 2017; Miranda et al. 2018).

This is the first study to estimate divergence times for fossil Vermilingua. The divergence between *Palaeomyrmidon* and *Cyclopes* is most likely close to the Late Oligocene/Early Miocene boundary, whereas *Protamandua* is predicted to have diverged from crown Myrmecophagidae in the Early Oligocene. These mean estimates indicate that the scant fossil material known for those taxa is much younger than the origin of the clades in which they are positioned, providing further evidence that the fossil record of Vermilingua is very poor (McDonald et al. 2008). The earliest record for Vermilingua, from the Early Miocene (Carlini et al. 1992), is very incomplete and has not yet been formally described, hampering the evaluation of its relationship to other anteaters.

Although caution is required because of the width of the 95% HPDs for divergence dates in those two nodes, taking the mean as the best estimate shows that there is no support for the proposal of Hirschfeld (1976), that *Protamandua* could have been the ancestor of all other Mymecophagidae. On the other hand, we confirmed her hypothesis that the divergence between *Cyclopes* and *Palaeomyrmidon* was considerably older than the age of the later. The status of *Palaemyrmidon* and *Protamandua* as sister to the other taxa is strongly corroborated by their long branches and the low frequency (1-2%) in which they present a small or zero branch length.

The situation for *Neotamandua* is somewhat different, however. This genus is known from a slightly better sample of fossil material, and it is predicted to have diverged from its sister taxon in Late Miocene, much more recently than the other fossil Vermilingua. The results of our clock analysis, including the frequency of times in which *Neotamandua* was recovered as ancestor of *M. tridactyla* (instead of its sister taxon), suggests that *Neotamandua* is most likely part of an anagenetic line of descent leading to *Myrmecophaga*. Patterson et al. (1992)

considered *N. conspicua* congeneric with *M. tridactyla*, whereas Hirschfeld (1976), Engelmann (1985), and Gaudin and Branham (1998) proposed that they belong to different genera. Given our results, the status of *Neotamandua* relative to *Myrmecophaga* seems more akin to that of a chronospecies (Mayden 1997; Silvestro et al. 2018), particularly considering the great morphological similarity of the taxa. Gaudin and Branham (1998) found a single unambiguous autapomorphy for *Neotamandua*, the horizontal inclination of the glenoid, which is posterodorsally inclined in *Myrmecophaga*. However, after the inspection of more specimens, we observed that this character is actually polymorphic for *Myrmecophaga,* leaving only size as a distinctive difference between it and *Neotamandua*. Nevertheless, we advocate for the maintenance of *Neotamandua* as a distinct genus, recognizing that in cases of continuous anagenetic changes, any taxonomic division is arbitrary and nomenclatural change unwarranted.

Hirschfeld (1976) hypothesized that *N. borealis* would be close to the ancestor of *Tamandua* and *Myrmecophaga*, but closer to the *Myrmecophaga* lineage. Considering its age (Laventan) and our results, this scenario is quite plausible. Also in agreement with the divergence times recovered in this study, *N. australis*, from the Colloncuran, would be even closer to the split between *Neotamandua*/*Myrmecophaga* and *Tamandua*, provided it actually is part of *Neotamandua*, which is difficult to determine due to the incompleteness of the material (Scillato-Yané and Carlini 1998; McDonald et al. 2008).

Assuming that all records of *Neotamandua* belong to the same lineage, they provide evidence for the presence of this taxon from the Middle Miocene (Colloncuran) to the Late Miocene (Huayquerian), the period in which *Neotamandua* would have given rise to *Myrmecophaga* according to our estimates. This would also be consistent with the hypothesis that *Myrmecophaga caroloameghinoi* (formerly *Nunezia carloamegnoi*; McKenna and Bell 1997), is the earliest record for *Myrmecophaga*. This taxon dates from the Monthermosan or the Huayquerian SALMA if we accept the synonym of *N. magna* with *Nunezia* proposed by Kraglievich (1934) (McDonald et al. 2008; Gaudin et al. 2018). The earliest record for *M. tridactyla* is more recent, from NALMA Irvingtonian stage (roughly equivalent to SALMA Uquian period, McDonald et al., 2008). If correct, this picture suggests a relatively continuous record for the lineages leading from *Neotamandua* to *Myrmecophaga.* However, it is not possible to establish how many and which of the proposed species for each genus are related by cladogenesis or anagenesis until more material becomes available and is properly included in a phylogenetic analysis.

Of the five species currently recognized for *Neotamandua* (McDonald et al. 2008), only two, *N. conspicua* and *N. borealis*, comprised the basis for our morphological dataset because the other species are very incomplete (*N. australis* and *N. magna*) or the material is missing or mistakenly identified (*N. greslebini*). The use of a composite taxon may also be a factor that could contribute to weaken the conclusions reached here. New in depth studies of the anatomy and relationships of *Neotamandua* are pivotal for the understanding of the evolution of the *Myrmecophaga* lineage.

We also have to be aware of the current limitations of the FBD model, which assumes that speciation, extinction and fossilization are constant through time (Heath et al. 2014), a premise that probably is at least partially violated for real datasets. Further studies are needed to corroborate the results presented here before an ancestor-descendant relationship between *Neotamadua* and *Mymecophaga* can be conclusively confirmed.

2.5 CONCLUSIONS

The combination of different sources of data for phylogenetic and dating analyses is a valuable approach to study the evolutionary history of extinct and extant taxa, even when separate analyses of those kinds of data are congruent. The use of more realistic models allowed us to empirically evaluate evolutionary processes that were long considered only theoretically. The models also produced novel insights even for a relatively well-studied group such as Vermilingua. Inclusion of fossils as tips in the analyses allowed us to incorporate a greater amount of information about those taxa, make divergence time estimates for fossil anteaters, and provide a plausible scenario for anagenetic evolution between the extinct genus *Neotamandua* and the extant *Myrmecophaga*. Future advances in models for morphological and temporal evolution offer the potential to integrate other evolutionary processes into our inferences, while improvements in our knowledge of the fossil record for Vermilingua can further increase our understanding of the evolution of this peculiar group of placental mammals.

ACKNOWLEDGMENTS

We would like to acknowledge Martin Ezcurra and Laura Chornogubsky (Museo Argentino de Ciencias Naturales - MACN), and Claudia Guimarães Costa (Pontifícia Universidade de Minas Gerais - PUC-MG) for kindly allowing us to study specimens under their care, Rafaela Missagia (Universidade Federal de Minas Gerais - UFMG), Leonardo Cotts

(Universidade Federal do Rio de Janeiro - UFRJ) and William Simpson (Field Museum of Natural History - FMNH) for photographing and sharing photos of vermilinguans, Fredrik Ronquist and Chi Zhang for help interpreting zero tip branch lengths in the implementation of the FBD model in MrBayes, Cayo Dias (UFMG) for writing and sharing the Phyton script used to count branch lengths in MrBayes outputs, and Mark Puttick for assistance in using the MCMCtreeR package. Rafaela Missagia also provided useful comments on an early version of the manuscript. Kenneth Angielczyk (FMNH) kindly helped us to revise a late version of the manuscript, providing many suggestions, which helped to improve our English and the manuscript content as a whole. We are also indebted to two anonymous reviewers and the editor who provided useful comments that helped us to improve the manuscript. We thank Coordenação de Aperfeiçoamento de Pessoal de Nível Superior (CAPES) for financial support via a monthly scholarship (Finance Code 0001) and Programa de Apoio à Pós-Graduação (PROAP). We also thank FAPEMIG, Fundação O Boticário and CNPq for research grants for this study.

REFERENCES

Abba A.M., Cassini G.H., Valverde G., Tilak M.-K., Vizcaíno S.F., Superina M., Delsuc F. 2015. Systematics of hairy armadillos and the taxonomic status of the Andean hairy armadillo (*Chaetophractus nationi*). J. Mammal. 96:673–689.

Arcila D., Pyron A.R., Tyler J.C., Ortí G., Betancur-R. R. 2015. An evaluation of fossil tip-dating versus node-age calibrations in tetraodontiform fishes (Teleostei: Percomorphaceae). Mol. Phylogenet. Evol. 82:131–145.

Barrett M., Donoghue M.J., Sober E. 1991. Against Consensus. Syst. Biol. 40:486–493.

Beck R.M.D., Lee M.S.Y. 2014. Ancient dates or accelerated rates? Morphological clocks and the antiquity of placental mammals. Proc. R. Soc. B Biol. Sci. 281:1–10.

Carlini A.A., Scillato-Yané G.J., Vizcaíno S.F., Dozo M.T. 1992. Un singular Myrmecophagidae (Xenarthra, Vermilingua) de edad Colhuehuapense (Oligoceno tardío, Mioceno temprano) de Patagonia, Argentina. Ameghiniana. 29:176.

Casali D.M. 2016. Evolução do aparelho hiolingual em Xenarthra (Mammalia: Eutheria) e considerações filogenéticas (Unpublished master's thesis).

Casali D.M., Martins-Santos E., Santos A.L.Q., Miranda F.R., Mahecha G.A.B., Perini F.A. 2017. Morphology of the tongue of Vermilingua (Xenarthra: Pilosa) and evolutionary considerations. J. Morphol. 278:1380–1399.

Casali D.M., Perini F.A. 2017. The evolution of hyoid apparatus in Xenarthra (Mammalia: Eutheria). Hist. Biol. 29:777–788.

Coimbra R.T.F., Miranda F.R., Lara C.C., Schetino M.A.A., Santos F.R. dos. 2017. Phylogeographic history of South American populations of the silky anteater *Cyclopes didactylus* (Pilosa: Cyclopedidae). Genet. Mol. Biol. 40:40–49.

Delsuc F., Ctzeflis F.M., Stanhope M.J., Douzery E.J.P. 2001. The evolution of armadillos, anteaters and sloths depicted by nuclear and mitochondrial phylogenies: implications for the status of the enigmatic fossil *Eurotamandua*. Proc. R. Soc. London. Ser. B Biol. Sci. 268:1605–1615.

Delsuc F., Kuch M., Gibb G.C., Hughes J., Szpak P., Southon J., Enk J., Duggan A.T., Poinar H.N. 2018. Resolving the phylogenetic position of Darwin's extinct ground sloth (*Mylodon darwinii*) using mitogenomic and nuclear exon data. Proc. R. Soc. B Biol. Sci. 285:1–10.

Delsuc F., Kuch M., Gibb G.C., Karpinski E., Hackenberger D., Szpak P., Martínez J.G., Mead J.I., McDonald H.G., MacPhee R.D.E., Billet G., Hautier L., Poinar H.N. 2019. Ancient mitogenomes reveal the evolutionary history and biogeography of sloths. Curr. Biol. 29:2031-2042.e6.

Delsuc F., Scally M., Madsen O., Stanhope M.J., de Jong W.W., Catzeflis F.M., Springer M.S., Douzery E.J.P. 2002. Molecular phylogeny of living xenarthrans and the impact of character and taxon sampling on the placental tree rooting. Mol. Biol. Evol. 19:1656–1671.

Delsuc F., Superina M., Tilak M.-K., Douzery E.J.P., Hassanin A. 2012. Molecular phylogenetics unveils the ancient evolutionary origins of the enigmatic fairy armadillos. Mol. Phylogenet. Evol. 62:673–680.

Delsuc F., Vizcaíno S.F., Douzery E.J.P. 2004. Influence of Tertiary paleoenvironmental changes on the diversification of South American mammals: a relaxed molecular clock study within xenarthrans. BMC Evol. Biol. 4:1–13.

Edgar R.C. 2004. MUSCLE: Multiple sequence alignment with high accuracy and high throughput. Nucleic Acids Res. 32:1792–1797.

Engelmann G.F. 1985. The phylogeny of the Xenarthra. In: Montgomery G.G., editor. The evolution and ecology of armadillos, sloths and vermilinguas. Washington: Smithsonian Institution Press. p. 51–64.

Fan Y., Wu R., Chen M.-H., Kuo L., Lewis P.O. 2011. Choosing among partition models in Bayesian phylogenetics. Mol. Biol. Evol. 28:523–532.

Feijó A., Cordeiro-Estrela P. 2016. Taxonomic revision of the *Dasypus kappleri* complex, with revalidations of *Dasypus pastasae* (Thomas, 1901) and *Dasypus beniensis* Lönnberg, 1942 (Cingulata, Dasypodidae). Zootaxa. 4170:271–297.

Feijó A., Patterson B.D., Cordeiro-Estrela P. 2018. Taxonomic revision of the long-nosed armadillos, Genus *Dasypus* Linnaeus, 1758 (Mammalia, Cingulata). PLoS One. 13:1–69.

Feijó A., Vilela J.F., Cheng J., Schetino M.A.A., Coimbra R.T.F., Bonvicino C.R., Santos F.R., Patterson B.D., Cordeiro-Estrela P. 2019. Phylogeny and molecular species delimitation of long-nosed armadillos (*Dasypus*: Cingulata) supports morphology-based taxonomy. Zool. J. Linn. Soc. 186:813–825.

Fisher D.C. 2008. Stratocladistics: Integrating Temporal Data and Character Data in Phylogenetic Inference. Annu. Rev. Ecol. Evol. Syst. 39:365–385.

Gardner A.L. 2008. Mammals of South America, Volume 1 - Marsupials, xenarthrans, shrews, and bats. London: The University of Chicago Press.

Gatesy J., O'Grady P., Baker R.H. 1999. Corroboration among data sets in simultaneous analysis: hidden support for phylogenetic relationships among higher level artiodactyl taxa. Cladistics. 15:271–313.

Gaudin T.J. 1993. Phylogeny of the Tardigrada (Mammalia, Xenarthra) and the evolution of locomotor function in the Xenarthra (Doctoral dissertation).

Gaudin T.J. 2004. Phylogenetic relationships among sloths (Mammalia, Xenarthra, Tardigrada): the craniodental evidence. Zool. J. Linn. Soc. 140:255–305.

Gaudin T.J., Branham D.G. 1998. The phylogeny of the Myrmecophagidae (Mammalia, Xenarthra, Vermilingua) and the relationship of *Eurotamandua* to the Vermilingua. J. Mamm. Evol. 5:237–265.

Gaudin T.J., Croft D.A. 2015. Paleogene Xenarthra and the evolution of South American mammals. J. Mammal. 96:622–634.

Gaudin T.J., Hicks P., Di Blanco Y. 2018. *Myrmecophaga tridactyla* (Pilosa: Myrmecophagidae). Mamm. Species. 50:1–13.

Gavryushkina A., Welch D., Stadler T., Drummond A.J. 2014. Bayesian inference of sampled ancestor trees for epidemiology and fossil calibration. PLoS Comput. Biol. 10:1–15.

Gibb G.C., Condamine F.L., Kuch M., Enk J., Moraes-Barros N., Superina M., Poinar H.N., Delsuc F. 2016. Shotgun mitogenomics provides a reference phylogenetic framework and timescale for living xenarthrans. Mol. Biol. Evol. 33:621–642.

Goloboff P.A., Arias J.S. 2019. Likelihood approximations of implied weights parsimony can be selected over the Mk model by the Akaike information criterion. Cladistics. 35:695–716.

Goloboff P.A., Torres A., Arias J.S. 2018a. Weighted parsimony outperforms other methods of phylogenetic inference under models appropriate for morphology. Cladistics. 34:407–437.

Goloboff P.A., Torres Galvis A., Arias J.S. 2018b. Parsimony and model-based phylogenetic methods for morphological data: comments on O'Reilly et al. Palaeontology. 61:625–630.

Heath T.A., Huelsenbeck J.P., Stadler T. 2014. The fossilized birth-death process for coherent calibration of divergence-time estimates. Proc. Natl. Acad. Sci. 111:E2957–E2966.

Hirschfeld S.E. 1976. A new fossil anteater (Edentata, Mammalia) from Colombia, S.A. and evolution of the Vermilingua. J. Paleontol. 50:419–432.

Huelsenbeck J.P., Ronquist F. 2001. MRBAYES: Bayesian inference of phylogenetic trees. Bioinformatics. 17:754–755.

Huelsenbeck J.P., Ronquist F., Nielsen R., Bollback J.P. 2001. Bayesian inference of phylogeny and its impact on evolutionary biology. Science (80-.). 294:2310–2314.

Kass R.E., Raftery A.E. 1995. Bayes Factors. J. Am. Stat. Assoc. 90:773–795.

Kraglievich L. 1934. La antigüedad Pliocena de las faunas de Monte Hermoso y Chapadmalal deducidas de su comparación con las que le precedieron y sucedieron. El Siglo Illus. 398:17–136.

Kück P., Longo G.C. 2014. FASconCAT-G: extensive functions for multiple sequence alignment preparations concerning phylogenetic studies. Front. Zool. 11:1–8.

Lanfear R., Frandsen P.B., Wright A.M., Senfeld T., Calcott B. 2016. PartitionFinder 2: new methods for selecting partitioned models of evolution for molecular and morphological phylogenetic analyses. Mol. Biol. Evol. 34:msw260.

Larsson A. 2014. AliView: A fast and lightweight alignment viewer and editor for large datasets. Bioinformatics. 30:3276–3278.

Lewis P.O. 2001. A likelihood approach to estimating phylogeny from discrete morphological character data. Syst. Biol. 50:913–925.

Mayden R.L. 1997. A hierarchy of species concepts: the denounement in the saga of the species problem. In: Claridge M.F., Dawah A.H., Wilson M.., editors. Species: the units of diversity. London: Chapman & Hall. p. 381–424.

McDonald G.H., Vizcaíno S.F., Bargo S.M. 2008. Skeletal anatomy and the fossil history of the Vermilingua. In: Vizcaíno S.F., Loughry W.J., editors. The Biology of the Xenarthra. Gainesville: University Press of Florida. p. 64–78.

McKenna M.C., Bell S.K. 1997. Classification of mammals: above the species level. New York: Columbia University Press.

McKenna M.C., Wyss A.R., Flynn J.J. 2006. Paleogene pseudoglyptodont xenarthrans from central Chile and Argentine Patagonia. Am. Museum Novit. 3536:1–18.

Meredith R.W., Janečka J.E., Gatesy J., Ryder O.A., Fisher C.A., Teeling E.C., Goodbla A., Eizirik E., Simão T.L.L., Stadler T., Rabosky D.L., Honeycutt R.L., Flynn J.J., Ingram C.M., Steiner C., Williams T.L., Robinson T.J., Burk-Herrick A., Westerman M., Ayoub N.A., Springer M.S., Murphy W.J. 2011. Impacts of the Cretaceous Terrestrial Revolution and KPg extinction on mammal diversification. Science (80-.). 334:521–524.

Miller M.A., Pfeiffer W., Schwartz T. 2010. Creating the CIPRES Science Gateway for inference of large phylogenetic trees. 2010 Gatew. Comput. Environ. Work. GCE 2010.:1–8.

Miranda F.R., Casali D.M., Perini F.A., Machado F.A., Santos F.R. 2018. Taxonomic review of the genus *Cyclopes* Gray, 1821 (Xenarthra: Pilosa), with the revalidation and description of new species. Zool. J. Linn. Soc. 183:687–721.

Möller-Krull M., Delsuc F., Churakov G., Marker C., Superina M., Brosius J., Douzery E.J.P., Schmitz J. 2007. Retroposed elements and their flanking regions resolve the evolutionary history of xenarthran mammals (armadillos, anteaters, and sloths). Mol. Biol. Evol. 24:2573–2582.

Naples V.L. 1999. Morphology, evolution and function of feeding in the giant anteater (*Myrmecophaga tridactyla*). J. Zool. 249:19–41.

O'Reilly J.E., Puttick M.N., Parry L., Tanner A.R., Tarver J.E., Fleming J., Pisani D., Donoghue P.C.J. 2016. Bayesian methods outperform parsimony but at the expense of precision in the estimation of phylogeny from discrete morphological data. Biol. Lett. 12:20160081.

O'Reilly J.E., Puttick M.N., Pisani D., Donoghue P.C.J. 2018. Probabilistic methods surpass parsimony when assessing clade support in phylogenetic analyses of discrete morphological data. Palaeontology. 61:105–118.

O'Reilly J.E., dos Reis M., Donoghue P.C.J. 2015. Dating tips for divergence-time estimation. Trends Genet. 31:637–650.

Owen R. 1856. On the anatomy of the Great Anteater (*Myrmecophaga jubata*, Linn.). Trans. Zool. Soc. London. 4:117–140.

Patterson B., Segall W., Turnbull W.D., Gaudin T.J. 1992. The ear region in Xenarthrans (=Edentata: Mammalia). Part II. Pilosa (sloths, anteaters), palaeanodonts, and a miscellany. Fieldiana Geol. 24:1–79.

Puttick M.N. 2019. MCMCtreeR: functions to prepare MCMCtree analyses and visualize posterior ages on trees. Bioinformatics. 24:5321–5322.

Puttick M.N., O'Reilly J.E., Oakley D., Tanner A.R., Fleming J.F., Clark J., Holloway L., Lozano-Fernandez J., Parry L.A., Tarver J.E., Pisani D., Donoghue P.C.J. 2017. Parsimony and maximum-likelihood phylogenetic analyses of morphology do not generally integrate uncertainty in inferring evolutionary history: a response to Brown et al. Proc. R. Soc. B Biol. Sci. 284:20171636.

Puttick M.N., O'Reilly J.E., Pisani D., Donoghue P.C.J. 2019. Probabilistic methods outperform parsimony in the phylogenetic analysis of data simulated without a probabilistic model. Palaeontology. 62:1–17.

de Queiroz A., Gatesy J. 2007. The supermatrix approach to systematics. Trends Ecol. Evol. 22:34–41.

R Core Team. 2019. R: A language and environment for statistical computing. https://www.r-project.org.

Rambaut A., Drummond A.J., Xie D., Baele G., Suchard M.A. 2018. Posterior summarization in bayesian phylogenetics using Tracer 1.7. Syst. Biol. 67:901–904.

Reiss K.Z. 1997. Myology of the feeding apparatus of myrmecophagid anteaters (Xenarthra : Myrmecophagidae). J. Mamm. Evol. 4:87–117.

Ronquist F., Huelsenbeck J.P. 2003. MrBayes 3: Bayesian phylogenetic inference under mixed models. Bioinformatics. 19:1572–1574.

Ronquist F., Klopfstein S., Vilhelmsen L., Schulmeister S., Murray D.L., Rasnitsyn A.P. 2012. A total-evidence approach to dating with fossils, applied to the early radiation of the Hymenoptera. Syst. Biol. 61:973–999.

Ronquist F., Lartillot N., Phillips M.J. 2016. Closing the gap between rocks and clocks using total-evidence dating. Philos. Trans. R. Soc. B Biol. Sci. 371:20150136.

Sambrook J., Russel D.W. 2001. Molecular cloning: A laboratory manual. Nova York: CSH Laboratory Press.

Santos Júnior J.E. dos, Santos F.R., Silveira F.A. 2015. Hitting an unintended target: Phylogeography of Bombus brasiliensis lepeletier, 1836 and the first new Brazilian bumblebee species in a century (Hymenoptera: Apidae). PLoS One. 10:1–21.

Scillato-Yané G.J., Carlini A.A. 1998. Nuevos Xenarthra del Friasense (Mioceno Medio) de Argentina. Stud. Geol. Salmant. 34:43–67.

Silvestro D., Warnock R.C.M., Gavryushkina A., Stadler T. 2018. Closing the gap between palaeontological and neontological speciation and extinction rate estimates. Nat. Commun. 9:1–14.

Taylor B.K. 1978. The anatomy of the forelimb in the anteater (*Tamandua*) and its functional implications. J. Morphol. 157:347–368.

Wetzel R.M. 1982. Systematic, distribution, ecology, and conservation of South American Edentates. In: Mares M.A., Genoways H.H., editors. Mammalian Biology in South America v.6. Pittsburg: University of Pittsburg. p. 345–375.

Wood H.M., Matzke N.J., Gillespie R.G., Griswold C.E. 2013. Treating fossils as terminal taxa in divergence time estimation reveals ancient vicariance patterns in the palpimanoid spiders. Syst. Biol. 62:264–284.

Wortley A.H., Scotland R.W. 2006. The effect of combining molecular and morphological data in publishedphylogenetic analyses. Syst. Biol. 55:677–685.

Wright A.M., Hillis D.M. 2014. Bayesian analysis using a simple likelihood model outperforms parsimony for estimation of phylogeny from discrete morphological data. PLoS One. 9:e109210.

Xie W., Lewis P.O., Fan Y., Kuo L., Chen M.-H. 2011. Improving marginal likelihood estimation for Bayesian phylogenetic model selection. Syst. Biol. 60:150–160.

Zhang C., Stadler T., Klopfstein S., Heath T.A., Ronquist F. 2016. Total-evidence dating under the fossilized birth-death process. Syst. Biol. 65:228–249.

SUPPLEMENTARY MATERIAL

Supplementary File S1. List of morphological characters used in the study.

Supplementary File S2. List of morphological characters excluded from the study.

Supplementary File S3. List of studied specimens.

Supplementary File S4. Nexus file with the morphological character matrix.

Supplementary File S5. Table with GenBank access numbers.

Supplementary File S6. Fasta file with the molecular alignment.

Supplementary File S7. Table with the best-fitting models and partitioning scheme selected by PartitionFinder2 for molecular data partitions.

Files available in:

https://drive.google.com/drive/folders/1V0iS_In_YtsCIuJYkU56cmjS38rpmJSo?usp=sharing

CHAPTER 3. Reassessing the phylogeny and divergence times of sloths (Mammalia: Pilosa: Folivora), exploring alternative morphological partitioning and dating models

ABSTRACT

Phylogenetic relationships among Folivora have been extensively studied in the last few decades using maximum parsimony approaches. Recently, Bayesian phylogenetic methods also began to be employed for this task. New advances, particularly in methods for data partitioning and tip-dating analyses with the fossilized birth-death process, have led to exciting new possibilities in Bayesian morphological phylogenetics. In that context, we assembled the largest morphological dataset ever applied in a study of sloths and reassessed their phylogeny and divergence times, further evaluating the performance of alternative models of morphological partitioning and dating in a Bayesian framework. The updated phylogeny of sloths is largely in agreement with previous morphological studies, with *Bradypus* recovered as sister to Eufolivora, the presence of two major sloth clades, Mylodontoidea and Megatherioidea, and the inclusion of *Choloepus* in Megalonychidae. The present study has, however, yielded some important advances in understanding the relationships of some genera with historically unresolved or controversial allocations. The origin of Folivora and of its two major clades occurred from the middle to late Eocene, and their diversification occurred during the late Oligocene. Other important clades – Scelidotheriidae, Mylodontidae, Megalonychidae and Megatheriidae – originated and diversified between the latest Oligocene and the early Miocene. Homoplasy-based partition models outperformed anatomical partitioning and unpartitioned analyses according to Bayes factors, with considerable impacts in phylogenetic relationships and posterior probabilities. Bayesian tree estimates obtained using homoplasy-partitioned models were in greater agreement with those inferred by maximum parsimony. We emphasize the importance of using model comparison with Bayes factors and suggest that the assessment of synapomorphies should not be neglected in Bayesian morphological phylogenetics.

KEYWORDS: Megatherioidea. Mylodontoidea. Morphology. Partitions. Divergence times. Synapomorphies.

3.1 INTRODUCTION

Sloths, previously referred to as Tardigrada or Phyllophaga (Fariña and Vizcaíno 2003), are now classified under the name Folivora (Delsuc et al. 2001; Gardner 2008) and constitute, together with Vermilingua (anteaters), the clade Pilosa (Gardner 2008; Gaudin and McDonald 2008; Gibb et al. 2016). Pilosa is part of Xenarthra (McKenna and Bell 1997; Gardner 2008; Gaudin and McDonald 2008; Gibb et al. 2016), along with Cingulata (armadillos, pampatheres and glyptodonts), which is one of the three main clades of placental mammals (Springer et al. 2004; Upham et al. 2019) and a significant component of the native South American fauna (Simpson 1948; Patterson and Pascual 1968; Gaudin and Croft 2015). Among xenarthans, sloths were the most successful clade, diversifying into approximately 100 genera throughout their evolutionary history (McKenna and Bell 1997; McDonald and De Iuliis 2008). Despite that, the vast majority of sloths are extinct today, with the exception of six species, classified into two genera, *Bradypus* and *Choloepus* (Gardner 2008; McDonald and De Iuliis 2008).

The oldest fossil record of sloths date from the Eocene-Oligocene transition, with abundant remains of the group extending into the Holocene (McDonald and De Iuliis 2008; Gaudin and Croft 2015). Sloths exhibited a substantial increase in diversity during the early and late Miocene (Varela et al. 2019), which was roughly maintained during the Pliocene and Pleistocene, but then declined suddenly at the end of the Quaternary, associated with the global megafaunal extinction events (McDonald and De Iuliis 2008). Studies that investigated the divergence time between sloths and their close relatives (e.g., Gibb et al. 2016; Varela et al. 2019) have suggested a slightly older origin for the group, so far undocumented in the fossil record. Historically, sloths presented a wide geographic distribution in the American continent, occupying territories from Patagonia to Alaska, and including representatives in Central America and the Antilles (McDonald and De Iuliis 2008; Pujos et al. 2017; Varela et al. 2019). Today, the two living genera are restricted to the tropical regions of South and Central America (Gardner 2008).

Such diversity and broad distribution in time and space were accompanied by a remarkable ecomorphological disparity. Sloths vary widely in body size and mass, ranging from a few kilograms to several tons (Raj Pant et al. 2014; Toledo et al. 2017). They show great anatomical variation associated with a variety of locomotory habits, with suspensory, arboreal, semi-arboreal, terrestrial, fossorial and semi-aquatic adaptations (Bargo et al. 2000; McDonald 2012; Nyakatura 2012; Pujos et al. 2012; Toledo et al. 2013, 2015; Amson et al. 2014), as well as variations related to diet, including adaptations for browsing, grazing and mixed feeding

strategies (de Muizon et al. 2004a; Bargo et al. 2006; Shockey and Anaya 2011; Naples and McAfee 2012, 2014; Pujos et al. 2012).

Phylogenetic relationships among Folivora have been extensively studied in the last few decades, mostly using morphological data and maximum parsimony (MP) criterion. Although speculative evolutionary hypotheses for the relationships of sloths had long been suggested (e.g., Hoffstetter 1954; Patterson and Pascual 1968; Paula Couto 1979), it was only with the study of Engelmann (1985) that cladistic methodology began to be applied to xenarthrans in general and folivorans in particular, to assess relationships and character support for taxa. Nonetheless, that study lacked a formal algorithmic analysis. The first study to apply a quantitative cladistic analysis for sloths was that of Gaudin (1995), using 85 ear region characters for 21 genera, with preliminary results of this study already available in two previous publications (Gaudin 1990; Patterson et al. 1992). A few years later, Gaudin (2004) expanded upon those previous studies, including 286 craniodental characters for 33 sloth genera, with the tree resulting from that analysis becoming the reference phylogenetic hypothesis for sloths until very recently. According to this phylogeny, four large groups could be recognized, and were considered families – Mylodontidae, Megalonychidae (including the living genus *Choloepus*), Nothrotheriidae and Megatheriidae – in addition to a fifth group exclusively composed of the living genus *Bradypus*, Bradypodidae. A clade uniting *Hapalops, Analcimorphus*, nothrotheriids and megatheriids was named Megatheria, which along with megalonychids, *Schismotherium* and *Pelecyodon,* composed Megatherioidea (Gaudin 2004).

Since then, many other studies have contributed to our understanding of the phylogenetic relationships of sloths (e.g., Carlini and Scillato-Yané 2004; Pujos 2006; Pujos et al. 2007; De Iuliis et al. 2011; Miño-Boilini et al. 2014; Rincón et al. 2015; Amson et al. 2016; McDonald et al. 2017; Boscaini et al. 2019b; Nieto et al. 2020), most of them including postcranial characters as well, but with a restricted taxonomic scope or a relatively small set of characters. Varela et al. (2019) was the first study to substantially expand the sampling of Gaudin (2004), including postcranial characters for representatives of all major groups and adding several recently described genera to the phylogeny. They generated a data matrix totaling 64 taxa and 361 characters, all obtained from previous studies. This was also the first morphological study to apply Bayesian inference (BI) methods to estimate the phylogeny and divergence times of sloths, and also to evaluate biogeographic and macroevolutionary patterns for the group. The topology recovered by Varela et al. (2019) corroborated the general resolution and the families recovered in Gaudin (2004), but with disagreements regarding the relationships within these groups. Their results also differed from those obtained in other

detailed studies carried out for Mylodontidae (Boscaini et al. 2019b) and Megatheria (Amson et al. 2016).

In parallel with morphological studies, efforts have been made in the past few decades to sequence ancient DNA from some species of fossil sloths, but samples were restricted to one or two fossil taxa (e.g., Greenwood et al. 2001; Poinar et al. 2003; Slater et al. 2016; Delsuc et al. 2018). More significant, however, were two recent studies that managed to include a greater number of Pleistocene and Holocene sloths in molecular phylogenies, with mitogenomic nucleotide data (Delsuc et al. 2019) and amino acid sequences obtained with paleoproteomics techniques (Presslee et al. 2019). Those studies achieved consistent results between themselves, but suggested topologies quite different from those previously recovered by morphological data. Although they provided very intriguing results, it would be premature to consider them as having provided conclusive evidence of the inaccuracy of all prior morphology-based phylogenetic inferences. Methodological issues, such as the limited taxonomic sample of those molecular studies, comprised solely of highly derived taxa, could be biasing their analyses to produce long-branch attraction artifacts (Bergsten 2005). Currently, only morphological data allows a representative sampling of most of the taxonomic diversity of sloths, and the current study focuses on further exploring sloth morphological phylogenetics with an expanded and revised dataset, using parsimony and Bayesian methods, focusing especially on the performance of the latter.

One possible source of error in phylogenetic reconstruction for statistical phylogenetic methods is the use of incorrect or inadequate models of evolution (Lemmon and Moriarty 2004; Brown and Lemmon 2007). Varela et al. (2019) explored models with alternative anatomical partitioning schemes for Folivora, as has become common practice in BI analyses of morphological data (Clarke and Middleton 2008; Tarasov and Génier 2015; Porto et al. 2021). However, only two alternative models were tested, and many other plausible anatomical partitioning hypotheses remained unexplored. Also, more recently, methods of homoplasy-based partitioning developed for molecular studies were extended to morphological analyses, constituting a promising alternative to anatomical partitioning (Rosa et al. 2019). Here we apply those partitioned models to investigate the phylogeny of sloths, but also take the opportunity to make this a case study of the performance of morphological data partitioning in Bayesian inference investigations.

In the last few years, new advances in modelling morphological data in time-calibrated analyses has consistently improved our inferences, including better practices to deal with uncertainty in fossil ages (Barido-Sottani et al. 2019); alternative tree priors (Matzke and

Wright 2016); alternative clock models, sampling regimes and diversification parameters (Simões et al. 2020b, 2020a); use of multiple clock partitions (Lee et al. 2014; Zhang and Wang 2019; Simões et al. 2020a); performance of dating algorithms and software (Bapst et al. 2016); and interaction with molecular data in total-evidence analyses (Ronquist et al. 2012b, 2016; Zhang et al. 2016; Luo et al. 2020). Despite that, details regarding the behavior of morphological data in dating analyses are still more poorly understood than they are for molecular data (Simões et al. 2020a; Barba-Montoya et al. 2021). For Folivora, the dating analyses performed by Varela et al. (2019) applied a single combination of clock and tree models, without evaluating plausible alternatives. The exploration of different models for the among-branch variation of clock rates, temporal patterns of diversification and fossil sampling conducted here aims to contribute further to the understanding of their performance in BI studies using morphological data.

In order to explore those empirical and methodological issues, we assembled the largest morphological dataset ever applied in a phylogenetic study of sloths, both in numbers of taxa and characters, employing a revised version of the data available in several previous studies, a few new characters, and a broad taxonomic sample, to produce an updated time-calibrated phylogeny and classification of sloths. We also evaluate synapomorphies associated with the recovered sloth clades, a step usually neglected in most studies applying Bayesian inferences to morphological datasets.

3.2 MATERIAL AND METHODS

3.2.1 Morphological dataset

We reevaluated the data used in most previous phylogenetic studies of sloths and their close outgroups (Gaudin 1995, 2004; De Iuliis 1996; Gaudin and Branham 1998; McDonald and de Muizon 2002; McDonald and Perea 2002; de Muizon et al. 2003; Pujos 2006; Pujos et al. 2007, 2016; De Iuliis et al. 2011; Miño-Boilini 2012; McDonald et al. 2013, 2017; Rincón et al. 2015; Amson et al. 2016; Casali and Perini 2017; Boscaini et al. 2019b; Cartelle et al. 2019). Some characters, although not modified in structure, were recoded after new evaluations and new observations of polymorphisms. Some of those characters were originally scored exclusively for less inclusive groups, and we were able to expand them here to all sloths. We also expanded the number of coded cells, especially for postcranial characters, after direct observations of specimens housed in museum collections, and, in a few cases, from high-quality photographs shared by colleagues (see Supplementary File S1 for a list of the specimens and

institutions). Those observations were complemented by descriptions and illustrations in the literature (Supplementary File S2).

Our taxonomic sampling included 68 sloth genera, and eight outgroups – all living and extinct genera of Vermilingua, and two representatives of Cingulata, *Dasypus* and *Euphractus*. We focused our taxonomic sampling on genera of sloths for which, at a minimum, the following were available: i) relatively complete cranial material, ii) incomplete cranial material associate with mandibular or postcranial elements, or, iii) mandibular material associated with several postcranial elements. A list of all genera included in this study, authorship, and literature consulted is available in Supplementary File S2.

The final dataset was composed of 510 characters, with 316 used in their original formulation, 182 modified for this study, and 12 new characters. See Supplementary File S3 for a detailed account of the characters, states, ordering, their origin, modifications and equivalence of characters among previous studies. Character ordering was applied for 63 of 127 multistate characters, mostly following what was proposed in previous studies, with a few modifications. Hypotheses of character ordering considered positional, orientational or structural morphoclines (Gaudin 2004). Those characters were treated as ordered in all maximum parsimony analyses, but models with and without ordering were statistically compared in Bayesian inferences, evaluating their relative fit to the data. The dataset was edited in Mesquite 3.61 (Maddison and Maddison 2019), and it is available as Supplementary File S4.

3.2.2 Phylogenetic Analyses

3.2.2.1 Maximum parsimony

Maximum parsimony analyses were conducted in TNT 1.5 (Goloboff et al. 2008; Goloboff and Catalano 2016), using equal (EW) and implied weights (IW, Goloboff 1993). For implied weights, we conducted analyses setting the concavity constant (k) to values of 1000, 100, 50, 20, 10 and 5, to evaluate the impact of increased weighting against homoplasy. Since only analyses with k set to 100, 10 and 5 produced different topologies, we focused on these results, along with those from EW. Searches used a combination of “New Technology” algorithms, sectorial searches and tree fusing, in their default configurations. We defined a minimum of ten hits for the minimum tree length, with ten initial additional sequences, holding 100,000 trees in memory, and collapsing zero-branch lengths. We also set the driver to check the level of analyses at every hit to improve the efficiency of searches. Subsequently, we applied traditional heuristic searches using TBR over the trees found in the first step, to ensure that we

recovered all most parsimonious trees (MPTs). For searches with EW, multiple MPTs were summarized using a 50% Majority-rule consensus tree. Supports were evaluated using standard bootstrap for EW, and Poisson bootstrap for IW analyses, with 1000 replications, showing the supports in the best trees from IW, and in the consensus of all MPTs for EW. A TNT script to reproduce those analyses is available as Supplementary File S5.

3.2.2.2 Bayesian inferences

3.2.2.2.1 Morphological partitions

We defined several alternative partitioning schemes to model rate heterogeneity in the dataset, using two major criteria. The first criterion used was anatomical partitioning (Clarke and Middleton 2008). We allocated all characters in eight mutually exclusive anatomical partitions – teeth (T), mandible (M), hyoid apparatus (H), cranium (excluding ear region, C), ear region (E), axial skeleton (X), anterior appendicular skeleton (A) and posterior appendicular skeleton (P). A single character for the presence or absence of osteoderms was considered along with those from the axial skeleton partition. Those subsets of characters comprised the most partitioned anatomical scheme, with combinations of those partitions resulting in seven anatomical partitioning schemes (A1-A7, Fig. 1, Table 1).

The second criterion used to define partitions was the degree of homoplasy presented by the characters in a given tree topology, with characters sharing the same levels of homoplasy composing separate partitions (Kjer and Honeycutt 2007; Rosa et al. 2019). The original version of this method (Kjer and Honeycutt 2007), proposed for molecular data, used character consistency indices (ci, Farris 1969) to segregate characters into partitions. Rosa et al. (2019) modified this method and validated its performance for morphological data. These authors suggested the use of fit values estimated in trees from IW parsimony analyses, since ci exhibits biases when calculated for binary versus multistate characters. Here, we propose a further modification to this method, to simply use the number of extra steps of a given character (i.e., the actual number of steps minus the minimum possible number of steps for that character) in any given topology. When the dataset is composed exclusively of unordered characters, this method produces the same partitions as the method of Rosa et al. (2019), except for how it deals with non-informative characters. It has three advantages:

i) Fit values (or distortion, the complementary metric used during IW tree searches in TNT) of ordered characters, as calculated in IW parsimony analyses, are obtained by decomposing the ordered multistate into multiple binary characters, calculating the fit for those binary characters, and summing the values. This results in overestimated homoplasy values for ordered characters. Although adequate for weighting during searches, the fit of ordered characters does not function well as a metric of homoplasy, since that was not its original purpose (Pablo Goloboff, personal communication). The number of extra steps, on the other hand, does not suffer from this shortcoming.

ii) The number of extra steps can be calculated for EW parsimony topologies as well as ci, but without the drawbacks pointed out by Rosa et al. (2019) for this metric. Also, like ci, this metric is even applicable to trees obtained from another optimality criterion.

iii) It joins, in the same partition, non-informative characters and those with no homoplasy, something showed by Rosa et al. (2019) to further improve the fit of the models partitioning by homoplasy, observable by inspecting the values recovered for the rate multiplier of those partitions.

We calculated the number of extra steps in EW and all three IW parsimony topologies, and defined partitions by allocating the characters according to their values for this index. To avoid too many overly small partitions, we defined the minimum partition size as equal to the smallest anatomical partition used this study, merging partitions with less than seven characters to those partitions with the most similar extra step character values. This led to a total of 11 or 12 homoplasy-based partitions – depending on the parsimony topology used to calculate the number of extra steps – and to four partitioning schemes – EW, IW100, IW10 and IW5 (Table 1).

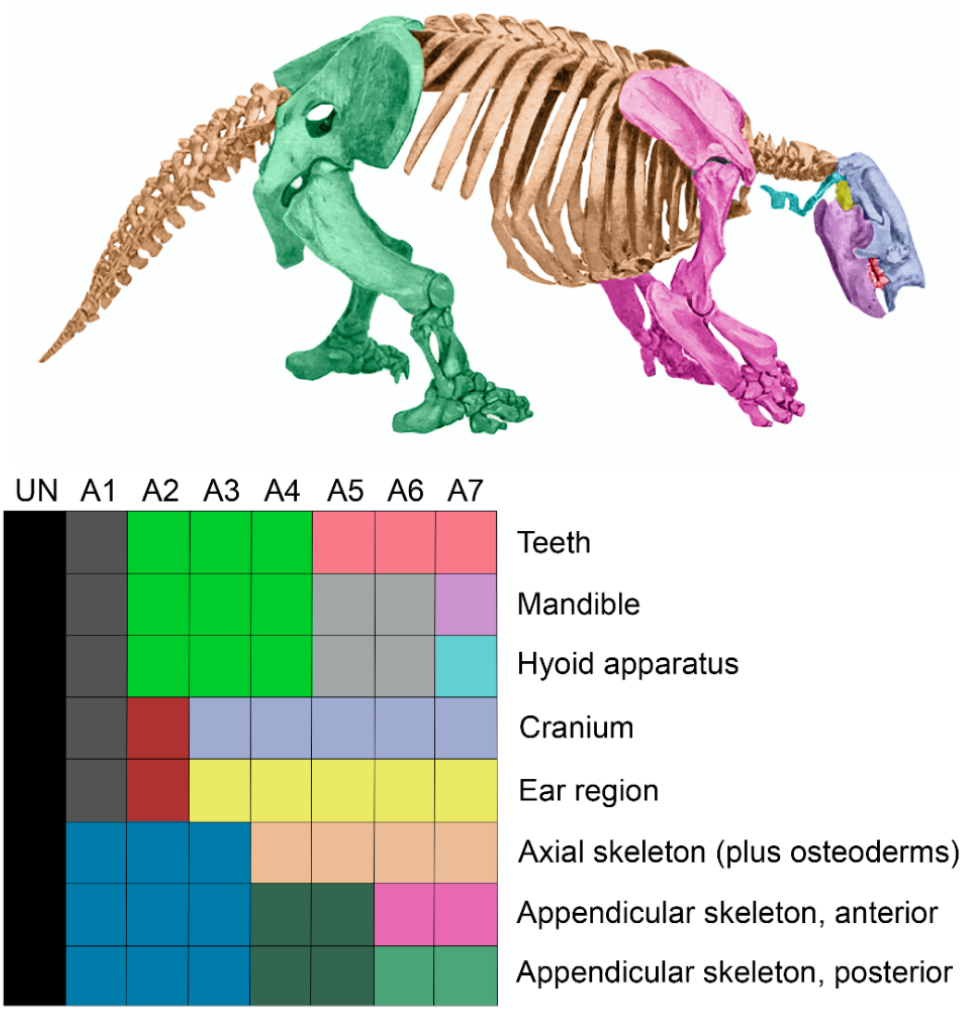

Figure 1. Anatomic partitions and partitioning schemes. Colored anatomic regions in the skeleton of *Paramylodon harlani* (modified from Stock 1925) correspond to the maximally partitioned data subsets, as used in model A7, whereas their combinations into composite partitions used in schemes A1 to A6 are indicated by other colors in the table.

Table 1. Partitioning criterion and partitions applied in Bayesian model-fitting and phylogenetic analyses.

Criterion	Partition	Characters	Binary	Multistate	Ordered	Informative	Missing	Inapplicable	Polymorphic
-	Complete dataset	510	383	127	63	500	0.38	0.03	0.02
Anatomy	Teeth (T)	35	17	18	4	34	0.10	0.10	0.02
Anatomy	Mandible (M)	42	29	13	11	42	0.28	0.03	0.03
Anatomy	Hyoid apparatus (H)	7	5	2	1	7	0.72	0.00	0.01
Anatomy	Cranium (C)	162	127	35	15	159	0.29	0.04	0.03
Anatomy	Ear region (E)	80	62	18	7	80	0.40	0.01	0.01
Anatomy	Axial skeleton (X)	10	8	2	1	9	0.66	0.00	0.01
Anatomy	Anterior appendicular (A)	88	72	16	10	85	0.52	0.01	0.02
Anatomy	Posterior appendicular (P)	86	63	23	14	84	0.49	0.01	0.02
Anatomy	MH	49	34	15	12	49	0.34	0.03	0.03
Anatomy	AP	174	135	39	24	169	0.50	0.01	0.02
Anatomy	TMH	84	51	33	16	83	0.24	0.06	0.03
Anatomy	XAP	184	143	41	25	178	0.51	0.01	0.02
Anatomy	CE	242	189	53	22	239	0.33	0.03	0.03
Anatomy	TMHCE	326	240	86	38	322	0.31	0.04	0.03
Homoplasy	EW_P1	101	90	11	6	91	0.41	0.04	0.01
Homoplasy	EW_P2	76	66	10	7	76	0.43	0.03	0.01
Homoplasy	EW_P3	64	54	10	2	64	0.39	0.03	0.02
Homoplasy	EW_P4	74	57	17	6	74	0.38	0.02	0.03
Homoplasy	EW_P5	62	43	19	9	62	0.39	0.02	0.03
Homoplasy	EW_P6	34	20	14	7	34	0.36	0.01	0.03

Criterion	Partition	Characters	Binary	Multistate	Ordered	Informative	Missing	Inapplicable	Polymorphic
Homoplasy	EW_P7	42	25	17	9	42	0.37	0.02	0.04
Homoplasy	EW_P8	21	11	10	6	21	0.26	0.04	0.05
Homoplasy	EW_P9	16	10	6	2	16	0.33	0.02	0.07
Homoplasy	EW_P10	7	3	4	2	7	0.22	0.05	0.06
Homoplasy	EW_P11	13	4	9	7	13	0.23	0.02	0.06
Homoplasy	IW_100_P1	103	92	11	6	93	0.40	0.04	0.01
Homoplasy	IW_100_P2	75	65	10	7	75	0.44	0.03	0.01
Homoplasy	IW_100_P3	69	59	10	2	69	0.40	0.02	0.02
Homoplasy	IW_100_P4	73	52	21	9	73	0.38	0.02	0.03
Homoplasy	IW_100_P5	61	45	16	6	61	0.39	0.02	0.03
Homoplasy	IW_100_P6	29	16	13	7	29	0.35	0.01	0.03
Homoplasy	IW_100_P7	45	28	17	9	45	0.36	0.02	0.04
Homoplasy	IW_100_P8	19	9	10	6	19	0.28	0.04	0.05
Homoplasy	IW_100_P9	16	10	6	2	16	0.33	0.02	0.07
Homoplasy	IW_100_P10	7	3	4	3	7	0.24	0.04	0.07
Homoplasy	IW_100_P11	13	4	9	6	13	0.22	0.02	0.05
Homoplasy	IW_10_P1	104	93	11	6	94	0.40	0.04	0.01
Homoplasy	IW_10_P2	74	65	9	6	74	0.45	0.03	0.01
Homoplasy	IW_10_P3	75	61	14	5	75	0.4	0.02	0.02
Homoplasy	IW_10_P4	64	48	16	5	64	0.39	0.02	0.03
Homoplasy	IW_10_P5	61	45	16	8	61	0.38	0.02	0.03
Homoplasy	IW_10_P6	37	22	15	8	37	0.34	0.03	0.03

Criterion	Partition	Characters	Binary	Multistate	Ordered	Informative	Missing	Inapplicable	Polymorphic
Homoplasy	IW_10_P7	39	22	17	8	39	0.36	0.02	0.04
Homoplasy	IW_10_P8	19	11	8	5	19	0.27	0.04	0.05
Homoplasy	IW_10_P9	15	7	8	2	15	0.30	0.03	0.06
Homoplasy	IW_10_P10	7	5	2	2	7	0.27	0.03	0.07
Homoplasy	IW_10_P11	15	4	11	8	15	0.24	0.03	0.05
Homoplasy	IW_5_P1	105	94	11	6	95	0.40	0.04	0.01
Homoplasy	IW_5_P2	73	64	9	6	73	0.45	0.03	0.01
Homoplasy	IW_5_P3	75	60	15	6	75	0.39	0.02	0.02
Homoplasy	IW_5_P4	65	49	16	5	65	0.39	0.02	0.03
Homoplasy	IW_5_P5	55	41	14	6	55	0.39	0.02	0.03
Homoplasy	IW_5_P6	41	25	16	9	41	0.34	0.03	0.03
Homoplasy	IW_5_P7	40	23	17	8	40	0.36	0.02	0.04
Homoplasy	IW_5_P8	18	11	7	5	18	0.28	0.04	0.05
Homoplasy	IW_5_P9	17	8	9	2	17	0.29	0.03	0.06
Homoplasy	IW_5_P10	7	4	3	3	7	0.26	0.02	0.08
Homoplasy	IW_5_P11	7	3	4	3	7	0.22	0.01	0.07
Homoplasy	IW_5_P12	7	1	6	4	7	0.24	0.05	0.04

3.2.2.2.2 Model fitting and selection

We estimated marginal likelihoods (MgL) for alternative models using Stepping-Stone (SS) sampling (Fan et al. 2011; Xie et al. 2011) in MrBayes 3.2.7a (Huelsenbeck and Ronquist 2001; Ronquist and Huelsenbeck 2003). We set three runs, with eight chains each, for 50M generations divided into 50 steps, sampling at every 1000 generations, with *nswaps* = 3. A step burn-in of 10M generations was discarded before the sampling of the main steps, and at each step, the 50% initial samples were discarded before summarizing MgL estimates. Chain temperatures were empirically adjusted to improve efficiency, ranging from 0.04-0.1. Convergence between runs was assessed with step trace plots in MrBayes, and inspecting the similarity among estimates of parallel runs. All MrBayes analyses were conducted in CIPRES Science Gateway (Miller et al. 2010).

Model fit was evaluated by comparing Bayes factors, using the Kass and Raftery (1995) statistics (KRS, following the terminology of Rosa et al. 2019), calculated as 2* ($\ln(MgL_{M0}) - \ln(MgL_{M1})$), representing $_{M0}$ and $_{M1}$ higher and lower MgL models, respectively. According to Kass and Raftery (1995), values between 0 and 2 for this statistic are only slightly better evidence in favor of the model with higher MgL, and barely worth mentioning. Values from 2 to 6 are considered positive evidence; from 6 to 10, strong evidence; and above 10, decisive evidence in favor of the model with higher marginal likelihoods.

For each partitioning scheme (or for the complete dataset, in unpartitioned analyses), two ways of modelling among-character rate variation (ACRV, Harrison and Larsson 2015) inside partitions were considered – equal rates (e), and per-partition variable rates (p), accommodated by a discrete lognormal distribution with four rate categories for each partition. Among-partition rate variation (APRV) was accounted for by partition-specific rate multipliers with linked branch lengths. The Mk model with ascertainment bias correction was applied (Lewis 2001), with coding set to variable, as we included some autapomorphic characters in the dataset. A total of 24 models were evaluated, 22 partitioned and two unpartitioned. Before fitting partitioned models to our dataset, we evaluated the impact of including ordering for some of the multistate characters, using unpartitioned analyses with both ACRV approaches. Since models including ordered characters produced a much better fit to data than those with all character unordered (KRS = 31.42 for equal rates and KRS = 101.17 for variable rates), all subsequent analyses for partitioned models included ordering for those characters.

3.2.2.2.3 Tree inferences and comparisons

Even though we used Bayes factors to select the best-fitting model, we conducted Bayesian inferences with all models, to evaluate their influence on tree topology and node supports. For all analyses, we set three runs, with eight chains each, for 20-60M generations, sampling at every 4000 generations and setting *nswaps* = 3 (see Supplementary File S6 for specific number of generations and temperature used for each model). A relative burn-in of 50% was applied before summarizing parameters. Tree samples were summarized into a maximum compatibility consensus tree (*contype* = *allcompat*) and supports evaluated using posterior probabilities (PP). Convergence for continuous parameters was assessed after visually inspecting trace plots, ESS > 200 and PRSF ~ 1.0 in MrBayes and Tracer 1.7. (Rambaut et al. 2018). For convergence of topologies, we used the function *analyze.rwty* in the package *rwty* (Warren et al. 2017) in R environment (R Core Team 2021) to inspect trace plots, and check if ESS > 200, ASDSF < 0.01 and correlation coefficients ≥ 0.99.

To compare topologies obtained from alternative models, we used normalized Robinson-Foulds distances (nRF, Robinson and Foulds 1981), which range from 0 (complete similarity among topologies) to 1 (complete dissimilarity). This metric was calculated comparing topologies obtained from MP and all Bayesian models to the reference topology obtained from the best-fitting Bayesian model, using the function *RF.dist* in R package *phangorn* (Schliep 2011).

We used the R package *ggplot2* (Wickham 2016) to plot MgL estimates (mean and range), nRF distances and the distributions of node supports for each model/analysis (including trees from MP analyses). Also, we plotted the estimates of rate multipliers obtained for each partition in all models, and summary statistics were calculated with the package *psych* (Revelle 2020). We calculated the signal-to-noise ratio (SNR) of each partition, following the procedure used in Rosa et al. (2019), with values > 0 indicating a prevalence of signal over noise, and values < 0 indicating the opposite.

3.2.3 Stratigraphic fit and divergence time estimates

We fixed the topology during dating analyses, since preliminary explorations indicated some persistent convergence issues when some clock and tree models were applied while co-estimating topology and divergence times. Also, there is some evidence from empirical and simulation studies that the co-estimation of topologies with a tip-dating approach for datasets mostly composed of fossil taxa and realistic levels of missing data may not be the best practice, since temporal data can override morphological signals in potentially detrimental ways (King 2021; Mongiardino Koch et al. 2021). The Bayesian topology obtained from the best-fitting model was a natural candidate to be used for this purpose, but we wish to investigate if topologies obtained in MP analyses could be more adequate. To evaluate this, we applied a non-phylogenetic comparison, avoiding the use of methods that would be biased in favor of one or the other criteria applied to obtain the trees (MP x BI). We compared the stratigraphic fit between all EW MPTs plus the topologies from IW analyses (1747 trees) to the post burn-in posterior samples obtained from BI analysis using the best-fitting model (7503 trees), excluding outgroups, following King (2021). For this comparison, we applied two widely used stratigraphic fit metrics using the function *StratPhyloCongruence* in R package *strap* (Bell and Lloyd 2015) – the stratigraphic consistency index (SCI, Huelsenbeck 1994) and the gap excess ratio (GER, Wills 1999). Age intervals were obtained after a survey from the literature (Supplementary File S7), assessing first and last appearance data for each taxon. Fossil ages were treated in two ways while dating the trees during stratigraphic fit evaluation – i) as known ranges of occurrence, applied to all trees (i.e., unequal sample sizes between MP and BI trees), and ii) as age uncertainties summarized into uniform distributions, from which 1000 samples were obtained for each phylogenetic method (i.e., equal sample sizes). Root length was set to 12.5 myrs, following the results of Varela et al. (2019), applying the *equal* dating method (Brusatte et al. 2008), and fixing topologies and the outgroup position. Boxplots with the distributions of those metrics were plotted using *ggplot2,* and summary statistics were calculated with package *psych* (Revelle 2020). To assess significance for differences in stratigraphic fit between MP and BI topologies, their medians were compared using the Wilcoxon Rank-Sum Test (Wilcoxon 1945) with *stats* function *wilcox.test*, considering $\alpha = 0.05$. We also compared the stratigraphic fit of the consensus topology from the Bayesian best-fitting model relative to individual IW topologies and to the median value of BI and MP trees.

To estimate divergence times, we used a tip-dating approach with the fossilized birth-death (FBD) process (Pyron 2011; Ronquist et al. 2012a; Heath et al. 2014; Zhang et al. 2016)

in MrBayes. This approach allowed us to consider the temporal information for all fossils included in our taxonomic sample. Uniform distributions with age uncertainty were defined for each fossil, since this practice seems to produce more accurate estimates then using fixed point estimates (Barido-Sottani et al. 2019). Additionally, we constrained the nodes of Cingulata, Pilosa and Vermilingua, and calibrated them using a uniform distribution with the 95% highest posterior density (HPD) range obtained from Gibb et al. (2016) for Cingulata and Pilosa, and from Casali et al. (2020) for Vermilingua. The root age prior was defined using the age of the oldest xenarthran, *Riostegotherium yanei* Oliveira & Bergqvist 1998, as the minimum age, with the maximum age defined by the upper limit of the 95% HPD obtained by Gibb et al. (2016) for that node.

We initially applied four alternative dating models, using combinations of clock (Independent rates – IGR and Autocorrelated rates – TK02) and fossil sampling (TIP – all fossils are terminals and SA – fossils can be ancestors) models. The base clock rate prior was sampled from a lognormal distribution, with mean and standard deviation parameters (-2.10, 0.07) defined using median and 95% HPD values of tree length obtained from the non-clock consensus tree from the best-fitting partitioned model, and the root age from Gibb et al. (2016), following the method used in Ronquist et al. (2012). FBD priors were kept at default configuration. Additionally, we investigated a fifth model, with all settings equal to those used in the best-fitting among the four previously tested dating models, but allowing fossilization, speciation and extinction rates to vary through time-bins (Zhang et al. 2016), i.e., a skyline fossilized birth-death (SFBD) process (Simões et al. 2020a). Those bins were defined considering the temporal distribution of taxic diversity present in our sample, obtained with the function *taxicDivCont* in R package *paleotree* (Bapst 2012). Periods marked by an increase and decrease in diversity were in overall agreement with the limits of geological epochs and their subdivisions (Fig. 2). This resulted in seven time-bins: i) Root age to the Eocene-Oligocene transition, ii) Oligocene, iii) early Miocene, iv) middle Miocene, v) late Miocene, vi) Pliocene, and vii) Pleistocene to recent. For all those dating models, the best-fitting partitioning scheme was applied, keeping ordering and coding as in non-clock analyses. Fossilization, speciation and extinction relative rates obtained with this analysis were plotted by time bins with *ggplot2*.

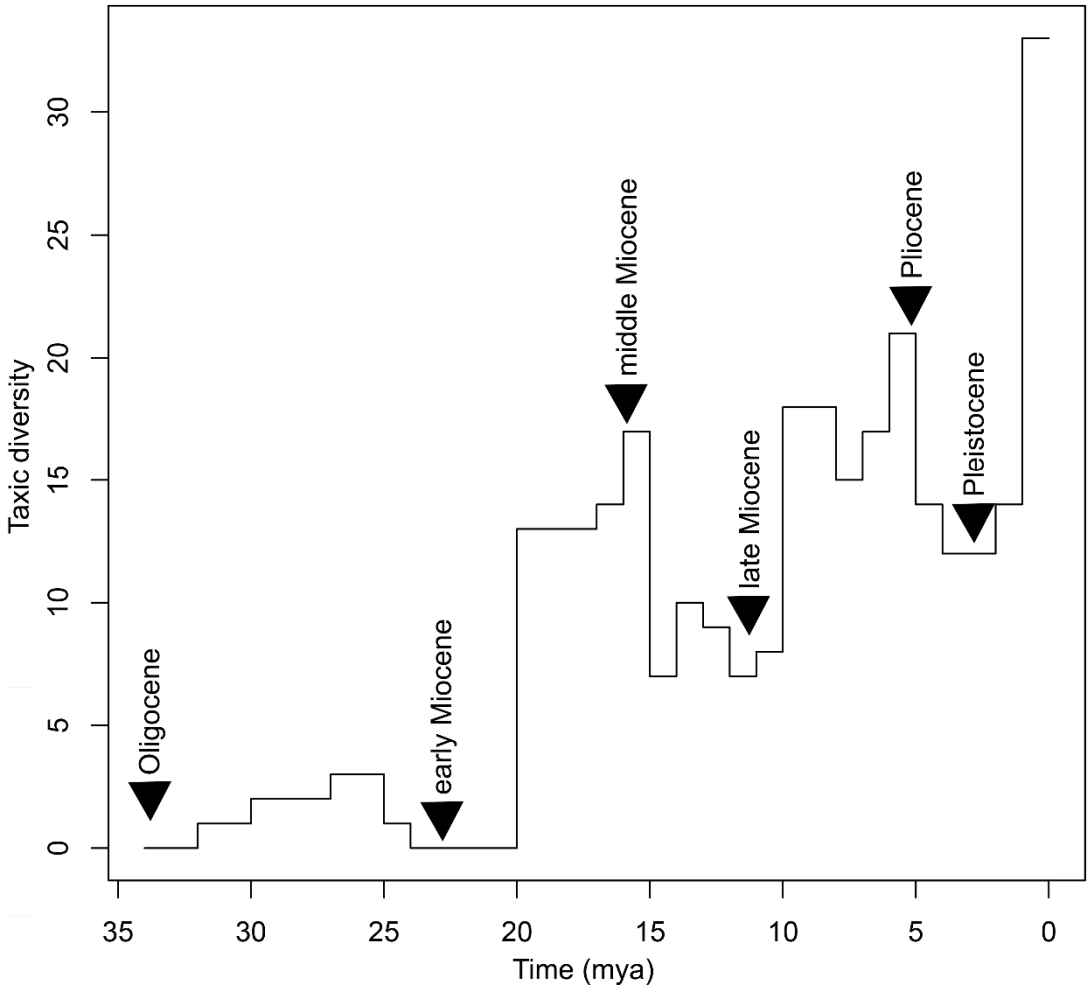

Figure 2. Diversity through time for sloth genera sampled here, and its association with geological periods. Time scale in million years ago (mya).

Model fitting was evaluated with Bayes factors, through KRS, as for non-clock partitioned models. For SS sampling, we set two runs, with four chains each, for 200M generations divided in 50 steps, sampling at every 1000 generations. A step burn-in of 10M generations was discarded before the sampling of the main steps, and at each step, the 50% initial samples were discarded before summarizing MgL estimates. Chain temperatures were set to 0.05 for all analyses. Convergence between runs was assessed with step trace plots in MrBayes, and inspecting the similarity among estimates of parallel runs.

We also conducted time-calibrated analyses with all five dating models, evaluating their impact on divergence times for selected clades. For those analyses, we set three runs, with four chains each, for 50M generations, sampling at every 10000, and *temp* = 0.05. A relative burn-

in of 50% was applied before summarizing parameters, which were checked for convergence as for non-clock models, except for topologies, that were fixed. Divergence ages (median and 95% HPDs) for selected clades representing the main named groups above genus-level were plotted using *ggplot2*. Divergence times for the models were summarized into Bayesian chronograms, depicted using *ggtree* (Yu et al. 2017) and *deeptime* (Gearty 2021) R packages. We evaluated the degree of overlap among distributions of median ages and also for distributions of 95% HPD lengths (i.e., upper minus lower limit values) between alternative models using Bhattacharyya coefficients (Bhattacharyya 1946), which rank the degree of overlap between distributions, ranging from 0 (no overlap) to 1 (complete overlap). Values below 0.05 and above 0.95 indicate clearly dissimilar and similar distributions, respectively (Guillerme and Cooper 2016). A nexus input file for the SFBD analysis is available as Supplementary File S8. It contains the structure to reproduce all Bayesian analyses performed in this study, including SS samplings, editing settings accordingly.

3.2.4 Assessing synapomorphies

Phylogenetic studies applying Bayesian inferences for morphological data rarely investigate the synapomorphies supporting the recovered clades, and when they do, MP optimizations are used to evolve characters in the tree while assessing character support (King 2019). This is not an ideal approach, since MP optimizations disregard the substitution model used to infer the trees in which characters are being evaluated, and do not consider branch length information, which potentially influences reconstructed ancestral states. King (2019) proposed an approach that compares the support of state transformations in alternative phylogenetic hypotheses, evaluating differences in their likelihood scores for subsets of trees from the posterior sample. Here we take a different approach, since we are interested in evaluating the synapomorphies for a single phylogenetic hypothesis, obtained from the best-fitting model chronogram.

We inferred ancestral states using marginal reconstructions with the function *estimate_ancestral_states* in R package *Claddis* (Lloyd 2016), with the rerooting method of Yang et al. (1995), with prior probabilities for parameters obtained from the data. This constitutes an empirical Bayes method (Huelsenbeck and Bollback 2001). Hierarchical Bayes methods, in which phylogenetic uncertainty is also integrated during ancestral state reconstruction, are time and computationally intensive to apply to as large a set of characters as we have here, and does not seem to positively affect ancestral state estimates (Hanson-Smith et

al. 2010). We applied the same substitution model and character ordering as used for tree inferences and the Bayesian chronogram obtained with the overall best-fitting model. State posterior probabilities were collapsed into the most likely state using the default threshold (0.01). We avoided reconstructing ancestral states for cases in which data for descendent tips and nodes were inapplicable or missing, and only considered as a synapomorphy those state transformations in which both ancestral and descendent nodes were estimated and non-polymorphic or uncertain. Additionally, we obtained a list of synapomorphies using traditional MP optimization in TNT, using unambiguous optimizations. We evaluated which synapomorphies were recovered by MP, BI, and both methods used to reconstruct ancestral states.

3.2.5 Updated classification

We proposed an updated and rank-free suprageneric classification of Folivora, naming groups that were recovered as monophyletic in the tree obtained from the overall best-fitting model. Even though we are not adopting formal ranks in that classification, we considered phylogenetic position, morphological distinctiveness and temporal information in order to standardize group suffixes for organizational purposes. Also, we tried to preserve the older names used in previous classifications of sloths to ensure stability, unless this contradicts the criteria defined above.

Abbreviations

Anatomical abbreviations: Cf, upper caniniform tooth; cf, lower caniniform tooth; Mf, upper molariform tooth; mf, lower molariform tooth; Mc, metacarpal; Mt, metatarsal.

Methodological abbreviations: ACRV, among-character rate variation; APRV, among-partition rate variation; ASDSF, average standard deviation of split frequencies; BI, Bayesian inference; ci, character consistency index; ESS, effective sample size; EW, equal weight; FBD, fossilized birth-death; GER, gap excess ratio; HPD, highest posterior density; IW, implied weight; KRS, Kass and Raftery statistic; MgL, marginal likelihood; MP, maximum parsimony; MPT, most parsimonious tree; nRF, normalized Robinson-Foulds distance; PP, posterior probability; PRSF, potential scale reduction factor; SA, sampling ancestors; SCI, stratigraphic consistency index; SFBD, skyline fossilized birth-death; SNR, signal-to-noise ratio; SS, stepping-stone; TBR, tree bisection and reconnection.

3.3 RESULTS

3.3.1 Maximum parsimony trees

EW parsimony analyses returned 1744 MPTs (TL = 2238), whereas searches using IW returned a single topology for each value of k (fit values: par_IW100 = 14.81; par_IW10 = 106.89, par_IW5 = 166.22).

3.3.2 Performance of Bayesian partitioned models

Models applying homoplasy partitioning (H models) fitted much better to the data than those partitioned by anatomy (A models), which, in turn, presented very similar fit among themselves and to unpartitioned models (UN models, Table 2, Fig. 3a). The best-fitting partitioned model, IW100_e, yielded strong evidence relative to the second-best model (KRS = 7.34), and decisive evidence (KSS > 10) relative to all other models compared. For H models, it was unnecessary to account for ACRV using lognormal distributions, with models that considered equal rates inside partitions being preferred, whereas the opposite was observed for A and UN models (Table 2, Fig. 3a).

3.3.3 Quantitative differences among topologies and node supports

Maximum parsimony, UN and A models' topologies were roughly equidistant from topologies obtained with H models (Table 2, Fig. 3b), although they present important qualitative differences (Fig. 4, Supplementary File S9), which will be detailed below. Among topologies obtained using H models, there was a smaller, but noticeable difference in nRF distances among partitioning schemes obtained when stronger weighting functions were applied (par_IW10 and par_IW5), if compared to partitioning schemes obtained with milder weighting (par_IW100) or the consensus from EW analysis (par_EW), although this was not so strongly reflected in MgL estimates (Table 2, Fig. 3).

Partitioning schemes also affected the distribution of node supports, with H models leading to higher average PPs and an increased prevalence of higher node supports than observed for alternative models (Table 2, Fig. 3c). Although UN and A models accounting for ACRV fitted the data better, their average node supports were equal to, or lower than those from models with equal rates inside partitions (Table 2), with only minor differences in their

distributions of node supports (Fig. 3c). Even though they are not strictly comparable, values of PPs for any BI analyses conducted here were higher than those for bootstrap values (BS) calculated for MP trees, and are shown for completeness (Table 2, Fig. 3c). Among MP trees, par_IW10 and par_IW5 returned slightly higher average supports (Table 2), accompanied by a slight difference in their overall distribution of supports relative to par_EW and par_IW100, which include slightly lower values in their distributions (Fig. 3c).

3.3.4 Partition rate multipliers

Estimates of rate multipliers were less precise for small anatomical partitions, especially for hyoid and axial partitions when ACRV was accounted for (Fig. 5, Supplementary File S10), and the same was observed for smaller partitions using the homoplasy criterion (right-end boxplots in Fig. 6, Supplementary File S10). Nevertheless, precision for partitions with more characters was greater while partitioning by homoplasy than when using anatomy. Rate multipliers of anatomical partitions in each model also showed a greater overlap of their distributions if compared to those from homoplasy partitioning (Figs. 5 and 6, Supplementary File S10). Signal-to-noise ratios were positive for all partitions, but, as expected, achieved lower values in those with less precise estimates, but also in the first partition of all homoplasy partitioning schemes. The relative decrease in signal was more pronounced for the smaller partitions (hyoid and axial anatomical partitions) when accounting for ACRV (Supplementary File S10).

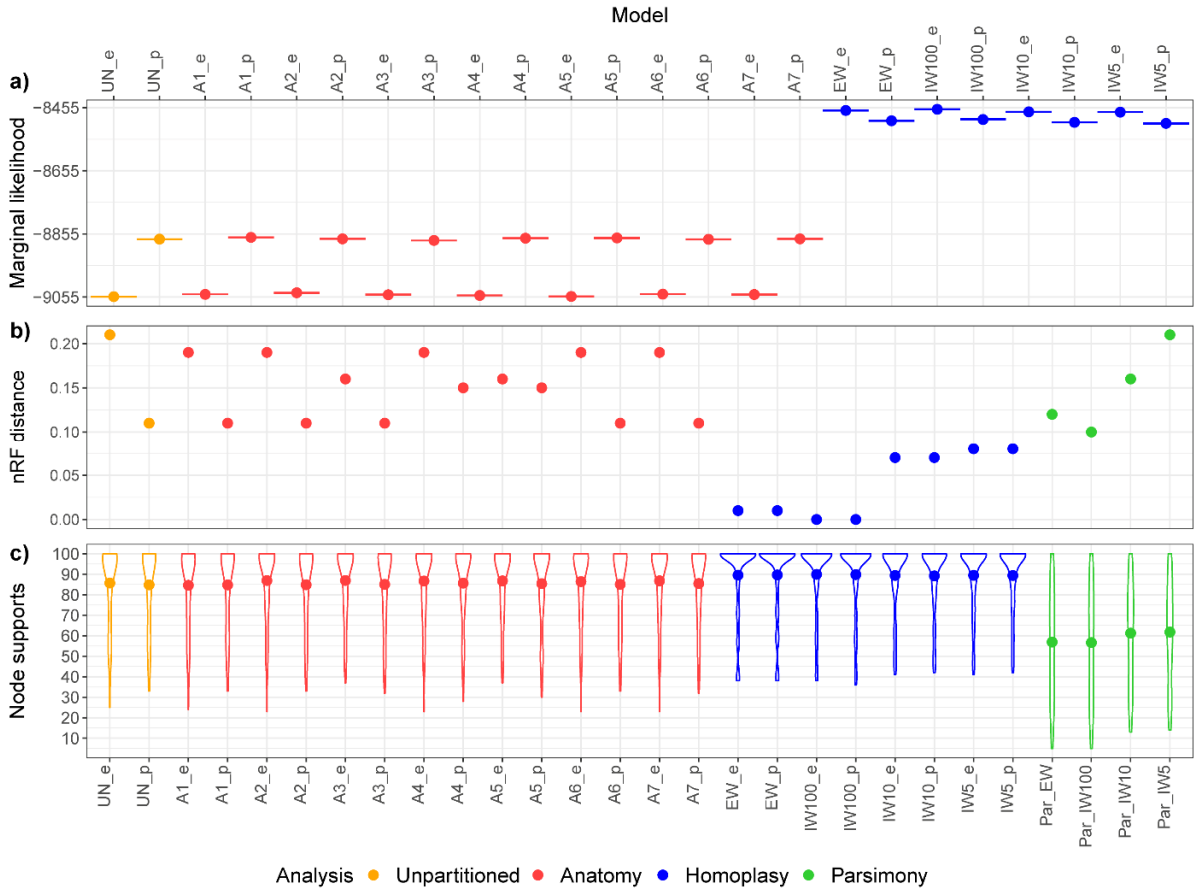

Figure 3. a) Marginal likelihoods of Bayesian models. b) Normalized Robinson-Foulds (nRF) distances among topologies (with IW100_e used as reference). c) Distribution of node supports, with posterior probabilities for Bayesian inferences and bootstrap values for maximum parsimony.

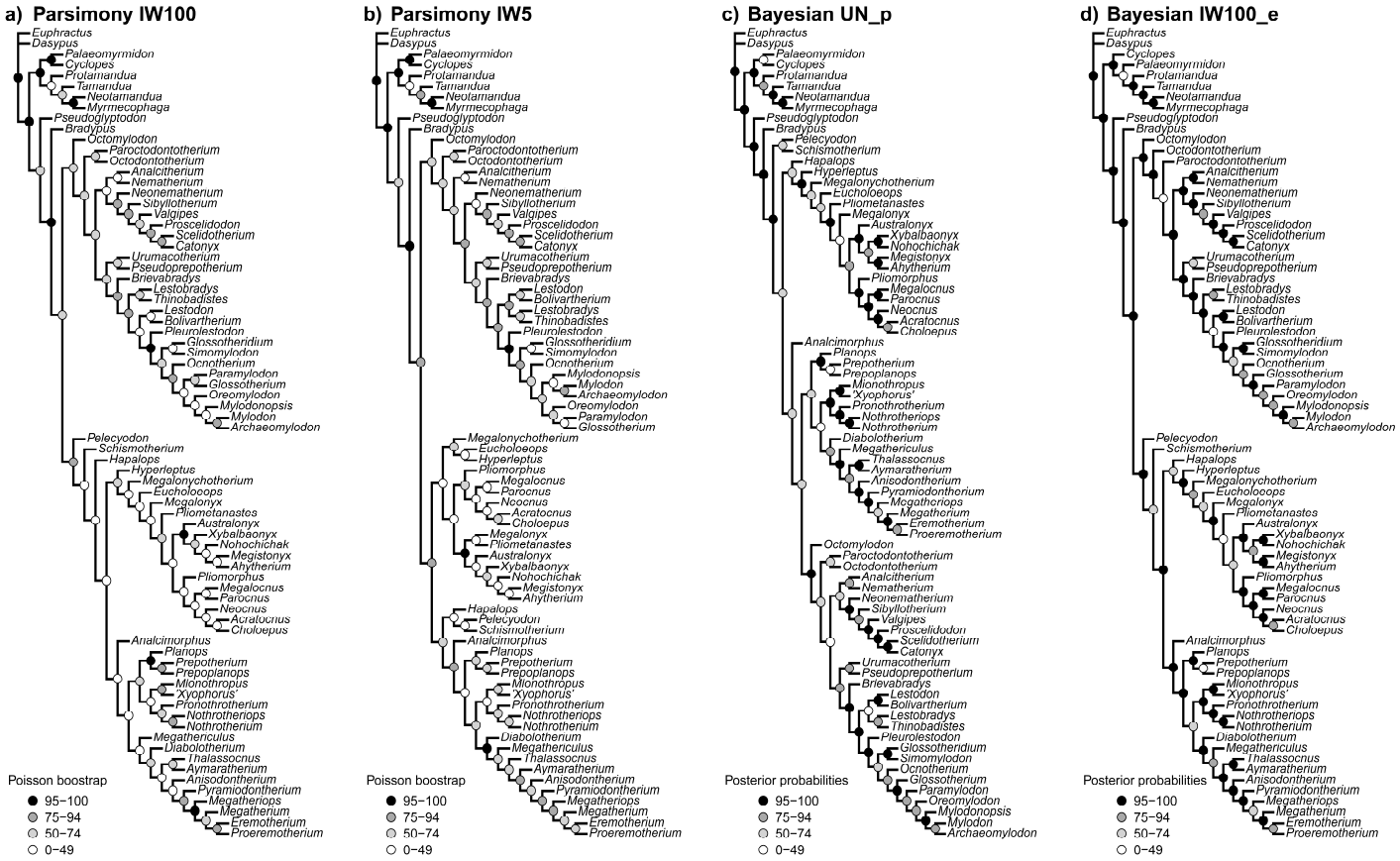

Figure 4. Selected trees, with node supports, depicting the overall variation in topologies obtained here. a) Parsimony IW100. b) Parsimony IW5. c) Bayesian UN_p. d) Bayesian IW100_e. All topologies and branch lengths for Bayesian trees are available in Supplementary File S9.

Table 2. Performance of alternative Bayesian partitioning schemes, with average marginal likelihoods of the three runs (MgL) and Kass and Raftery (1995) statistic used to compare models. Normalized Robinson-Foulds distances (nRF) for all trees from Bayesian inferences and maximum parsimony analyses were calculated relative to the topology of the best-fitting Bayesian model. Average node supports (Avg. supp.) refer to posterior probabilities for Bayesian inferences and bootstrap values for maximum parsimony.

Analysis	Model	Run1	Run2	Run3	Avg. MgL	KRS	nRF	Avg. supp.
Homoplasy	IW100_e	-8460.96	-8459.25	-8460.53	-8460.25	0.00	0.00	90
Homoplasy	EW_e	-8462.96	-8465.15	-8463.65	-8463.92	7.34	0.01	90
Homoplasy	IW10_e	-8467.48	-8468.84	-8468.53	-8468.28	16.06	0.07	89
Homoplasy	IW5_e	-8470.10	-8468.34	-8469.30	-8469.25	18.00	0.08	89
Homoplasy	IW100_p	-8494.33	-8492.94	-8490.48	-8492.58	64.66	0.00	90
Homoplasy	EW_p	-8496.83	-8497.93	-8495.01	-8496.59	72.68	0.01	90
Homoplasy	IW10_p	-8501.19	-8502.34	-8501.18	-8501.57	82.64	0.07	89
Homoplasy	IW5_p	-8506.66	-8504.36	-8503.32	-8504.78	89.06	0.08	89
Anatomy	A1_p	-8865.03	-8865.86	-8867.23	-8866.04	811.58	0.11	85
Anatomy	A5_p	-8865.48	-8868.73	-8869.22	-8867.81	815.12	0.15	85
Anatomy	A4_p	-8867.23	-8870.41	-8868.38	-8868.67	816.84	0.15	86
Anatomy	A2_p	-8870.85	-8871.23	-8870.03	-8870.70	820.90	0.11	85
Anatomy	A7_p	-8871.75	-8869.82	-8870.59	-8870.72	820.94	0.11	85
Unpartitioned	UN_p	-8872.69	-8871.23	-8870.70	-8871.54	822.58	0.11	85
Anatomy	A6_p	-8871.63	-8871.52	-8873.49	-8872.21	823.92	0.11	85
Anatomy	A3_p	-8875.51	-8876.01	-8875.53	-8875.68	830.86	0.11	85
Anatomy	A2_e	-9042.51	-9041.37	-9040.71	-9041.53	1162.56	0.19	87
Anatomy	A6_e	-9046.54	-9045.91	-9045.55	-9046.00	1171.50	0.19	86
Anatomy	A1_e	-9046.69	-9046.33	-9046.83	-9046.62	1172.74	0.19	85
Anatomy	A7_e	-9046.73	-9045.87	-9048.80	-9047.13	1173.76	0.19	87
Anatomy	A3_e	-9048.23	-9046.59	-9048.37	-9047.73	1174.96	0.16	87
Anatomy	A4_e	-9048.85	-9050.43	-9050.81	-9050.03	1179.56	0.19	87
Anatomy	A5_e	-9053.15	-9052.28	-9053.85	-9053.09	1185.68	0.16	87
Unpartitioned	UN_e	-9052.84	-9053.59	-9055.05	-9053.83	1187.16	0.21	86
Par_EW	-	-	-	-	-	-	0.12	57
Par_IW100	-	-	-	-	-	-	0.10	57
Par_IW10	-	-	-	-	-	-	0.16	61
Par_IW5	-	-	-	-	-	-	0.21	62

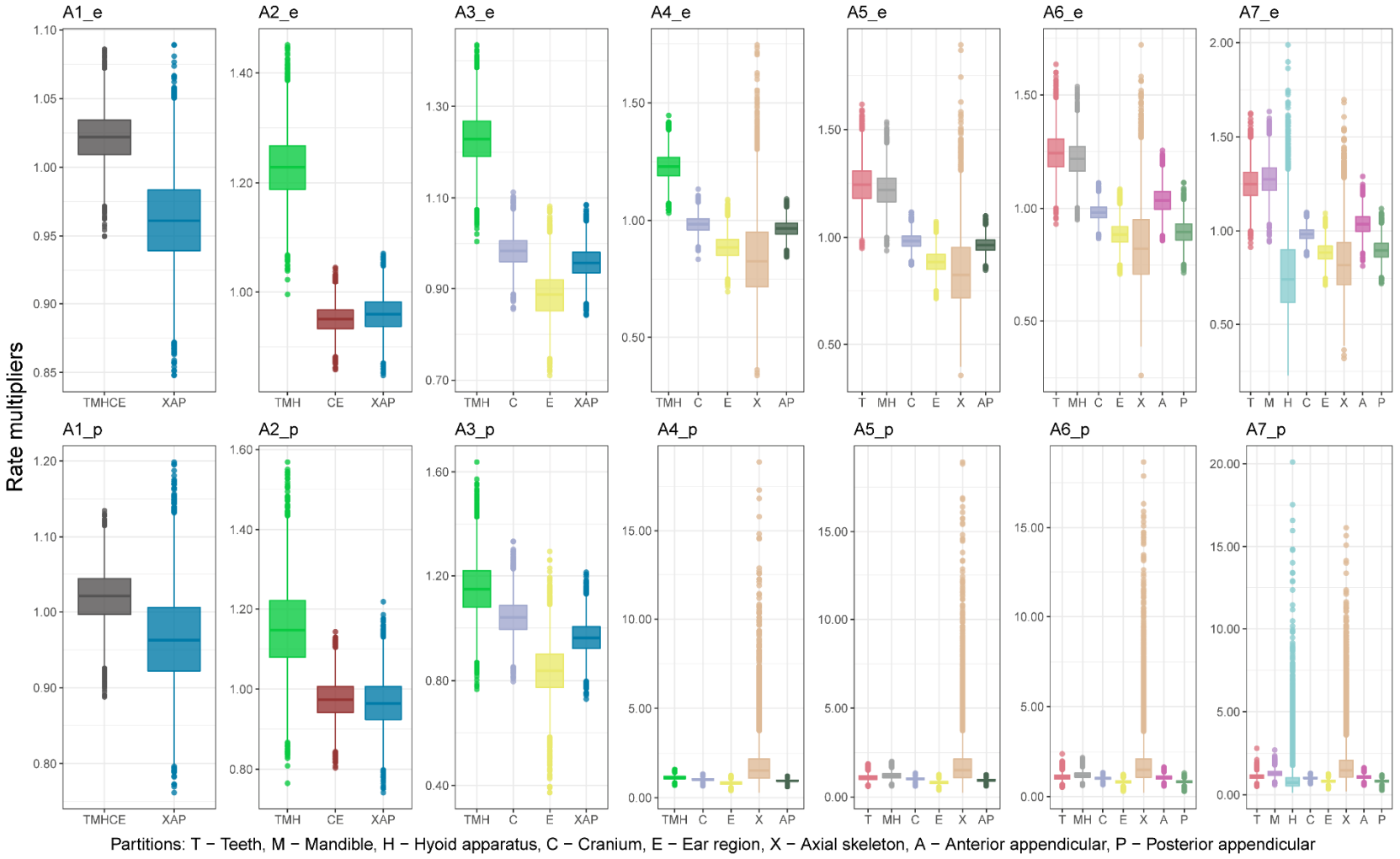

Figure 5. Estimated rate multipliers for anatomical partitions in each model. Partition colors as in Figure 1.

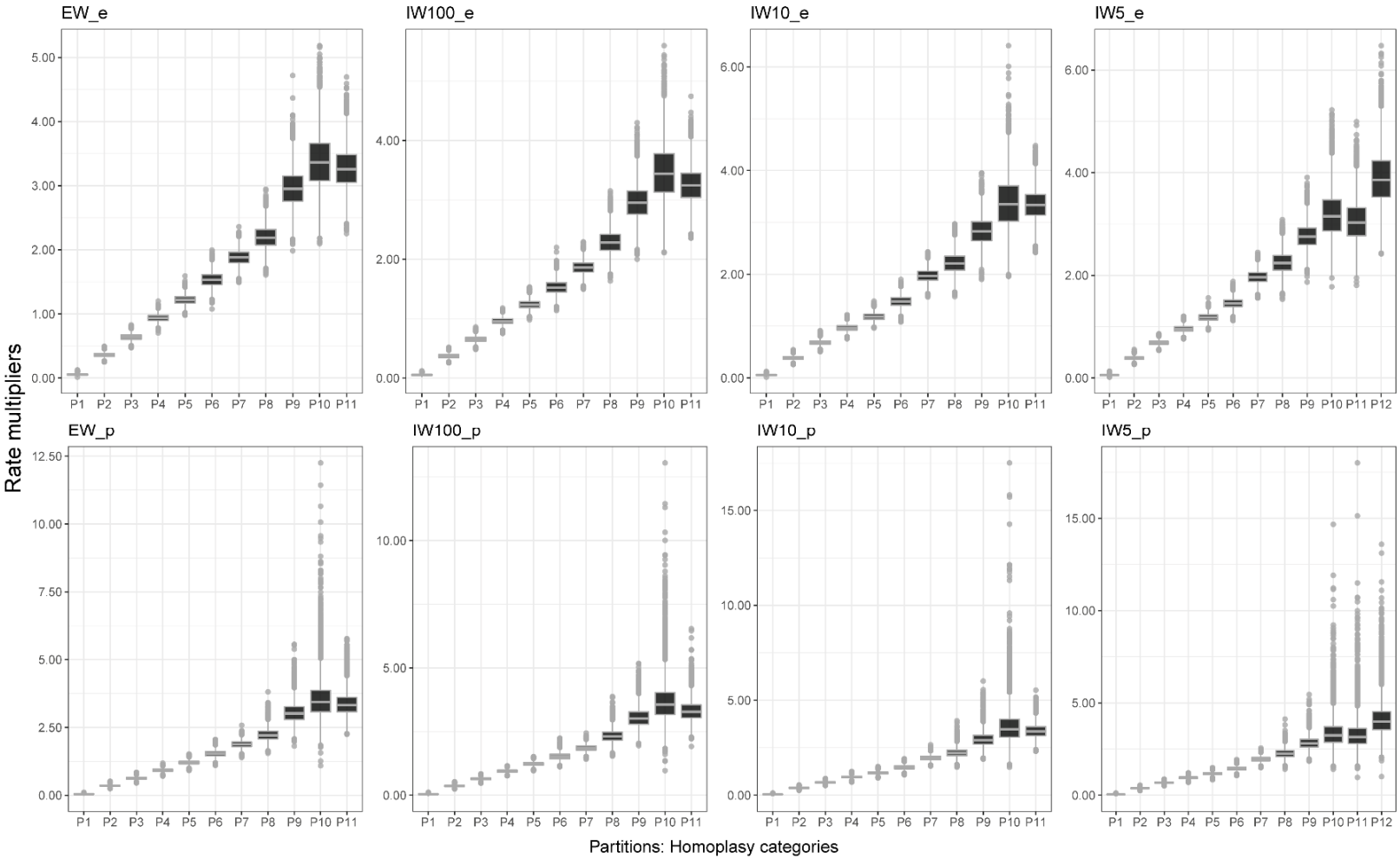

Figure 6. Estimated rate multipliers for homoplasy-based partitions in each model.

3.3.5 Stratigraphic fit

Results for SCI and GER indicated that BI and MP topologies showed more stratigraphic fit than expected by chance (with the exception of a single MP topology when measured with SCI and using ages as uncertain, p = 0.065, Supplementary File S11). Bayesian topologies fitted better to stratigraphic data than topologies obtained with maximum parsimony (Fig. 7), with this difference being statistically significant (Supplementary File S12). The BI consensus topology showed a stratigraphic fit above the median of the BI posterior sample, except when using ages as uncertain for GER. The stratigraphic fit of the BI consensus is also higher than that of IW individual topologies and that from the median stratigraphic-fit MP trees, for all metrics evaluated (Supplementary File S12). Hence, this topology was fixed for all dating models evaluated here.

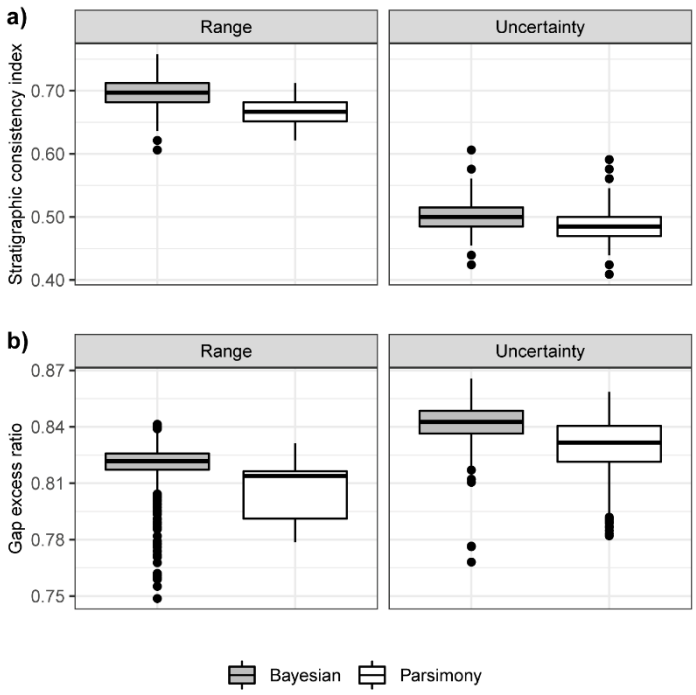

Figure 7. Stratigraphic fit of maximum parsimony and Bayesian topologies evaluated with two metrics, considering fossil age intervals as known ranges or as stratigraphic uncertainty. A) Stratigraphic consistency index (SCI). B) Gap excess ratio (GER).

3.3.6 Performance of dating models

Among the five models used to estimate divergence-times for sloths, FBD_TK02_TIP fit the data decisively better relative to the second-best model, SFBD_TK02_TIP (KRS = 18.07, Table 3). Autocorrelated clock models outperformed models with independent rates, and models in which all taxa were sampled as terminals outperformed those in which ancestors were sampled (Table 3). No taxon in SA models presented zero branch lengths, and very small branch lengths (< 0.01) were only observed in the model FBD_IGR_SA, for *Anisodontherium* and *Pyramiodontherium*. Overall, ages for the selected clades were very consistent among models, with their median values contained in the 95% HPD of alternative models, with a few exceptions, mostly observed in clades closer to the root (e.g., Folivora and Eufolivora, Fig. 8, Supplementary File S13). Those clades also presented more imprecise estimates, with wider 95% HPDs. Bhattacharyya coefficients indicate very similar age estimates among models, with all comparisons of median ages showing clearly similar distributions (Table 4, upper triangular). For 95% HPD lengths, four of ten comparisons were not clearly similar, but distributions still presented a great degree of overlap (≥ 0.9, Table 4, lower triangular). In TK02 models, and even more pronounced in the analysis using a SFBD process, clades closer to the root were estimated as older than in IGR models, which, in turn, recovered slightly older estimates for more nested clades (Fig. 8, Supplementary File S13). Models including sampled ancestors (SA) consistently led to slightly younger estimates relative to those in which all taxa were sampled as tips, but with more modest effects on divergence ages that those observed for the alternative clock model (Fig. 8, Supplementary File S13).

Table 3. Performance of alternative Bayesian dating models, with average marginal likelihoods (MgL) of the two runs and Kass and Raftery (1995) statistic used to compare models.

Model	Run1	Run2	MgL	KRS
FBD_TK02_TIP	-8217.14	-8219.14	-8218.14	0.00
SFBD_TK02_TIP	-8226.75	-8227.60	-8227.18	18.07
FBD_TK02_SA	-8287.73	-8284.73	-8286.23	136.17
FBD_IGR_TIP	-8297.83	-8297.22	-8297.52	158.76
FBD_IGR_SA	-8322.98	-8326.77	-8324.87	213.46

Table 4. Bhattacharyya coefficients calculated for distributions of medians (upper triangular) and 95% HPD length (lower triangular) of node ages estimated with alternative models.

Models	FBD_IGR_SA	FBD_IGR_TIP	FBD_TK02_SA	FBD_TK02_TIP	SFBD_TK02_TIP
FBD_IGR_SA	-	1.00	0.98	0.98	0.97
FBD_IGR_TIP	0.96	-	0.98	0.98	0.96
FBD_TK02_SA	0.93	0.90	-	1.00	0.97
FBD_TK02_TIP	0.96	0.94	0.95	-	0.97
SFBD_TK02_TIP	0.95	0.92	0.96	0.96	-

Figure 8. Divergence ages (median and 95% HPD) for all dating models, showed for the main groups of Folivora of the present classification. Time scale in million years ago (mya).

3.3.7 Phylogeny and divergence times

In the following phylogenetic account for major sloth clades, we will consider the Bayesian chronogram from the best-fitting dating model (Fig. 9) as the reference for topology and divergence ages, which will be presented using medians, and 95% HPD intervals in brackets. Node supports refer to the Bayesian topology from the best-fitting partitioned model that was fixed for divergence time estimates. Alternative topological arrangements will be compared to the reference tree and the reader should refer to Supplementary File S9 for additional details of those topologies, including branch lengths and node supports. In general, topological differences among models and methods were associated with low to intermediate supports (BS < 70, PP < 95). For each major clade in the Bayesian chronogram, the total number of synapomorphies obtained exclusively by the Bayesian method of ancestral state reconstruction (indicated by "BI" after the character) are listed, and also those obtained with both methods. See Supplementary File S14 for the plots of ancestral states reconstructed with BI, and Supplementary File S15 for the complete synapomorphy list, including those recovered exclusively by the MP ancestral reconstruction method, as well as the synapomorphies for minor clades. Authorship and first use of names adopted in the classification scheme used below are detailed in Supplementary File S16.

According to the results from the best-fitting dating model, FBF_TK02_TIP, the origin of Folivora and of its major clades (i.e., Mylodontoidea and Megatherioidea) took place between the middle and the late Eocene, whereas their diversification occurred during the late Oligocene. The origin and diversification of other important less inclusive clades (i.e., Scelidotheriidae, Mylodontidae, Megalonychidae and Megatheriidae) occurred between the latest Oligocene and the early Miocene (Fig. 9). In the dating model in which FBD parameters were allowed to change through time (SFBD_TK02_TIP), we observed a trend of increase in extinction rates towards the present, whereas speciation and fossilization remained relatively more stable. Fossilization rates increase slightly in the Oligocene, and speciation shows a positive trend in the early Miocene, with a speciation rate twice that observed for any other time bin. Except for speciation rates, very wide 95% HPDs were obtained for those estimates (Fig. 10, Supplementary File S17).

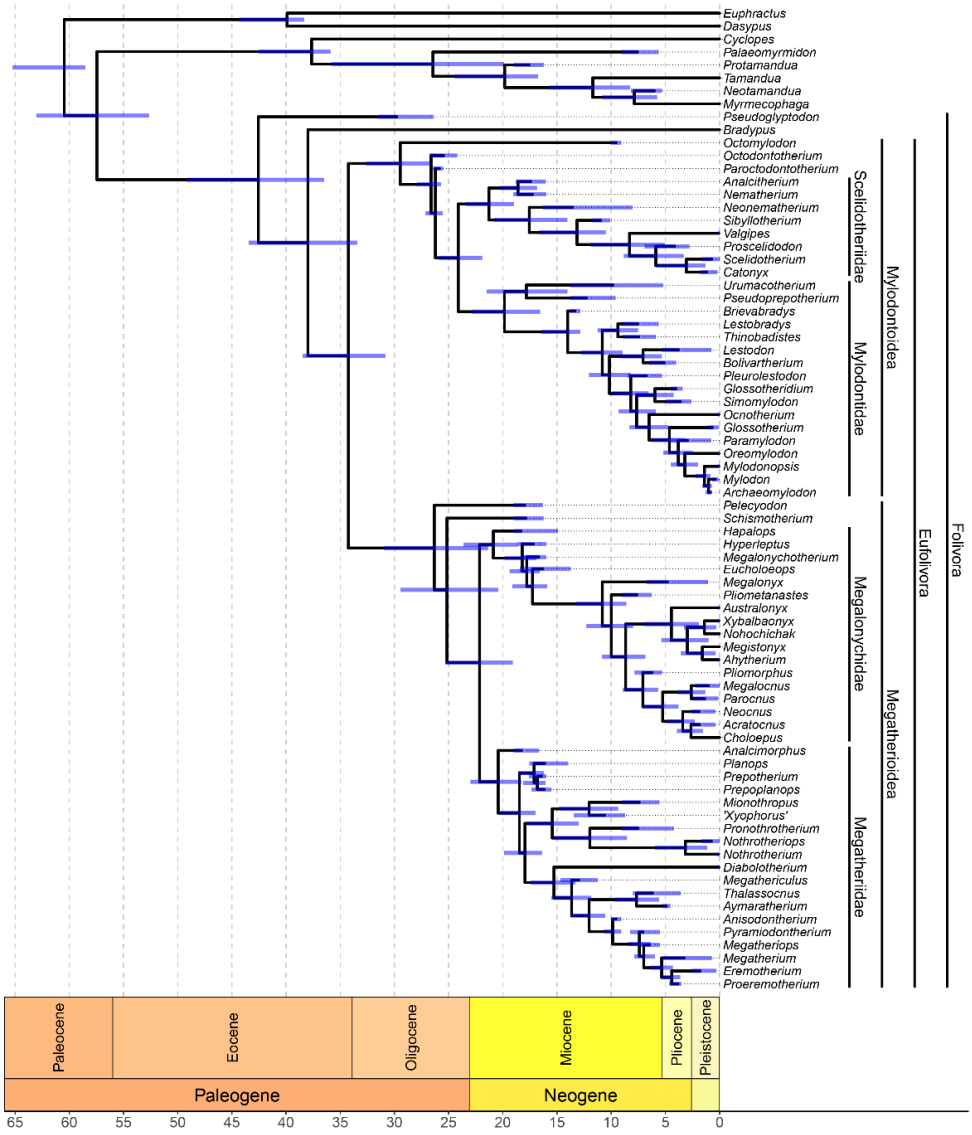

Figure 9. Bayesian chronogram for the best-fitting dating model (FBD_TK02_TIP). Blue bars depict uncertainty in estimates of node and tip ages. Main sloth clades are named at the right.

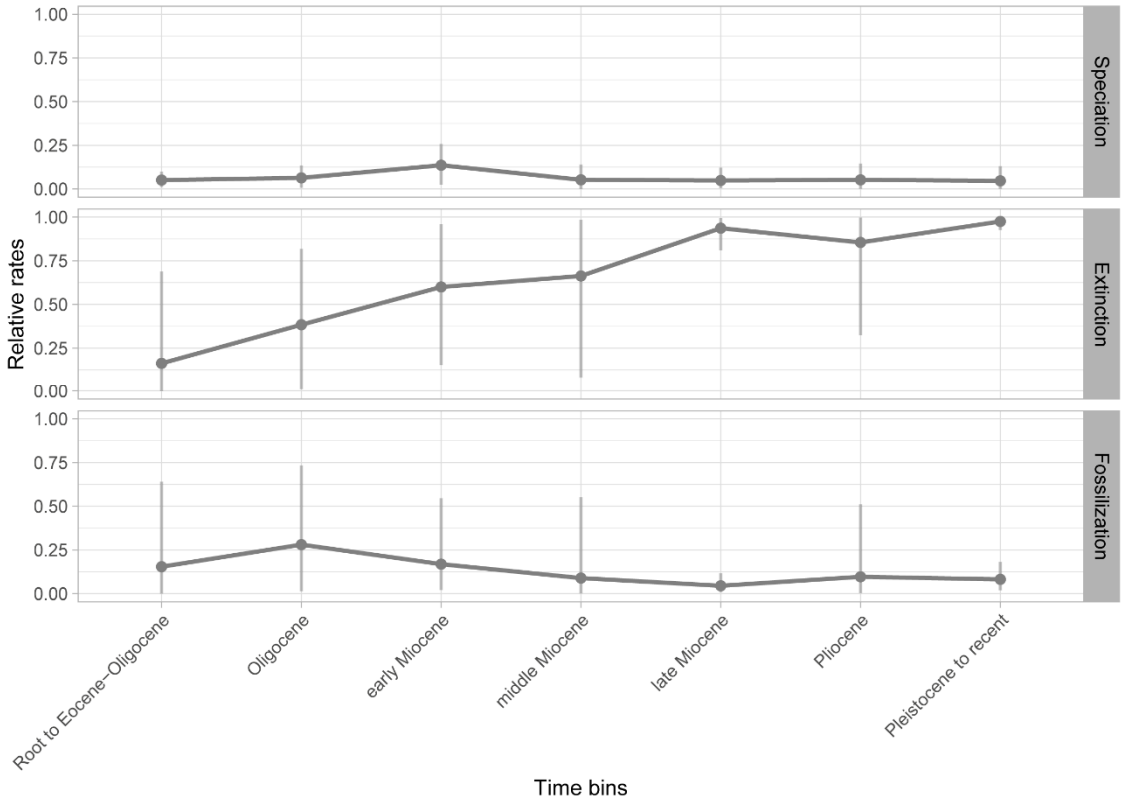

Figure 10. Relative rates (median and 95% HPD) of speciation, extinction and fossilization obtained with a skyline fossilized birth-death process for seven consecutive time bins.

FOLIVORA

PP = 100, Age = 42.56 [36.48 – 49.19]

The clade containing extant and extinct sloths was consistently recovered in all analyses performed in this study.

Folivora was supported by four synapomorphies (three for both methods and one exclusive for BI): mandibular horizontal ramus two times longer than its depth; presence of a mediolateral bulge in the horizontal ramus of mandible, at the level of toothrow (BI); fusion of mandibular symphysis; and the presence of an ascending process of jugal.

FOLIVORA minus Pseudoglyptodon

PP = 100, Age = 37.98 [33.43 – 43.47]

The clade is composed of the living genus *Bradypus* and Eufolivora. It was consistently recovered in all analyses performed in this study, except in par_EW consensus, in which *Psuedoglyptodon, Bradypus* and Eufolivora were arranged in a polytomy.

The clade was supported by nine synapomorphies (two for both methods and seven exclusively for BI): a large basin for the modified orthodentine core; ovate cf1 cross-section (BI); anteroposteriorly ovate Mf1 cross-section (BI); anteroposteriorly ovate mf1 cross-section (B1); bilobate Mf2 and Mf3 cross-section (BI); bilobate mf2 cross-section (BI); ascending ramus of mandible not covering the posterior teeth in lateral view (BI); presence of posterior external opening of mandibular canal; and maximum length of nasal bones greater than, or equal to, twice the width of both nasals, but less than three times (BI).

EUFOLIVORA

PP = 100, Age = 34.25 [30.81 – 38.47]

All sloths excluding *Pseudoglyptodon* and *Bradypus*. It is composed of two major clades, Mylodontoidea and Megatherioidea, and was consistently recovered in all analyses performed in this study.

Eufolivora was supported by eight synapomorphies (five for both methods and three exclusively for BI): parallel lateral edges of the mandibular spout (BI); orbital portion of lacrimal greater than facial portion; presence of middle process of jugal; tip of zygomatic process of squamosal extends anterior to fronto-parietal suture (BI); nuchal and exoccipital crests diverge distally (BI); tympanohyal wide distally, contributing to the formation of the

stylohyal fossa; fusion of the acromion with the coracoid process of the scapula; and femoral entepicondyle and ectepicondyle strongly projected beyond condyles.

MYLODONTOIDEA

PP = 100, Age = 29.46 [26.67 – 32.60]

The clade is composed of Scelidotheriidae, Mylodontidae and three stem mylodontoid genera, *Octomylodon, Octodontotherium* and *Paroctodontotherium*, this pattern being consistently recovered in all analyses performed in this study. Those three genera are recovered as successive sister groups to (Scelidotheriidae, Mylodontidae) in analyses with all H, UN_p and some A models. On the other hand, *Octodontotherium* and *Paroctodontotherium* are sister taxa and more closely related to (Scelidotheriidae, Mylodontidae) in MP analyses, and in some A models. In other analyses, using UN_e and other A models, the three genera were recovered as a clade and sister to Mylodontidae or to Mylodontinae, depending on the analysis.

Mylodontoidea was supported by eight synapomorphies (four for both methods and four exclusively for BI): absence of a mediolateral bulge in horizontal ramus of mandible, at toothrow (BI); absence of a medial ridge running along anterior edge of coronoid process; short and deep angular process (BI); condyles at or just above level of toothrow; mandibular symphysis longer than molariform toothrow (BI); snout elevated anteriorly; absence of prominent lateral walls in lacrimal foramen; and dorsal edge of entotympanic with a strong concave curvature in lateral view, with dorsal projection at anterior end (BI).

SCELIDOTHERIIDAE plus MYLODONTIDAE

PP = 98, Age = 24.11 [21.90 – 25.95]

As stated above, the group uniting the two clades was recovered in most of our analyses, except for UN_e and some A models, in which Mylodontidae (or Mylodontinae) is more closely related to *Octomylodon, Octodontotherium* and *Paroctodontotherium* than to Scelidotheriidae. The clade was supported by 4 synapomorphies, all exclusive to BI ancestral state reconstructions: Cf1 closer to Mf1 than to anterior edge of maxilla (BI); presence of fossa anterior to Cf1 (BI); Mf1 straight in lateral view (BI); and a high and narrow braincase (BI).

SCELIDOTHERIIDAE

PP = 100, Age = 21.28 [18.99 – 23.42]

This taxon, which is composed of the clades Nematheriinae and Scelidotheriinae, was recovered in all H and UN model analyses, and in some A models, par_EW and par_IW100 topologies. For other A models, Nematheriinae was recovered as sister to (Scelidotheriinae (Mylodontinae (stem mylodontoids))), whereas for par_IW10 and par_IW5 analyses, it was recovered as sister to the clade uniting Scelidotheriinae and Mylodontinae.

Scelidotheriidae was supported by 21 synapomorphies (seven for both methods and 14 exclusively for BI): long axis of molariforms oblique to toothrow along its entire length; molariform morphology of Cf1/cf1 (BI); subtriangular cf1 cross-section (BI); ellipsoid mf1 cross-section (BI); subtriangular Mf2 and Mf3 cross-section (BI); S-shaped mf3 cross-section (BI); presence of a medial ridge running along anterior edge of coronoid process (BI); presence of symphysial keel (BI); snout length greater than, but no more than twice its width; uniform snout in dorsal view; large supraoccipital exposure on cranial roof, expanded anteriorly at midline; absence of fossa at the anterior edge of maxilla, lateral to external nares; equivalent anterior extent of lateral and medial palatal processes of maxilla (BI); external occipital protuberance immediately posterior to dorsal nuchal crest (BI); circular shape of ectotympanic in lateral view (BI); lateral process of entotympanic extending above anterior portion of tympanic, forming a portion of the roof of tympanic cavity (BI); promontorium dorsoventrally elongate, flat anteriorly and globose posteriorly (BI); deltoid crest facing anteriorly, reaching the medial side of the humerus in anterior view; humeral head widely exposed, raised above the tubercules (BI); posterior end of pubic cornu reaching half of anteroposterior length of acetabulum, less extended than ischiatic cornu (BI); and concave cuboid facet of astragalus.

NEMATHERIINAE

PP = 100, Age = 18.60 [16.85 – 20.28]

This clade contains the genera *Nematherium* and *Analcitherium*, and was recovered in all analyses performed in this study.

Nematheriinae was supported by seven synapomorphies, all recovered with both methods: anteroposteriorly ovate Mf4 cross-section; snout depressed anteriorly; external nares not greatly enlarged; absence of pterygoid inflation; presence of lacrimal eminence; presence of prominent lateral walls in lacrimal foramen; and jugal and lacrimal anteriorly overlapping facial portion of maxilla.

SCELIDOTHERIINAE

PP = 100, Age = 17.55 [14.03 – 20.82]

The clade includes the genera *Neonematherium, Sibyllotherium, Valgipes, Proscelidodon, Catonyx* and *Scelidotherium*, and was recovered in all analyses performed in this study. The relationships among those genera were very consistent among analyses: (*Neonematherium*, (*Sibyllotherium*, (*Valgipes*, (*Proscelidodon*, (*Catonyx*, *Scelidotherium*))))). It was recovered in all but one analysis, par_EW, in which *Neonematherium* and *Sibyllotherium* are in a polytomy with the remaining scelidotheriines.

Scelidotheriinae was supported by six synapomorphies, all but one recovered by both methods: flat occlusal surface of molariforms; subtriangular Mf1 cross-section (BI); roughly horizontal profile of dorsal surface of the skull, in lateral view; presence of ventral extension in maxilla for dental alveoli; medial palatal process of maxilla extending anterior to lateral process; and well-developed, free-standing paracondylar processes.

MYLODONTIDAE

PP = 100, Age = 19.84 [16.56 – 22.90]

This taxon, composed of the clades Urumacotheriinae and Mylodontinae, was recovered in all analyses performed in this study, except the analysis using the UN_e model, in which Urumacotheriinae was recovered as sister to a clade composed of stem mylodontoids and Mylodontinae.

Mylodontidae was supported by 29 synapomorphies (13 for both methods and 16 exclusively for BI): Cf1 larger than the largest molariform (BI); anteroposteriorly ovate Mf2 and Mf3 cross-section (BI); anteroposteriorly ovate mf2 cross-section (BI); elongate and irregularly lobate mf3 cross-section (BI); presence of a corkscrew-like rotation in the plane of articulation of mandibular condyle; presence of buccinator fossa of maxilla; frontal and parietal flattened anteroposteriorly and mediolaterally; frontal sinus extends into nasal and parietal bones (BI); ectotympanic oriented anteromedially; absence of styliform process of ectotympanic; mastoid broadly exposed laterally (BI); stylomastoid canal ventrolaterally directed (BI); absence of entepicondylar notch (BI); lateral and medial epicondyles equally expanded in anterior view; olecranon quadrate in lateral view, with anterior and posterior margins parallel or diverging proximally; oval shape of radial head, in proximal view (BI); straight posterior border of radius, in lateral view; roughly straight radial diaphysis (BI); quadrangular laterodistal corner of

scaphoid, in dorsal view; intermediate tibial length, more than two times the width, but less than three times; lateral facet of anterior border of tibial proximal epiphysis located posterior to medial facet (BI); two deep grooves for tendons of *m. flexor hallucis longus*, *m. flexor digitorum longus* and *m. tibialis caudalis*; fibular facet of astragalus restricted to anterior surface (BI); discoid process of astragalus flat or roughly so, in lateral view; proximodistal length of the astragalus greater than or equal to anteroposterior length (BI); calcaneus tuberous and expanded, with distal apex rounded (BI); confluence between sustentacular facet and cuboid surface of calcaneus (BI); presence of an oblique crest on plantar side of calcaneus (BI); and broadly contiguous facets for cuboid and metatarsal III, in metatarsal IV.

URUMACOTHERIINAE

PP = 60, Age = 17.82 [14.03 – 21.51]

This clade was originally proposed with fewer taxa (Negri and Ferigolo 2004), but was expanded here to include both *Urumacotherium* and *Pseudoprepotherium.* It did not receive high node support, despite being present in trees from all analyses.

Urumacotheriinae was supported by seven synapomorphies (five for both methods and two exclusively for BI): molariform morphology of Cf1/cf1 (BI); posterior edge of mandibular condyle inclined posterodorsally; eversion of lateral edge of symphyseal spout (BI); premolariform portion of palate roughly equal or longer than the length of molariform toothrow; presence of a distinct neck at the base of occipital condyles; occipital condyles elongated anteroposteriorly in ventral view; and lesser tubercle of humerus proximally projected as much as greater tubercle.

MYLODONTINAE

PP = 100, Age = 14.01 [12.85 – 16.46]

This clade is composed of the genus *Brievabradys* and the clades Lestodontini (*sensu* Gaudin 2004) and Mylodontini. Mylodontinae is present in trees from all analyses, with the arrangement: (*Brievabradys*, (Lestodontini/"Lestodontini", Mylodontini)). Nevertheless, Lestodontini was not recovered as monophyletic in our reference topology, nor in the majority of analyses of this study. The exceptions were UN and A models with ACRV modeled per partition (_p) and par_IW5. Because of that, we recognized two clades here, Thinobadistini and Lestodontini (*sensu* McKenna and Bell 1997). The clade which is more closely related to Mylodontini varies among analyses – (*Thinobadistes*, *Lestobradys*) in some, (*Lestodon*,

Bolivartherium) in others. In par_EW, Thinobadistini is not recovered and *Thinobadistes* and *Lestobradys* are both in a polytomy with Lestodontini and Mylodontini.

Mylodontinae was supported by ten synapomorphies (three for both methods and seven exclusively for BI): cf1 larger than largest molariform (BI); Cf1 equidistant from the anterior edge of the maxilla and from Mf1 (BI); absence of fossa anterior to Cf1 (BI); presence of anterior projection of alveoli of Cf1/cf1; Mf1 recurved posteriorly in lateral view (BI); trigonal Cf1 cross-section (BI); trigonal cf1 cross-section (BI); mandibular symphysis shorter or roughly equal to molariform toothrow; presence of symphysial keel (BI); and length of symphysial spout shorter than or equal to its width.

THINOBADISTINI

PP = 81, Age = 9.38 [7.52 – 11.26]

The clade is composed of *Thinobadistes* and *Lestobradys* and was recovered in all analyses, with the exception of par_EW.

Thinobadistini was supported by a single synapomorphy, obtained with both methods: The presence of a diastema between Mf1 and Mf2.

LESTODONTINI

PP = 100, Age = 7.06 [5.32 – 9.16]

The clade is composed of *Lestodon* and *Bolivartherium* and was recovered in all analyses.

Lestodontini was supported by 11 synapomorphies (six for both methods and five exclusively for BI): presence of a well-developed diastema between Cf1/cf1 and molariforms; Cf1 closer to anterior edge of maxilla than to Mf1; Cf1/cf1 displaced laterally relative to molariform toothrow; anteroposteriorly ovate mf1 cross-section (BI); anteroposteriorly ovate mf2 cross-section (BI); maximum length of nasal bones greater than or equal to three times the width of both nasals (BI); attachment of the base of jugal to skull dorsal to Mf2 (BI); well-developed buccinator fossa of maxilla, with a deep depression; absence of a crest at median suture of palatine; dorsally situated infraorbital canal; and posteroventrally inclined occipital condyle in lateral view (BI).

MYLODONTINI

PP = 100, Age = 8.19 [6.54 – 9.95]

This clade is composed of ten genera, with the following arrangement in all analyses using H models: (*Pleurolestodon,* ((*Simomylodon, Glossotheridium*), (*Ocnotherium*, (*Glossotherium,* (*Paramylodon*, (*Oreomylodon*, (*Mylodonopsis*, (*Archaeomylodon*, *Mylodon*)))))))). For UN and A models not accounting for ACRV (_e), and MP trees, several alternative arrangements can be observed, regarding the positions of *Pleurolestodon*, *Ocnotherium, Oreomylodon, Glossotherium* and *Paramylodon*, whereas the clades (*Simomylodon*, *Glossotheridium*) and (*Mylodonopsis*, (*Archaeomylodon*, *Mylodon*)) are stable.

Mylodontini was supported by 11 synapomorphies (seven for both methods and four exclusively for BI): Cf1 smaller than the smallest molariform; cf1 smaller than the smallest molariform (BI); ovate Cf1 cross-section; presence of internal ridge running obliquely or vertically from ventral edge of ascending ramus, near the base of the angle, towards the last tooth; length of coronoid process greater than its height (BI); absence of a mandibular fossa posterior to cf1 (BI); temporal lines laterally situated, do not approximate midline of skull roof; posterior segments of temporal lines run anterior to but closely parallel the nuchal crest; medial palatal processes of maxilla anterior to lateral process; presence of osteoderms; and a slightly obtuse (around 120°) angle formed by discoid and odontoid facets of astragalus, in distal view (BI).

MEGATHERIOIDEA

PP = 99, Age = 26.32 [21.32 – 30.99]

The clade, composed of *Pelecyodon*, *Schismotherium*, Megalonychidae and Megatheriidae, was recovered in all analyses using MP methods and all Bayesian analyses using H models. In analyses with UN and A models, it was recovered as paraphyletic, with Mylodontoidea closely related to Megatheriidae or Megatheriinae. When Megatherioidea was recovered as monophyletic, *Pelecyodon* and *Schismotherium* emerged as successive sister taxa of a clade containing megalonychids and megatheriids (H models, par_EW and par_IW100), or, together with *Hapalops*, composing a clade that is more closely related to megatheriids than to megalonychids (par_IW10 and par_IW5). When Megatherioidea was paraphyletic (A models), *Pelecyodon* and *Schismotherium* compose a sister clade to all other eufolivorans.

Megatherioidea was supported by 43 synapomorphies (18 for both methods and 25 exclusively for BI): left and right molariform toothrows parallel in occlusal view (BI); cementum slightly

thicker than the orthodentine; occlusal surface of molariforms with strong transverse crests (BI); Mf4 curved anteriorly in lateral view; circular Mf1 cross-section (BI); mediolaterally ovate to rectangular mf1 cross-section (BI); mediolaterally ovate to rectangular Mf2 and Mf3 cross-section (BI); mediolaterally ovate to rectangular mf2 cross-section (BI); circular mf3 cross-section; inferior edge of mandible with strongly convex ventral bulge (BI); presence of a constriction at the junction of horizontal and ascending rami of mandible (BI); elongate and narrow angular process (BI); symphysis ending well anterior to the level of mf1; presence of symphysial keel (BI); symphysial spout equal to, or slightly shorter than the length of molariform toothrow (BI); eversion of lateral edge of symphyseal spout (BI); lateral edges of the spout converging anteriorly (BI); presence of a mandibular fossa posterior to cf1; roughly horizontal dorsal surface of the skull; temporal lines meet in the dorsal midline to form a sagittal crest; presence of fossa at the root of zygoma, anterodorsal to paroccipital process; presence of buccinator fossa of maxilla; presence of maxillary fossa behind last upper tooth; palate concave anteriorly, and convex posteriorly to dentition (BI); interpterygoid region broader than interpalatine region (BI); absence of pterygoid inflation (BI); presence of lacrimal eminence; anterior overlap of jugal and lacrimal over facial portion of maxilla; short and deep middle process of jugal (BI); tip of zygomatic process of squamosal at or posterior to fronto-parietal suture (BI); presence of a marked postorbital constriction (BI); occipital condyle elongated anteroposteriorly, in ventral view; absence of a median ridge of basisphenoid (BI); ventral edge of entotympanic extended into anteroventral process; posteroventral stylomastoid canal (BI); rugose posterior surface of glenoid; well-developed entoglenoid process; convex posterior margin of ulnar diaphysis, in lateral view (BI); presence of deep notch for medial cruciate (posterior) ligament in femur (BI); equivalent transverse diameters of discoid and odontoid facets of astragalus, in dorsal view (BI); posterior surface of fibular facet of astragalus greatly reduced dorsoventraly (BI); roughly right-angled facets for cuboid and metatarsal IV, in metatarsal V; and laterally oriented expansion of metatarsal V.

MEGALONYCHIDAE plus MEGATHERIIDAE

PP = 100, Age = 22.14 [19.08 – 25.29]

The clade, which includes all megatherioids excepting the genera *Pelecyodon* and *Schismotherium*, was recovered in all Bayesian analyses using H models, and in par_EW and par_IW100, although in these MP analyses, *Hapalops* was not recovered closely associated with megalonychids, but as sister to the clade uniting all other megalonychids and megatheriids. In par_IW10 and par_IW5, a distinct arrangement was obtained, with a clade (*Hapalops*,

(*Pelecyodon*, *Schismotherium*)) recovered as sister to Megatheriidae. In trees from analyses with UN and A models, in which Megatherioidea was recovered as paraphyletic, the clade uniting Megalonychidae and Megatheriidae is also absent.

The clade was supported by 16 synapomorphies (11 for both methods and five exclusively for BI): Cf1 and cf1 slightly depressed ventrally relative to molariforms; presence of a well-developed diastema between Cf1/cf1 and molariforms; ovate mediolaterally to rectangular Mf1 cross-section (B1); mandibular symphysis longer than molariform toothrow; horizontal orientation of spout, in lateral view; external opening of mandibular canal opens anterolaterally, on ascending ramus (B1); tip of zygomatic process anterior to fronto-parietal suture; nuchal crest splits dorsally into anterior and posterior crests, with a raised triangular area in the dorsal surface of the skull roof (B1); nuchal crest overhangs occiput posteriorly; presence of a distinct neck at the base of occipital condyles (B1); rugose ectotympanic external surface; presence of an ectotympanic medial expansion; presence of pterygoid lateral groove for *m. tensor veli palatini*; medial extent of trochlear notch of ulna equal to or less than that of the olecranon (B1); straight posterior margin of ulnar diaphysis in lateral view; and lateroproximal process of tuber calcis more distal than medioproximal process.

MEGALONYCHIDAE

PP = 63, Age = 20.88 [18.61 – 23.61]

The position of *Hapalops* as a stem megalonychid was recovered in all BI analyses, but was poorly supported. The clade containing all other Megalonychidae will be detailed below.

Megalonychidae was supported by seven synapomorphies (one for both methods and six exclusively for BI): Cf1 closer to anterior edge of maxilla than to Mf1 (BI); maximum height of coronoid process greater than its anteroposterior length (BI); large supraoccipital exposure on cranial roof, expanded anteriorly at midline; triangular occiput in posterior view (BI); presence of paroccipital process foramen (BI); eustachian tube opening formed by entotympanic and ectotympanic (BI); and absence of a deep notch for medial cruciate (posterior) ligament in femur (BI).

MEGALONYCHIDAE minus Hapalops

PP = 100, Age = 18.21 [16.90 – 19.84]

This clade is composed of the Santacrucian genera *Hyperleptus, Megalonychotherium* and *Eucholoeops*, and by Megalonychinae. In all BI analyses and in par_IW, those three genera

diverge successively, following the arrangement (*Hyperleptus*, (*Megalonychotherium*, (*Eucholoeops*, Megalonychinae))). In par_IW10 and par_IW5, they form a clade (*Megalonychotherium*, (*Hyperleptus*, *Eucholoeops*)), which is sister to Megalonychinae, and in par_EW, *Megalonychotherium* and *Hyperleptus* are in a polytomy with *Eucholoeops* and Megalonychinae.

The clade was supported by 18 synapomorphies (11 for both methods and seven exclusively for BI): Cf1 within size range of molariforms; presence of fossa on palatal surface of maxilla posterior to Cf1; maximum height of coronoid process shorter than its anteroposterior length (BI); snout elevated anteriorly; snout flared anteriorly, in dorsal view (BI); maximum length of nasal bones less than twice the width of both nasals; uniform nasal width in its anterior half, with lateral margins parallel (BI); well-developed buccinator fossa of maxilla, with a deep depression (BI); mediolateral width of premaxillary lateral rami greater than the anteroposterior length of incisive foramen; presence of a plate-like area anterior to incisive foramen; presence of pterygoid inflation (BI); elongate, triangular middle process of jugal (BI); dorsally situated infraorbital canal; deep zygomatic process, almost covers the entire squamosal exposure; pointed free end of zygomatic process; postorbital process of frontal roughly at the level of maxillary foramen; uniformly wide nuchal crest (BI); and medial expansion of entotympanic dorsal to basicranium.

MEGALONYCHINAE

PP = 100, Age = 10.82 [8.60 – 13.21]

This clade is composed of the genera *Megalonyx* (Megalonychini) and *Pliometanastes*, plus a clade uniting *Pliomorphus*, Antillean megalonychines and *Choloepus* – Choloepodini, and a clade of intertropical megalonychids – Ahytheriini. Alternative arrangements were observed for the relationships among *Megalonyx, Pliometanastes,* and the other megalonychines: as successive sister taxa, diverging earlier than all other megalonychines – *Megalonyx* earliest (H models EW and IW100, par_EW and par_IW100), *Pliometanastes* earliest (UN and A models, especially those including ACRV); *Megalonyx* and *Pliometanastes* as sister taxa to each other, and this clade sister to all other megalonychines (A models with equal rates, excepting A1_e); or as sister to intertropical sloths (H models IW10 and IW5, par_IW10 and par_IW5).

Megalonychinae was supported by 59 synapomorphies (24 for both methods and 35 exclusively for BI): Cf1 and cf1 strongly depressed relative to molariforms; Cf1 smaller than smallest molariform (BI); long axis of molariforms oblique to toothrow along its entire length; trapezoidal Mf2 and Mf3 cross-section; trapezoidal mf2 cross-section; trigonal Mf4 cross-

section; mandibular horizontal ramus length less than two times its depth (BI); ascending ramus of mandible completely covers the posterior teeth in lateral view (BI); three processes of ascending mandibular ramus equidistant (BI); absence of a medial ridge running along anterior edge of coronoid process (BI); maximum height of coronoid process shorter than its anteroposterior length (BI); intermediate development of angular process; symphysial spout much shorter than the length of molariform toothrow (BI); posterior external opening of mandibular canal opens laterally on horizontal ramus (BI); low and broad braincase (BI); reflexed basicranial/basifacial axis; nuchal crest continuous with dorsal edge of zygomatic process of squamosal (BI); premolariform portion of palate roughly equal to, or longer than molariform toothrow (BI); presence of fossa at the anterior edge of maxilla, lateral to external nares (BI); presence of ventral extension in maxilla for dental alveoli (BI); ventral extension in maxilla for dental alveoli only posteriorly (BI); jugal does not participate in rim of maxillary foramen (BI); absence of dorsal process of premaxilla; presence of a crest at median suture of palatine (BI); presence of alisphenoid-parietal contact (BI); anteroventrally inclined zygomatic process of squamosal; absence of a marked postorbital constriction (BI); postorbital process well anterior to maxillary foramen; semicircular occiput, in posterior view (BI); hypoglossal foramen smaller than jugular foramen (BI); basioccipital narrow and convex mediolaterally (BI); median fusion of posterior alae of vomer; ectotympanic fused dorsally; carotid foramen fully exposed in ventral view (BI); anteroposteriorly oriented entotympanic (BI); dorsal edge of entotympanic with a strong concave curvature in lateral view, with dorsal projection at anterior end (BI); lateral process of entotympanic extending above anterior portion of tympanic, forming a portion of the roof of tympanic cavity (BI); bulbous, mediolaterally expanded paroccipital process; absence of paroccipital process foramen (BI); nuchal and exoccipital crests diverge proximally and converge distally (BI); posteroventrolateral stylomastoid canal; entotympanic, ectotympanic and pterygoid composing eustachian tube opening (BI); hypoglossal foramen recessed dorsally, lies at same level as jugular foramen; presence of a groove connecting the internal opening of the posterior lacerate foramen to foramen magnum; glenoid fossa ventral to superficies meatus; mediolaterally widened glenoid fossa (BI); smooth posterior surface of glenoid; glenoid fossa well-separated from porus acusticus (BI); laterally directed root of zygoma; deltoid crest faces anteriorly, reaching the medial side of the humerus in anterior view (BI); strongly marked brachiocephalicus crest of humerus (BI); quadrangular laterodistal corner of scaphoid, in dorsal view (BI); fusion of trapezium and metacarpal I, forming the carpal-metacarpal complex; absence of a strong concavity between greater trochanter and the head of femur (BI); moderately developed lesser trochanter of femur, with a

laminar projection; femoral patellar trochlea isolated or only abuts the condylar surfaces; medial trochlear ridge protruded anteriorly to lateral trochlear ridge (BI); distal epiphyses of femur twisted with respect to the main axis; and an obtuse (around 120°) angle formed by facets for cuboid and metatarsal IV, in metatarsal V.

CHOLOEPODINI plus AHYTHERIINI

PP = 69, Age = 8.66 [6.84 – 10.85]

This clade was recovered in most of the analyses performed in this study but was not well-supported. The exceptions for the presence of the clade were two analyses with H models – IW10 and IW5, par_IW10 and par_IW5, in which the intertropical megalonychids were recovered more closely related to a clade uniting *Megalonyx* and *Pliometanastes*.

The clade was supported by 11 synapomorphies (seven for both methods and four exclusively for BI): mandibular symphysis extends posterior or to the level to mf1; lateral edge of symphyseal spout not everted; temporal lines approximate midline, but do not meet to form a sagittal crest (BI); presence of a contact between maxilla and lacrimal, within orbit; absence of a crest at median suture of palatine; interpterygoid region narrower than interpalatine region (BI); presence of pterygoid inflation; presence of a median ridge of basisphenoid (BI); jugular foramen well-separated from hypoglossal foramen; presence of glenoid posterior shelf; and convex posterior margin of ulnar diaphysis in lateral view (BI).

AHYTHERIINI

PP = 100, Age = 4.44 [1.93 – 6.98]

This clade, composed of the intertropical megalonychids *Australonyx, Ahytherium, Megistonyx, Nohochichak* and *Xibalbaonyx*, was consistently recovered in all of our analyses, with two alternative arrangements: (*Australonyx,* ((*Ahytherium, Megistonyx*), (*Nohochichak*, *Xibalbaonyx*))) in all BI analyses and in par_EW, and (*Australonyx,* (*Xibalbaonyx*, (*Nohochichak*, (*Ahytherium, Megistonyx*)))) for IW parsimony analyses.

Ahytheriini was supported by 23 synapomorphies (13 for both methods and ten exclusively for BI): absence of fossa on palatal surface of maxilla posterior to Cf1; circular Mf1 cross-section (BI); ascending ramus of mandible partially covers posterior teeth in lateral view (BI); coronoid process not hooked posteriorly (BI); posterior external opening of mandibular canal opens anterolaterally, on ascending ramus; high and narrow braincase (BI); nasal uniform width in its posterior half, lateral margins parallel (BI); interpterygoid and posterior interpalatine regions

of roughly equal width (BI); large sinus in pterygoid; ventrally situated infraorbital canal; absence of alisphenoid-parietal contact (BI); presence of a marked postorbital constriction; postorbital process of frontal roughly at the level of maxillary foramen (BI); triangular occiput in posterior view (BI); occipital condyles situated well dorsal to the dentition (BI); anteromedially orientation of entotympanic (BI); weakly marked brachiocephalicus crest of humerus (BI); humeral head almost hidden behind the tubercles; anconeal process of ulna not extended anteriorly, not overhanging trochlear notch; widest extension of pronator ridge at the proximal half of radial diaphysis (BI); proximal half of femur narrower than distal half; intermediate tibial length, more than two times the width, but less than three times; and fusion of metatarsal I with entocuneiform.

CHOLOEPODINI

PP = 98, Age = 7.07 [5.67 – 8.93]

This clade is composed of the genus *Pliomorphus*; the Antillean megalonychines *Megalocnus*, *Parocnus*, *Neocnus*, and *Acratocnus*; and, the living sloth genus *Choloepus*. It was consistently recovered in our analyses with the arrangement (*Pliomorphus*, ((*Megalocnus*, *Parocnus*), (*Neocnus*, (*Acratocnus*, *Choloepus*)))). In one exception – in par_EW, *Neocnus*, *Acratocnus* and *Choloepus* were recovered in a polytomy.

Choloepodini was supported by eight synapomorphies (six for both methods and two exclusively for BI): snout downturned anteroventrally, in lateral view; evenly convex dorsal surface of the skull; minimum width of palate between toothrows equal or less than width of Mf2; absence of postorbital process of zygomatic arch; occiput wider than deep; presence of recessus meatus (BI); presence of a strong concavity between greater trochanter and the head of femur (BI); and patellar trochlea confluent with lateral, but not with medial condylar surface.

MEGATHERIIDAE

PP = 100, Age = 20.43 [18.28 – 22.99]

This clade is composed of the genus *Analcimorphus* and the clades Prepotheriinae, Nothrotheriinae and Megatheriinae. Megatheriidae was recovered in all MP analyses and all BI analyses with H models, and was absent in all analyses with UN and A models, given the nested position of Mylodontoidea in this clade. *Analcimorphus* was consistently recovered as a stem member of this clade.

Megatheriidae was supported by 12 synapomorphies (eight for both methods and four exclusively for BI): presence of fossa anterior to Cf1 (BI); snout length greater than its width, but no longer than two times the width; uniform nasal width in its posterior half, with lateral margins parallel (BI); premolariform portion of palate roughly equal or longer than molariform toothrow; absence of a crest at median suture of palatine (BI); absence of a marked postorbital constriction; well-developed ventral nuchal crest; carotid foramen fully covered in ventral view; entotympanic dorsal edge with a strong concave curvature in lateral view, and a dorsal projection at anterior end; entotympanic forming almost the entire floor of the tympanic cavity medial wall; nuchal and exoccipital crests parallel (BI); and lateral expansion of metatarsal V proximolaterally oriented.

MEGATHERIIDAE minus Analcimorphus

PP = 100, Age = 18.47 [16.97 – 20.24]

This clade is composed of the clades Prepotheriinae, Nothrotheriinae and Megatheriinae, which were recovered in two alternative arrangements: (Prepotheriinae, (Nothrotheriinae, Megatheriinae)) for H models, par_IW10 and par IW5, and (Megatheriinae, (Nothrotheriinae, Prepotheriinae)) for par_EW and par_IW_100. For A models that contain the clade, both arrangements were observed.

The clade was supported by 17 synapomorphies (ten for both methods and seven exclusively for BI): Cf1 closer to Mf1 than to anterior edge of maxilla (BI); deep zygomatic process, almost covers the entire squamosal exposure; occiput vertical or slightly inclined posterodorsally; sessile occipital condyles (BI); median fusion of posterior alae of vomer; medial expansion of entotympanic dorsal to basicranium; occipital artery passes through a closed canal in mastoid; absence of intertrochanteric ridge; moderately developed lesser trochanter of femur, with a laminar projection (BI); distal epiphyses of femur twisted with respect to the main axis (BI); lateral facet of anterior border of tibial proximal epiphysis located posterior to medial facet (BI); distal fibular articulation for tibia posterolaterally positioned; odontoid process well defined only on distal half of proximodistal length of tibial surface (BI); slightly obtuse (around 120°) angle formed by discoid and odontoid facets of astragalus, in distal view; process for navicular on astragalus at the level of the odontoid facet; transverse diameter of discoid facet of astragalus smaller than that of odontoid facet (BI); and obtuse (around 120°) angle formed by facets for cuboid and metatarsal IV, in metatarsal V.

PREPOTHERIINAE

PP = 99, Age = 17.11 [16.20 – 18.61]

The clade is composed of the genera *Prepotherium*, *Planops* and *Prepoplanops* and was consistently recovered in all of our analyses. *Planops* was recovered as the sister taxon to a clade uniting the other two genera in all but four analyses, those with H models – IW10_e, IW10_p, IW5_e and IW5_p. In these cases, *Prepotherium* assumed a stem position.

Prepotheriinae was supported by 14 synapomorphies (ten for both methods and four exclusively for BI): absence of fossa anterior to Cf1 (BI); posterior segments of temporal lines run anterior to but closely parallel the nuchal crest (BI); postorbital process roughly at the level of maxillary foramen; triangular occiput in posterior view (BI); condyles lie just posterior, almost continuous with hypoglossal foramina (BI); absence of styliform process of ectotympanic; anteroposterior orientation of entotympanic; ventrolateral orientation of stylohyal articulation; presence of glenoid posterior shelf; strongly marked brachiocephalicus crest of humerus; medial epicondyle of humerus rounded to slightly pointed laterally; proximal half of femur wider than distal half; calcaneus tuberous and expanded, with distal apex rounded; and confluence of sustentacular facet and cuboid surface of calcaneus.

NOTHROTHERIINAE plus MEGATHERIINAE

PP = 54, Age = 17.96 [16.39 – 19.87]

This clade, which unites the clades Nothrotheriinae and Megatheriinae, was recovered only for H models and par_IW10 and par IW5, as stated above, and was poorly supported.

The clade was supported by 4 synapomorphies, recovered with both methods: presence of lingual and labial grooves in mf3; temporal lines approximate midline but do not meet to form a sagittal crest on skull roof; well-developed buccinator fossa of maxilla, with a deep depression; and Glaserian fissure opening into a distinct groove in squamosal lying medial to entoglenoid process.

NOTHROTHERIINAE

PP = 100, Age = 15.44 [13.02 – 17.76]

The clade is composed of five genera consistently recovered in all analyses with the following arrangement: ((“*Xyophorus”*, *Mionothropus*), (*Pronothrotherium*, (*Nothrotherium, Nothrotheriops*))).

Nothrotheriinae was supported by 24 synapomorphies (12 for both methods and 12 exclusively for BI): trapezoidal Mf2 and Mf3 cross-section (BI); absence of a corkscrew-like rotation in the plane of articulation of mandibular condyle, in dorsal view (BI); presence of angle at the junction of symphysis and lower edge of horizontal ramus of mandible in lateral view (BI); large supraoccipital exposure on cranial roof, expanded anteriorly at midline; posterior segments of temporal lines run anterior to but closely parallel the nuchal crest (BI); nasal expands posteriorly, lateral margins divergent (BI); lateral and medial palatal processes of maxilla of equivalent length; interpterygoid and posterior interpalatine regions of roughly equal width; presence of pterygoid/vomer contact (BI); large sinus in pterygoid; alisphenoid-parietal contact present (BI); external occipital protuberance ventral to dorsal nuchal crest, in line with ventral nuchal crest (BI); posterior edge of occipital condyles ends at or anterior to posterior edge of foramen magnum superior border; very large exposure of vomer in nasopharynx, covers presphenoid and much of basisphenoid; pterygoid does not participate in bony wall of tympanic cavity; anteroventral process of tegmen tympani as a large bony mass; occipital artery passes through a short canal in mastoid, perforating paroccipital process; glenoid fossa well-separated from porus acusticus (BI); anteriorly directed root of zygoma; humeral head widely exposed, raised above the tubercles (BI); proximolateral process of metacarpal II does not extensively overlap metacarpal III proximally, contacting magnum (BI); absence of a detached sulcus delimitating, both medially and laterally, the articular surface of the femoral head in anterior view (BI); absence of a strong concavity between greater trochanter and the head of femur; and femoral patellar trochlea isolated or only abuts the condylar surfaces.

MEGATHERIINAE

PP = 100, Age = 15.28 [13.30 – 17.45]

The clade, which was recovered in all of our analyses, is composed of the stem genera *Diabolotherium* and *Megathericulus* and the clades Thalassocnini and Megatheriini. The arrangement (*Diabolotherium*, (*Megathericulus*, (Thalassocnini, Megatheriini))) was recovered in all BI analyses and in par_IW10. In par_EW and par_IW100, the order of divergence between *Diabolotherium* and *Megathericulus* is reversed, whereas in par_IW5, *Aymaratherium* and *Thalassocnus* are successively sister taxa to Megatheriini, not forming a clade.

Megatheriinae was supported by 16 synapomorphies (11 for both methods and five exclusively for BI): Cf1 and cf1 dorsoventrally aligned with molariforms; absence of a well-developed diastema between Cf1/cf1 and molariforms; Cf1 within size range of molariforms; cf1 within size range of molariforms; molariform morphology of Cf1/cf1; trapezoidal Cf1 cross-section;

trapezoidal cf1 cross-section; absence of a mandibular fossa posterior to cf1; nuchal crest continuous with dorsal edge of zygomatic process of squamosal (BI); anteroventrally inclined zygomatic process of squamosal; postorbital process roughly at the level of maxillary foramen (BI); distinct neck present at the base of occipital condyles (BI); carotid foramen partially covered ventrally by entotympanic and ectotympanic, in ventral view; glenoid fossa well-separated from porus acusticus (BI); absence of entepicondylar foramen of humerus; and medial (trochlear) portion of trochlear notch extends proximal to lateral (capitular) portion (BI).

THALASSOCNINI plus MEGATHERIINI

PP = 99, Age = 12.03 [10.56 – 13.75]

This clade was consistently recovered in all analyses performed in this study although, as stated above, a monophyletic Thalassocnini is absent from par_IW5.

The clade was supported by nine synapomorphies (seven for both methods and two exclusively for BI): premolariform portion of palate much shorter than the length of molariform toothrow (BI); lateral and medial palatal processes of maxilla of equivalent length; ectotympanic fused dorsally; hypoglossal foramen recessed dorsally, lies at same level as jugular foramen (BI); hemispherical glenoid fossa; three shallow grooves for tendons of *m. flexor hallucis longus*, *m. flexor digitorum longus* and *m. tibialis caudalis*; odontoid process of astragalus well defined along entire proximodistal length of tibial surface; discoid and odontoid facets of astragalus roughly at right angles to one another in distal view; and proximodistal length of astragalus greater than or equal to anteroposterior length.

THALASSOCNINI

PP = 100, Age = 7.67 [5.60 – 9.67]

This clade was recovered in all analyses performed in this study, except, as stated above, in par_IW5, in which *Aymaratherium* and *Thalassocnus* are successive sister taxa to Megatheriini.

Thalassocnini was supported by five synapomorphies (one for both methods and four exclusively for BI): horizontal ramus of mandible length greater than or equal to two times the depth, but less than three times (BI); straight anterior edge of symphysis, in lateral view (BI); lesser tubercle of humerus less proximally projected than greater tubercle (BI); presence of entepicondylar foramen of humerus; and confluence of sustentacular facet and cuboid surface of calcaneus (BI).

MEGATHERIINI

PP = 100, Age = 9.85 [9.07 – 10.67]

This clade was consistently recovered in all analyses performed in this study with an invariable arrangement: (*Anisodontherium*, (*Pyramiodontherium*, (*Megatheriops*, (*Megatherium*, (*Proeremotherium*, *Eremotherium*))))).

Megatheriini was supported by eight synapomorphies, all but one, recovered with both methods: thickness of cementum much larger than orthodentine; mf3 smaller than next smallest molariform; reflexed basicranial/basifacial axis; profile of nasal region and braincase relatively horizontal, but nasal region depressed relative to braincase; maximum length of nasal bones greater than or equal to three times the width of both nasals (BI); presence of ventral extension in maxilla for dental alveoli; concave mediolateral contour of palate; and occipital condyles situated well dorsal to the dentition.

3.4 DISCUSSION

3.4.1 Morphological data partitioning

Our results strongly indicate that homoplasy partitioning outperforms anatomical partitioning and unpartitioned analyses, resulting in higher marginal likelihoods, higher node supports (PP) and more precise estimates of rate multipliers (Figs. 3, 5 and 6). These results agree with a previous analysis of three empirical datasets using the homoplasy criterion to partition morphological datasets in Bayesian inferences (Rosa et al. 2019). The results obtained here are also aligned with those from a systematic exploration of empirical and simulated datasets, which indicated that anatomical partitioning does not improve tree topologies relative to unpartitioned analyses (Casali et al. 2021 – Chapter 1), even though they can be preferred to unpartitioned models with Bayes factor comparisons (Clarke and Middleton 2008; Tarasov and Génier 2015; Varela et al. 2019; Porto et al. 2021). Additionally, we observed that small partitions (< 10 characters) substantially decreased the precision of estimates and the signal-to-noise ratio, and they should be avoided whenever possible.

A possible reason for the inferior performance of the anatomical partitions relative to homoplasy is that subsets defined by this criterion may not provide an adequate segregation of characters by their evolutionary rates, since anatomical partitions are composed of characters of variable nature, like changes in shape, size, proportions, relative organization, and the presence or absence of disparate kinds of structures (Casali et al. 2021 – Chapter 1). It is unlikely that all those characters share similar evolutionary rates only because they are located

in a same anatomic region. The inferior performance of those models also suggest that sloths do not present a modular pattern of evolution associated with the proposed partitions (Clarke and Middleton 2008; Melo et al. 2016), with the characters considered here showing a considerable degree of evolutionary independence inside anatomical partitions. The preference for anatomical partitioning models which account for ACRV relative to those with equal rates further supports this interpretation.

The approach of defining partitions by homoplasy may raise some questions, since the degrees of homoplasy are calculated using trees from MP analyses, which are not immune to biased reconstructions due to long-branch attraction (LBA, Felsenstein 1978; Bergsten 2005). Since LBA artifacts are not restricted to MP analyses (Bergsten 2005), it seems more likely that performing BI with models that do not properly account for rate heterogeneity among characters due to homoplasy may result in reconstruction artifacts, and this may be more pronounced in datasets with much character conflict. Here we explored the effect of using four alternative MP topologies to calculate the number of extra steps for characters, and we observed that this had a small but non-negligible effect in the defined partitions, so we suggest that future studies should not restrict themselves to using the default IW setting in TNT (k = 3), as has been done in previous studies (Rosa et al. 2019; Brazeau et al. 2020; Lucena and Almeida 2021; Porto and Almeida 2021). Bayes factor comparisons unambiguously prefer models which account for heterogeneity among partitions due to homoplasy, indicating that the segregation of characters in partitions obtained from any of the MP topologies is still a more efficient approach than the anatomical partitioning schemes, since it is unnecessary to model ACRV for homoplasy-based partitions, as already demonstrated by Rosa et al. (2019). It remains to be seen if different homoplasy metrics, like the retention index (Farris 1989), which have different properties and limitations (Sanderson and Donoghue 1989; Murphy et al. 2021), would confirm the general behavior of partitioning by homoplasy observed here and in previous studies.

Trees obtained by unpartitioned and anatomically partitioned models resulted in topologies quite distinct from those obtained with models partitioning by homoplasy, as well as from those resulting from MP analyses (Fig. 4). Unpartitioned and anatomically partitioned models did not recovered Megatherioidea as monophyletic, although this clade has been consistently recovered in previous phylogenetic analyses of sloths (Gaudin 2004; Amson et al. 2016; Varela et al. 2019) and is supported by 43 synapomorphies in the present study. Inferences using homoplasy partitioning and MP analyses were in greater agreement among themselves when we compare the topologies qualitatively, although nRF distances obscure these patterns. Since Bayes factor comparisons allowed us to determine that models with

homoplasy partitioning as better-fitted for our dataset, we can also infer, indirectly, that topologies obtained with MP were also more reliable than those from BI with data unpartitioned or partitioned by anatomy. Previous empirical studies (e.g., Nylander et al. 2004) reported that trees from IW parsimony analyses were topologically more similar to those derived from unpartitioned BI analyses than to those resulting from EW parsimony, but we did not observe such a pattern here. Porto and Almeida (2021), on the other hand, recovered very similar topologies with IW maximum parsimony analyses and Bayesian inferences applying anatomical and homoplasy-based partitioning for morphological data.

For the morphological characters of sloths, the greatest difference observed among topologies seems to be related to the absence of adequate data partitioning, as indicated by Bayes factor comparisons. Although the relative performance of MP and BI methods for morphological data has been much debated in the last few years (e.g., Goloboff et al. 2018; Puttick et al. 2019; Smith 2019), our results indicate that some relevant differences in tree topologies may be more related to how we model character heterogeneity within morphological datasets in Bayesian phylogenetics than to the choice between MP and BI methods. Further studies considering partitioned models applied to morphology are necessary to understand how generalized this pattern is.

The major differences among trees obtained with alternative partitioning schemes suggest that some kind of artificial attraction between Megatheriidae/Megatheriinae and Mylodontoidea was occurring in trees from unpartitioned and anatomically partitioned models. Most taxa from those clades are highly derived with respect to postcranial characters related to locomotion, with members of both clades achieving partial or complete pedolateral stances (McDonald 2012; Toledo et al. 2018). This reorganization in posture lead to several similar, and by our current understanding, convergent modifications in the posterior appendicular skeleton: more robust long bones (femora, tibiae and fibulae); highly modified astragali, with a marked odontoid process; calcanei with a tuberous tuber calcis; a modified Mt V which broadly contacts the ground; and the loss of phalanges in the most lateral pedal digits. Additionally, the molariform morphology of upper and lower first teeth (Cf/cf) in Scelidotheriinae and Megatheriinae, lacking a diastema and other associated changes, probably evolved independently, since all those characters are in conflict with a greater number of cranial and postcranial characters that indicate a monophyletic Megatherioidea. Our results suggest that if the degree of homoplasy of characters like those are not accounted for in the model, those changes may be incorrectly treated as evidence of phylogenetic proximity in Bayesian analyses. It may also be worth noting that, with the exception of *Octodontotherium* and

Paroctodontotherium, all Mylodontoidea used in this analysis come from the early Miocene or later, whereas the origin of the clade is inferred here in the late Eocene. This indicates that primitive morphologies may be missing, thereby making long-branch attractions more likely, especially when patterns of homoplasy are not considered.

3.4.2 Evaluating divergence times using morphology

We observed greater stratigraphic consistency for non-clock BI than for MP topologies, contrasting with a previous study in which parsimony performed, on average, slightly better (Sansom et al. 2018). On the other hand, a recent study suggested that this may be dataset specific (King 2021). As observed for partitioning, there are other relevant differences between analyses beyond the method used for phylogenetic inference, so restricting the discussion to comparisons of MP or BI approaches may not fully account for all details. King (2021) showed that tip-dated BI produces topologies with higher stratigraphic consistency when compared to those obtained with MP and non-clock BI, since temporal information is included during tree inference. Also, other parameters like diversification rates are also consequential to the stratigraphic fit of inferred topologies (King 2021).

Although estimates with all five models used for dating analyses were similar, some small differences can be observed for particular nodes depending on the models applied (Fig. 8). We observed that the most influential factor affecting the divergence ages for our dataset was the clock model, and the one with autocorrelated rates outperformed the widely used (and often assumed) independent rates models. Simões et al. (2020a) also recovered this model as the best-fitting for sphenodontians, and this pattern may be common for other morphological datasets, so we further recommend that morphological clock analyses should always be included in Bayes factor comparisons, instead of assuming a single clock model. The autocorrelated model led to slightly older divergences close to the root and slightly younger in nested nodes, the opposite of what was observed by Simões et al. (2020a), suggesting that this behavior is dataset dependent. In another difference from Simões et al. (2020a), sampling ancestors in our study was not as consequential for the results as were the clock models. Analyses with SA recovered younger, not older estimates, suggesting those results are not general for dating of morphological datasets. Those models also allow us to make inferences about the nature of the evolutionary rates across the branches of the tree, or the plausibility of ancestor-descendent relationships among the taxa examined. Our results indicate that sloths conform to a gradualist regime of evolutionary rates across branches, and that anagenetic

relationships are not often supported, not even for the outgroup *Neotamandua*, previously found to be in a purportedly anagenetic relationship with *Myrmecophaga* (Casali et al. 2020 – Chapter 2).

The standard fossilized birth-death process makes seemingly unrealistic assumptions of constant rates of speciation, extinction and fossilization through time (Heath et al. 2014). More flexible assumptions (Gavryushkina et al. 2014; Zhang et al. 2016) may be more realistic from both biological and geological perspectives. Notwithstanding, the model considering the variation in those parameters was not preferred relative to a model keeping them constant though time. Since the number of alternative possible combinations of time bins and constancy or variation in FBD parameters can be extremely high, a pragmatic approach informed by biological and geological information, as used here, should be applied. Allowing parameters to vary across time bins may also be an overly simplistic approach, and alternatives allowing lineage-specific birth-death models are already available (Barido-Sottani et al. 2020), although little is known of how those models perform in dating analyses in general, and even less about how they perform with morphological data, specifically.

3.4.3 The importance of synapomorphies in statistical phylogenetics

We advocate here that including synapomorphies as evidence of phylogenetic relationships provides an invaluable link between the characters used to infer the tree and recovered clades, irrespective of the method used for tree inference, since they provide biological evidence of clade support, complementary to posterior probabilities.

Unlike maximum parsimony analyses, maximum likelihood (ML) and Bayesian phylogenetic methods do not hold a necessary relationship between monophyletic groups and synapomorphies (Assis 2015). During tree searches, uncertainty in ancestral states assigned to internal nodes is integrated into the process (topological uncertainty is also integrated in BI analyses), and an additional procedure of ancestral state reconstruction is necessary to obtain estimates of character states at nodes, with their relative probabilities (Ronquist 2004). Assessing synapomorphies in statistical phylogenetics, therefore, does not occur simultaneously with clade recognition, since clades are defined by the overall likelihood of the trees in ML analyses and by the posterior probabilities of clades in BI (a maximum a posteriori Bayesian tree is another, although less recommended, estimate of Bayesian results; O'Reilly and Donoghue 2018). This indirect relationship might be responsible for how rarely an

assessment of synapomorphies is conducted by empiricists when Bayesian methods are applied to morphology (King 2019).

The empirical Bayes method applied here showed overall consistency in the synapomorphies recovered with parsimony optimizations for the same topology, although a few synapomorphies were exclusively recovered by one or the other method. The method applied here can be improved and a deeper exploration of its performance is necessary, something beyond the scope of the present study. We collapsed node state probabilities for the most probable state using the minimum default threshold (0.01), whereas higher cutoff values would probably exclude some synapomorphies exclusively recovered with BI. It is unclear which cutoff value should be applied, and whether or how it should be adjusted according to the maximum number of states in a character. It may be that the best approach would be to define the cutoff values by empirical properties specific for a given dataset or character. Also, using joint instead of marginal reconstructions of ancestral states (Joy et al. 2016) may be more suited to the purpose of assessing synapomorphies, since it already returns the most probable state and a consistent history of node reconstructions. Our results indicate that the posterior probabilities and number of synapomorphies recovered for each clade are not always associated, something that will also demand quantitative evaluation to be properly understood. This is not surprising, however, considering the absence of a direct relation between clades and synapomorphies in Bayesian inferences, as discussed above.

3.4.4 The phylogeny of Folivora

There is a general agreement among the results obtained here, and those from previous morphological phylogenetic studies of sloths (e.g., Gaudin 2004; Amson et al. 2016; Varela et al. 2019; Boscaini et al. 2019b), something that is not unexpected since all those studies share many similar or identical characters. On the other hand, our main results disagree with those obtained from studies with a more modest sample of characters or taxa (e.g., Gaudin 1995; Pujos et al. 2007; Rincón et al. 2015), which likely contained less information to resolve those phylogenetic relationships.

The position of the peculiar genus *Pseudoglyptodon*, as sister to all other sloths, is further corroborated here, in agreement with the results of Varela et al. (2019) and Boscaini et al. (2019b). As discussed in those two studies, our knowledge for this taxon is limited. Nevertheless, its position was well supported here, both by posterior probability and synapomorphies. The position of *Bradypus* as sister to Eufolivora, observed in most

morphological studies to date (e.g., Gaudin 2004; Amson et al. 2016; Varela et al. 2019; Boscaini et al. 2019b), is also recovered here, in contrast with molecular evidence which places *Bradypus* among Megatherioidea (Delsuc et al. 2019; Presslee et al. 2019). The hypothesis of a closer relationship between *Bradypus* and some megatherioid clade was proposed in older morphological studies (Guth 1961; Patterson and Pascual 1968; Webb 1985; Gaudin 1990; Patterson et al. 1992), especially due to shared similarities in the ear region anatomy. Varela et al. (2019) also reported that in analyses in which the topology was co-estimated with divergence-times, *Bradypus* was associated with megatherioids, specifically with *Schismotherium* and *Pelecyodon*, and the results of Carlini and Scillato-Yané (2004) also associated *Bradypus* with *Schismotherium*. We obtained similar results in some preliminary attempts to co-estimate topology with tip-dating and FBD process, but due to convergence issues, those results were not considered further here. As discussed by Varela et al. (2019), accounting for diversification and fossilization dynamics may improve phylogenetic inferences for taxa with long unsampled branches, as is the case of *Bradypus*, but potential issues in co-estimating topology and divergence times in datasets composed mostly of fossil taxa should also be considered (King 2021; Mongiardino Koch et al. 2021). Although well supported here and in previous morphological studies, it is not possible to rule out the possibility that the position of *Bradypus* as sister to Eufolivora is a product of long-branch attraction due to its highly derived and probably paedomorphic features (Gaudin 1995, 2004; Hautier et al. 2016). Additionally, the absence of fossils attributed to the genus (McDonald and De Iuliis 2008) render unlikely a divergence from Eufolivora in the middle Eocene (Varela et al. 2019 and this study). In a total-evidence analysis performed by Presslee et al. (2019), *Bradypus* was recovered as sister to all other megatherioids, thereby implying a much shorter ghost lineage, as also observed analyzing molecular data alone (Slater et al. 2016; Delsuc et al. 2019; Presslee et al. 2019, but see the discussion about the Antillean megalonychines below).

The division of Eufolivora in two major clades, Megatherioidea and Mylodontoidea has been consistently recovered not only with morphological (Gaudin and Wible 2004; Varela et al. 2019), but also with molecular data analyses (Delsuc et al. 2019; Presslee et al. 2019). However, the content of those clades is somewhat different in molecular studies, with the living genus *Choloepus* included among mylodontoids, and *Bradypus* among megatherioids, as already discussed. Both Megatherioidea and Mylodontoidea were recovered here with high posterior probabilities (> 95%) and with several synapomorphies associated with each of them. In the case of unpartitioned and anatomically partitioned Bayesian analyses, homoplasy could have biased our data, so that the two clades were not recovered in these analyses. Something

similar may have affected previous studies which included a reduced set of characters (e.g., White and MacPhee 2001; Pujos et al. 2007; Rincón et al. 2015).

Mylodontoidea in our study is equivalent to the clade named Mylodontidae in most previous phylogenetic evaluations (Gaudin 2004; Haro et al. 2016, 2017; Brambilla and Ibarra 2018; Boscaini et al. 2019b; Cartelle et al. 2019; Varela et al. 2019; De Iuliis et al. 2020). In those studies, the Oligocene genera *Octodontotherium* and *Paroctodontotherium* were recovered as more closely related to Mylodontinae than to Scelidotheriinae. In Varela et al. (2019), those Oligocene genera comprise a clade with *Octomylodon*, *Pseudoprepotherium*, *Urumacotherium*, *Brievabradys* and other few genera known from very fragmentary remains and not sampled in our study. Our main results were quite distinct, placing *Octomylodon*, *Octodontotherium*, and *Paroctodontotherium* as successive sister taxa to a clade uniting Mylodontidae and Scelidotheriidae. The two Oligocene genera are amongst the oldest known sloths, and a stem position of *Octodontotherium* relative to sloths in general or to mylodontoids specifically has been previously suggested (e.g., Hoffstetter 1954, 1956; Engelmann 1985; Pujos and De Iuliis 2007). This stem position of *Octodontotherium* and *Paroctodontotherium* in Mylodontoidea, as recovered in most analyses performed in this study (including the best-fitting model of BI and all MP trees), is more stratigraphically consistent than the nested position obtained in previous studies. The clade excluding those stem mylodontoids is well-supported by posterior probability in the reference topology, but only four synapomorphies could be associated with it. More postcranial material of Oligocene mylodontoids are being discovered (Pujos et al. 2021), and could contribute to a better understanding of the phylogenetic position of these enigmatic taxa in future studies.

The clade Scelidotheriidae recovered here, with Nematheriinae as sister to Scelidotheriinae, was absent in trees from previous phylogenetic analyses (Gaudin 2004; Boscaini et al. 2019b; Varela et al. 2019; Nieto et al. 2020), although *Analcitherium* was recovered as sister to Scelidotheriinae in Varela et al. (2019). Most other studies place *Nematherium* as sister to a clade uniting scelidotheriines and mylodontids, as in trees obtained here with our poorly fitting BI models, and in IW parsimony analyses with stronger weights. In more narrowly focused investigations of scelidotheres, *Nematherium* has often been used as a sole outgroup of Scelidotheriinae (McDonald and Perea 2002; Cartelle et al. 2009; Miño-Boilini 2012; Miño-Boilini et al. 2014); hence, its position was not evaluated. Although some previous authors have associated *Nematherium* with scelidotheriines (Engelmann 1985; McKenna and Bell 1997), this is the first study to provide quantitative phylogenetic support for this association, which was maximally supported by posterior probability and by more than 20

synapomorphies. Scelidotheriinae has been recovered as monophyletic in all studies in which this was investigated (Gaudin 2004; Haro et al. 2016, 2017; Boscaini et al. 2019b; Varela et al. 2019; Nieto et al. 2020), and it was also well-supported here. Arrangements within Scelidotheriinae have varied considerably among prior studies (McDonald and Perea 2002; Cartelle et al. 2009; Miño-Boilini 2012; Miño-Boilini et al. 2014; Varela et al. 2019). The arrangement obtained here was not identical to any of these proposals, but holds some similarity with them, as indicated by the stem position of *Neonematherium* and *Sibyllotherium* (Miño-Boilini 2012; Miño-Boilini et al. 2014), and the close association of *Catonyx* and *Scelidotherium* (Nieto et al. 2020).

Our topology for Mylodontidae (Mylodontinae of previous studies) strongly resembles the results obtained by Boscaini et al. (2019b) and De Iuliis et al. (2020), and to some extent, those of Gaudin (2004) and other studies that used Gaudin's characters as the core of their datasets (Haro et al. 2016, 2017; Brambilla and Ibarra 2018; Boscaini et al. 2019a; Cartelle et al. 2019; Román-Carrión and Brambilla 2019). As in Boscaini et al. (2019b) and De Iuliis et al. (2020), we recovered a dichotomy between a clade composed of *Urumacotherium* and *Pseudoprepotherium* (Urumacotheriinae) and the remaining mylodontids, which include *Octodontotherium* and *Paroctodontotherium* in the trees of Boscaini et al. (2019b) and De Iuliis et al. (2020). Urumacotheriinae was consistently recovered in our analyses, and seven synapomorphies are associated with this node, but it was poorly supported by posterior probability, something that could be related to the scant material known for those genera, especially for *Urumacotherium*.

Mylodontinae here is equivalent to node M recovered in Boscaini et al. (2019b, Figure 1), a clade composed of the stem genus *Brievabradys*, and the Mylodontini and Lestodontini (*sensu* Gaudin 2004). It is also similar to the Mylodontinae of Varela et al. (2019), except for the inclusion of *Brievabradys*. Unlike earlier studies, Lestodontini was paraphyletic in the majority of the analyses performed here, including the best-fitting BI model. We provisionally recognized two clades here, Thinobadistini and Lestodontini (*sensu* McKenna and Bell 1997) in our efforts to remain consistent in naming only monophyletic clades in our classification. It is not unlikely that future studies may reestablish a monophyletic Lestodontini (*sensu* Gaudin 2004), since it was recovered in almost all other recent studies of mylodontines which included at least *Lestodon* and *Thinobadistes* (Gaudin 2004; Brambilla and Ibarra 2018; Boscaini et al. 2019b; Cartelle et al. 2019; Román-Carrión and Brambilla 2019; Varela et al. 2019; De Iuliis et al. 2020). Also, Thinobadistini received low posterior probability and was supported by only a single synapomorphy.

Both Lestodontini (*sensu* McKenna and Bell 1997) and Mylodontini are supported by maximum PPs and 11 synapomorphies each. This last clade was also recovered by Boscaini et al. (2019b) and De Iuliis et al. (2020), but is paraphyletic in most other studies, with *Mylodon* being recovered outside the clade and Lestodontini (*sensu* Gaudin 2004) or *Mirandabradys* Rincón et al. 2015 being included in it (Gaudin 2004; Haro et al. 2016, 2017; Brambilla and Ibarra 2018; Boscaini et al. 2019a; Cartelle et al. 2019; Román-Carrión and Brambilla 2019; Varela et al. 2019). We observed an overall congruence while comparing the internal relationships of Mylodontini obtained here to those in Boscaini et al. (2019b) and De Iuliis et al. (2020), with differences in taxonomic sampling probably leading to the few disagreements. As in Boscaini et al. (2019b) and De Iuliis et al. (2020), our reference tree recovered a stem *Pleurolestodon* as sister to the remaining Mylodontini, followed by a clade composed of *Simomylodon* and *Glossotheridium*.

A few Mylodontini were included in this study but not in Boscaini et al. (2019b) and De Iuliis et al. (2020). The first was *Ocnotherium*, an understudied Pleistocene mylodontid which diverged after *Simomylodon* and *Glossotheridium* in our reference topology and in most analyses performed here. However, we also recovered it as sister to all other Mylodontini in some analyses. Although this genus may superficially resemble *Glossotherium*, some of its characters show clear evidence of its stem position among Mylodontini, such as an anteroposteriorly ovate mf1 and mf2, as in Lestodontini, and the presence of an astragalar sulcus tali, a primitive feature for Eufolivora (Supplementary File S14, character 465). *Ocnotherium* was also recovered closer to the base of Mylodontini by Haro et al. (2017), associated with *Simomylodon*. *Oreomylodon* was considered a separate genus from *Glossotherium* in our study, following Román-Carrión and Brambilla (2019), but a subsequent analysis at the species-level showed that it nests within *Glossotherium*, despite its unusual muzzle morphology (De Iuliis et al. 2020). In our study, all analyses but one recovered this taxon as sister to a clade composed of *Mylodonopsis*, *Archaeomylodon* and *Mylodon*, whereas in par_IW5, it was recovered as sister to a clade composed of *Glossotherium* and *Paramylodon*. In both cases, supports were not high for these associations. Although in a different arrangement, *Oreomylodon* also assumed an intermediate phylogenetic position between *Mylodon* and *Glossotherium*/*Paramylodon* in Román-Carrión and Brambilla (2019). De Iuliis et al. (2020) did not include *Archaeomylodon* or *Mylodonopsis* in their sample. On the other hand, *Kiyumylodon* Rinderknecht 2007 was not included in our study, nor in the phylogeny by Román-Carrión and Brambilla (2019), both employing only a genus-level sample. Including all those taxa, along with a species-level evaluation, would be necessary to definitively assess the

taxonomic status of *Oreomylodon*. Another understudied taxon, *Mylodonopsis*, was consistently recovered as sister to a clade composed of *Mylodon* and *Archaeomylodon*, with the association of *Mylodon* and *Mylodonopsis* having already been suggested by the results of Haro et al. (2016). Their unique premaxillary morphology reinforces the phylogenetic proximity of these two genera. As in the present study, *Archaeomylodon* was recovered as sister to *Mylodon* in Brambilla and Ibarra (2018), but not in Román-Carrión and Brambilla (2019).

Within Megatherioidea, *Pelecyodon* and *Schismotherium* occupy a stem position, sister to a well-supported clade uniting Megalonychidae and Megatheriidae (Megatheria of previous studies) in all Bayesian analyses performed here. Those two Santacrucian taxa are joined by *Hapalops* in equal weights parsimony and par_IW100 models. This arrangement is very similar to that recovered in most previous studies which included those taxa (Gaudin 2004; Amson et al. 2016; Varela et al. 2019), although we recovered them as successive divergences, whereas most of those studies allied *Pelecyodon* and *Schismotherium* as sister taxa. In parsimony analyses with stronger weights, they comprise a clade along with *Hapalops,* more closely related to megatheriids than to megalonychids (i.e., Schismotheriinae, according to McKenna and Bell 1997), whereas in Carlini and Scillato-Yané (2004), *Schismotherium* was recovered as a megalonychid. Gaudin (1995) also include those Santacrucian genera in his analysis, and the ear region characters indicated a stem position among sloths, diverging after *Bradypus*. Although admittedly speculative, this may be additional evidence of a closer association of *Bradypus*, *Pelecyodon* and *Schismotherium*, which could have been obscured if the position of *Bradypus* in morphological phylogenies is indeed the result of long-branch attraction artifacts. If true, this could be confusing the assessment of the correct polarity of those ear region characters.

Hapalops was recovered in all our Bayesian inferences as a stem Megalonychidae, sister to all other taxa in the clade, as in previous studies (Amson et al. 2016; Varela et al. 2019). In some parsimony analyses, *Hapalops* assumed a stem position in Megatherioidea, sister to Megalonychidae plus Megatheriidae, as observed by Carlini and Scillato-Yané (2004). In other MP results, and as in Gaudin (2004), *Hapalops* was recovered closer to Megatheriidae than to Megalonychidae. Unlike the total-group Megalonychidae, the clade containing Megalonychidae minus *Hapalops* was well-supported here. In this clade, other Santacrucian genera, namely, *Hyperleptus, Megalonychotherium* and *Eucholoeops*, occupy a stem position relative to the remaining taxa (i.e., Megalonychinae), an arrangement corroborated by most of the previous studies evaluating the phylogeny of the clade (Carlini and Scillato-Yané 2004; Gaudin 2004; Pujos et al. 2007; McDonald et al. 2013, 2017, 2020; Stinnesbeck et al. 2017,

2020; Rincón et al. 2018, 2021; Varela et al. 2019). In our reference topology, and in the majority of analyses performed here, *Megalonyx* and *Pliometanastes* were recovered as sister taxa to all other megalonychines, in an arrangement that was recovered in several previous studies (Gaudin 2004; McDonald et al. 2017, 2020; Stinnesbeck et al. 2017, 2020; Rincón et al. 2021). In other analyses, those genera were more closely related to a clade composed of intertropical genera (i.e., Ahytheriini) than to the other genera of Megalonychinae (McDonald et al. 2013; Rincón et al. 2018; Varela et al. 2019). We also observed this last arrangement in some BI and MP analyses. Megalonychinae was well-supported both from maximum PPs and by 59 synapomorphies. However, the alternative internal resolutions discussed above were all poorly supported by posterior probabilities, although the clade Ahytheriini plus Choloepodini present in the reference topology received support from 11 synapomorphies.

The clade containing all intertropical megalonychines, Ahytheriini, was recovered in all analyses performed here and was well-supported by PP and synapomorphies in the reference tree. Except for some MP analyses which did not recover a clade with *Nohochichak* and *Xibalbaonyx*, our results are in agreement with most previously published phylogenies (McDonald et al. 2013, 2017; Stinnesbeck et al. 2017, 2020; Rincón et al. 2018; Varela et al. 2019). McDonald and Carranza-Castañeda (2017), on the other hand, recovered *Ahytherium* as more closely related to *Australonyx* than to *Megistonyx*. This phylogenetic result also returned unusual relationships for other megalonychids, and probably had its accuracy affected by the inclusion of some very fragmentary material for genera not sampled here, like *Zacatzontli* McDonald and Carranza-Castañeda 2017 or *Deseadognathus* Carlini and Scillato-Yané 2004. A diphyletic origin of intertropical megalonychines was recently suggested (McDonald et al. 2020; Rincón et al. 2021), and this arrangement is in disagreement with all other investigations cited above and with our results here, indicating that we may need more studies to unravel the phylogenetic relationship of this clade of intriguing sloths.

Choloepodini, the clade including the living genus *Choloepus*, Antillean megalonychines and *Pliomorphus*, was also recovered and well-supported in all of our analyses, with an identical or very similar arrangement to that observed in most previous studies (Gaudin 2004; McDonald et al. 2013, 2017; Stinnesbeck et al. 2017, 2020; Rincón et al. 2018; Varela et al. 2019). In some of them, a closer association of *Choloepus* to *Neocnus* than to *Acratocnus* was observed (Gaudin 2004; Varela et al. 2019), whereas in others (McDonald et al. 2017; Stinnesbeck et al. 2017, 2020), *Pliomorphus* emerged as sister to Ahytheriini plus Choloepodini. In Pujos et al. (2007), *Acratocnus* was recovered as more closely related to *Pliometanastes* than to *Megalocnus*. Since *Diabolotherium* was recovered as its sister taxon,

this is likely an artifact related to convergent postcranial climbing adaptations in those taxa. White and MacPhee (2001) hypothesized a diphyletic origin for Antillean sloths, with *Neocnus* and *Acractocnus* more closely related to *Choloepus*, *Bradypus* and *Hapalops*, whereas *Megalocnus* and *Parocnus* were closer to *Paramylodon*. Considering the restricted taxonomic sampling used in that study, it is very likely that those unusual results are also artifacts caused by postcranial convergences related to the arboreal and terrestrial habits of those two groups of taxa, respectively (White and MacPhee 2001). Additionally, body size differences among taxa associated with these two locomotory categories were likely associated with morphological convergences that may have biased the phylogenetic results. Two other recent studies did not recover a monophyletic Choloepodini as well, with some intertropical megalonychines being more closely related to *Parocnus* and *Megalocnus* (McDonald et al. 2020; Rincón et al. 2021). This arrangement is clearly associated with the diphyletic origin of intertropical megalonychines discussed above. Sampling all Megalonychinae evaluated here and in those two studies would be a necessary first step to illuminate the relationships among those taxa.

Recent molecular phylogenies suggest a very distinct relationship for most of the genera included here in Choloepodini, with *Choloepus* being recovered as a member of or sister to Mylodontidae, and Antillean sloths as sister to all other sloths in the tree, rendering Megalonychidae polyphyletic (Delsuc et al. 2019; Presslee et al. 2019). These molecular results are partially aligned with pre-cladistic suggestions that *Choloepus* could be closely related to mylodontids (Guth 1961; Webb 1985). To some extent, *Choloepus* is a taxon as enigmatic as *Bradypus*, because of its derived postcranial morphology (Buchholtz and Stepien 2009; Nyakatura 2012), its mixture of megalonychid and mylodontoid craniomandibular characters, and the presence of numerous autapomorphies (Gaudin 2004). Although it was firmly placed among Choelopodini in our study, mostly supported by postcranial and ear region characters, *Choloepus'* phylogenetic relationships remain contentious, and further total-evidence analyses may help to shed additional light on this issue. Presslee et al.'s (2019) total-evidence analysis combined their molecular data with the morphological dataset of Varela et al. (2019), and recovered *Choloepus* as sister to all other Mylodontoidea. This seems unlikely, due to the implied minimum age for this divergence, considering that *Choloepus* lacks a fossil record, just like *Bradypus* (McDonald and De Iuliis 2008). This arrangement may have been influenced by the unusual relationships suggested for Mylodontoidea by the morphological data of Varela et al. (2019), as previously discussed. If *Choloepus* is indeed a member of Mylodontoidea, a more nested position, as recovered by protein data alone, seems more reasonable. The mismatch between morphological and molecular evidence regarding the position of Antillean sloths is,

however, harder to reconcile with the morphological evidence, suggesting an astonishing convergent pattern for Antillean sloths relative to other megalonychids. Also, those molecular results imply an extensive ghost lineage, since the Antillean taxa sampled in all previous morphological phylogenies are from the Quaternary (White and MacPhee 2001; Steadman et al. 2005). Oligocene remains in the Antilles suggest an earlier colonization of the islands by purported megalonychids (McDonald and DeIuliis 2008), but the very fragmentary nature of that material makes its association with Pleistocene-Holocene taxa more uncertain (MacPhee and Iturralde-Vinent 1995; White and MacPhee 2001).

Megatheriidae here refers to the clade named Megatheria in Gaudin (2004), also recovered by Varela et al. (2019). This clade was well-supported in our study, both by posterior probability and synapomorphies. In Amson et al. (2016), this clade was recovered excluding *Analcimorphus*, which was associated with the megalonychids. The resulting clade is equivalent to the Megatheriidae minus *Analcimorphus* of our study, which was also well-supported here. On the other hand, the relationship among the three groups composing this clade – prepotheriines, megatheriines and nothrotheriines – are contentious. While previous studies recovered a closer association of Prepotheriinae to Megatherinae than to Nothrotheriinae (Gaudin 1995, 2004; Amson et al. 2016; Varela et al. 2019), our main results pointed to a closer association between Nothrotheriinae and Megatheriinae, to the exclusion of Prepotheriinae, as in Pujos et al. (2007). However, this clade was not well-supported. We also recovered another arrangement, with a clade uniting Nothrotheriinae and Prepotheriinae, to the exclusion of Megatheriinae, as in some alternative results reported by Varela et al. (2019). More detailed studies are required to resolve the phylogenetic arrangements inside Megatheriidae, an evolutionary enigma that has remained open at least since De Iuliis (1995). For the time being, we suggest considering Megatheriidae to be composed of Megatheriinae, Nothrotheriinae, and Prepotheriinae.

A monophyletic and well-supported Prepotheriinae was recovered here, with *Planops* as sister to the other two genera in most analyses. An arrangement with *Prepotherium* assuming a stem position was also observed here for trees from more poorly fitting BI models. Varela et al. (2019), which was the only other study to test the monophyly of this group, did not find it well-supported, and the arrangement obtained was different from ours, with a stem position for *Prepoplanops*. In both studies, however, those internal relationships are not well supported. Nothrotheriinae has been recovered as a monophyletic group in several studies, in which it was considered a family-level clade, although the content and internal relationships of this clade has varied (Gaudin 2004; De Iuliis et al. 2011; Amson et al. 2016; Pujos et al. 2016; Varela et al.

2019). The well-supported internal arrangement recovered here is very similar that obtained by Amson et al. (2016), excluding *Thalassocnus*, but differs from most of the previous analyses (McDonald and de Muizon 2002; de Muizon et al. 2003, 2004b; De Iuliis et al. 2011; Varela et al. 2019). However, only the last of those investigations included megatheriines as well, properly testing the affinities of *Thalassocnus*. Another recently described genus, *Aymaratherium,* was also recovered outside of Nothrotheriinae in the present study, whereas Varela et al. (2019) found it associated with this group, as originally assigned by Pujos et al. (2016). The provisional taxon "*Xyophorus*", presents clear nothrotheriine affinities, as opposed to the other *Xyophorus* species (Brandoni 2014; Brandoni et al. 2019), and was recovered here as sister to *Mionothropus*. *Pronothrotherium* was recovered as sister to a clade composed of *Nothrotheriops* and *Nothrotherium*, as in De Iuliis et al. (2011) and Pujos et al. (2016), but in contrast to other studies, which recovered *Mionothropus* as sister to the Pleistocene genera (Gaudin 2004; Amson et al. 2016; Varela et al. 2019) or in a clade uniting *Mionothropus* and *Pronothrotherium* (McDonald and de Muizon 2002; de Muizon et al. 2003).

Megatheriinae (Megatheriidae of previous studies), was also recovered in all analyses here, and was well-supported. Its content is not identical to that obtained in any previous study, but exhibits patterns similar to those observed in some of them (e.g., Brandoni 2006; Pujos 2006; Amson et al. 2016; Varela et al. 2019). Two successive stem genera, *Diabolotherium* and *Megathericulus* were recovered here, whereas in Varela et al. (2019) they form a sister clade to all other megatheriines. Although the affinity of *Diabolotherium* with megatheriids has become clear in recent years (Pujos et al. 2011, 2014, 2016; Varela et al. 2019), several postcranial characters point to convergence with climbing megalonychids, something that may explain its original association with that clade (Pujos et al. 2007). Those postcranial characters also have some influence on its stem phylogenetic position in this study, as sister to all other megatheriines (except in two MP trees in which *Megathericulus* diverges earlier). The stem position of *Megathericulus* was recovered in other studies as well (Brandoni 2006; Pujos 2006). A clade containing Thalassocnini (*Thalassocnus* and *Aymaratherium*) and Megatheriini was well-supported in most analyses here, including those with the best-fitting BI model, and this is consistent with the results of Amson et al. (2016), associating *Thalassocnus* with megatheriines instead of nothrotheriines. This relationship is supported by nine synapomorphies, including characters related to the extended anterior portion of the maxilla and premaxilla and a well-defined odontoid process of the astragalus. Humeral and calcaneal morphology are responsible for the association of *Thalassocnus* and *Aymaratherium*, something already noted by Pujos et al. (2016). This clade was recovered in all but one analysis here, and

is maximally supported by PP in the reference tree, although only five synapomorphies could be associated with it. Cranial remains of *Aymaratherium* are unknown and its peculiar, and probably derived dental morphology suggest that the original association of this genus with nothrotheriines (Pujos et al. 2016; Varela et al. 2019), or its novel link to megatheriines in this study, may be provisional, demanding further investigation. Megatheriini is consistently recovered here, and is well-supported. Its internal relationships exhibit an arrangement very similar to those obtained in previous studies (Brandoni 2006; Pujos 2006; Varela et al. 2019). Nonetheless, our results indicate successive divergences of *Pyramiodontherium*, *Megatheriops* and the remaining Megatheriini, in contrast to Brandoni (2006) or Pujos (2006), which recovered those two genera in a same clade or in polytomies. We also recovered a closer association of *Eremotherium* with *Proeremotherium*, and not to *Megatherium*, as observed in Varela et al. (2019).

3.4.5 Divergence ages and macroevolutionary patterns of Folivora

Divergence ages for Folivora (middle Eocene) and Eufolivora (late Eocene/early Oligocene) presented here (Fig. 9) are in overall agreement with those obtained with morphological data by Varela et al. (2019). On the other hand, for Mylodontoidea (Mylodontidae in Varela et al. 2019), our estimates were considerably younger, in the early Oligocene-late Oligocene transition, and outside the 95% HPD they obtained, which suggested a late Eocene divergence for this clade. This probably relates to the very distinct topologies recovered for mylodontoids between the two studies. As already discussed, our phylogenetic hypothesis placed the oldest known representatives of this clade, *Octodontotherium* and *Paroctodontotherium*, as successive sister taxa to a clade formed by Scelidotheriidae and Mylodontidae, whereas Varela et al. (2019), recovered these taxa in "Orophodontoidea". This poorly supported clade, nested within Mylodontidae, probably pushed the divergence among mylodontoid clades further into the past (Varela et al. 2019). We recovered an early Miocene age for the initial diversifications of both Scelidotheriidae and Mylodontidae, consistent with the most comparable clades present in Varela et al. (2019, Scelidotheriinae and Mylodontinae, respectively). These comparisons are limited by the different taxonomic content of those groups, with taxa recovered here as stem members of those clades (e.g., *Nematherium, Pseudoprepotherium*) being recovered in alternative phylogenetic positions in their study. The age of divergence of Megatherioidea, in the late Oligocene, was only slightly younger than the early Oligocene age recovered by Varela et al. (2019), but well within the 95% HPD recovered

by these authors. Also, we recovered younger divergence ages – in the early Miocene – for both Megalonychidae and Megatheriidae (Megatheria in Varela et al. 2019), with our median estimates being younger than the lower limit of their 95% HPDs. According to those authors, the initial divergence for each of those clades was in the late Oligocene. The reason for these disagreements is less clear, since we recovered similar overall topologies for those clades, despite some minor differences in their internal arrangements. Also, both studies employed very similar node calibrations closer to the root, informed by previous molecular time-calibrated inferences for Xenarthra. Differences in character and taxonomic sampling in each study may bear some responsibility for explaining those discordances, as well as the indirect influences of age estimates for other nodes on the tree.

Comparing the divergence ages estimated in our study with those obtained in two recent molecular analyses of sloths (Delsuc et al. 2019; Presslee et al. 2019) is challenging, since they refer to quite distinct phylogenetic hypotheses, so we will focus on three major nodes which are to some extent comparable – Folivora, Mylodontoidea and Megatherioidea – despite differences in their contents among the three studies. The root node of Folivora in molecular studies roughly compares to the Folivora minus *Pseudoglyptodon* node in our study, but as discussed before, in the molecular analyses, *Bradypus* is included in Eufolivora, among Megatherioidea, and *Choloepus* is placed among Mylodontoidea. Moreover, we will consider the combined analyses of nucleotide and protein data of Presslee et al. (2019) for comparisons, since their protein-only estimates were much younger and in greater disagreement with the nucleotide data of Delsuc et al. (2019). The initial divergence for Folivora was dated at the Eocene-Oligocene transition in all three studies. Our estimates were slightly older, but within the ranges obtained by molecular estimates. The divergence of Mylodontoidea obtained here, in the Oligocene, was very similar to the one obtained with nucleotide data (Delsuc et al. 2019), whereas the paleoproteomic plus nucleotide dataset (Presslee et al. 2019) suggests a much more recent age, at the Oligocene-Miocene transition, even though their 95% HPD include the median value obtained in our study. We inferred a late Oligocene divergence for Megatherioidea, slightly younger than that obtained with nucleotide data (early Oligocene, Delsuc et al. 2019), but older than that obtained with protein plus nucleotide data (early Miocene, Presslee et al. 2019). Once again, our estimates were still within 95% HPDs from both molecular studies. It seems premature to try to fully understand the source of those minor disagreements, given the available evidence, since the two types of molecular data disagree between themselves to some extent. Empirical datasets have showed that there are not necessary conflicts between divergence ages inferred from molecular and morphological datasets (Barba-

Montoya et al. 2021). It is possible that the differing taxonomic samples among studies may partially explain their distinct estimates, and not just the nature of the data, as was discussed for topological differences.

Even though a model including an SFBD process was not preferred here (it was the second-best model), it is worth discussing what its estimates suggest about sloth macroevolutionary patterns, in light of our current knowledge. According to this model, folivoran extinction rates increased almost continuously through time (Fig. 10). The most precise estimates were for the late Miocene and for the Pleistocene, whereas estimates for other time bins were associated with much uncertainty, with wide and overlapping HPDs. The late Miocene and Pleistocene correspond roughly to periods previously associated with a greater loss of diversity in sloths – the latest Miocene-early Pliocene decline in diversity (Varela et al. 2019), and the massive extinction in the late Pleistocene-early Holocene (Steadman et al. 2005; McDonald and De Iuliis 2008; Pujos et al. 2017; Varela et al. 2019). A third decline in diversity, during the middle Miocene, as observed by Varela et al. (2019), could be related to a slowdown in speciation rates after the peak observed here in the early Miocene. In contrast to extinction rates, speciation rates were estimated with greater precision, and the peak observed in the early Miocene can be correlated with the increased diversification in several major clades and the abundant fossil record of Santacrucian sloths, which include stem representatives of most of those groups (Scott 1903; McDonald and De Iuliis 2008; Bargo et al. 2019). A peak in diversity in the early late Miocene was not observed here, and according to Varela et al. (2019), this peak was mostly related to the diversification of mylodontoids. This pattern could be a consequence of the long branch separating Mylodontinae from "Orophodontinae" in their phylogenetic tree, but absent in our study. Our results suggest that fossilization rates were slightly higher in the early evolution of sloths, especially during the Oligocene. As was the case for extinction, the uncertainty around those estimates was also quite high, and this scenario is not well-supported by the scant folivoran fossil record of this period. Nevertheless, many Oligocene sloths have been discovered in the last few decades (Engelmann 1987; MacPhee and Iturralde-Vinent 1995; Carlini and Scillato-Yané 2004; McKenna et al. 2006; Pujos and De Iuliis 2007; Shockey and Anaya 2011; Pujos et al. 2021), and it is likely that many others are still unknown, since the early diversification of sloths occurred in the late Eocene and throughout the Oligocene (Delsuc et al. 2019; Presslee et al. 2019; Varela et al. 2019 and this study).

Even though we include a representative sample of folivoran taxonomic diversity, many other genera and species of sloths are currently recognized (McKenna and Bell 1997; McDonald and De Iuliis 2008; Pujos et al. 2017), and more detailed evaluations of

macroevolutionary patterns will require analyses that consider those taxa as well. Because of that, we refrain from associating those putative macroevolutionary patterns with specific geological, climatic or biological causes until a better and more stable picture of these patterns become available.

3.4.6 Limitations and future directions

The present study involved the most extensive taxonomic and character sample ever applied in a phylogenetic investigation of Folivora. This was made possible by joining data used in previous studies, data that was then carefully reevaluated. Despite that, only a few new characters were added, and only relatively complete taxa were considered. Efforts to include more taxa in the sloths' phylogenetic tree are necessary, especially as more complete material for some genera and species becomes available (e.g., McDonald et al. 2020). Also, coding new characters from less explored anatomical regions, like the endocranial cavities (e.g., Boscaini et al. 2020b, 2020a) or the axial skeleton (Gaudin 1999), could be an important additional source of evidence to illuminate the phylogenetic relationships of sloths.

A recent and positive tendency in sloth phylogenetic studies has been the use of species instead of genera for most terminal taxa (Boscaini et al. 2019b; De Iuliis et al. 2020; Nieto et al. 2020). This is a much needed improvement, since the practice of using composite taxa can have important shortcomings (Prendini 2001). On the other hand, working with composite tips also allows the minimization of missing data (Campbell and Lapointe 2009), so common in datasets composed mostly or entirely of fossil taxa. A compromise approach is possible, whenever sufficient material is available along with a clear taxonomy, as applied in Boscaini et al. (2019b) for mylodontoid sloths. Expanding this practice to megatherioids as well will firstly demand a clearer species-level taxonomy, especially for some Santacrucian genera with less well understood species limits, despite some recent efforts in this direction (De Iuliis and Pujos 2006; De Iuliis et al. 2014; Racco et al. 2018).

Finally, it is of great importance to employ total-evidence analyses combining morphological and molecular datasets, with a goal toward understanding why those datasets are in disagreement about the position of certain taxa, including the two living genera. One of the recent molecular studies (Presslee et al. 2019) performed a preliminary combined analysis joining nucleotides and proteins to the morphological dataset of Varela et al. (2019). Ideally, more molecular data should be considered, in order to minimize the chances that methodological artifacts have created the disagreements among trees. This would of course

require molecular samples from stratigraphically older genera and species. Ancient DNA is limited in this respect, given the biological limits imposed by degradation of the genetic material, but paleoproteomics seems to be a more promising approach (Buckley 2018; Schweitzer et al. 2019). Ideally, the inclusion of paleoproteomic data for Oligocene, Miocene and Pliocene taxa would allow us to evaluate if current molecular inferences, which are so far restricted to Pleistocene samples, provide a trustworthy depiction of sloth phylogenetic relationships. We could then also better evaluate the relationship between molecular evidence and the evidence contained in morphological characters.

3.5 CONCLUSIONS

We provided an updated time-calibrated phylogeny and suprageneric classification for sloths, which was largely in agreement with previous morphological studies, and distinct from recent molecular-based investigations. The present study has, however, yielded some important advances in our understanding of the relationships of some genera with historically unresolved or controversial allocations, such as *Octodontotherium, Paroctodontotherium, Ocnotherium*, *Mylodonopsis, Thalassocnus* and *Aymaratherium*. Hopefully, future comprehensive analyses combining morphology and molecular data can depict a consensus scenario on sloth evolution. With a systematic evaluation of Bayesian inference methods for our morphological dataset, we also showed the importance of properly evaluating partitioning and dating models using Bayes factor comparisons, and we further recommend that future studies using Bayesian phylogenetic methods for morphological datasets also adopt similar practices. Lastly, we suggest that synapomorphies should not be neglected in Bayesian morphological phylogenetics, since they constitute an indispensable source of evidence for phylogenetic relationships, complementing posterior probabilities.

ACKNOWLEDGEMENTS

We thank institutions, curators and staff members who kindly gave us access to the specimens under their care: J. Meng and J. Galkin (AMNH), W. Simpson, A. Stroup and K. Angielczyk (FMNH), M. Ezcurra, L. Chornogubsky and A. Kramarz (MACN), M. Reguero, A. Scarano and A. Carlini (MLP), M. Taglioretti and F. Scaglia (MMP), C. de Muizon and G. Billet (MNHN), C. Cartelle, L. Santos and M. A. Veloso (MCL PUC-MG), C. Costa (MCN-M PUC-MG) and D. Brinkman (YPM). We also thank F. Miranda, L. Cotts, L. Vilaboim, B. Rossi and S. Stinnesbeck for sharing photographs of specimens. We are indebted to L. Vilaboim, A. Miño-Boilini, G. Gasparini, A. P. Martins and COMUT for their help in obtaining literature. Enlightening discussions with F. Freitas, G. Garbino and C. Dias were invaluable to improve the methodology of the study. D. Casali was funded by Coordenação de Aperfeiçoamento de Pessoal de Nível Superior (CAPES), via a monthly scholarship (CODE 0001) and the Programa de Apoio à Pós-Graduação (PROAP), and received grants from the FMNH and the Paleontological Society, which assisted significantly in the completion of the study.

REFERENCES

Amson E., de Muizon C., Gaudin T.J. 2016. A reappraisal of the phylogeny of the Megatheria (Mammalia: Tardigrada), with an emphasis on the relationships of the Thalassocninae, the marine sloths. Zool. J. Linn. Soc. 179:217–236.

Amson E., de Muizon C., Laurin M., Argot C., de Buffrénil V. 2014. Gradual adaptation of bone structure to aquatic lifestyle in extinct sloths from Peru. Proc. R. Soc. B Biol. Sci. 281:20140192.

Assis L.C.S. 2015. Homology assessment in parsimony and model-based analyses: two sides of the same coin. Cladistics. 31:315–320.

Bapst D.W. 2012. Paleotree: An R package for paleontological and phylogenetic analyses of evolution. Methods Ecol. Evol. 3:803–807.

Bapst D.W., Wright A.M., Matzke N.J., Lloyd G.T. 2016. Topology, divergence dates, and macroevolutionary inferences vary between different tip-dating approaches applied to fossil theropods (Dinosauria). Biol. Lett. 12:20160237.

Barba-Montoya J., Tao Q., Kumar S. 2021. Molecular and morphological clocks for estimating evolutionary divergence times. Preprint. 0:1–24.

Bargo M.S., Toledo N., Vizcaíno S.F. 2006. Muzzle of South American pleistocene ground sloths (Xenarthra, Tardigrada). J. Morphol. 267:248–263.

Bargo M.S., Vizcaíno S.F., Archuby F.M., Blanco R.E. 2000. Limb bone proportions, strength and digging in some Lujanian (Late Pleistocene-Early Holocene) mylodontid ground sloths (Mammalia, Xenarthra). J. Vertebr. Paleontol. 20:601–610.

Bargo S.M., de Iuliis G., Toledo N. 2019. Early Miocene sloths (Xenarthra, Folivora) from the Río Santa Cruz valley (southern Patagonia, Argentina). Ameghino, 1887 revisited. Publ. Electron. la Asoc. Paleontol. Argentina. 19:102–137.

Barido-Sottani J., Aguirre-Fernández G., Hopkins M.J., Stadler T., Warnock R. 2019. Ignoring stratigraphic age uncertainty leads to erroneous estimates of species divergence times under the fossilized birth–death process. Proc. R. Soc. B Biol. Sci. 286:20190685.

Barido-Sottani J., Vaughan T.G., Stadler T. 2020. A multitype birth–death model for Bayesian inference of lineage-specific birth and death Rates. Syst. Biol. 69:973–986.

Bell M.A., Lloyd G.T. 2015. Strap: An R package for plotting phylogenies against stratigraphy and assessing their stratigraphic congruence. Palaeontology. 58:379–389.

Bergsten J. 2005. A review of long-branch attraction. Cladistics. 21:163–193.

Bhattacharyya A. 1946. On a measure of divergence between two multinomial populations. Sankhyā Indian J. Stat. 7:401–406.

Boscaini A., Gaudin T.J., Quispe B.M., Münch P., Antoine P.O., Pujos F. 2019a. New well-preserved craniodental remains of *Simomylodon uccasamamensis* (Xenarthra: Mylodontidae) from the Pliocene of the Bolivian Altiplano: Phylogenetic, chronostratigraphic and palaeobiogeographical implications. Zool. J. Linn. Soc. 185:459–486.

Boscaini A., Iurino D.A., Mamani Quispe B., Andrade Flores R., Sardella R., Pujos F., Gaudin T.J. 2020a. Cranial anatomy and paleoneurology of the extinct sloth *Catonyx tarijensis* (Xenarthra, Mylodontidae) from the Late Pleistocene of Oruro, southwestern Bolivia. Front. Ecol. Evol. 8:1–16.

Boscaini A., Iurino D.A., Sardella R., Tirao G., Gaudin T.J., Pujos F. 2020b. Digital cranial endocasts of the extinct sloth *Glossotherium robustum* (Xenarthra, Mylodontidae) from the Late Pleistocene of Argentina: Description and comparison with the extant sloths. J. Mamm. Evol. 27:55–71.

Boscaini A., Pujos F., Gaudin T.J. 2019b. A reappraisal of the phylogeny of Mylodontidae (Mammalia, Xenarthra) and the divergence of mylodontine and lestodontine sloths. Zool. Scr. 48:691–710.

Brambilla L., Ibarra D.A. 2018. *Archaeomylodon sampedrinensis*, gen. et sp. nov., a new mylodontine from the middle Pleistocene of Pampean Region, Argentina. J. Vertebr. Paleontol. 38:1–13.

Brandoni D. 2006. Los Megatheriinae (Xenarthra, Tardigrada, Megatheriidae) terciarios de Argentina. sistemática, evolución y biogeografia. La Plata: Universidad Nacional de La Plata.

Brandoni D. 2014. *"Xyophorus"* sp. en el Mioceno medio de Chubut: implicancias sistemáticas, biogeográficas y biocronológicas del registro de un Nothrotheriinae en el Neógeno de la Argentina. Ameghiniana. 51:94–105.

Brandoni D., González Ruiz L., Reato A., Martin G. 2019. Chronological implications of the nothrotheriid *"Xyophorus"* (Mammalia, Xenarthra) from the Collón Curá Formation (Miocene of Patagonia, Argentina). Hist. Biol. 31:879–887.

Brazeau M.D., Giles S., Dearden R.P., Jerve A., Ariunchimeg Y.A., Zorig E., Sansom R., Guillerme T., Castiello M. 2020. Endochondral bone in an Early Devonian 'placoderm' from Mongolia. Nat. Ecol. Evol. 4:1477–1484.

Brown J.M., Lemmon A.R. 2007. The importance of data partitioning and the utility of Bayes factors in Bayesian phylogenetics. Syst. Biol. 56:643–655.

Brusatte S.L., Benton M.J., Ruta M., Lloyd G.T. 2008. Superiority, competition, and opportunism in the evolutionary radiation of dinosaurs. Science (80-.). 321:1485–1488.

Buchholtz E.A., Stepien C.C. 2009. Anatomical transformation in mammals: Developmental origin of aberrant cervical anatomy in tree sloths. Evol. Dev. 11:69–79.

Buckley M. 2018. Paleoproteomics: an introduction to the analysis of ancient proteins by soft ionisation mass spectrometry. In: Lindqvist C., Rajora O.P., editors. Paleogenomics. Cham: Springer. p. 31–52.

Campbell V., Lapointe F.J. 2009. The use and validity of composite taxa in phylogenetic analysis. Syst. Biol. 58:560–572.

Carlini A.A., Scillato-Yané G.J. 2004. The oldest Megalonychidae (Xenarthra: Tardigrada); phylogenetic relationships and an emended diagnosis of the family. Neues Jahrb. für Geol. und Paläontologie-Abhandlungen. 233:423–443.

Cartelle C., De Iuliis G., Boscaini A., Pujos F. 2019. Anatomy, possible sexual dimorphism, and phylogenetic affinities of a new mylodontine sloth from the late Pleistocene of intertropical Brazil. J. Syst. Palaeontol. 17:1957–1988.

Cartelle C., De Iuliis G., Ferreira R.L. 2009. Systematic revision of tropical Brazilian scelidotheriine sloths (Xenarthra, Mylodontoidea). J. Vertebr. Paleontol. 29:555–566.

Casali D. de M., Freitas F. V., Perini F.A. 2021. Anatomical partitioning have little influence in topologies from Bayesian phylogenetic analyses of morphological data. PhD Thesis. Chapter 1.

Casali D. de M., Dos Santos Júnior J.E., Miranda F.R., Santos F.R., Perini F.A. 2020. Total-evidence phylogeny and divergence times of Vermilingua (Mammalia: Pilosa). Syst. Biodivers. 18:216–227.

Casali D.M., Perini F.A. 2017. The evolution of hyoid apparatus in Xenarthra (Mammalia: Eutheria). Hist. Biol. 29:777–788.

Clarke J.A., Middleton K.M. 2008. Mosaicism, modules, and the evolution of birds: results from a Bayesian approach to the study of morphological evolution using discrete character data. Syst. Biol. 57:185–201.

Delsuc F., Ctzeflis F.M., Stanhope M.J., Douzery E.J.P. 2001. The evolution of armadillos, anteaters and sloths depicted by nuclear and mitochondrial phylogenies: implications for the status of the enigmatic fossil *Eurotamandua*. Proc. R. Soc. London. Ser. B Biol. Sci. 268:1605–1615.

Delsuc F., Kuch M., Gibb G.C., Hughes J., Szpak P., Southon J., Enk J., Duggan A.T., Poinar H.N. 2018. Resolving the phylogenetic position of Darwin's extinct ground sloth (*Mylodon darwinii*) using mitogenomic and nuclear exon data. Proc. R. Soc. B Biol. Sci. 285:1–10.

Delsuc F., Kuch M., Gibb G.C., Karpinski E., Hackenberger D., Szpak P., Martínez J.G., Mead J.I., McDonald H.G., MacPhee R.D.E., Billet G., Hautier L., Poinar H.N. 2019. Ancient mitogenomes reveal the evolutionary history and biogeography of sloths. Curr. Biol. 29:2031-2042.e6.

Engelmann G.F. 1985. The phylogeny of the Xenarthra. In: Montgomery G.G., editor. The evolution and ecology of armadillos, sloths and vermilinguas. Washington: Smithsonian Institution Press. p. 51–64.

Engelmann G.F. 1987. A new Deseadan sloth (Mammalia: Xenarthra) from Salla, Bolivia, and its implications for the primitive condition of the dentition in edentates. J. Vertebr. Paleontol. 7:217–223.

Fan Y., Wu R., Chen M.-H., Kuo L., Lewis P.O. 2011. Choosing among partition models in Bayesian phylogenetics. Mol. Biol. Evol. 28:523–532.

Fariña R.A., Vizcaíno S.F. 2003. Slow moving or browsers? A note on nomenclature. Morphological studies in fossil and extant Xenarthra (Mammalia). Senckenb. Biol. 83:34.

Farris J.S. 1969. A successive approximations approach to character weighting. Syst. Zool. 18:374.

Farris J.S. 1989. The retention index and the rescaled consistency index. Cladistics. 5:417–419.

Felsenstein J. 1978. Cases in which parsimony or compatibility methods will be positively misleading. Syst. Biol. 27:401–410.

Gardner A.L. 2008. Mammals of South America, Volume 1 - Marsupials, xenarthrans, shrews, and bats. London: The University of Chicago Press.

Gaudin T.J. 1990. The ear region of the Pilosa (Mammalia, Xenarthra) and the phylogeny of the Tardigrada. J. Vertebr. Paleontol. 10:24A.

Gaudin T.J. 1995. The ear region of edentates and the phylogeny of the Tardigrada (Mammalia, Xenarthra). J. Vertebr. Paleontol. 15:672–705.

Gaudin T.J. 1999. The morphology of xenarthrous vertebrae (Mammalia: Xenarthra). Fieldiana, Geol. 41:1–38.

Gaudin T.J. 2004. Phylogenetic relationships among sloths (Mammalia, Xenarthra, Tardigrada): the craniodental evidence. Zool. J. Linn. Soc. 140:255–305.

Gaudin T.J., Branham D.G. 1998. The phylogeny of the Myrmecophagidae (Mammalia, Xenarthra, Vermilingua) and the relationship of *Eurotamandua* to the Vermilingua. J. Mamm. Evol. 5:237–265.

Gaudin T.J., Croft D.A. 2015. Paleogene Xenarthra and the evolution of South American mammals. J. Mammal. 96:622–634.

Gaudin T.J., McDonald H.G. 2008. Morphology-based investigations of the phylogenetic relationships among extant and fossil xenarthrans. In: Vizcaíno S.F., Loughry W.J., editors. The biology of the Xenarthra. Gainesville: University of Florida Press. p. 24–36.

Gaudin T.J., Wible J.R. 2004. On the cranial osteology of the yellow armadillo *Euphractus sexcintus* (Dasypodidae, Xenarthra, Placentalia). Ann. Carnegie Museum. 73:117–196.

Gavryushkina A., Welch D., Stadler T., Drummond A.J. 2014. Bayesian inference of sampled ancestor trees for epidemiology and fossil calibration. PLoS Comput. Biol. 10:1–15.

Gearty W. 2021. deeptime: Plotting tools for anyone working in deep time. https://github.com/willgearty/deeptime.

Gibb G.C., Condamine F.L., Kuch M., Enk J., Moraes-Barros N., Superina M., Poinar H.N., Delsuc F. 2016. Shotgun mitogenomics provides a reference phylogenetic framework and timescale for living xenarthrans. Mol. Biol. Evol. 33:621–642.

Goloboff P. 1993. Estimating character weights during tree search. Cladistics. 9:83–91.

Goloboff P.A., Catalano S.A. 2016. TNT version 1.5, including a full implementation of phylogenetic morphometrics. Cladistics. 32:221–238.

Goloboff P.A., Farris J.S., Nixon K.C. 2008. TNT, a free program for phylogenetic analysis. Cladistics. 24:774–786.

Goloboff P.A., Torres A., Arias J.S. 2018. Weighted parsimony outperforms other methods of phylogenetic inference under models appropriate for morphology. Cladistics. 34:407–437.

Greenwood A., Castresana J., Feldmaier-Fuchs G., Pääbo S. 2001. A molecular phylogeny of two extinct sloths. Mol. Phylogenet. Evol. 18:94–103.

Guillerme T., Cooper N. 2016. Effects of missing data on topological inference using a Total Evidence approach. Mol. Phylogenet. Evol. 94:146–158.

Guth C. 1961. La région temporale des Edentés. Le Puy: Imprimierie Jeanne D'Arc.

Hanson-Smith V., Kolaczkowski B., Thornton J.W. 2010. Robustness of ancestral sequence reconstruction to phylogenetic uncertainty. Mol. Biol. Evol. 27:1988–1999.

Haro J.A., Tauber A.A., Krapovickas J.M. 2016. The manus of *Mylodon darwinii* Owen (Tardigrada, Mylodontidae) and its phylogenetic implications. J. Vertebr. Paleontol. 36:e1188824.

Haro J.A., Tauber A.A., Krapovickas J.M. 2017. Thoracic member (pectoral girdle and forelimb) bones of *Mylodon darwinii* Owen (Xenarthra, Mylodontidae) from the Late Pleistocene of Central Argentina and their phylogenetic implications. PalZ. 91:439–457.

Harrison L.B., Larsson H.C.E. 2015. Among-character rate variation distributions in phylogenetic analysis of discrete morphological characters. Syst. Biol. 64:307–324.

Hautier L., Gomes Rodrigues H., Billet G., Asher R.J. 2016. The hidden teeth of sloths: evolutionary vestiges and the development of a simplified dentition. Sci. Rep. 6:27763.

Heath T.A., Huelsenbeck J.P., Stadler T. 2014. The fossilized birth-death process for coherent calibration of divergence-time estimates. Proc. Natl. Acad. Sci. 111:E2957–E2966.

Hoffstetter R. 1954. Phylogenie des Edentes xenarthres. Bull. du Museum Natl. d'Histoire Nat. 2:433–438.

Hoffstetter R. 1956. Contribuition a L'étude des Orophodontoidea, gravigrades cuirassés de la Patagonie. An. Paléontologie. 42:27–40.

Huelsenbeck J.P. 1994. Comparing the stratigraphic record to estimates of phylogeny. Paleobiology. 20:470–483.

Huelsenbeck J.P., Bollback J.P. 2001. Empirical and hierarchical bayesian estimation of ancestral states. Syst. Biol. 50:351–366.

Huelsenbeck J.P., Ronquist F. 2001. MRBAYES: Bayesian inference of phylogenetic trees. Bioinformatics. 17:754–755.

De Iuliis G. 1996. A systematic review of the Megatheriinae (Mammalia: Xenarthra: Megatheriidae). Toronto: University of Toronto.

De Iuliis G., Boscaini A., Pujos F., Mcafee R.K., Cartelle C., Tsuji L.J.S., Rook L. 2020. On the status of the giant mylodontine sloth *Glossotherium wegneri* (Spillmann, 1931) (Xenarthra, Folivora) from the late Pleistocene of Ecuador. Comptes Rendus Palevol. 2020.

De Iuliis G., Gaudin T.J., Vicars M.J. 2011. A new genus and species of nothrotheriid sloth (Xenarthra, Tardigrada, Nothrotheriidae) from the Late Miocene (Huayquerian) of Peru. Palaeontology. 54:171–205.

De Iuliis G., Pujos F. 2006. On the systematics of *Hapalops* (Xenarthra: Megatherioidea). J. Vertebr. Paleontol. 26:55A.

De Iuliis G., Pujos F., Toledo N., Bargo M.S., Vizcaíno S.F. 2014. *Eucholoeops* Ameghino, 1887 (Xenarthra, Tardigrada, Megalonychidae) from the Santa Cruz Formation, Argentine Patagonia: implications for the systematics of Santacrucian sloths. Geodiversitas. 36:209–255.

Joy J.B., Liang R.H., McCloskey R.M., Nguyen T., Poon A.F.Y. 2016. Ancestral reconstruction. PLoS Comput. Biol. 12:1–20.

Kass R.E., Raftery A.E. 1995. Bayes Factors. J. Am. Stat. Assoc. 90:773–795.

King B. 2019. Which morphological characters are influential in a Bayesian phylogenetic analysis? Examples from the earliest osteichthyans. Biol. Lett. 15:20190288.

King B. 2021. Bayesian tip-dated phylogenetics in paleontology: topological effects and stratigraphic fit. Syst. Biol. 70:283–294.

Kjer K.M., Honeycutt R.L. 2007. Site specific rates of mitochondrial genomes and the phylogeny of Eutheria. BMC Evol. Biol. 7:1–9.

Lee M.S.Y., Cau A., Naish D., Dyke G.J. 2014. Morphological clocks in paleontology, and a Mid-Cretaceous origin of crown aves. Syst. Biol. 63:442–449.

Lemmon A.R., Moriarty E.C. 2004. The importance of proper model assumption in Bayesian phylogenetics. Syst. Biol. 53:265–277.

Lewis P.O. 2001. A likelihood approach to estimating phylogeny from discrete morphological character data. Syst. Biol. 50:913–925.

Lloyd G.T. 2016. Estimating morphological diversity and tempo with discrete character-taxon matrices: implementation, challenges, progress, and future directions. Biol. J. Linn. Soc. 118:131–151.

Lucena D.A.A., Almeida E.A.B. 2021. Morphology and Bayesian tip-dating recover deep Cretaceous-age divergences among major chrysidid lineages (Hymenoptera: Chrysididae). Zool. J. Linn. Soc. 0:1–44.

Luo A., Duchêne D.A., Zhang C., Zhu C.D., Ho S.Y.W. 2020. A simulation-based evaluation of tip-dating under the fossilized birth-death process. Syst. Biol. 69:325–344.

MacPhee R.D.E., Iturralde-Vinent M.A. 1995. Origin of the Greater Antillean land mammal fauna, 1: new Tertiary fossils from Cuba and Puerto Rico. Am. Museum Novit. 3141:1–30.

Maddison W.P., Maddison D.R. 2019. Mesquite: a modular system for evolutionary analysis. http://www.mesquiteproject.org.

Matzke N.J., Wright A. 2016. Inferring node dates from tip dates in fossil Canidae: the importance of tree priors. Biol. Lett. 12:20160328.

McDonald H.G. 2012. Evolution of the pedolateral foot in ground sloths: Patterns of change in the astragalus. J. Mamm. Evol. 19:209–215.

McDonald H.G., Arroyo-Cabrales J., Alarcón-Durán I., Espinosa-Martínez D. V. 2020. First record of *Meizonyx salvadorensis* (Mammalia: Xenarthra: Pilosa) from the late Pleistocene of Mexico and its evolutionary implications. J. Syst. Palaeontol. 18:1829–1851.

McDonald H.G., Carranza-Castañeda O. 2017. Increased xenarthran diversity of the Great American Biotic Interchange: a new genus and species of ground sloth (Mammalia, Xenarthra, Megalonychidae) from the Hemphillian (late Miocene) of Jalisco, Mexico. J. Paleontol. 91:1069–1082.

McDonald H.G., Chatters J.C., Gaudin T.J. 2017. A new genus of megalonychid ground sloth (Mammalia, Xenarthra) from the late Pleistocene of Quintana Roo, Mexico. J. Vertebr. Paleontol. 37:e1307206.

McDonald H.G., De Iuliis G. 2008. Fossil history of sloths. In: Vizcaino S.F., Loughry W.J., editors. The Biology of the Xenarthra. Gainesville: University Press of Florida. p. 39–55.

McDonald H.G., de Muizon C. 2002. The cranial anatomy of *Thalassocnus* (Xenarthra, Mammalia), a derived nothrothere from the Neogene of the Pisco Formation (Peru). J. Vertebr. Paleontol. 22:349–365.

McDonald H.G., Perea D. 2002. The large scelidothere *Catonyx tarijensis* (Xenarthra , Mylodontidae) from the Pleistocene of Uruguay. J. Vertebr. Paleontol. 22:677–683.

McDonald H.G., Rincón A.D., Gaudin T.J. 2013. A new genus of megalonychid sloth (Mammalia, Xenarthra) from the late Pleistocene (Lujanian) of Sierra de Perija, Zulia State, Venezuela. J. Vertebr. Paleontol. 33:1226–1238.

McKenna M.C., Bell S.K. 1997. Classification of mammals: above the species level. New York: Columbia University Press.

McKenna M.C., Wyss A.R., Flynn J.J. 2006. Paleogene pseudoglyptodont xenarthrans from central Chile and Argentine Patagonia. Am. Museum Novit. 3536:1–18.

Melo D., Porto A., Cheverud J.M., Marroig G. 2016. Modularity: genes, development, and evolution. Annu. Rev. Ecol. Evol. Syst. 47:463–486.

Miller M.A., Pfeiffer W., Schwartz T. 2010. Creating the CIPRES Science Gateway for inference of large phylogenetic trees. 2010 Gatew. Comput. Environ. Work. GCE 2010.:1–8.

Miño-Boilini Á.R. 2012. Sistemática y evolución de los Scelidotheriinae (Xenarthra, Mylodontidae) cuaternarios de la Argentina. Importancia bioestratigráfica, paleobiogeográfica y peleoambiental. La Plata: Universidad Nacional de La Plata.

Miño-Boilini Á.R., Carlini A.A., Scillato-Yané G.J. 2014. Revisión sistemática y taxonómica del género *Scelidotherium* Owen, 1839 (Xenarthra, Phyllophaga, Mylodontidae). Rev. Bras. Paleontol. 17:43–58.

Mongiardino Koch N., Garwood R.J., Parry L.A. 2021. Fossils improve phylogenetic analyses of morphological characters. Proc. R. Soc. B Biol. Sci. 288:20210044.

de Muizon C., McDonald H.G., Salas R., Urbina M. 2003. A new early species of the aquatic sloth *Thalassocnus* (Mammalia, Xenarthra) from the Late Miocene of Peru. J. Vertebr. Paleontol. 23:886–894.

de Muizon C., McDonald H.G., Salas R., Urbina M. 2004a. The evolution of feeding adaptations of the aquatic sloth *Thalassocnus*. J. Vertebr. Paleontol. 24:398–410.

de Muizon C., McDonald H.G., Salas R., Urbina M. 2004b. The youngest species of the aquatic sloth *Thalassocnus* and a reassessment of the relationship of the nothrothere sloths (Mammalia: Xenarthra). J. Vertebr. Paleontol. 24:387–397.

Murphy J.L., Puttick M.N., O'Reilly J.E., Pisani D., Donoghue P.C.J. 2021. Empirical distributions of homoplasy in morphological data. Palaeontology. 0:1–14.

Naples V.L., McAfee R.K. 2012. Reconstruction of the cranial musculature and masticatory function of the Pleistocene panamerican ground sloth *Eremotherium laurillardi* (Mammalia, Xenarthra, Megatheriidae). Hist. Biol. 24:187–206.

Naples V.L., McAfee R.K. 2014. Chewing through the Miocene: an examination of the feeding musculature in the ground sloth *Hapalops* from South America (Mammalia: Pilosa). F1000Research. 3:1–26.

Negri F., Ferigolo J. 2004. Urumacotheriinae, nova subfamília de Mylodontidae (Mammalia, Tardigrada) do Mioceno superior-Plioceno, América do Sul. Rev. Bras. Paleontol. 7:281–288.

Nieto G.L., Haro J.A., McDonald H.G., Miño-Boilini Á.R., Tauber A.A., Krapovickas J.M., Fabianelli M.N., Rosas F.M. 2020. The Skeleton of the Manus of *Scelidotherium* (Xenarthra, Mylodontidae) specimens from the Pleistocene of the Province of Córdoba, Argentina, and its Systematic Implications. J. Mamm. Evol. 0:0.

Nyakatura J.A. 2012. The convergent evolution of suspensory posture and locomotion in tree sloths. J. Mamm. Evol. 19:225–234.

Nylander J.A.A., Ronquist F., Huelsenbeck J.P., Nieves-Aldrey J.L. 2004. Bayesian phylogenetic analysis of combined data. Syst. Biol. 53:47–67.

O'Reilly J.E., Donoghue P.C.J. 2018. The efficacy of consensus tree methods for summarizing phylogenetic relationships from a posterior sample of trees estimated from morphological data. Syst. Biol. 67:354–362.

Patterson B., Pascual R. 1968. The fossil mammal fauna of South America. Q. Rev. Biol. 43:409–451.

Patterson B., Segall W., Turnbull W.D., Gaudin T.J. 1992. The ear region in Xenarthrans (=Edentata: Mammalia). Part II. Pilosa (sloths, anteaters), palaeanodonts, and a miscellany. Fieldiana Geol. 24:1–79.

Paula Couto C. de. 1979. Tratado de Paleomastozoologia. Rio de Janeiro: Academia Brasileira de Ciencias.

Poinar H., Kuch M., McDonald G., Martin P., Pääbo S. 2003. Nuclear gene sequences from a late Pleistocene sloth coprolite. Curr. Biol. 13:1150–1152.

Porto D.S., Almeida E.A.B. 2021. Corbiculate bees (Hymenoptera: Apidae): exploring the limits of morphological data to solve a hard phylogenetic problem. Insect Syst. Divers. 5:1–40.

Porto D.S., Almeida E.A.B., Pennell M.W. 2021. Investigating morphological complexes using informational dissonance and Bayes factors: A case study in corbiculate bees. Syst. Biol. 70:295–306.

Prendini L. 2001. Species or supraspecific taxa as terminals in cladistic analysis? Groundplans versus exemplars revisited. Syst. Biol. 50:290–300.

Presslee S., Slater G.J., Pujos F., Forasiepi A.M., Fischer R., Molloy K., Mackie M., Olsen J. V, Kramarz A., Taglioretti M., Scaglia F., Lezcano M., Lanata J.L., Southon J., Feranec R., Bloch J., Hajduk A., Martin F.M., Salas Gismondi R., Reguero M., de Muizon C., Greenwood A., Chait B.T., Penkman K., Collins M., MacPhee R.D.E. 2019. Palaeoproteomics resolves sloth relationships. Nat. Ecol. Evol. 3:1121–1130.

Pujos F. 2006. *Megatherium celendinense* sp. nov. from the Pleistocene of the Peruvian Andes and the phylogenetic relationships of megatheriines. Palaeontology. 49:285–306.

Pujos F., Ciancio M.R., Forasiepi A.M., Pujos M., Candela A.M., Vera B., Reguero M.A., Combina A.M., Cerdeño E. 2021. The late Oligocene xenarthran fauna of Quebrada Fiera (Mendoza, Argentina) and its implications for sloth origins and the diversity of Palaeogene cingulates. Pap. Palaeontol. 0:1–44.

Pujos F., Gaudin T.J., De Iuliis G., Cartelle C. 2012. Recent advances on variability, morpho-functional adaptations, dental terminology, and evolution of sloths. J. Mamm. Evol. 19:159–169.

Pujos F., De Iuliis G. 2007. Late Oligocene Megatherioidea fauna (Mammalia: Xenarthra) from Salla-Luribay (Bolivia): new data on basal sloth radiation and Cingulata-Tardigrada split. J. Vertebr. Paleontol. 27:132–144.

Pujos F., De Iuliis G., Argot C., Werdelin L. 2007. A peculiar climbing Megalonychidae from the Pleistocene of Peru and its implication for sloth history. Zool. J. Linn. Soc. 149:179–235.

Pujos F., De Iuliis G., Cartelle C. 2017. A paleogeographic overview of tropical fossil sloths: towards an understanding of the origin of extant suspensory sloths? J. Mamm. Evol. 24:19–38.

Pujos F., De Iuliis G., Mamani Quispe B., Adnet S., Andrade Flores R., Billet G., Fernández-Monescillo M., Marivaux L., Münch P., Prámparo M.B., Antoine P.-O. 2016. A new nothrotheriid xenarthran from the Early Pliocene of Pomata-Ayte (Bolivia): new insights into the caniniform-molariform transition in sloths. Zool. J. Linn. Soc. 178:679–712.

Pujos F., De Iuliis G., Mamani Quispe B., Flores R.A. 2014. *Lakukullus anatisrostratus* , gen. et sp. nov., a new massive nothrotheriid sloth (Xenarthra, Pilosa) from the middle Miocene of Bolivia. J. Vertebr. Paleontol. 34:1243–1248.

Pujos F., De Iuliis G., Quispe B.M. 2011. *Hiskatherium saintandrei*, gen. et sp. nov.: An unusual sloth from the Santacrucian of Quebrada Honda (Bolivia) and an overview of middle Miocene, small megatherioids. J. Vertebr. Paleontol. 31:1131–1149.

Puttick M.N., O'Reilly J.E., Pisani D., Donoghue P.C.J. 2019. Probabilistic methods outperform parsimony in the phylogenetic analysis of data simulated without a probabilistic model. Palaeontology. 62:1–17.

Pyron R.A. 2011. Divergence time estimation using fossils as terminal taxa and the origins of Lissamphibia. Syst. Biol. 60:466–81.

R Core Team. 2021. R: A language and environment for statistical computing. https://www.r-project.org/.

Racco A., Fernicola J.C., Bargo M.S., Vizcaíno S.F., Iuliis G. De. 2018. On the type of *Schismotherium fractum* Ameghino, 1887 (Xenarthra, Folivora, Megatherioidea) from the Early Miocene Santa Cruz Formation (Santa Cruz Province, Argentina). Ameghiniana. 55:117–125.

Raj Pant S., Goswami A., Finarelli J.A. 2014. Complex body size trends in the evolution of sloths (Xenarthra: Pilosa). BMC Evol. Biol. 14:1–8.

Rambaut A., Drummond A.J., Xie D., Baele G., Suchard M.A. 2018. Posterior summarization in bayesian phylogenetics using Tracer 1.7. Syst. Biol. 67:901–904.

Revelle W. 2020. psych: Procedures for psychological, psychometric, and personality research. https://cran.r-project.org/package=psych.

Rincón A.D., Lemoine L.A., Mcdonald H.G. 2021. A new addition to Pleistocene megalonychid sloth diversity in the northern Neotropics. J. South Am. Earth Sci. 110:103379.

Rincón A.D., McDonald H.G., Solórzano A., Flores M.N., Ruiz-Ramoni D. 2015. A new enigmatic Late Miocene mylodontoid sloth from northern South America. R. Soc. Open Sci. 2:140256.

Rincón A.D., Solórzano A., McDonald H.G., Montellano-Ballesteros M. 2018. Two new megalonychid sloths (Mammalia: Xenarthra) from the Urumaco Formation (late Miocene), and their phylogenetic affinities. J. Syst. Palaeontol.:1–13.

Robinson D.F., Foulds L.R. 1981. Comparison of phylogenetic trees. Math. Biosci. 53:131–147.

Román-Carrión J.L., Brambilla L. 2019. Comparative skull osteology of *Oreomylodon wegneri* (Xenarthra, Mylodontinae): defining the taxonomic status of the Ecuadorian endemic mylodontid. J. Vertebr. Paleontol. 39:e1674860.

Ronquist F. 2004. Bayesian inference of character evolution. Trends Ecol. Evol. 19:475–481.

Ronquist F., Huelsenbeck J.P. 2003. MrBayes 3: Bayesian phylogenetic inference under mixed models. Bioinformatics. 19:1572–1574.

Ronquist F., Klopfstein S., Vilhelmsen L., Schulmeister S., Murray D.L., Rasnitsyn A.P. 2012a. A total-evidence approach to dating with fossils, applied to the early radiation of the Hymenoptera. Syst. Biol. 61:973–999.

Ronquist F., Lartillot N., Phillips M.J. 2016. Closing the gap between rocks and clocks using total-evidence dating. Philos. Trans. R. Soc. B Biol. Sci. 371:20150136.

Ronquist F., Teslenko M., van der Mark P., Ayres D.L., Darling A., Höhna S., Larget B., Liu L., Suchard M. a, Huelsenbeck J.P. 2012b. MrBayes 3.2: efficient Bayesian phylogenetic inference and model choice across a large model space. Syst. Biol. 61:539–42.

Rosa B.B., Melo G.A.R., Barbeitos M.S. 2019. Homoplasy-based partitioning outperforms alternatives in Bayesian analysis of discrete morphological data. Syst. Biol. 68:657–671.

Sanderson M.J., Donoghue M.J. 1989. Patterns of variation in levels of homoplasy. Evolution (N. Y). 43:1781–1795.

Sansom R.S., Choate P.G., Keating J.N., Randle E. 2018. Parsimony, not Bayesian analysis, recovers more stratigraphically congruent phylogenetic trees. Biol. Lett. 14:20180263.

Schliep K.P. 2011. phangorn: phylogenetic analysis in R. Bioinformatics. 27:592–593.

Schweitzer M.H., Schroeter E.R., Cleland T.P., Zheng W. 2019. Paleoproteomics of Mesozoic dinosaurs and other Mesozoic fossils. Proteomics. 19:1800251.

Scott W.B. 1903. Mammalia of the Santa Cruz beds. Part I. Edentata. In: Scott W.B., editor. Reports of the Princeton University Expeditions to Patagonia 1896-1899. Princeton: Princeton University Press. p. 1–364.

Shockey B.J., Anaya F. 2011. Grazing in a new Late Oligocene mylodontid sloth and a mylodontid radiation as a component of the Eocene-Oligocene faunal turnover and the early spread of grasslands/savannas in South America. J. Mamm. Evol. 18:101–115.

Simões T.R., Caldwell M.W., Pierce S.E. 2020a. Sphenodontian phylogeny and the impact of model choice in Bayesian morphological clock estimates of divergence times and evolutionary rates. BMC Biol. 18:1–30.

Simões T.R., Vernygora O., Caldwell M.W., Pierce S.E. 2020b. Megaevolutionary dynamics and the timing of evolutionary innovation in reptiles. Nat. Commun. 11.

Simpson G.G. 1948. The beginning of the age of mammals in South America. Bull. Am. Museum Nat. Hist. 91:1–232.

Slater G.J., Cui P., Forasiepi A.M., Lenz D., Tsangaras K., Voirin B., de Moraes-Barros N., MacPhee R.D.E., Greenwood A.D. 2016. Evolutionary relationships among extinct and extant sloths: The evidence of mitogenomes and retroviruses. Genome Biol. Evol. 8:607–621.

Smith M.R. 2019. Bayesian and parsimony approaches reconstruct informative trees from simulated morphological datasets. Biol. Lett. 15:20180632.

Springer M.S., Stanhope M.J., Madsen O., de Jong W.W. 2004. Molecules consolidate the placental mammal tree. Trends Ecol. Evol. 19:430–438.

Steadman D.W., Martin P.S., MacPhee R.D.E., Jull A.J.T., McDonald H.G., Woods C.A., Iturralde-Vinent M., Hodgins G.W.L. 2005. Asynchronous extinction of late Quaternary sloths on continents and islands. Proc. Natl. Acad. Sci. 102:11763–11768.

Stinnesbeck S.R., Frey E., Olguín J.A., Stinnesbeck W., Zell P., Mallison H., González González A., Aceves Núñez E., Velázquez Morlet A., Terrazas Mata A., Benavente Sanvicente M., Hering F., Rojas Sandoval C. 2017. *Xibalbaonyx oviceps*, a new megalonychid ground sloth (Folivora, Xenarthra) from the Late Pleistocene of the Yucatán Peninsula, Mexico, and its paleobiogeographic significance. PalZ. 91:245–271.

Stinnesbeck S.R., Stinnesbeck W., Frey E., Avilés Olguín J., González A.G. 2020. *Xibalbaonyx exinferis* n. sp. (Megalonychidae), a new Pleistocene ground sloth from the Yucatán Peninsula, Mexico. Hist. Biol. 00:1–12.

Stock C. 1925. Cenozoic gravigrade edentates of western North America, with special reference to the Pleistocene Megalonychinae and Mylodontidae of Rancho La Brea. Carnegie Inst. Washingt. 331:1–206.

Tarasov S., Génier F. 2015. Innovative bayesian and parsimony phylogeny of dung beetles (coleoptera, scarabaeidae, scarabaeinae) enhanced by ontology-based partitioning of morphological characters. PLoS One. 10.

Toledo N., Bargo M.S., Vizcaíno S.F. 2013. Muscular reconstruction and functional morphology of the forelimb of Early Miocene sloths (Xenarthra, Folivora) of Patagonia. Anat. Rec. 296:305–325.

Toledo N., Bargo M.S., Vizcaíno S.F. 2015. Muscular reconstruction and functional morphology of the hind limb of Santacrucian (Early Miocene) sloths (Xenarthra, Folivora) of Patagonia. Anat. Rec. 298:842–864.

Toledo N., Bargo M.S., Vizcaíno S.F., De Iuliis G., Pujos F. 2017. Evolution of body size in anteaters and sloths (Xenarthra, Pilosa): Phylogeny, metabolism, diet and substrate preferences. Earth Environ. Sci. Trans. R. Soc. Edinburgh. 106:289–301.

Toledo N., De Iuliis G., Vizcaíno S.F., Bargo M.S. 2018. The concept of a pedolateral pes revisited: The giant sloths *Megatherium* and *Eremotherium* (Xenarthra, Folivora, Megatheriinae) as a Case Study. J. Mamm. Evol. 25:525–537.

Upham N.S., Esselstyn J.A., Jetz W. 2019. Inferring the mammal tree: Species-level sets of phylogenies for questions in ecology, evolution, and conservation. PLOS Biol. 17:e3000494.

Varela L., Tambusso P.S., McDonald H.G., Fariña R.A. 2019. Phylogeny, macroevolutionary trends and historical biogeography of sloths: insights from a Bayesian morphological clock analysis. Syst. Biol. 68:204–218.

Warren D.L., Geneva A.J., Lanfear R. 2017. RWTY (R We There Yet): An R package for examining convergence of Bayesian phylogenetic analyses. Mol. Biol. Evol. 34:1016–1020.

Webb S.D. 1985. The interrelationships of tree sloths and ground sloths. In: Montgomery G.G., editor. The evolution and ecology of armadillos, sloths and vermilinguas. Washington: Smithsonian Institution Press. p. 105–112.

White J.L., MacPhee R.D.E. 2001. Sloths of the West Indies: A systematic and phylogenetic review. In: Woods C.A., Sergile F.E., editors. Biogeography of the West Indies: Patterns and Perspectives. New York: CRC Press. p. 201–235.

Wickham H. 2016. ggplot2: Elegant graphics for data analysis. https://ggplot2.tidyverse.org.

Wilcoxon F. 1945. Individual comparisons by ranking methods. Biometrics Bull. 1:80.

Wills M.A. 1999. Congruence between phylogeny and stratigraphy: Randomization tests and the gap excess ratio. Syst. Biol. 48:559–580.

Xie W., Lewis P.O., Fan Y., Kuo L., Chen M.-H. 2011. Improving marginal likelihood estimation for Bayesian phylogenetic model selection. Syst. Biol. 60:150–160.

Yang Z., Kumar S., Nei M. 1995. A new method of inference of ancestral nucleotide and amino acid sequences. Genetics. 141:1641–1650.

Yu G., Smith D.K., Zhu H., Guan Y., Lam T.T. 2017. ggtree: an R package for visualization and annotation of phylogenetic trees with their covariates and other associated data. Methods Ecol. Evol. 8:28–36.

Zhang C., Stadler T., Klopfstein S., Heath T.A., Ronquist F. 2016. Total-evidence dating under the fossilized birth-death process. Syst. Biol. 65:228–249.

Zhang C., Wang M. 2019. Bayesian tip dating reveals heterogeneous morphological clocks in Mesozoic birds. R. Soc. Open Sci. 6:182062.

SUPPLEMENTARY MATERIAL

Supplementary File S1. List of observed specimens and associated material.

Supplementary File S2. Table with taxonomic authorship for genera and consulted literature used as a complement in character codings.

Supplementary File S3. List of morphological characters.

Supplementary File S4. Nexus file with the morphological character matrix.

Supplementary File S5. TNT script for reproduce maximum parsimony analyses.

Supplementary File S6. Table with complementary MCMC specifications for non-clock Bayesian phylogenetic analyses.

Supplementary File S7. Table with temporal, geological and geographical information for fossil taxa.

Supplementary File S8. Nexus input file to reproduce all Bayesian analyses.

Supplementary File S9. Plots of resulting trees from all phylogenetic analyses (majority-rule consensus for Bayesian inferences and equal-weights parsimony; most-parsimonious tree for implied-weight parsimony), with branch lengths (for Bayesian inferences) and node supports (posterior probabilities for Bayesian inferences; standard boostrap for equal-weights parsimony; and Poisson boostrap for implied-weights parsimony).

Supplementary File S10. Tables with summary statistics for estimated partition rate multipliers obtained with Bayesian inferences.

Supplementary File S11. RDS file with results of stratigraphic consistency indices (R file).

Supplementary File S12. Tables with summary and test statistics for stratigraphic consistency indices.

Supplementary File S13. Plots of divergence time estimates for all five dating models. Bars at nodes depicting the uncertainty in age estimates (95% HPD).

Supplementary File S14. Plots with Bayesian ancestral state reconstruction for all 510 characters. Slide 511 depict node numbers to be used as reference for the synapomorphy list (Supplementary File S15).

Supplementary File S15. List of synapomorphies for all nodes of the best-fitting Bayesian chronogram, obtained with Bayesian and parsimony ancestral state reconstructions.

Supplementary File S16. Updated suprageneric classification of Folivora and the authorship of clade names.

Supplementary File S17. Table with relative rates (median and 95% HPD) of speciation, extinction and fossilization obtained with a skyline fossilized birth-death process for seven consecutive time bins.

Files available in:

https://drive.google.com/drive/folders/1754XoW4MOtzFRmNiLCCpRXwOlvV5BfSv?usp=sharing

CHAPTER 4. Morphological disparity and evolutionary rates of cranial and postcranial characters in Folivora (Mammalia: Pilosa)

ABSTRACT

Sloth morphological evolution has been widely studied qualitatively, with comparative anatomy and morpho-functional approaches, or through quantitative assessments of morphological variation using morphometrics. Only recently, however, folivoran morphological disparity and evolutionary rates began to be evaluated using discrete character data. Nonetheless, patterns of morphological evolution in separate character partitions have not been investigated, neither the relative influence of, at one hand, the phylogeny, and on the other, the dietary and locomotory adaptations of sloths. Here we evaluate those patterns using a phylomorphospace approach, quantifying morphological disparity and evolutionary rates, and investigating possible drivers of morphological evolution for cranial and postcranial characters in Folivora. The evolution of the morphology in those partitions is associated with distinct patterns of disparity among clades and ecological groups, even though the two partitions do not differ substantially in evolutionary tempo. Historical processes shaped the morphological evolution of sloths more consistently than ecological ones, although changes in postcranial characters also seem to be associated to locomotory adaptations, in which morphological convergences were much more common. We discuss important methodological trade-offs in investigations of partitioned datasets mostly composed of fossil taxa, stressing the importance of adequate sampling while conducting such inferences.

KEYWORDS: Sloths. Morphology. Partitions. Phylomorphospace. Diet. Locomotion.

4.1 INTRODUCTION

Sloths (Folivora), along with anteaters (Vermilingua), are members of the clade Pilosa and, together with its sister clade Cingulata (armadillos and their fossil kin), comprise Xenarthra (Gaudin 2004; Gibb et al. 2016), one of the main placental mammal lineages (O'Leary et al. 2013; Upham et al. 2019). Folivora is a diversified group, with approximately 100 recognized genera, most of them extinct, the extant diversity being restricted to only two genera, *Bradypus* Linnaeus 1758 and *Choloepus* Illiger 1811 (McKenna and Bell 1997; Gardner 2008; McDonald and De Iuliis 2008). This diversity of extinct and extant sloths is also reflected in morphology,

with marked differences associated with each of the main clades (Gaudin 2004; Varela et al. 2019; Casali et al. 2021 – Chapter 3). According to the most recent phylogenies based on morphological data, most sloths can be included in one of two major clades, Mylodontoidea and Megatherioidea, the first being composed of Scelidotheriidae and Mylodontidae and the second, of Megalonychidae and Megatheriidae (Casali et al. 2021 – Chapter 3).

Sloths present disparate ecological adaptations (Pujos et al. 2012; Gaudin and Croft 2015). Although all living and fossil sloths are considered herbivorous, dietary specializations have been inferred for several taxa, which have been classified as browsers, mixed-feeders or grazers (Naples 1982, 1987, 1989; Bargo and Vizcaíno 2008; Bargo et al. 2009, 2012; Naples and McAfee 2012; Saarinen and Karme 2017; Kalthoff and Green 2018). However, for some taxa, mostly among mylodontoids, data from craniomandibular morphology and dental wear patterns point to conflicting dietary classifications, making the distinction between grazers and mixed feeders less clear (Bargo and Vizcaíno 2008; Saarinen and Karme 2017).

Locomotory habits are also diverse throughout the evolutionary history of sloths, but can be more generally associated with either climbing or terrestrial (including graviportal) adaptations (White 1993, 1997; Pujos et al. 2007; Bargo et al. 2012; McDonald 2012; Nyakatura 2012; Toledo et al. 2012, 2013, 2015). Nevertheless, other types of substrate uses, like digging (Bargo et al. 2000; Pujos et al. 2012; Toledo et al. 2012; Gaudin and Croft 2015) or semi-aquatic adaptations can also be recognized (Amson et al. 2014, 2015a, 2015c, 2015b). Climbing habits range from facultative semi-arboreal forms (White 1993, 1997; Toledo et al. 2013, 2015) to fully suspensory taxa (living sloths, Nyakatura 2012), also encompassing climbing capabilities probably unrelated to an arboreal lifestyle (Pujos et al. 2011). Additionally, some terrestrial taxa may have been able to assume a bipedal posture (Coombs 1983; Casinos 1996; Brandoni et al. 2004).

Empirical morphospaces have been widely used to investigate patterns of morphological evolution, including adaptation, convergence, morphological disparity and evolutionary rates (Sidlauskas 2008; Lloyd 2016, 2018). Previous studies on sloth morphology applied a morphospace evaluation for morphometric data from dental (Green 2009; Green and Resar 2012; Resar et al. 2013; Saarinen and Karme 2017; Kalthoff and Green 2018) and postcranial elements (White 1997; Bargo et al. 2012; Toledo et al. 2012; Toledo 2016; Amson and Nyakatura 2018; de Oliveira and Santos 2018; Vizcaíno et al. 2018; Grass 2019; Serio et al. 2020). Often, and especially for postcranial data, this was done in a broader taxonomic context, along with other xenarthrans and other placental mammals, providing some insights on how their morphology relates to phylogeny and/or adaptation. One of the limitations of this approach

is that the morphology of sloths in particular, and xenarthrans in general, is quite unique when compared to other placental mammals, presenting a combination of primitive and derived traits (McDonald 2003).

Dental microwear patterns suggest that mylodontoids, which are considered grazers or mixed-feeders, present a distinguishable wear pattern when compared with browsing sloths, although differences within this last group are also noticeable, including between *Bradypus* and *Choloepus*, suggesting some degree of dietary specialization among browsers (Green 2009; Green and Resar 2012; Resar et al. 2013; Saarinen and Karme 2017; Kalthoff and Green 2018). On the other hand, postcranial morphospaces separate suspensory living sloths from terrestrial and semi-arboreal sloths, the latter usually being recovered close to taxa with inferred digging capabilities (Bargo et al. 2012; Toledo et al. 2012; Toledo 2016; de Oliveira and Santos 2018; Vizcaíno et al. 2018; Serio et al. 2020). This pattern was observed especially when anterior appendicular elements were investigated, although scapular morphology suggests a lesser degree of differentiation between suspensory and semi-arboreal taxa (Toledo 2016; Grass 2019). Some studies, which included a larger taxonomic fossil sample while investigating humeral morphology, also pointed to some historical signal, with terrestrial mylodontoids and megatheriids occupying slightly distinct morphospace regions, whereas stem megatherioids, megalonychids, stem megatheriids and nothrotherines cluster together, along with other semi-arboreal taxa (de Oliveira and Santos 2018; Serio et al. 2020).

Other studies examined the evolution of adaptive ecological characters themselves, suggesting an ancestral browsing diet and scansorial locomotory adaptations for sloths (Pujos et al. 2012; Gaudin and Croft 2015), whereas Varela et al. (2019) were the first to use discrete morphological characters to investigate patterns of disparity and morphological evolutionary rates for different folivoran clades, an approach further explored in the present study.

Discrete character matrices offer several advantages when comparing the morphology of fragmentary and incomplete taxa (Oyston et al. 2015, 2016; Schaeffer et al. 2020). This is particularly true for Folivora, a clade mostly comprised of extinct taxa, for which many are missing some anatomical information, although the group as a whole possess a remarkably good fossil record and several complete taxa especially for the last 20 Ma time span. Discrete character matrices allow to minimize this loss of information, although showing stronger historical signals, since they are usually constructed with the goal of inferring phylogeny. On the other hand, morphometric data is more closely associated with functional morphology and adaptive evolution (Anderson and Friedman 2012; Schaeffer et al. 2020). Nevertheless, the specific dataset used for this study also contains many homoplastic characters, some of which

can be associated with functional adaptations (Casali et al. 2021 – Chapter 3). Also, several previous studies, for different taxonomic groups, observed congruent disparity patterns obtained from cladistic and morphometric data (Anderson and Friedman 2012; Hetherington et al. 2015; Romano et al. 2017; Schaeffer et al. 2020, but see Mongiardino Koch et al. 2017). For rate analyses, on the other hand, discrete characters are to be preferred, since methods of ancestral state reconstruction are usually necessary to infer branch evolutionary rates. Those methods are much better developed for discrete, rather than continuous characters (Soul and Wright 2021), and ancestral states estimates are often improved when fossil taxa are included in the taxonomic sample (Puttick 2016).

The vertebrate skeleton is a modular morphological complex, and it is well known that different character partitions may evolve with different rates and lead to distinct phylogenetic patterns (Clarke and Middleton 2008; Mounce et al. 2016). Recent studies investigating morphological disparity and evolutionary rates for discrete character partitions in vertebrates showed that, when all morphological characters are treated as a homogeneous source of evidence, unique patterns exclusive to some of these character subset may be obscured (Stubbs et al. 2019; Simões et al. 2020; Wang et al. 2021).

We apply here a partition-oriented approach, separately investigating cranial and postcranial morphological evolution in sloths. This allows us to provide a general characterization of the patterns of morphological evolution in these morphological complexes for a broad sample of sloths, also investigating how they are associated with historical (phylogenetic) and ecological (adaptive) factors.

4.2 MATERIAL AND METHODS

4.2.1 Morphological dataset and phylogenetic tree

We obtained discrete morphological characters from a previous genus-level phylogenetic study of Folivora (Casali et al. 2021 – Chapter 3) – a dataset comprised of 510 characters (383 binary, 127 multistate, being 63 ordered). Those characters were separated into two data partitions. The cranial partition (326 binary, 240 multistate, being 86 ordered) was composed of characters from the skull (including ear region characters), mandible, teeth and hyoid apparatus. The postcranial partition (184 binary, 143 multistate, being 41 ordered) was composed mostly of appendicular skeleton characters, with a few characters from the axial skeleton. For a detailed account of those characters, see Casali et al. (2021 – Chapter 3). The dataset is available as Supplementary File S1.

Partition datasets were pruned of outgroups and of sloth taxa that were associated with incalculable distances (i.e., absence of coded characters for a given pair of taxa). For evaluating the minimum number of taxa to be removed due to incalculable distances, we calculated the maximum observable rescaled distance (MORD) with functions *calculate_morphological_distances* and *trim_matrix* in the package *Claddis* (Lloyd 2016) in the R programing environment (R Core Team 2021). Also, we removed those taxa that presented a 75% or higher proportion of missing data in at least one of the two partitions (Supplementary File S2). Preliminary explorations showed that most taxa with this high level of missing data were artificially being displaced to extreme values along the axes of the morphospace, which resulted in their isolation from all other data points, even from those similar in character coding. In both cases, if a taxon was removed from one partition, it was also removed from the other, ensuring that results of partitions were comparable. The resulting datasets included 41 taxa, with at least one representative of all major groups recognized in the classification of Casali et al. (2021 – Chapter 3), which is herewith considered as the main systematic scheme.

As a reference tree, we adopted the Bayesian chronogram from the best-fitting model from Casali et al. (2021 – Chapter 3), pruned to match the taxonomic sample of the present datasets. The complete tree is available as Supplementary File S3.

4.2.2 Definition of clades and ecological groups

To study the influence of historical factors in the morphological evolution of Folivora, we applied two phylogenetic divisions of sloths: i) less inclusive clades: Scelidotheriidae, Mylodontidae, Megatheriidae and Megalonychidae, and ii) more inclusive clades – Mylodontoidea and Megatherioidea.

Dietary and locomotory categories were obtained from the literature (Supplementary File S4). To classify taxa that were not previously evaluated, we applied the same criteria used by studies which investigated morphologically similar and phylogenetically related taxa. We worked with general but still biologically meaningful ecological subsets, avoiding overly small groups, which could affect the precision of estimates of morphological disparity (Lloyd 2016; Gerber 2019).

For dietary categorization, we relied on previous classifications that considered evidence from anatomical features of the muzzle and mandibular spout, as well as overall tooth morphology and dental wear patterns. More rarely, data from masticatory musculature

reconstructions and paleofecal content was available, and was also considered. Since there are considerable disagreements among classifications stemming from alternative sources of evidence for taxa associated with mixed feeding and grazing, we considered both diets in a single category – mixed/grazer – whereas all other specialized folivorans were classified as browsers.

We assigned sloth taxa to one of two locomotory categories – scansorial and terrestrial. These assignments were also informed by literature that applied anatomical and morpho-functional inferences to assess locomotory habits. We considered both fully arboreal living and semi-arboreal extinct sloths as scansorial. This category was also applied to *Diabolotherium* Pujos et al. 2007, which presents climbing adaptations probably unrelated to arboreal substrates (Pujos et al. 2011). All other taxa possessing terrestrial (= ambulatory) adaptations were grouped together in a single category, irrespective of substrate use. When different species of a genus differed in their locomotory adaptations, as is the case for *Thalassocnus* Muizon and McDonald 1995, we assigned the genus the primitive condition, to avoid introducing categories that would include only one or a couple of taxa, which could make qualitative analyses impossible.

4.2.3 Morphological disparity

For each partition in the dataset, we inferred character ancestral states with the function *estimate_ancestral_states* in the R package *Claddis*, only reconstructing nodes with observed states for both descendants, whereas tip nodes were not inferred. Ancestral states for inapplicable characters were also not estimated, and polymorphic states were considered equally likely. The threshold used to collapse ancestral states to the most probable state was kept at the default value (= 0.01). Then we calculated morphological distances of discrete characters with MORD (Lloyd 2016), applying an arcsine square root transformation with the function *calculate_morphological_distances*, in *Claddis*. Polymorphisms were evaluated using their minimum distances, inapplicable characters were treated as missing, and character dependencies were disregarded. With the distances obtained, we conducted principal coordinate analyses (PCoA) with the function *pcoa* in the R package *ape* (Paradis and Schliep 2019), applying a Cailliez correction for negative eigenvalues (Cailliez 1983). The first two PCoA axes were used for plotting graphs to visualize the data, but disparity analyses were conducted considering all axes. Reconstructed ancestors were included in the phylomorphospace

visualizations, but were not shown in traditional morphospaces and were removed from disparity analyses.

Disparity for dietary category groups was investigated using the cranial dataset exclusively, whereas for locomotory categories, only data from postcranial characters were considered. Before calculating the disparity index, we performed 1000 bootstrap replications for each group, rarefying the samples according to the size of the smallest group involved in each comparison, to ensure that differences in sample sizes were not affecting results. Disparity was assessed with the widely used sum of variances (SV) index, which is relatively insensitive to outliers and a good descriptor of changes in space occupancy (Guillerme et al. 2020), and is not much affected by moderate differences in group sizes and levels of missing data (Ciampaglio et al. 2001; Hopkins and Gerber 2017). To assess significance in disparity between groups, we compared medians applying a two-sided Wilcoxon rank-sum test (Wilcoxon 1945), with $\alpha = 0.01$, using the *stats* function *wilcox.test*. In cases of multiple comparisons, a Holm-Bonferroni p-value correction was applied (Holm 1979). To evaluate the degree of overlapping among distributions of values of SV obtained from bootstrapped data for each group, we applied the Bhattacharyya coefficient (BC, Bhattacharyya 1946). Following Guillerme and Cooper (2016), when $BC < 0.05$, we considered distributions clearly different; and clearly similar when $BC > 0.95$. Those calculations and tests were conducted in R package *dispRity* (Guillerme 2018), with functions *custom.subsets*, *boot.matrix, dispRity,* and *test.dispRity*.

4.2.4 Ancestral state reconstructions and phylogenetic signal of ecological characters

To be able to associate ecological categories with all branches of the tree for subsequent rate analyses, we estimated the ancestral diet and locomotion for all nodes of the tree. We reconstructed ancestral states with the R package and the function *corHMM* (Boyko and Beaulieu 2021), using marginal reconstructions (Joy et al. 2016). We fitted alternative versions of the Mk model (Lewis 2001), considering equal rates (ER) and all rates different (ARD) models of among-state rate heterogeneity (Paradis et al. 2004), and evaluated the presence of one or two rate regimes across branches (Beaulieu et al. 2013), resulting in four alternative models for each ecological character.

Those models were compared using sample size corrected Akaike information criteria – AICc, and Akaike weights – AICw (Burnham and Anderson 2002). In model selection, following Harmon (2018), we considered necessary a distance of, at least, four AICc units between the model with lower AICc (i.e., the best-fitting model) and the second best-fitting

model. Also, we required an AICw value greater than 0.9 for the best-fitting model; otherwise, the less parametrized model was applied irrespective of its relative fit (Harmon 2018). We also investigated the phylogenetic signal of ecological characters using the D statistic (Fritz and Purvis 2010), calculated by function *phylo.d* in the R package *caper* (Orme et al. 2018). Values of $D \leq 0$ relate to a strongly clumped distribution of character states in the tree, indicating a strong phylogenetic signal, with 0 being the value expected when characters evolved by a Brownian motion process. Values between 0 and 1 suggest a progressively weaker signal, with 1 indicating that characters evolved according to a stochastic process obtained by randomly permutating the data across the tips. Finally, values > 1 indicate an overdispersion of character states in the phylogeny, beyond random expectation. Significance was assessed relative to Brownian motion and permutational random patterns, using 10000 permutations, with probabilities ≥ 0.95 indicating phylogenetic signal compatible with those patterns.

4.2.5 Morphological evolutionary rates

Branch rates were evaluated with the function *test_rates* in the R package *Claddis*. which first reconstructs ancestral states for all morphological characters. Subsequently, this method considers the number of changes observed in each branch, calculated over the product of the branch duration (in millions of years) and the number of characters that can be observed at both ends of this given branch (Lloyd 2016). Ancestral states were reconstructed applying the same settings as used in disparity analyses, and for branch rate calculations, all polymorphic, uncertain and inapplicable states were considered as missing.

To test the influence of historical factors on morphological evolutionary rate shifts, we considered four rate regimes for each dataset partition, totaling 14 alternative models: i) a null model, with no rate shifts (1 rate regime); ii) six individual clade models (same clades as in disparity analyses), comparing the focal clade average morphological evolutionary rate relative to a background average rate comprised of the rates of all other branches not associated with the focal clade (2 rate regimes); iii) six models assuming that two of the less inclusive clades had distinct rates from all other tree branches (3 rate regimes); and iv) a model considering distinct average rates for each less inclusive clade, plus a background average rate (5 rate regimes). To evaluate the influence of ecological factors, we applied a model with branches associated with the derived ecological category presenting an average rate different from those associated with the primitive state (2 rate regimes). For each dataset partition, the fit of models to the data was evaluated with AICc and AICw. For the cranial dataset, we should note that

Mylodontoidea and the ecological (diet) rate shifts are identical, but they are included for the sake of completeness. To allow comparison among partitions, branch rates (i.e., the number of character changes per million years) were normalized by their respective partition length.

Plots were produced using R packages *phytools* (Revell 2012), *ggplot2* (Wickham 2016), *ggphylomorpho* (Barr 2017), *ggtree* (Yu et al. 2017), *ggpubr* (Kassambara 2020), *ggrepel* (Slowikowski 2021) and *deeptime* (Gearty 2021). A script to fully reproduce all analyses employed in this study is available as Supplementary File S5.

Abbreviations

AICc, sample size corrected Akaike information criteria; AICw, Akaike weights; ARD, all rates different; BC, Bhattacharyya coefficient; ER, equal rates; MORD, maximum observable rescaled distance; PCoA, principal coordinate analysis; SV, sum of variances.

4.3 RESULTS

4.3.1 Overall morphospace patterns

As is usual for morphospaces/phylomorphospaces obtained from discrete morphological characters, especially when PCoA analyses are performed applying corrections for negative eigenvalues, the variance explained by each axis was quite modest. For cranial data, PCo1 explained 22.93% of the variance, and PCo2 13.24% (Fig. 1). For postcranial data, PCo1 was responsible for 9.48% of the variance, whereas for PCo2, 4.38% was explained (Fig. 2).

For the cranial dataset, the first axis of morphospace provided evidence of a clear separation between megatherioid and mylodontoid sloths, with *Bradypus* closely associated with the former, especially with stem megatherioids (Fig. 1). The other living genus, *Choloepus*, although clearly associated with megalonychids in morphospace, was somewhat separated from the other genera of this clade and displaced towards higher values of the PCo1, a region of morphospace occupied by mylodontoids (Fig. 1). Both living genera occupy a central position in PCo1, between megatherioids and mylodontoids. The PCo2 roughly separates the Megalonychidae from Megatheriidae and Mylodontidae from Scelidotheriidae, although stem members of some of those clades were associated with the clusters of other clades (Fig. 1). Among megatherioids, the stem genera *Pelecyodon* Ameghino 1891 and *Schismotherium* Ameghino 1887, as well as the stem megalonychids *Hapalops* Ameghino 1887 and

Eucholoeops Ameghino 1887*,* were placed closer to megatheriids. For mylodontoids, the stem genus *Octodontotherium* Ameghino 1895 was associated with mylodontids, whereas *Pseudoprepotherium* Hoffstetter 1961*,* a stem mylodontid, was closely associated with scelidotheriids (Fig. 1). These cases are suggestive of the retention of an ancestral morphology, according to the disposition of the branches of the phylomorphospace.

For the postcranial dataset, three major clusters could be recognized. There was a main group encompassing most sloths sampled here, with representatives from all less inclusive clades. The first axis separated this major group from Mylodontinae, which group far away on the positive values of PCo1, whereas PCo2 separated both from Megatheriini (Fig. 2). In the first group, there was some spatial structure associated with less inclusive clades, despite some noticeable exceptions, like the association of the stem megatheriid *Analcimorphus* Ameghino 1891, stem megatheriine *Diabolotherium*, and the stem scelidotheriid *Nematherium* Ameghino 1887 with megalonychids (Fig. 2). The proximity to scelidotheriines of less derived megatheriids, of the megalonychids *Parocnus* Miller 1929 and *Megalocnus* Leidy 1868, and of the stem mylodontid *Pseudoprepotherium*, is suggestive of morphological convergence, with their branches approximating to the central region of the phylomorphospace (Fig. 2). The stem megatherioids *Schismotherium* and *Pelecyodon* were situated close to megalonychids. The living genus *Bradypus* was placed between scansorial megalonychids and the terrestrial nothrotheriines, prepotheriines and *Octodontotherium.* The branches of the phylomorphospace indicate that the proximity of *Bradypus* to those terrestrial taxa may result from convergent evolution, since the ancestral node of the tree was recovered clustering with scansorial megalonychids (Fig. 2). PCoA eigenvalues and eigenvectors are available as Supplementary File S6.

4.3.2 Morphological disparity

Bootstrapped and rarefied disparity estimates were very similar to those obtained for the original data, with little impact on the estimated sum of variances for groups with greater sample sizes (> 10), whereas estimates for smaller groups were slightly more affected by the bootstrap procedure, as expected (Table 1). We considered the bootstrapped and rarefied data in the following results.

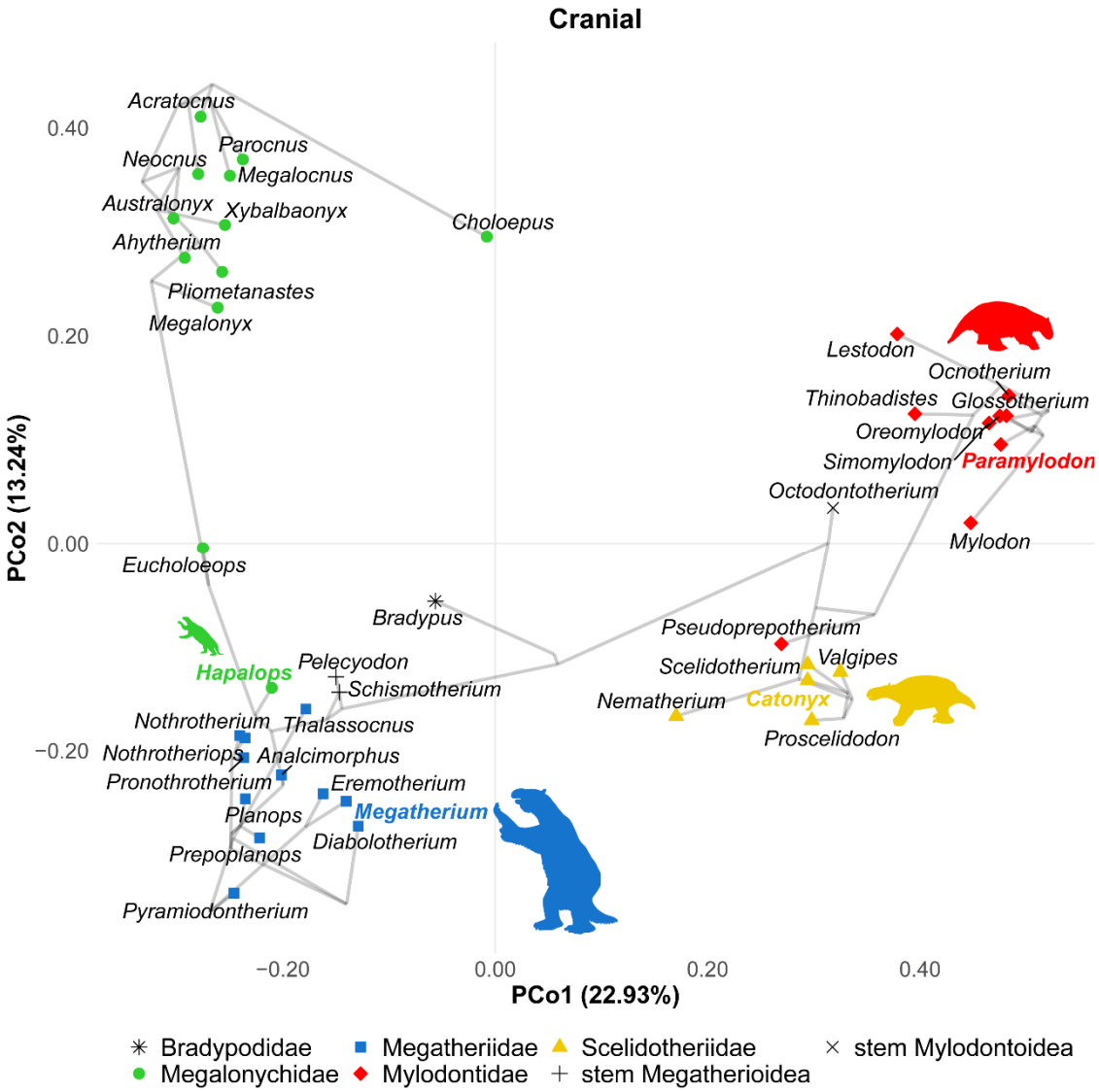

Figure 1. First two axes of cranial phylomorphospace, obtained after a principal coordinate analysis. Less inclusive clades (Scelidotheriidae, Mylodontidae, Megatheriidae and Megalonychidae) are shown in colors, and stem taxa not allocated to any of these clades are shown in black. Silhouettes for taxa with names indicated with bold face and colored obtained from phylopic.org.

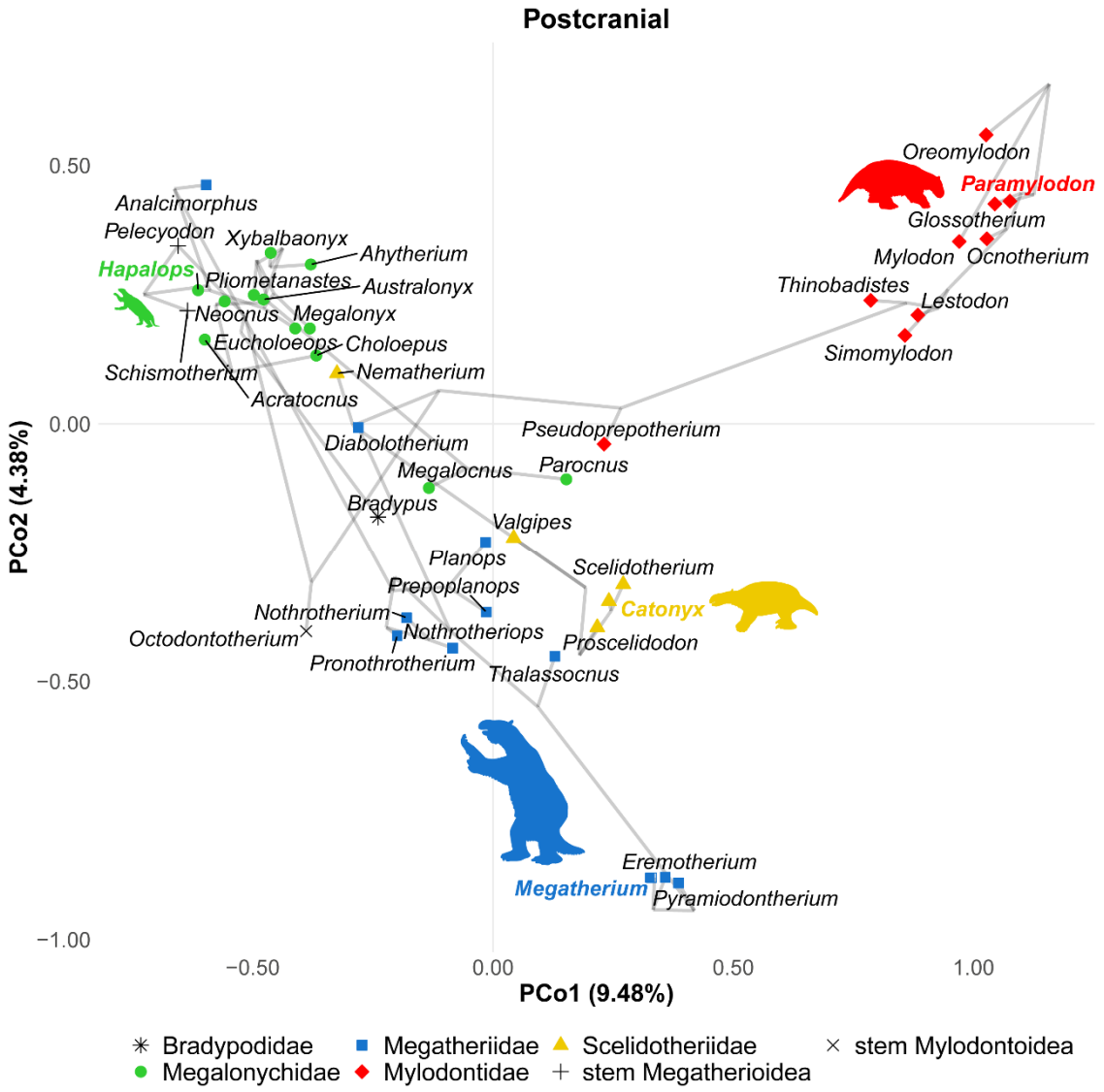

Figure 2. First two axes of postcranial phylomorphospace, obtained after a principal coordinate analysis. Less inclusive clades (Scelidotheriidae, Mylodontidae, Megatheriidae and Megalonychidae) are shown in colors, and stem taxa not allocated to any of these clades are shown in black. Silhouettes for taxa with names indicated with bold face and colored obtained from phylopic.org.

Table 1. Morphological disparity per partition dataset, for each clade and ecological group. The observed sum of variances – SV (Obs.) do not apply to rarefied samples. Median and confidence interval (CI) values for bootstrapped and rarefied data (BS).

Dataset	Group	Sample size	SV (Obs.)	Median (BS)	CI (BS)
Cranial	Megatheriidae	11	0.33	0.30	0.25 – 0.32
Cranial	Megatheriidae	5	-	0.31	0.21 – 0.35
Cranial	Megalonychidae	12	0.31	0.29	0.24 – 0.32
Cranial	Megalonychidae	5	-	0.28	0.19 – 0.35
Cranial	Mylodontidae	9	0.23	0.21	0.14 – 0.25
Cranial	Mylodontidae	5	-	0.21	0.12 – 0.27
Cranial	Scelidotheriidae	5	0.18	0.16	0.06 – 0.19
Cranial	Megatherioidea	25	0.37	0.36	0.33 – 0.38
Cranial	Megatherioidea	15	-	0.36	0.32 – 0.39
Cranial	Mylodontoidea	15	0.28	0.27	0.23 – 0.29
Cranial	Browser	26	0.38	0.36	0.33 – 0.39
Cranial	Browser	15	-	0.36	0.32 – 0.40
Cranial	Mixed/Grazer	15	0.28	0.27	0.23 – 0.29
Postcranial	Megatheriidae	11	3.31	3.04	2.68 – 3.23
Postcranial	Megatheriidae	5	-	3.04	2.24 – 3.45
Postcranial	Megalonychidae	12	2.99	2.76	2.42 – 2.92
Postcranial	Megalonychidae	5	-	2.79	2.01 – 3.14
Postcranial	Mylodontidae	9	2.87	2.57	2.12 – 2.82
Postcranial	Mylodontidae	5	-	2.56	1.83 – 3.01
Postcranial	Scelidotheriidae	5	2.94	2.45	1.29 – 2.94
Postcranial	Megatherioidea	25	3.23	3.10	2.94 – 3.21
Postcranial	Megatherioidea	15	-	3.10	2.88 – 3.26
Postcranial	Mylodontoidea	15	3.25	3.05	2.77 – 3.23
Postcranial	Scansorial	10	2.90	2.63	2.23 – 2.83
Postcranial	Terrestrial	31	3.40	3.29	3.18 – 3.36
Postcranial	Terrestrial	10	-	3.30	3.02 – 3.47

Among the less inclusive clades, there was a clear separation along the first two axes of morphospace when cranial data was considered (Fig. 3a). The median disparity was greater for Megatheriidae, followed by Megalonychidae, Mylodontidae, and Scelidotheriidae (Fig. 3b, Table 1), and those differences were found to be statistically significant (Table 2). Despite that,

those two first axes of morphospace indicate a broader occupancy of Megalonychidae relative to that of Megatheriidae (Fig. 3a), and there is considerable overlap in the disparity of those two clades (Fig. 3b, Tables 1 and 2). There is also a moderate overlap in the disparity of Scelidotheriidae and Mylodontidae (Fig. 3b, Tables 1 and 2). On the other hand, the degree of overlap for disparity estimates among less inclusive clades pertaining to different more inclusive clades is much smaller, with the SV distributions of Scelidotheriidae x Megatheriidae and Scelidotheriidae x Megalonychidae being the only cases in which distributions were clearly different according to BC (Fig. 3b, Tables 1 and 2). None of the comparisons among less inclusive clades indicated clearly similar distributions (Table 2).

For the postcranial dataset, the morphospace yielded a much greater superposition among less inclusive clades, with only Mylodontidae being well-separated from the others (Fig. 3c). The values for median disparity follow the same relative order as observed for cranial data, and group differences were also statistically significant (Fig. 3d, Tables 1 and 2). In contrast to the pattern observed for cranial data, the degree of overlap among estimates of postcranial disparity in Megalonychidae relative to that in Megatheriidae is only moderate, whereas that of Scelidotheriidae and Mylodontidae is much greater (Fig. 3d, Tables 1 and 2). Also, unlike cranial disparity, postcranial estimates of the sum of variance for Megalonychidae moderately overlapped those obtained for each mylodontoid clade (Fig. 3d, Tables 1 and 2). On the other hand, the distribution of sum of variances for Megatheriidae presented only a small overlapping with those of Scelidotheriidae and Mylodontidae, as observed for the cranial dataset (Fig. 3d, Tables 1 and 2). No comparison among those less inclusive clades indicated clearly similar or dissimilar distributions according to BC (Table 2).

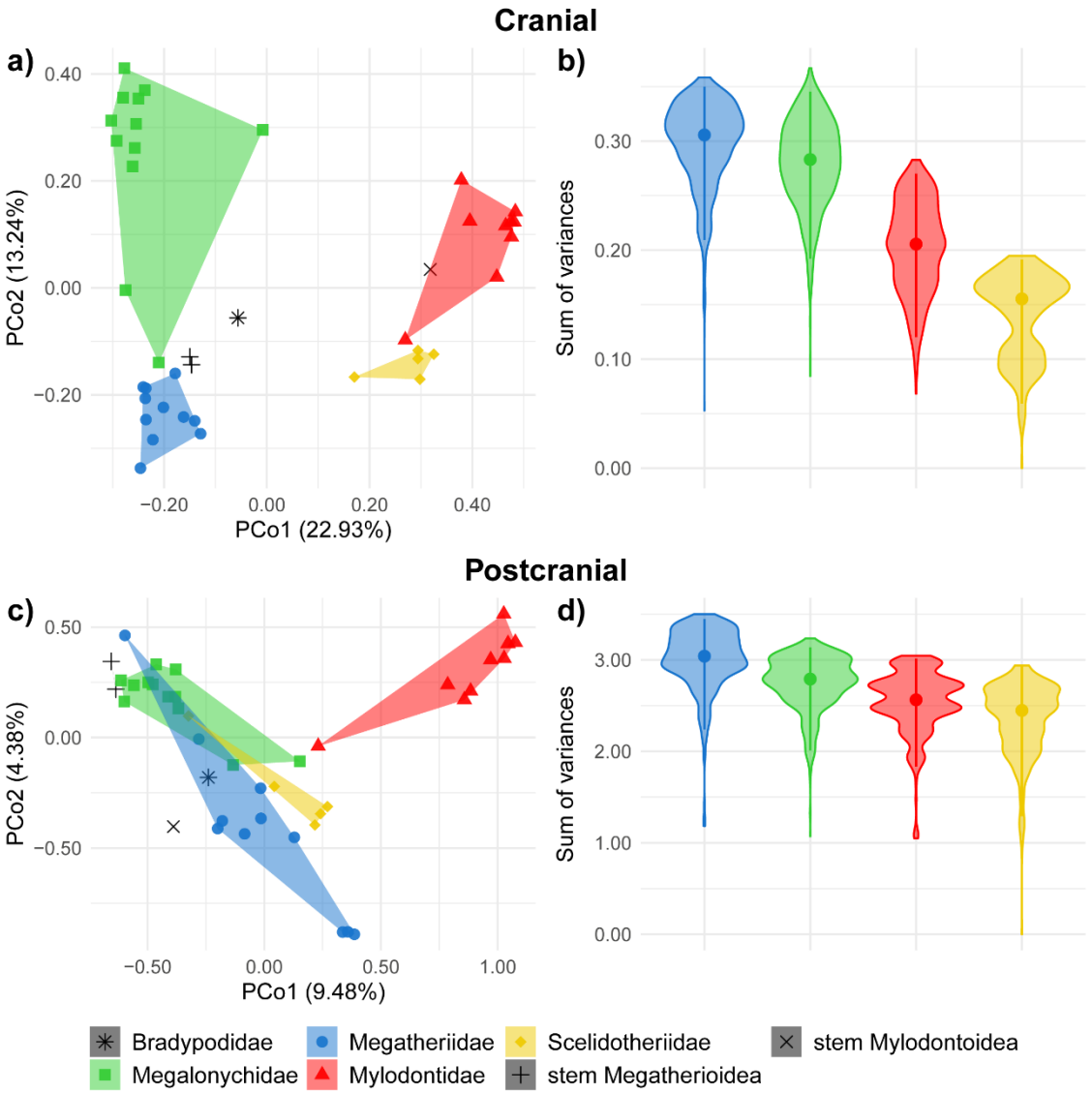

Figure 3. Morphological disparity of less inclusive clades – Scelidotheriidae, Mylodontidae, Megatheriidae and Megalonychidae – for cranial and postcranial datasets. In morphospace plots, the first two PCoA axes are shown. Bradypodidae (= *Bradypus*), stem megatherioids and stem mylodontoids were included for completeness in the morphospace, but were absent in disparity calculations. Violin plots depicting sum of variances (SV) distributions obtained from bootstrapped and rarefied data. a) Cranial data, morphospace occupancy. b) Cranial data, SV. c) Postcranial data, morphospace occupancy. d) Postcranial data, SV.

Table 2. Comparisons of morphological disparity (sum of variances) for pairs of clades and ecological groups, for each partition dataset. Significance of median differences according to Wilcoxon rank-sum test (P-value), and degree of overlapping between distributions according to Bhattacharyya Coefficients (BC).

Dataset	Groups	P-value	BC
Cranial	Megatheriidae : Megalonychidae	< 0.01	0.92
Cranial	Megatheriidae : Mylodontidae	< 0.01	0.12
Cranial	Megatheriidae : Scelidotheriidae	< 0.01	0.00
Cranial	Megalonychidae : Mylodontidae	< 0.01	0.19
Cranial	Megalonychidae : Scelidotheriidae	< 0.01	0.00
Cranial	Mylodontidae : Scelidotheriidae	< 0.01	0.52
Cranial	Megatherioidea : Mylodontoidea	< 0.01	0.00
Cranial	Browser : Mixed/Grazer	< 0.01	0.00
Postcranial	Megatheriidae : Megalonychidae	< 0.01	0.48
Postcranial	Megatheriidae : Mylodontidae	< 0.01	0.28
Postcranial	Megatheriidae : Scelidotheriidae	< 0.01	0.30
Postcranial	Megalonychidae : Mylodontidae	< 0.01	0.78
Postcranial	Megalonychidae : Scelidotheriidae	< 0.01	0.55
Postcranial	Mylodontidae : Scelidotheriidae	< 0.01	0.81
Postcranial	Megatherioidea : Mylodontoidea	< 0.01	0.91
Postcranial	Scansorial : Terrestrial	< 0.01	0.00

Morphospace occupancy of Megatherioidea was greater than that of Mylodontoidea when we consider the cranial dataset, and those clades occupy clearly distinct morphospace regions (Fig. 4a-b, Table 1). The disparity difference was statistically significant for medians and there was a clear lack of overlap in distributions (Fig. 4b, Table 2). For postcranial data, a different pattern was observed, with a partial overlap between clades in morphospace, which presented similar degrees of morphological disparity (Fig. 4c-d, Table 1). Medians were still significantly different, but BC indicates that distributions of the disparity index extensively overlap, despite not being clearly similar according to the ≥ 95 threshold adopted here (Fig. 4d, Table 2).

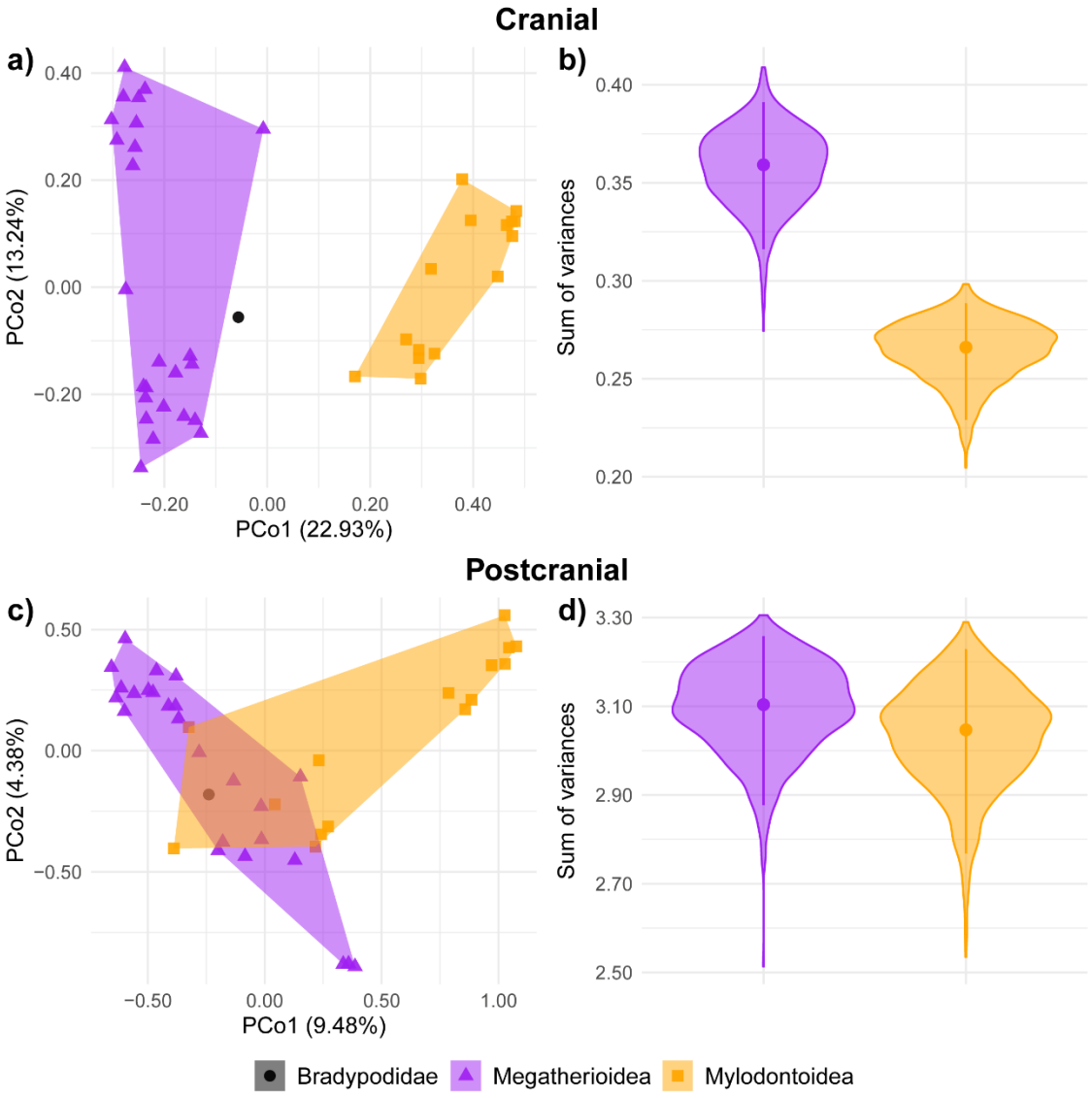

Figure 4. Morphological disparity of more inclusive clades – Mylodontoidea and Megatherioidea – for cranial and postcranial datasets. In morphospace plots, the first two PCoA axes are shown. Bradypodidae (= *Bradypus*) was included for completeness, but was absent in disparity calculations. Violin plots depicting sum of variances (SV) distributions obtained from bootstrapped and rarefied data. a) Cranial data, morphospace occupancy. b) Cranial data, SV. c) Postcranial data, morphospace occupancy. d) Postcranial data, SV.

For dietary categories, results were almost identical to those observed for more inclusive clades in cranial dataset, given the high similarity among those groupings. Browsers, including *Bradypus* and all megatherioids, occupy a distinct region of the morphospace and showed greater disparity relative to mixed feeders/grazers (Fig. 5a-b, Table 1). Locomotory categories presented a partial overlap in morphospace, but terrestrial locomotory habits were associated with a much greater disparity than that observed for scansorial sloths (Fig. 5c-d, Table 1). For both ecological groups, their estimated disparity values do not overlap, being significantly different according to medians and with clearly different distributions according to Bhattacharyya coefficients (Fig. 5, Tables 1 and 2).

4.3.3 Ancestral states and phylogenetic signal

For both ecological traits, ER models were preferred relative to ARD, and models with a single rate regime across branches fitted much better than two-rate models. In both cases, the best model, ER1, did not fulfill the criteria defined a priori to consider it better fitted than the second best-fitted model. However, ER1 was preferred because it was the simplest model tested (Supplementary File S7).

The ancestral dietary category of Folivora was reconstructed as browser, which was maintained in Eufolivora and in all Megatherioidea (Fig. 6a). The ancestor of Mylodontoidea and all nodes within this clade were reconstructed as mixed feeder/grazers (Fig. 6a). The D statistic (D = -1.10) indicate a very clumped distribution for this trait, which indicates a strong phylogenetic signal more extreme than, but still consistent with, the expectations of Brownian motion (probability = 0.99), and far from a random pattern (probability = 0.00).

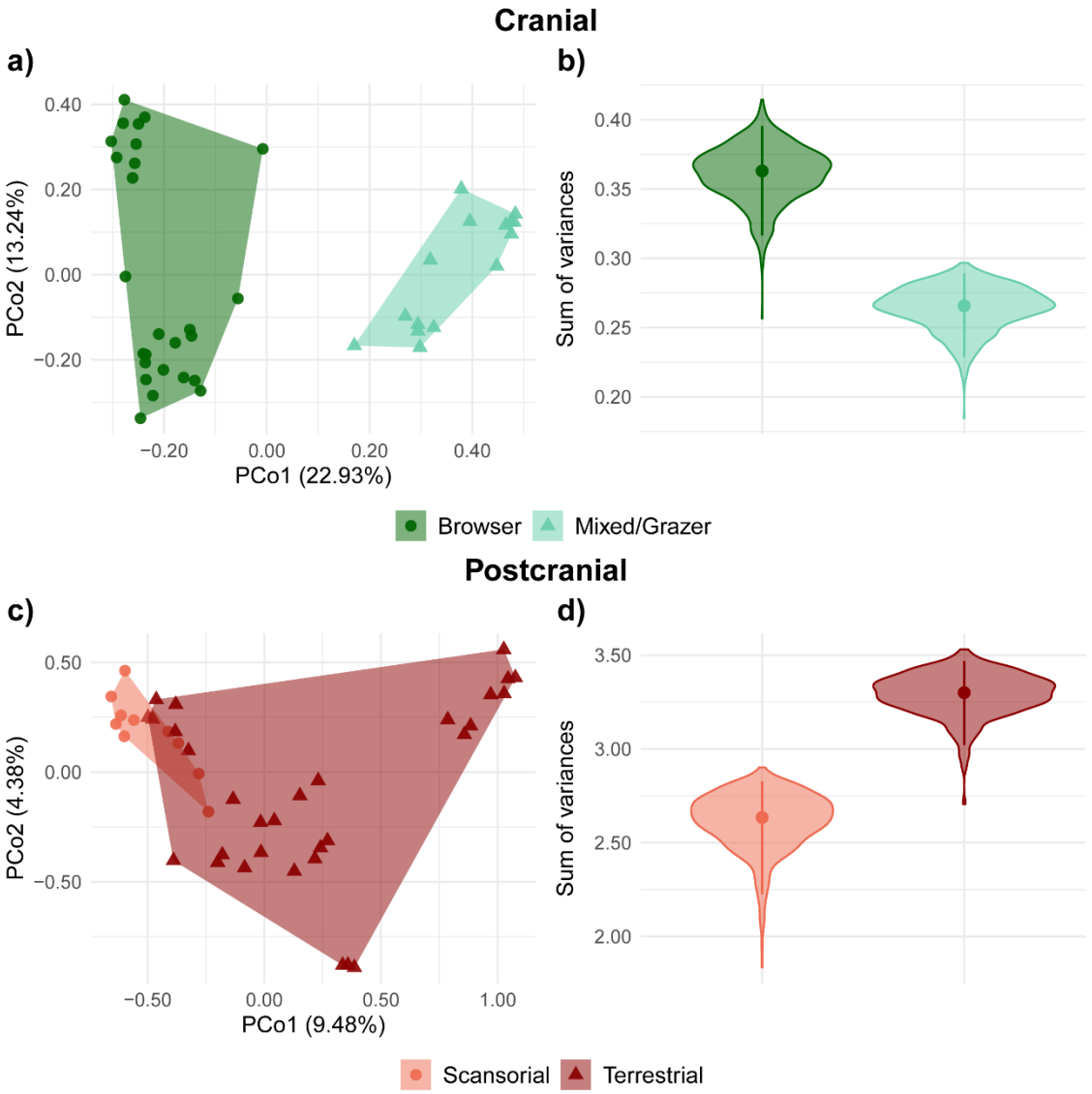

Figure 5. Morphological disparity of cranial dataset for dietary categories, and postcranial dataset for locomotory categories. In morphospace plots, the first two PCoA axes are shown. Violin plots depicting SV distributions obtained from bootstrapped and rarefied data. a) Cranial data, morphospace occupancy. b) Cranial data, sum of variances (SV). c) Postcranial data, morphospace occupancy. d) Postcranial data, SV.

Scansorial habits were, most likely, the ancestral sloth locomotory adaptation. This was also reconstructed as the ancestral locomotory mode for the ancestors of Eufolivora, Megatherioidea, Megatheriidae and Megalonychidae (Fig. 6b). Three independent origins of terrestrial adaptations were observed, in Mylodontoidea, Megatherioidea minus *Analcimorphus*, and Megalonychinae (Fig. 6b). Reversions to scansorial habits evolved independently in *Diabolotherium*, and in the ancestor of the clade uniting *Choloepus*, *Acratocnus* Anthony 1916 and *Neocnus* Arredondo 1961 (Fig. 6b). The D statistic for this

character (D = 0.33) suggested a relatively weak phylogenetic signal that could not be well-described by Brownian motion (probability = 0.25), but even less by a pattern obtained from random permutations of the data (probability = 0.01).

4.3.4 Morphological evolutionary rates

Average cranial and postcranial evolutionary rates were extremely similar (Table 3). The average cranial rates of Mylodontoidea, Scelidotheriidae and Mylodontidae were lower than their respective background evolutionary rates, whereas those of Megatherioidea, Megatheriidae and Megalonychidae were higher than the background (Fig. 7, Table 3). Comparing the less inclusive clades among themselves, Megalonychidae presented a higher average morphological evolutionary rate, followed by Megatheriidae, Mylodontidae and Scelidotheriidae, and among more inclusive clades, Megatherioidea showed a higher evolutionaty rate than Mylodontoidea (Fig. 7, Table 3). Among dietary categories, mixed feeders/grazers showed a lower morphological evolutionary rate than browsers (Fig. 6c, Table 3), in agreement with disparity results.

For postcranial data, clade evolutionary rates showed the same relationship to background rates as those recovered for cranial evolutionary rates, with the exception of Scelidotheriidae, which presented a slightly higher average rate than the average rate of all other branches, and Mylodontoidea, which presented an average evolutionary rate similar to the background (Fig. 7, Table 3). Megatheriidae and Megalonychidae showed very similar postcranial evolutionary rates among themselves, and both showed higher rates than those observed for Mylodontidae and Scelidotheriidae. (Fig. 7, Table 3). Also, Megatherioidea yielded a higher average evolutionary rate than Mylodontoidea (Fig. 7, Table 3). Sloths with terrestrial locomotory habits were associated with a faster postcranial evolution than those with scansorial adaptations (Fig. 6d, Table 3), aligned with its greater disparity.

The best-fitting rate shift model for both cranial and postcranial datasets was the All model, that considered five independent evolutionary rates – one for each less inclusive clade plus the background rate (Table 3). In both cases, AICc > 4 and AICw > 0.9 indicated that those models can be preferred relative to alternative rate shift models, and also relative to a null model without a rate shift (Table 3).

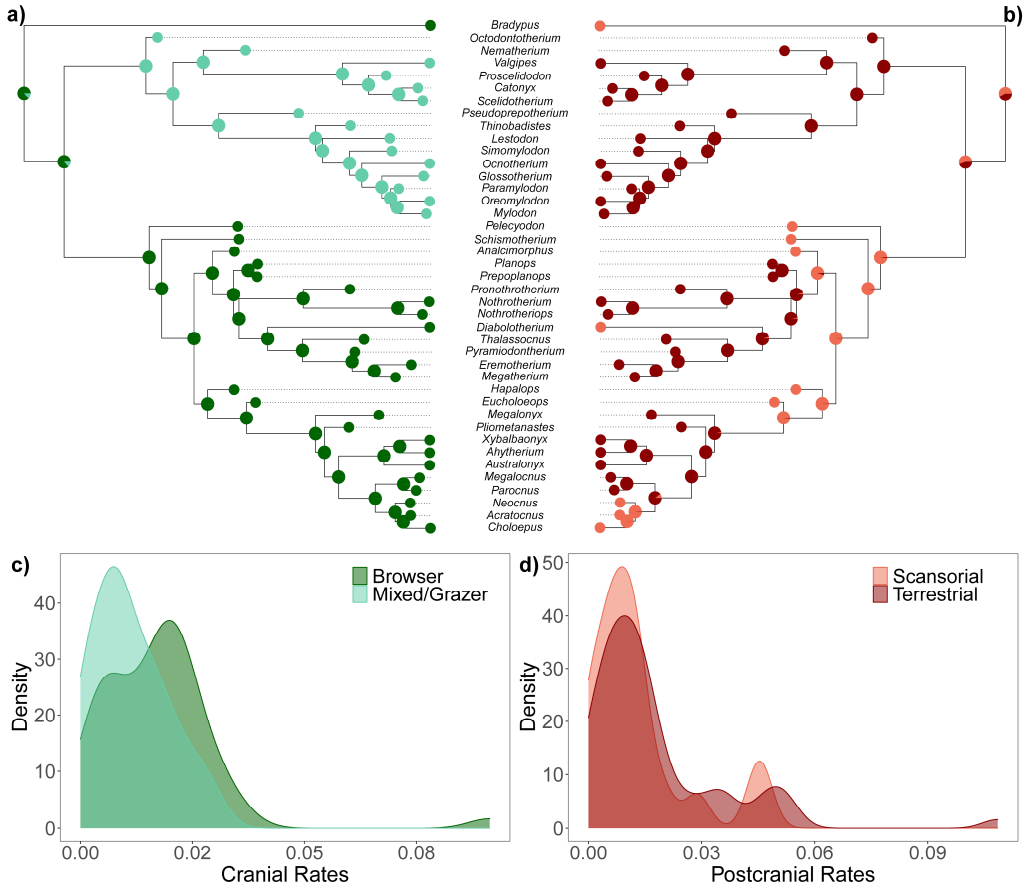

Figure 6. Ancestral state reconstructions of ecological habits in Folivora. a) Diet. b) Locomotion. Their respective distributions of morphological evolutionary rates are depicted below. c) Cranial dataset. d) Postcranial dataset.

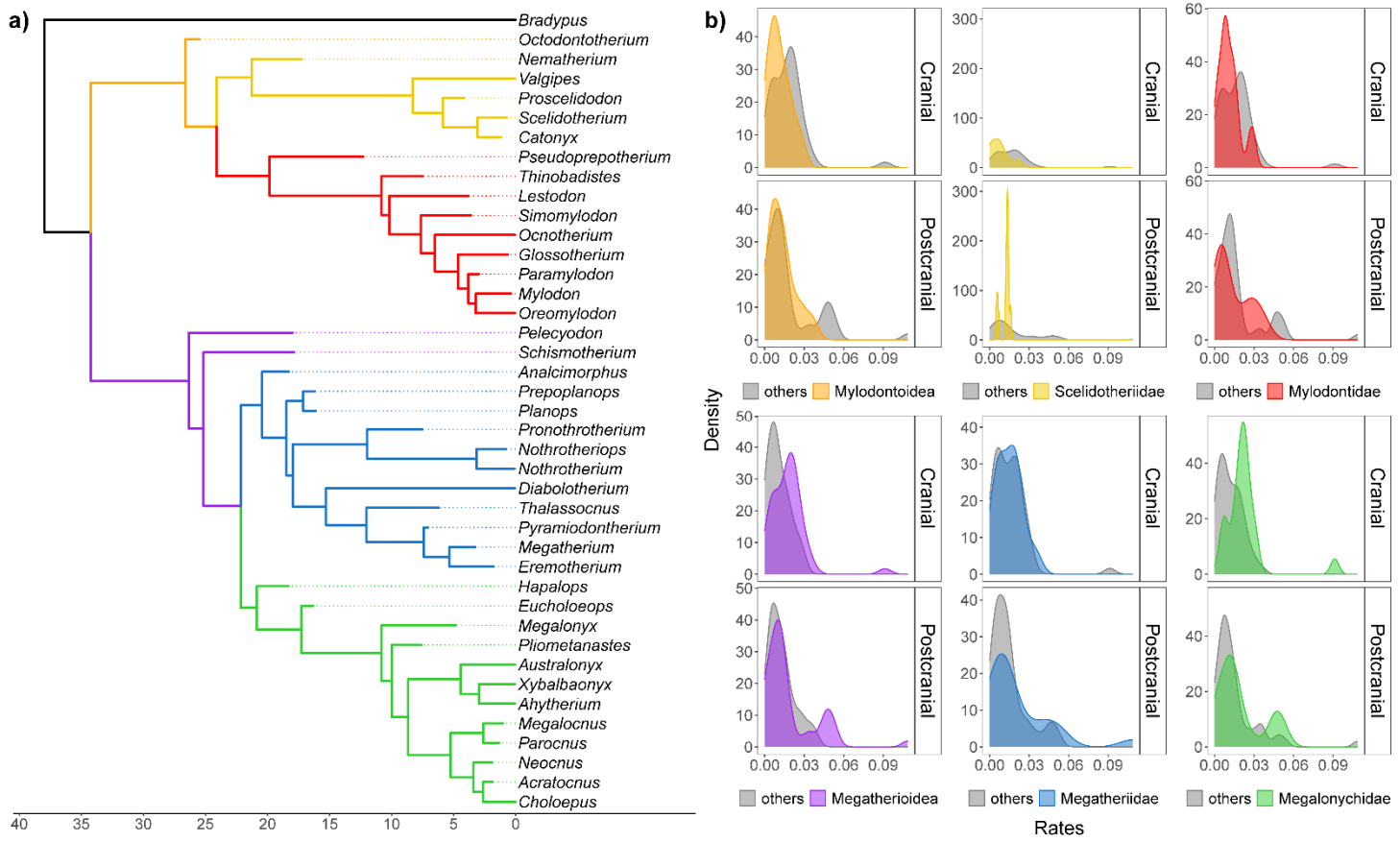

Figure 7. a) Time-scaled phylogeny (scale in millions of years ago) colored by clade. b) clade distributions of morphological evolutionary rates for cranial and postcranial partition datasets relative to the background rate (others). For Megatheriioidea and Mylodontoidea, only the ancestral branches and stem taxa are colored in the tree, but rates apply to all lineages descending from those branches.

Table 3. Model comparison for each partition dataset and rate shift hypothesis, indicating the number of rate regimes (Rates). Focal rates refer to the average rate of each group compared to the background average rate (Backgr.), and to each other, in models with more than two rate regimes. In Null models, a single average rate is considered for the whole tree (i.e., no rate shifts), and in All models, all four less inclusive clades had their average rates compared to each other and to the background rate. *Average focal rates as observed for each less inclusive clade.

Dataset	Model	Rates	Focal	Backgr.	AICc	AICw
Cranial	Null	1	0.012	-	862.14	0.00
Cranial	Megalonychidae x others	2	0.023	0.010	728.39	0.00
Cranial	Megatheriidae x others	2	0.013	0.012	863.99	0.00
Cranial	Scelidotheriidae x others	2	0.007	0.013	837.62	0.00
Cranial	Mylodontidae x others	2	0.011	0.013	861.47	0.00
Cranial	Megatherioidea x others	2	0.016	0.009	786.25	0.00
Cranial	Mylodontoidea x others	2	0.010	0.013	851.23	0.00
Cranial	Megalonychidae x Megatheriidae x others	3	*	0.009	713.24	0.04
Cranial	Megalonychidae x Scelidotheriidae x others	3	*	0.010	722.18	0.00
Cranial	Megalonychidae x Mylodontidae x others	3	*	0.010	728.36	0.00
Cranial	Megatheriidae x Scelidotheriidae x others	3	*	0.013	839.57	0.00
Cranial	Megatheriidae x Mylodontidae x others	3	*	0.013	863.62	0.00
Cranial	Scelidotheriidae x Mylodontidae x others	3	*	0.014	833.18	0.00
Cranial	All	5	*	0.008	707.00	0.96
Cranial	Mixed/Grazer x Browser	2	0.010	0.013	851.23	0.00
Postcranial	Null	1	0.012	-	542.63	0.00
Postcranial	Megalonychidae x others	2	0.017	0.011	533.07	0.00
Postcranial	Megatheriidae x others	2	0.017	0.011	532.41	0.00
Postcranial	Scelidotheriidae x others	2	0.013	0.012	544.70	0.00
Postcranial	Mylodontidae x others	2	0.012	0.013	544.33	0.00
Postcranial	Megatherioidea x others	2	0.014	0.010	533.86	0.00
Postcranial	Mylodontoidea x others	2	0.012	0.012	544.71	0.00
Postcranial	Megalonychidae x Megatheriidae x others	3	*	0.010	513.26	0.00
Postcranial	Megalonychidae x Scelidotheriidae x others	3	*	0.011	534.48	0.00
Postcranial	Megalonychidae x Mylodontidae x others	3	*	0.011	535.16	0.00
Postcranial	Megatheriidae x Scelidotheriidae x others	3	*	0.011	533.60	0.00
Postcranial	Megatheriidae x Mylodontidae x others	3	*	0.011	534.39	0.00
Postcranial	Scelidotheriidae x Mylodontidae x others	3	*	0.013	546.49	0.00
Postcranial	All	5	*	0.006	497.43	1.00
Postcranial	Terrestrial x Scansorial	2	0.015	0.008	515.74	0.00

4.4 DISCUSSION

Cranial data showed disparity patterns and morphological evolutionary rates clearly associated with the phylogenetic structure represented by the less inclusive sloth clades considered in this study. The first two axes of the morphospace were highly informative for distinguishing these groups. The few exception of this clear phylogenetic pattern are stem members of Megalonychidae and Mylodontidae, which are taxa known for retaining many primitive cranial characters in their respective clades (Gaudin 2004; Boscaini et al. 2019; Casali et al. 2021 – Chapter 3).

According to morphological phylogenies, *Choloepus* is closely related with the Antillean taxa, whereas Bradypodidae is the sister taxon of all other sloths. Nevertheless, it is worth noting that the proximity of *Bradypus* to megatherioids, and to a lesser extent, the displacement of *Choloepus* toward the region occupied by mylodontoids in morphospace, echoes their phylogenetic associations as recovered in recent molecular investigations including extant and extinct sloths (Slater et al. 2016; Delsuc et al. 2019; Presslee et al. 2019). If these molecular studies are taken at face value, this may indicate a phylogenetic component in morphology despite the position of extant sloths differing in the two approaches. Notwithstanding, morphospaces depict phenetic and not phylogenetic distances; hence, those patterns are also fully compatible with scenarios of evolutionary convergence (Oyston et al. 2016). The similar position assumed by *Bradypus* and *Choloepus* in PCo1, between mylodontoid and megatherioid sloths, is suggestive of cranial convergence between these taxa, which may originate in part from allometric effects related to their relatively small body size (Raj Pant et al. 2014), but also from the absence of intermediate morphologies in the sample, reflecting their long phylogenetic history, undocumented in the fossil record (McDonald and De Iuliis 2008).

It was not possible to disentangle the influences of the phylogenetic relationships of more inclusive clades – Megatherioidea and Mylodontoidea – from those of dietary categories, which showed a strong phylogenetic signal. Some cranial characters are undoubtedly influenced by dietary adaptations in sloths, like those from the teeth, hyoid apparatus, mandible, snout, and several other structures dispersed in the skull and associated with entheses for the masticatory musculature (Naples 1987; Bargo and Vizcaíno 2008; Bargo et al. 2009; Pérez et al. 2010; McAfee 2011; Naples and McAfee 2014; Casali and Perini 2017; Saarinen and Karme 2017). Alternatively, other characters of the skull, like those from the ear region, have been associated with both phylogenetic and functional signals (Patterson et al. 1989, 1992; Gaudin

1995, 2011; Boscaini et al. 2018). Studies focusing on more restricted sets of characters may be necessary to properly investigate in greater detail the causal influences of cranial disparity in sloths. The very poor fit of the model segregating evolutionary rates by dietary categories – which is equivalent to that separating Mylodontoidea rates from those of the remainder of sloths – highlights that a historical signal in morphology at the level of less inclusive clades was more important for cranial evolution than diet may have been.

Postcranial skeletal anatomy has been mostly associated with functional locomotory adaptations in sloths (Bargo et al. 2000; Toledo et al. 2013, 2015; Amson et al. 2014, 2015c, 2015a, 2015b). This adaptive influence is quite distinct from that of the phylogeny, as indicated by the low phylogenetic signal of locomotory adaptations. The fit of the model considering rate differences among ecological categories was the third best-fitting model, providing some indirect evidence that locomotory adaptations may have also played an important role in postcranial evolutionary tempo. Although long-term evolutionary change is continuously shaped by extrinsic ecological factors, intrinsic developmental constraints are also important, limiting or biasing morphological evolution within major clades (Oyston et al. 2015; Jablonski 2020). Previous studies applying a morphospace approach to investigate the evolution of postcranial morphology in xenarthrans, using morphometric data, also produced a mixture of historical and functional or ecological signals (Amson and Nyakatura 2018; de Oliveira and Santos 2018; Serio et al. 2020; Toledo et al. 2021), which can be hard to fully disentangle, as we also observe here.

Postcranial data showed less phylogenetic structure in morphospace, greater overlap in clade disparity patterns, and a marked difference in disparity among locomotory categories. The phylomorphospace also indicated multiple instances of convergent evolution among sloths. Some of those convergences can be related to locomotory adaptations, like the association of *Analcimorphus*, *Diabolotherium* and to a lesser extent, *Nematherium* to scansorial megalonychids, and that of *Parocnus* and *Megalocnus* to terrestrial taxa occupying a position in the center of the phylomorphospace. Among these patterns, that of *Nematherium* was most surprising, since it has been frequently associated with terrestrial adaptations, climbing only occasionally (White 1997; Toledo et al. 2012, 2013, 2015). However, in a more recent work Toledo (2016) considered *Nematherium* a semi-arboreal taxon, an interpretation also supported by present data. The closer association of *Octodontotherium*, scelidotheriines and *Pseudoprepotherium* to terrestrial megatherioids may reflect a mixture of the retention of primitive characters along with derived convergent morphologies related to pedolateral stance, especially for Scelidotheriinae (McDonald 2012). Another noticeable convergent event

indicated in the postcranial phylomorphospace is that of *Bradypus* towards the morphospace region occupied by terrestrial megatheriids. This clearly derives from its stem position as sister to all other sloths associated with a morphology adapted to climbing, which was rendered primitive to sloths. If we consider its possible association to megatherioids, as in recent molecular phylogenies (Delsuc et al. 2019; Presslee et al. 2019), a very distinct scenario of convergence from terrestrial to scansorial habits should be taken into account.

The Megalonychidae associated with terrestrial adaptations, as *Megalonyx* Harlan (1825) and the genera included in Ahytheriini, did not show much dissimilarity relative to their scansorial kin, and it is unlikely that adult individuals of these taxa presented a semi-arboreal lifestyle (De Iuliis et al. 2009; Grass 2019). One possible explanation for this pattern would be that those taxa adapted to terrestrial habits with little postcranial modification, co-opted the semi-arboreal skeleton of stem megalonychids to perform exclusive ambulatory functions.

The isolated position of Mylodontinae in the PCo1 can be related to several postcranial characters which distinguishes its skeleton from that of Scelidotheriidae and primitive Mylodontidae, especially in the forelimb (Boscaini et al. 2019; Casali et al. 2021 – Chapter 3). However, associating this pattern with ecological adaptations is not straightforward since Scelidotheriidae and primitive Mylodontidae were also terrestrial and probably showed digging and burrowing capabilities (Coombs 1983; Pujos et al. 2012). Megatheriini was also recovered well-separated from other megatheriids along negative values of PCo2, a distribution probably related to large body sizes and the presence of facultative bipedality (Coombs 1983; Casinos 1996; Raj Pant et al. 2014; Toledo et al. 2017).

The reduced disparity and morphological evolutionary rates in scansorial sloths may be the product of strong stabilizing selection for climbing adaptations, despite variations associated with particular alternative climbing habits in sloths (White 1993, 1997; Pujos et al. 2007, 2011; Bargo et al. 2012; Nyakatura 2012; Toledo et al. 2012, 2013). In contrast, much more disparate morphologies and faster evolutionary rates were observed among terrestrial taxa, and it is possible that specific substrate uses, like digging in Mylodontinae (Bargo et al. 2000; Pujos et al. 2012) should also be considered in order to fully understand sloth postcranial evolution. The inclusion of those fine-grained categories is challenging, though. For example, we still have a very incomplete understanding of fossorial adaptations in sloths, which were probably not restricted to terrestrial taxa (Toledo et al. 2012; Gaudin and Croft 2015). Also, those substrate uses may interact with the locomotory categories as we applied here, generating even more restricted groups, what may lead to reduced sample sizes, which make disparity analyses less precise (Lloyd 2016; Gerber 2019).

Morphological disparity and evolutionary rates in Folivora were, in general, greater for megatherioids than for mylodontoids, and this was compatible with the overall rate – but not disparity – patterns observed by Varela et al. (2019). This comparison, nevertheless, should be viewed with caution, because there are important differences in methodology between our studies. We investigated disparity and morphological evolutionary rates for separate partitions, summarizing it with an index for each group, whereas Varela et al. (2019) analyzed how those metrics change through time for the complete skeleton. Working with a complete dataset may lead to the least loss of information caused by incompatible distances between taxa or distortions caused by taxa with higher levels of missing data (Lloyd 2016; Gerber 2019; Schaeffer et al. 2020). On the other hand, separate partitions may elucidate patterns that are unique for subsets of characters, which may be obscured by evaluating complete datasets (Stubbs et al. 2019; Simões et al. 2020; Wang et al. 2021), but with the cost of losing information due to unequal completeness for some taxa in a given partition. This latter aspect is usually more aggravated with multiple time-bins required in disparity and rates through time analyses.

Another trade-off was also observed here, between using a sufficiently detailed ecological categorization on the one hand, and, on the other, ensuring adequate sample sizes for each of the groups being investigated. The proposed practice of including reconstructed ancestors in disparity analyses (Brusatte et al. 2011; Butler et al. 2012; Varela et al. 2019) could help to minimize this problem to some extent, but also introduces an undesirable phylogenetic smoothing to morphological distances (Lloyd 2016, 2018). As new taxa and additional fossil material becomes available, it will be more practical to evaluate multiple partitions with minimal taxonomic exclusion, whereas rare ecological adaptations may be more feasible to apply in species-level datasets, potentially improving sample sizes for those smaller groups.

4.5 CONCLUSIONS

The evolution of cranial and postcranial morphology in sloths is associated with distinct patterns of disparity among clades and ecological groups, even though the two partitions do not differ substantially in evolutionary tempo. Historical processes shaped the evolution of sloths more consistently than ecological ones, although changes in postcranial characters seem also to be associated to locomotory adaptations, at least more than cranial characters are affected by variations in diet. Nevertheless, this may be in part due to the greater overall variation in locomotory mode and more uniformity in dietary adaptations, which, in turn, may stem from

our limited ability to make fine distinctions in diet of extinct taxa. Exploration of cranial subdivisions may prove to be more informative in understanding the possible drivers of the evolution of this morphological complex. Additionally, the usage of fine-grained ecological categories and methodological trade-offs should be taken into account when these evolutionary patterns are investigated quantitatively.

ACKNOWLEDGEMENTS

We thank institutions, curators and staff members who kindly gave us access to the specimens under their care: J. Meng and J. Galkin (AMNH), W. Simpson, A. Stroup and K. Angielczyk (FMNH), M. Ezcurra, L. Chornogubsky and A. Kramarz (MACN), M. Reguero, A. Scarano and A. Carlini (MLP), M. Taglioretti and F. Scaglia (MMP), C. de Muizon and G. Billet (MNHN), C. Cartelle, L. Santos and M. A. Veloso (MCL PUC-MG), C. Costa (MCN-M PUC-MG) and D. Brinkman (YPM). We also thank L. Vilaboim, B. Rossi and S. Stinnesbeck for sharing photographs of specimens. D. Casali was funded by Coordenação de Aperfeiçoamento de Pessoal de Nível Superior (CAPES), via a monthly scholarship (CODE 0001) and the Programa de Apoio à Pós-Graduação (PROAP), and received grants from the FMNH and the Paleontological Society, which assisted significantly in the completion of the study.

REFERENCES

Ameghino F. 1887. Enumeración sistemática de las especies de mamíferos fósiles coleccionados por Cárlos Ameghino en los terrenos eocenos de la Patagonia. Boletín del Mus. La Plata. 1:1–26.

Ameghino F. 1891. Observaciones críticas sobre los mamíferos eocenos de la Patagonia austral. Rev. Argentina Hist. Nat. 1:328–382.

Ameghino F. 1895. Première contribution à la connaissance de la faune mammalogique des couches à *Pyrotherium*. Boletín del Inst. Geográfico Argentino. 15:1–60.

Amson E., Argot C., McDonald H.G., de Muizon C. 2015a. Osteology and functional morphology of the forelimb of the marine sloth *Thalassocnus* (Mammalia, Tardigrada). J. Mamm. Evol. 22:169–242.

Amson E., Argot C., McDonald H.G., de Muizon C. 2015b. Osteology and functional morphology of the hind limb of the marine sloth *Thalassocnus* (Mammalia, Tardigrada). J. Mamm. Evol. 22:355–419.

Amson E., Argot C., McDonald H.G., de Muizon C. 2015c. Osteology and functional morphology of the axial postcranium of the marine sloth *Thalassocnus* (Mammalia, Tardigrada) with paleobiological implications. J. Mamm. Evol. 22:473–518.

Amson E., de Muizon C., Laurin M., Argot C., de Buffrénil V. 2014. Gradual adaptation of bone structure to aquatic lifestyle in extinct sloths from Peru. Proc. R. Soc. B Biol. Sci. 281:20140192.

Amson E., Nyakatura J.A. 2018. Palaeobiological inferences based on long bone epiphyseal and diaphyseal structure - the forelimb of xenarthrans (Mammalia). bioRxiv. 318121:1–20.

Anderson P.S.L., Friedman M. 2012. Using cladistic characters to predict functional variety: experiments using early gnathostomes. J. Vertebr. Paleontol. 32:1254–1270.

Anthony H.E. 1916. Preliminary report on fossil mammals from Porto Rico, with descriptions of new genus of ground sloth and two new genera of hystricomorph rodents. Ann. N. Y. Acad. Sci. 27:193–203.

Arredondo O. 1961. Descripciones preliminares de dos nuevos géneros y especies de edentados del Pleistoceno Cubano. Bol. del Grup. Explor. Científicas. 1:19–40.

Bargo M.S., Toledo N., Vizcaíno S.F. 2012. Paleobiology of Santacrucian sloths and anteaters. In: Vizcaíno S.F., Kay R.F., Bargo M.S., editors. Early Miocene Paleobiology in Patagonia. Cambridge University. p. 216–242.

Bargo M.S., Vizcaíno S.F. 2008. Paleobiology of Pleistocene ground sloths (Xenarthra, Tardigrada): Biomechanics, morphogeometry and ecomorphology applied to the masticatory apparatus. Ameghiniana. 45:175–196.

Bargo M.S., Vizcaíno S.F., Archuby F.M., Blanco R.E. 2000. Limb bone proportions, strength and digging in some Lujanian (Late Pleistocene-Early Holocene) mylodontid ground sloths (Mammalia, Xenarthra). J. Vertebr. Paleontol. 20:601–610.

Bargo M.S., Vizcaíno S.F., Kay R.F. 2009. Predominance of orthal masticatory movements in the Early Miocene *Eucholaeops* (Mammalia, Xenarthra, Tardigrada, Megalonychidae) and other megatherioid sloths. J. Vertebr. Paleontol. 29:870–880.

Barr W.A. 2017. ggphylomorpho. https://github.com/wabarr/ggphylomorpho.

Beaulieu J.M., O'Meara B.C., Donoghue M.J. 2013. Identifying hidden rate changes in the evolution of a binary morphological character: The evolution of plant habit in campanulid angiosperms. Syst. Biol. 62:725–737.

Bhattacharyya A. 1946. On a measure of divergence between two multinomial populations. Sankhyā Indian J. Stat. 7:401–406.

Boscaini A., Iurino D.A., Billet G., Hautier L., Sardella R., Tirao G., Gaudin T.J., Pujos F. 2018. Phylogenetic and functional implications of the ear region anatomy of *Glossotherium robustum* (Xenarthra, Mylodontidae) from the Late Pleistocene of Argentina. Sci. Nat. 105:28.

Boscaini A., Pujos F., Gaudin T.J. 2019. A reappraisal of the phylogeny of Mylodontidae (Mammalia, Xenarthra) and the divergence of mylodontine and lestodontine sloths. Zool. Scr. 48:691–710.

Boyko J.D., Beaulieu J.M. 2021. Generalized hidden Markov models for phylogenetic comparative datasets. Methods Ecol. Evol. 12:468–478.

Brandoni D., Carlini A.A., Pujos F., Scillato-Yané G.J. 2004. The pes of *Pyramiodontherium bergi* (Moreno & Mercerat, 1891) (Mammalia, Xenarthra, Phyllophaga): the most complete pes of a Tertiary Megatheriinae. Geodiversitas. 26:643–659.

Brusatte S.L., Montanari S., Yi H., Norell M.A. 2011. Phylogenetic corrections for morphological disparity analysis: new methodology and case studies. Paleobiology. 37:1–22.

Burnham K.P., Anderson D.R. 2002. Model selection and multimodel inference: A practical information-theoretic approach. New York: Springer-Verlag.

Butler R.J., Brusatte S.L., Andres B., Benson R.B.J. 2012. How do geological sampling biases affect studies of morphological evolution in deep time? A case study of pterosaur (Reptilia: Archosauria) disparity. Evolution (N. Y). 66:147–162.

Cailliez F. 1983. The analytical solution of the additive constant problem. Psychometrika. 48:305–308.

Casali D.M., Boscaini A., Gaudin T.J., Perini F.A. 2021. Reassessing the phylogeny and divergence times of sloths (Mammalia: Pilosa: Folivora), exploring alternative morphological partitioning and dating models. PhD Thesis. Chapter 3.

Casali D.M., Perini F.A. 2017. The evolution of hyoid apparatus in Xenarthra (Mammalia: Eutheria). Hist. Biol. 29:777–788.

Casinos A. 1996. Bipedalism and quadrupedalism in *Megatherium*: an attempt at biomechanical reconstruction. Lethaia. 29:87–96.

Ciampaglio C.N., Kemp M., McShea D.W. 2001. Detecting changes in morphospace occupation patterns in the fossil record: characterization and analysis of measures of disparity. Paleobiology. 27:695–715.

Clarke J.A., Middleton K.M. 2008. Mosaicism, modules, and the evolution of birds: results from a Bayesian approach to the study of morphological evolution using discrete character data. Syst. Biol. 57:185–201.

Coombs M.C. 1983. Large mammalian clawed herbivores: A comparative study. Trans. Am. Philos. Soc. 73:1.

Delsuc F., Kuch M., Gibb G.C., Karpinski E., Hackenberger D., Szpak P., Martínez J.G., Mead J.I., McDonald H.G., MacPhee R.D.E., Billet G., Hautier L., Poinar H.N. 2019. Ancient mitogenomes reveal the evolutionary history and biogeography of sloths. Curr. Biol. 29:2031-2042.e6.

Fritz S.A., Purvis A. 2010. Selectivity in mammalian extinction risk and threat types: a new measure of phylogenetic signal strength in binary traits. Conserv. Biol. 24:1042–1051.

Gardner A.L. 2008. Mammals of South America, Volume 1 - Marsupials, xenarthrans, shrews, and bats. London: The University of Chicago Press.

Gaudin T.J. 1995. The ear region of edentates and the phylogeny of the Tardigrada (Mammalia, Xenarthra). J. Vertebr. Paleontol. 15:672–705.

Gaudin T.J. 2004. Phylogenetic relationships among sloths (Mammalia, Xenarthra, Tardigrada): the craniodental evidence. Zool. J. Linn. Soc. 140:255–305.

Gaudin T.J. 2011. On the osteology of the auditory region and orbital wall in the extinct West Indian sloth Genus *Neocnus* Arredondo, 1961 (Placentalia, Xenarthra, Megalonychidae. Ann. Carnegie Museum. 80:5–28.

Gaudin T.J., Croft D.A. 2015. Paleogene Xenarthra and the evolution of South American mammals. J. Mammal. 96:622–634.

Gearty W. 2021. deeptime: Plotting tools for anyone working in deep time. https://github.com/willgearty/deeptime.

Gerber S. 2019. Use and misuse of discrete character data for morphospace and disparity analyses. Palaeontology. 62:305–319.

Gibb G.C., Condamine F.L., Kuch M., Enk J., Moraes-Barros N., Superina M., Poinar H.N., Delsuc F. 2016. Shotgun mitogenomics provides a reference phylogenetic framework and timescale for living xenarthrans. Mol. Biol. Evol. 33:621–642.

Grass A.D. 2019. Inferring differential behavior between giant ground sloth adults and juveniles through scapula morphology. J. Vertebr. Paleontol. 39:e1569018.

Green J.L. 2009. Dental microwear in the orthodentine of the Xenarthra (Mammalia) and its use in reconstructing the palaeodiet of extinct taxa: the case study of *Nothrotheriops* shastensis (Xenarthra, Tardigrada, Nothrotheriidae). Zool. J. Linn. Soc. 156:201–222.

Green J.L., Resar N.A. 2012. The link between dental microwear and feeding ecology in tree sloths and armadillos (Mammalia: Xenarthra). Biol. J. Linn. Soc. 107:277–294.

Guillerme T. 2018. dispRity: A modular R package for measuring disparity. Methods Ecol. Evol. 9:1755–1763.

Guillerme T., Cooper N. 2016. Effects of missing data on topological inference using a Total Evidence approach. Mol. Phylogenet. Evol. 94:146–158.

Guillerme T., Puttick M.N., Marcy A.E., Weisbecker V. 2020. Shifting spaces: Which disparity or dissimilarity measurement best summarize occupancy in multidimensional spaces? Ecol. Evol. 10:7261–7275.

Harlan R. 1825. Fauna Americana: being a description of the mammiferous animals inhabiting North America. Philadelphia: Anthony Finley.

Harmon L.J. 2018. Phylogenetic comparative methods: Learning from trees. https://lukejharmon.github.io/pcm/.

Hetherington A.J., Sherratt E., Ruta M., Wilkinson M., Deline B., Donoghue P.C.J. 2015. Do cladistic and morphometric data capture common patterns of morphological disparity? Palaeontology. 58:393–399.

Hoffstetter R. 1961. Description d'un squelette de *Planops* (Gravigrade du Miocène de Patagonie). Mammalia. 25:57–96.

Holm S. 1979. A simple sequentially rejective multiple test procedure. Scand. J. Stat. 6:65–70.

Hopkins M.J., Gerber S. 2017. Morphological disparity. In: Nuno de la Rosa L., Müller G., editors. Evolutionary Developmental Biology. Cham: Springer International Publishing. p. 1–12.

Illiger J.K.W. 1811. Prodromus systematis mammalium et avium additis terminis zoographicis utriusque classis, eorumque versione germanica. Berlin: Salfield, C.

De Iuliis G., Pujos F., Cartelle C. 2009. A new ground sloth (Mammalia: Xenarthra) from the Quaternary of Brazil. Comptes Rendus - Palevol. 8:705–715.

Jablonski D. 2020. Developmental bias, macroevolution, and the fossil record. Evol. Dev. 22:103–125.

Joy J.B., Liang R.H., McCloskey R.M., Nguyen T., Poon A.F.Y. 2016. Ancestral reconstruction. PLoS Comput. Biol. 12:1–20.

Kalthoff D.C., Green J.L. 2018. Feeding ecology in Oligocene mylodontoid sloths (Mammalia, Xenarthra) as revealed by orthodentine microwear analysis. J. Mamm. Evol. 25:551–564.

Kassambara A. 2020. ggpubr: "ggplot2" based publication ready plots. https://CRAN.R-project.org/package=ggpubr.

Leidy J. 1868. Notice of some vertebrate remains from the West Indian islands. Proc. Acad. Nat. Sci. Philadelphia. 20:178–180.

Lewis P.O. 2001. A likelihood approach to estimating phylogeny from discrete morphological character data. Syst. Biol. 50:913–925.

Linnaeus C. 1758. Systema Naturae per regna tria naturae, secundum classes, ordines, genera, species, cum characteribus, differentiis, synonymis, locis. Holmie: Laurentius Salvius.

Lloyd G.T. 2016. Estimating morphological diversity and tempo with discrete character-taxon matrices: implementation, challenges, progress, and future directions. Biol. J. Linn. Soc. 118:131–151.

Lloyd G.T. 2018. Journeys through discrete-character morphospace: synthesizing phylogeny, tempo, and disparity. Palaeontology. 61:637–645.

McAfee R.K. 2011. Feeding mechanics and dietary implications in the fossil sloth *Neocnus* (Mammalia: Xenarthra: Megalonychidae) from haiti. J. Morphol. 272:1204–1216.

McDonald H.G. 2003. Xenarthran skeletal anatomy: primitive or derived. Senckenb. Biol. 83:5–17.

McDonald H.G. 2012. Evolution of the pedolateral foot in ground sloths: Patterns of change in the astragalus. J. Mamm. Evol. 19:209–215.

McDonald H.G., De Iuliis G. 2008. Fossil history of sloths. In: Vizcaíno S.F., Loughry W.J., editors. The Biology of the Xenarthra. Gainesville: University Press of Florida. p. 39–55.

McKenna M.C., Bell S.K. 1997. Classification of mammals: above the species level. New York: Columbia University Press.

Miller G.S. 1929. A second collection of mammals from caves near St. Michel, Haiti. Smithson. Misc. Collect. 81:1–30.

Mongiardino Koch N., Ceccarelli F.S., Ojanguren-Affilastro A.A., Ramírez M.J. 2017. Discrete and morphometric traits reveal contrasting patterns and processes in the macroevolutionary history of a clade of scorpions. J. Evol. Biol. 30:814–825.

Mounce R.C.P., Sansom R., Wills M.A. 2016. Sampling diverse characters improves phylogenies: Craniodental and postcranial characters of vertebrates often imply different trees. Evolution (N. Y). 70:666–686.

de Muizon C., McDonald H.G. 1995. An aquatic sloth from the pliocene of peru. Nature. 375:224–227.

Naples V.L. 1982. Cranial osteology and function in the tree sloths, *Bradypus* and *Choloepus*. Am. Museum Novit. 2739:1–41.

Naples V.L. 1987. Reconstruction of cranial morphology and analysis of function in the Pleistocene ground sloth *Nothrotheriops shastense* (Mammalia, Megatheriidae). Contrib. Sci. Nat. Hist. Museum Los Angeles Cty. 389:1–21.

Naples V.L. 1989. The feeding mechanism in the Pleistocene ground sloth, *Glossotherium*. Contrib. Sci. 415:1–23.

Naples V.L., McAfee R.K. 2012. Reconstruction of the cranial musculature and masticatory function of the Pleistocene panamerican ground sloth *Eremotherium laurillardi* (Mammalia, Xenarthra, Megatheriidae). Hist. Biol. 24:187–206.

Naples V.L., McAfee R.K. 2014. Chewing through the Miocene: an examination of the feeding musculature in the ground sloth *Hapalops* from South America (Mammalia: Pilosa). F1000Research. 3:1–26.

Nyakatura J.A. 2012. The convergent evolution of suspensory posture and locomotion in tree sloths. J. Mamm. Evol. 19:225–234.

O'Leary M.A., Bloch J.I., Flynn J.J., Gaudin T.J., Giallombardo A., Giannini N.P., Goldberg S.L., Kraatz B.P., Luo Z.-X., Meng J., Ni X., Novacek M.J., Perini F.A., Randall Z.S., Rougier G.W., Sargis E.J., Silcox M.T., Simmons N.B., Spaulding M., Velazco P.M., Weksler M., Wible J.R., Cirranello A.L. 2013. The placental mammal ancestor and the Post-K-Pg radiation of Placentals. Science (80-.). 339:662–667.

de Oliveira A.M., Santos C.M.D. 2018. Functional morphology and paleoecology of Pilosa (Xenarthra, Mammalia) based on a two-dimensional geometric Morphometrics study of the Humerus. J. Morphol.:1–13.

Orme D., Freckleton R., Thomas G., Petzoldt T., Fritz S., Isaac N., Pearse W. 2018. caper: Comparative analyses of phylogenetics and evolution in R. https://CRAN.R-project.org/package=caper.

Oyston J.W., Hughes M., Gerber S., Wills M.A. 2016. Why should we investigate the morphological disparity of plant clades? Ann. Bot. 117:859–879.

Oyston J.W., Hughes M., Wagner P.J., Gerber S., Wills M.A. 2015. What limits the morphological disparity of clades? Interface Focus. 5:20150042.

Paradis E., Claude J., Strimmer K. 2004. APE: Analyses of phylogenetics and evolution in R language. Bioinformatics. 20:289–290.

Paradis E., Schliep K. 2019. Ape 5.0: An environment for modern phylogenetics and evolutionary analyses in R. Bioinformatics. 35:526–528.

Patterson B., Segall W., Turnbull W.D., Gaudin T.J. 1992. The ear region in Xenarthrans (=Edentata: Mammalia). Part II. Pilosa (sloths, anteaters), palaeanodonts, and a miscellany. Fieldiana Geol. 24:1–79.

Patterson B., Turnbull W.D., Segall W. 1989. The ear region in xenarthrans (=Edentata: Mammalia). Part I. Cingulates. Fieldiana Geol. 18:1–45.

Pérez L.M., Toledo N., De Iuliis G., Bargo M.S., Vizcaíno S.F. 2010. Morphology and function of the hyoid apparatus of fossil xenarthrans (Mammalia). J. Morphol. 271:1119–1133.

Presslee S., Slater G.J., Pujos F., Forasiepi A.M., Fischer R., Molloy K., Mackie M., Olsen J. V, Kramarz A., Taglioretti M., Scaglia F., Lezcano M., Lanata J.L., Southon J., Feranec R., Bloch J., Hajduk A., Martin F.M., Salas Gismondi R., Reguero M., de Muizon C., Greenwood A., Chait B.T., Penkman K., Collins M., MacPhee R.D.E. 2019. Palaeoproteomics resolves sloth relationships. Nat. Ecol. Evol. 3:1121–1130.

Pujos F., Gaudin T.J., De Iuliis G., Cartelle C. 2012. Recent advances on variability, morpho-functional adaptations, dental terminology, and evolution of sloths. J. Mamm. Evol. 19:159–169.

Pujos F., De Iuliis G., Argot C., Werdelin L. 2007. A peculiar climbing Megalonychidae from the Pleistocene of Peru and its implication for sloth history. Zool. J. Linn. Soc. 149:179–235.

Pujos F., De Iuliis G., Quispe B.M. 2011. *Hiskatherium saintandrei*, gen. et sp. nov.: An unusual sloth from the Santacrucian of Quebrada Honda (Bolivia) and an overview of middle Miocene, small megatherioids. J. Vertebr. Paleontol. 31:1131–1149.

Puttick M.N. 2016. Partially incorrect fossil data augment analyses of discrete trait evolution in living species. Biol. Lett. 12:20160392.

R Core Team. 2021. R: A language and environment for statistical computing. https://www.r-project.org/.

Raj Pant S., Goswami A., Finarelli J.A. 2014. Complex body size trends in the evolution of sloths (Xenarthra: Pilosa). BMC Evol. Biol. 14:1–8.

Resar N.A., Green J.L., McAfee R.K. 2013. Reconstructing paleodiet in ground sloths (Mammalia , Xenarthra) using dental microwear analysis. Kirtilandia. 58:61–72.

Revell L.J. 2012. phytools: an R package for phylogenetic comparative biology (and other things). Methods Ecol. Evol. 3:217–223.

Romano M., Brocklehurst N., Fröbisch J. 2017. Discrete and continuous character-based disparity analyses converge to the same macroevolutionary signal: A case study from captorhinids. Sci. Rep. 7:17531.

Saarinen J., Karme A. 2017. Tooth wear and diets of extant and fossil xenarthrans (Mammalia, Xenarthra) – Applying a new mesowear approach. Palaeogeogr. Palaeoclimatol. Palaeoecol. 476:42–54.

Schaeffer J., Benton M.J., Rayfield E.J., Stubbs T.L. 2020. Morphological disparity in theropod jaws: comparing discrete characters and geometric morphometrics. Palaeontology. 63:283–299.

Serio C., Raia P., Meloro C. 2020. Locomotory adaptations in 3D humerus geometry of Xenarthra: testing for convergence. Front. Ecol. Evol. 8:1–12.

Sidlauskas B. 2008. Continuous and arrested morphological diversification in sister clades of characiform fishes: A phylomorphospace approach. Evolution (N. Y). 62:3135–3156.

Simões T.R., Caldwell M.W., Pierce S.E. 2020. Sphenodontian phylogeny and the impact of model choice in Bayesian morphological clock estimates of divergence times and evolutionary rates. BMC Biol. 18:1–30.

Slater G.J., Cui P., Forasiepi A.M., Lenz D., Tsangaras K., Voirin B., de Moraes-Barros N., MacPhee R.D.E., Greenwood A.D. 2016. Evolutionary relationships among extinct and extant sloths: The evidence of mitogenomes and retroviruses. Genome Biol. Evol. 8:607–621.

Slowikowski K. 2021. ggrepel: Automatically position non-overlapping text labels with "ggplot2." https://CRAN.R-project.org/package=ggrepel.

Soul L.C., Wright D.F. 2021. Phylogenetic comparative methods: A user's guide for paleontologists. Cambridge University Press.

Stubbs T.L., Benton M.J., Elsler A., Prieto-Márquez A. 2019. Morphological innovation and the evolution of hadrosaurid dinosaurs. Paleobiology. 45:347–362.

Toledo N. 2016. Paleobiological integration of Santacrucian sloths (Early Miocene of Patagonia). Ameghiniana. 53:100.

Toledo N., Bargo M.S., Cassini G.H., Vizcaíno S.F. 2012. The forelimb of Early Miocene sloths (Mammalia, Xenarthra, Folivora): morphometrics and functional implications for substrate preferences. J. Mamm. Evol. 19:185–198.

Toledo N., Bargo M.S., Vizcaíno S.F. 2013. Muscular reconstruction and functional morphology of the forelimb of Early Miocene sloths (Xenarthra, Folivora) of Patagonia. Anat. Rec. 296:305–325.

Toledo N., Bargo M.S., Vizcaíno S.F. 2015. Muscular reconstruction and functional morphology of the hind limb of Santacrucian (Early Miocene) sloths (Xenarthra, Folivora) of Patagonia. Anat. Rec. 298:842–864.

Toledo N., Bargo M.S., Vizcaíno S.F., De Iuliis G., Pujos F. 2017. Evolution of body size in anteaters and sloths (Xenarthra, Pilosa): Phylogeny, metabolism, diet and substrate preferences. Earth Environ. Sci. Trans. R. Soc. Edinburgh. 106:289–301.

Toledo N., Muñoz N.A., Cassini G.H. 2021. Ulna of extant xenarthrans: shape, size, and function. J. Mamm. Evol. 28:35–45.

Upham N.S., Esselstyn J.A., Jetz W. 2019. Inferring the mammal tree: Species-level sets of phylogenies for questions in ecology, evolution, and conservation. PLOS Biol. 17:e3000494.

Varela L., Tambusso P.S., McDonald H.G., Fariña R.A. 2019. Phylogeny, macroevolutionary trends and historical biogeography of sloths: insights from a Bayesian morphological clock analysis. Syst. Biol. 68:204–218.

Vizcaíno S.F., Toledo N., Bargo M.S. 2018. Advantages and limitations in the use of extant xenarthrans (Mammalia) as morphological models for paleobiological reconstruction. J. Mamm. Evol. 25:495–505.

Wang M., Lloyd G.T., Zhang C., Zhou Z. 2021. The patterns and modes of the evolution of disparity in Mesozoic birds. Proc. R. Soc. B Biol. Sci. 288:1–10.

White J.L. 1993. Indicators of locomotor habits in Xenarthrans: evidence for locomotor heterogeneity among fossil sloths. J. Vertebr. Paleontol. 13:230–242.

White J.L. 1997. Locomotor adaptations in Miocene xenarthrans. In: Kay R.F., Madden R.H., Cifelli R.L., Flynn J.J., editors. Vertebrate Paleontology in the Neotropics: The Miocene Fauna of La Venta, Colombia. Washington: Smithsonian Institution Press. p. 246–264.

Wickham H. 2016. ggplot2: Elegant graphics for data analysis. https://ggplot2.tidyverse.org.

Wilcoxon F. 1945. Individual comparisons by ranking methods. Biometrics Bull. 1:80.

Yu G., Smith D.K., Zhu H., Guan Y., Lam T.T. 2017. ggtree: an R package for visualization and annotation of phylogenetic trees with their covariates and other associated data. Methods Ecol. Evol. 8:28–36.

SUPPLEMENTARY MATERIAL

Supplementary File S1. Nexus file with the morphological character matrix.

Supplementary File S2. Table with missing data prevalence per anatomical partition and status (included or excluded) for all sloth taxa originally included in the dataset.

Supplementary File S3. Tree file with the Bayesian chronogram used in analyses.

Supplementary File S4. Tables with dietary and locomotory categories considered for each taxon, and the consulted literature.

Supplementary File S5. R script to reproduce all the analyses performed in the study.

Supplementary File S6. Tables with eigenvectors and eigenvalues from PCoA analyses.

Supplementary File S7. Tables summarizing the fit of models applied in ancestral states reconstructions of diet and locomotion.

Files available in:

https://drive.google.com/drive/folders/1Na5ECv7fzx2MXE7bNXzz6G_A2Y_lYmcW?usp=sharing

CONCLUSIONS

Morphological evolution is undeniably heterogeneous and this is clearly expressed at different levels of organization of the phenotype, from anatomic complexes to individual characters, requiring analytical tools that account for this evolutionary heterogeneity. Despite its conceptual plausibility, the method of data partitioning by anatomy is mostly inconsequential to the main parameter of interest in phylogenetic analyses, the tree topology. Evidence stemming from simulations and empirical data suggest that those models are not very efficient ways to segregate characters according to their evolutionary rates, whereas this can be easily achieved using homoplasy-based partitions in phylogenetic analyses. Nevertheless, those anatomically-oriented partitions can be valuable when studying morphological disparity and evolutionary rates, allowing to investigate distinct patterns for regions of interest that can be obscured when complete datasets are evaluated.

Phylogenetic investigations of Vermilingua and Folivora returned overall similar results with those previously obtained, but provided some important insights. For Vermilingua, the inclusion of molecular data impacted the position of a fossil taxa, highlighting the indirect effect of sampling additional taxa and characters, and the presence of hidden phylogenetic signals in separate datasets, which become evident when they are combined. For Folivora, the consistency with previously published results is affected by the partitioning model applied, and Bayes factor preferred models based on homoplasy partitioning, which lead to topological estimates more similar to those of parsimony inferences. Despite recovering a topology consistent with those of previous studies, contentious taxa were more precisely positioned here, dated trees were obtained – for Vermilingua, for the first time – and additional synapomorphies were recovered for groups already recognized. Also, both studies showed the importance of model selection in Bayesian phylogenetics, not only for data partitioning, but also for clock and tree models in dating analyses using morphological data.

While investigating the patterns of morphological evolution in sloths, partitioning of cranial and postcranial data was fundamental to shed light in the distinct pattern provided by these partitions, with cranial morphology mostly reflecting phylogenetic inertia, whereas for postcranium, ecological adaptations seem to have played a more important role, resulting in considerably less phylogenetic structure, with several convergent patterns related to the functional morphology of sloths. This study also provided evidence of methodological trade-offs related to data partitioning and missing data, and of detailed categorizations of ecological categories and sample sizes.